SLAC–438
SLAC/SSRL–0073
UC–410
(SSRL–M)

X-RAY STANDING WAVE STUDY OF THE Bi/GaAs AND Bi/GaP INTERFACES*

Alberto Herrera-Gómez

Stanford Linear Accelerator Center
Stanford Synchrotron Radiation Laboratory
Stanford University, Stanford, California 94309

April 1994

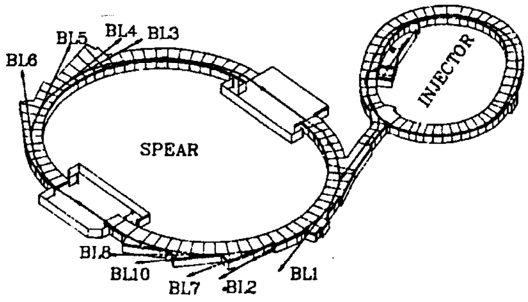

Prepared for the Department of Energy under Contract number DE-AC03-76SF00515

Printed in the United States of America. Available from the National Technical
Information Service, U.S. Department of Commerce, 5285 Port Royal Road,
Springfield, Virginia 22161

---

* Ph.D. thesis

to Gemma

Abstract

Interfaces are one of the most important elements determining the characteristics of electronic devices. Composite semiconductors, specifically the III-V family, are technologically attractive because of their mobility and optical properties, and also because they offer the possibility of engineering such properties as the size of the band gap. Nevertheless, Si has remained the most utilized semiconductor material, primarily because the fabrication of practical MOSFETs with III-V semiconductors remains elusive. Additionally, even though metal/III-V semiconductor junctions are extensively used in devices, the difficulties of understanding these Schottky barriers is evident from the present chaos in the literature concerning barrier formation.

A large research effort is directed to the study of simple systems for which detailed and unambiguous experimental results can be obtained concerning their electronic and geometric structure. Structural techniques, such as X-Ray Standing Wave (XSW) and Low Energy Electron Diffraction (LEED), have successfully been applied to determine the geometric structure of ideal monolayers of adsorbates on semiconductor surfaces. On the other hand, XSW offers the possibility of extending these structural studies to more realistic (less ideal) systems.

Examples of such complex interfaces are the structures formed by one monolayer of Bi on the (110) surface of GaAs and GaP. While better matched Column V elements form epitaxial continuous monolayers on III–V semiconductor (110) surfaces (as Sb/GaAs, Sb/InP, and Bi/InP), Bi is too large to accommodate on GaAs and GaP surfaces with long range order, and vacancies appear to allow relaxation. For the ideal systems, symmetry imposes the presence of only two nonequivalent adatom sites (one bonded to the substrate anion and the other to the substrate cation). However, for Bi/GaAs and Bi/GaP, more than two different sites are present because the position of Bi atoms next to a vacancy is not necessarily equivalent to that between other Bi atoms.

The geometry of the Bi/GaAs and Bi/GaP systems was determined here by triangulating XSW results from three Bragg planes. A methodology was developed that provides an intrinsic check of the validity of assuming two sites for the overlayer structures. An experimental method was developed that allows the three reflections to be measured on the same sample, thus reducing the number of experimental variables, such as the degree of disorder. The traditional method of analysis was not accurate enough for this data, so a more reliable and faster method of data fitting was developed. A configuration used in the present work, which previously has been widely used, presents an intrinsic multireflection problem. This issue is discussed in depth, and the appropriate method is determined for analyzing the data obtained with this configuration.

The results indicate that the two-site approximation for the Bi structure is suitable to the Bi/GaAs interface, and that Bi grows on GaAs in sites close to the bulk continuation of the crystal. For the case of Bi/GaP, the two-site model proved to be too simplistic to completely describe the structure. Nevertheless, it can be concluded that the Bi adatoms grow on GaP also assuming positions close to the bulk continuation of the crystal.

The position of P, both at the clean GaP and Bi/GaP interface, was also studied. Results indicate that, for the clean GaP surface, P relaxes with a small outwards rotation, with the axis of the rotation located at the second-layer Ga site. Whereas, for the Bi-covered case, relaxation consists of a contraction towards the second-layer Ga site.

Acknowledgments

The culmination of my graduate work would not have been possible without the help of many people and institutions to whom I am profoundly grateful.

For the enlightenment and pleasure of working close to him all these years, I am forever indebted to my advisor Prof. William Spicer, who made sure that I got the whole and more of the Ph.D. experience, and whose support had no boundaries.

I am grateful to Tom Kendelewicz, whose suggestions, guidance, and support were fundamental to realization of the work presented in this dissertation.

I am also indebted to Joe Woicik, a key element in this work, for his tenacious support and attention at every stage of the research process, and for his delightful and clear guidance through many issues of this project.

It was helpful to share so many interests with Ken Miyano, who was also a key element in this work. I am grateful for his constant encouragement and support.

I acknowledge the importance of my collaboration with Paul Meissner, which was a significant turning point during my early years as a student.

I will always remember the people with whom I interacted during these wonderful years at Stanford. I am especially thankful to Prof. Walter Harrison for his always-open-door policy; to Dave King for sharing his expertise so many times; and to Masao Yamada, Chris Spindt, Albert Green, and Anita Wahi, for sharing their experience.

I thank Gloria Barnes and Paula Perron for all their help, and Ron Morris, Barry Karlin, and Steve Southworth for their outstanding technical assistance. I also want to salute all the visionary people who made of Stanford such an extraordinary place.

This work was supported by DARPA-ONR (N00014-89-J-1083) and ONR (N00014-92-J-1280). The partial support of CONACyT-México during the first years of this program is gratefully recognized.

Although it is not possible to acknowledge my wife as a co-author, this work was not a one, but a two-person effort.

Table of Contents

List of Tables

List of Illustrations

Chapter 1. Introduction

1.1 Fundamental studies of simple interfaces

Interfaces are one of the most important aspects determining the characteristics of electronic devices. The great interest in interfaces is explained by the enormous and still growing economic impact of the semiconductor industry, which is now considered the largest in the world [1]. A deeper understanding of interfaces increases our ability to predict and control their properties. This allows for the design and fabrication of new devices.

Composite semiconductors, specifically the III-V family, are technologically attractive because of their mobility and optical properties, and also because they offer the possibility of engineering such properties as the size of the band gap. Nevertheless, Si has remained as the most utilized semiconductor material, primarily because the fabrication of practical MOSFETs with III-V semiconductors remains elusive. Additionally, even though metal/III-V semiconductor junctions are extensively used in devices, the difficulties of understanding these Schottky barriers is evident from the present chaos in the literature concerning barrier formation. Still, a consensus exists about the need of a better and deeper understanding of interfaces to III-V semiconductors.

A large research effort is directed to the study of simple systems for which detailed and unambiguous experimental results can be obtained concerning their electronic and geometric structure. Structural techniques, such as X-Ray Standing Wave (XSW) [2] and Low–Energy Electron Diffraction (LEED) [3, 4], have successfully been applied to determine the geometric structure of ideal monolayers of absorbates on III-V semiconductor surfaces. Scanning Tunneling Microscopy (STM) is an extremely useful technique that can be used in conjunction with XSW and LEED, although its generally poor resolution does not provide coordinates of the structure with enough detail.

XSW has many advantages over LEED, such as chemically selectivity. In contrast to LEED, the presence of a thin overlayer does not fundamentally affect the ability of XSW to measure the reconstruction of the substrate outermost layer.

With XSW, it is possible to determine the atomic location of adsorbates scattered across the substrate surface for coverage of a fraction of a monolayer [2]. This is because XSW does not depend on the correlation between the position of the adsorbates. The XSW technique is suitable to study systems where vacancies are present (such as the systems discussed in this thesis) because vacancies do not contribute to the signal. For this reason, XSW offers the possibility of extending structural studies beyond ideal systems.

Such complex interfaces are the structures formed by one monolayer of Bi on the (110) surfaces of GaAs and GaP. This thesis presents an XSW study of the structure of these systems.

1.2 Properties of the systems formed by one monolayer of Bi on the (110) surface of GaAs and GaP

Many of the properties of the Bi/GaAs and Bi/GaP systems can be better understood by contrasting them with those of ideal V/III-V interfaces. This section describes in a comparative way background information on the systems subject to this dissertation.

1.2.1 Morphology of the Bi/GaAs and Bi/GaP interfaces

The (110) surface of III–V semiconductors is very characteristic because the substrate atoms form zigzag chains, which run along the $(1\bar{1}0)$ direction (see Fig. 1.1 or 1.2). The structure of the overlayers formed by Bi and Sb on those surfaces has very special properties. These adatoms do not disrupt the substrate surface with strong reactions, neither do they present strong clustering. The first monolayer tends to grow in an orderly fashion (Stranski-Krastanov type growth), and imitates the substrate surface by forming zigzag chains along the $(1\bar{1}0)$ direction, with a one-to-one correspondence with the substrate atoms. Ideal monolayers, with long-term order and low density of surface defects, are the cases of Sb on GaAs [3, 5], Sb on InP [4, 6], and of Bi on InP [4], with the zigzag chains running indefinitely.

The systems subject to this thesis depart, one slightly (Bi/GaAs [7]) and the other largely (Bi/GaP [8]), from the ideal behavior. The Bi adatoms are too large [9] (see Table 1.1) to accommodate in long ordered chains on GaAs and on GaP. Table 1.2 displays some of the properties of the Bi/GaAs and Bi/GaP interfaces (obtained by previous studies), and how they compare with the ideal V/III–V systems mentioned above.

As for the Sb/GaAs [10], Sb/InP [11], and Bi/InP [12] cases, photoemission spectroscopy (PES) studies of Bi/GaAs [7] and Bi/GaP [13] show two main chemical species, one bonded to the anion and the other to the cation. This is not surprising because the (110) substrate surface unit cell of III-V semiconductors has one anion and one cation, and PES is "directly" sensitive to the different chemical environments of the surface atoms.

The tetrahedral covalent radii can provide a sense of the degree of mismatch between the overlayer and the substrate because, although the bonding of the adatoms to the substrate is not tetrahedral, the sum of the tetrahedral covalent radii describe very closely the actual bond length, at least for the ideal cases [3, 4]. The numbers presented in Table 1.2 as "mismatch" are the differences between the average of the substrate tetrahedral covalent radii and the adatom tetrahedral covalent radio [9]. Notice that the mismatch for the ideal cases is rather large.

With a even larger mismatch, the zigzag chains formed by Bi on GaAs and GaP are interrupted by vacancies to allow relaxation by expansion of the chains along the chain direction. In the case of Bi/GaP, the relaxation of the Bi atoms along the chain is noticeable from the STM results, which shows an expansion of approximately 7% in that direction [8]. Figures 1.1 and 1.2 show simplified schematics of previous STM results on the Bi/GaAs [7] and Bi/GaP [8] systems. The vacancies form rows running along the (001) direction, perpendicular to the adatoms zigzag chains. The length of the Bi zigzag chains are shorter and the vacancy rows are wider for the Bi/GaP interface, which has the largest mismatch.

For both Bi/GaAs [7] and Bi/GaP [8] interfaces, the (1×1) LEED symmetry has an underlying (6×1) pattern. This is because, in both cases, the length of the overlayer surface unit cell adds to 6 substrate surface unit cells (see Figs. 1.1 and 1.2, and Table 1.2). The intensity of the (6×1) spots is very dependent on the details of the preparation of the surface [3], which is not surprising because LEED results are dependent on the vacancy population.

Gap states originating in the vacancy region may account for the inability to obtain flat bands on the Bi/GaAs [7] and Bi/GaP [13] systems, in contrast to the ideal interfaces [14, 15, 16], for which flat band conditions can be achieved for both p and n types.

1.2.2 Generalities of the geometric structure of column V monolayers on III–V semiconductor (110) surfaces

For the case of the ideal monolayers, the long-range order of the adatom chains, the one-to-one correspondence of the adatoms to the substrate atoms, and the (1×1) LEED symmetry impose the presence of only two nonequivalent adatom sites—one bonding to the cation and the other to the anion of the substrate surface unit cell. This is, of course, consistent with the PES results, which finds only two main chemical species. For the case of Bi on GaAs and GaP, the presence of these vacancies breaks the symmetry because the adatom sites at the edge of the chains are not equivalent to those near the center of the chains, so their positions are not necessarily the same. Nevertheless, we will use a two-site model to describe the Bi sites of the Bi/GaAs and Bi/GaP interfaces. Due to the intrinsic complications of introducing too many variables, all structural studies on these types of systems to date (including those presented in this thesis) utilize a (1×1) model.

Using two sites in Tight Binding Total Energy (TBTE) calculations, LaFemina et al. [17] found basically two geometric structures that locally minimize the total energy of ideal column V monolayers on III-V semiconductors. These structural candidates are displayed in Fig. 1.3. The Epitaxially Continued Layer Structure (ECLS) is called so because the adatoms take positions near the bulk continuation of the substrate. In the Epitaxial On Top Structure (EOTS), the adatoms are on top of the outermost substrate atoms. The calculations indicate that for lower mismatch, ECLS is favored, and for larger mismatch, EOTS is favored. Let's remark that these calculations consider two sites; in principle, then, their conclusions are only valid for the ideal cases, where the zigzag chains are continuous. All the ideal cases mentioned are in the lower mismatch side, so ECLS is favored over EOTS in all of them (see Table 1.2).

1.2.3 Experimental structural techniques

Scanning Tunneling Microscopy is an very useful technique because it provides an overall view of the interface. However, STM does not provide the structure in enough detail. Other techniques with greater resolution have to be used to determine the geometry. It is important that the resolution is precise enough to at least discriminate between the structural candidates proposed by the theoretical calculations.

X-Ray Standing Wave is a very powerful technique, and is becoming a clear choice for surface structure determination. Although XSW was established during the sixties, the technique was reborn in the eighties due to the availability of synchrotron radiation. Table 1.3 makes a comparison among four structural techniques: STM, Extended X-Ray Absorption Fine Structure (EXAFS), dynamical LEED, and XSW.

Dynamical LEED is the main competitor of XSW, although XSW has many clear advantages. First of all, XSW results are very simply related to the horizontal and vertical atomic coordinates, and the resolution on these parameters are better than for LEED. The XSW technique is chemically selective, while LEED is not; XSW is not affected by the lack of correlation between the adatoms, so it can be used to study the sitting point for submonolayers of adatoms, while LEED cannot. The presence of vacancies does not affect

XSW data because vacancies contribute with no XSW signal, while they influence LEED patterns. In contrast to LEED, the presence of a thin overlayer does not fundamentally affect the ability of XSW to measure substrate relaxation. Although the interpretation of both XSW and LEED results needs some initial assumptions (such as the number of nonequivalent sites), XSW provides the specific answer under those assumptions, and not just support for a possible best candidate, as in the LEED case. Finally, the analysis of the results is much simpler for XSW.

1.2.4 Previous structural results

Coincidentally, LEED [3, 4] and/or XSW [5, 6] studies have been carried out on the ideal systems, where the calculations favor ECLS (see Table 1.2). These studies find, at the least, a qualitative agreement with the theoretical method [17].

For the Bi/GaAs system, TBTE calculations favor ECLS over EOTS by 0.06 eV [18]. This difference is much smaller than 0.43 eV, which is the difference in the Sb/GaAs case [17]. LEED studies [3] compare fits to the experimental data using the ECLS and EOTS models. ECLS is also favored by this technique.

Unpublished TBTE calculations [19] on the Bi/GaP system have been carried out using a (1×1) model. For this case, the difference between the energy formation of a ECLS and of a EOTS type chain is, if any, favoring EOTS. No published LEED structural studies on this system is known to the author.

1.3 Background and overview of the XSW technique

A more detailed treatment is provided in Chapters 4 and 5 and Appendix 1. There are many excellent treatments of the Dynamical Diffraction of X-Rays applied to XSW [20].

1.3.1 Generalities

The XSW technique relies on the fact that when an X-ray impinges on a crystalline substrate near a Bragg condition, the incident beam is strongly reflected, and the superposition of the incident and reflected beam forms an X-ray standing wave that has the periodicity of the reflecting Bragg planes of the crystal lattice (see Fig. 1.4). Meanwhile, the atoms in the substrate and on the surface are photoexcited by the electric field of the standing wave. From the Electric Dipole approximation, the excitation rate varies as the square of the total electric field amplitude (see Section 5.1.1). The key element that makes this technique sensitive to the atomic positions is the spatial modulation of the electric field amplitude of the standing wave over an interplanar distance, so the field strength seen by a particular atom depends on its position with respect to the planes.

It is possible to experimentally measure the strength of the electric field seen by a particular atom by monitoring the yield (Y) from any product of its excitation. For example, we can select a particular atomic specie by counting the total number of electrons photoemitted from one of its distinct core levels. In this work, the excitation rate of the Bi atoms was measured by monitoring the photoelectron yield from the Bi 4d core levels, using a Cylindrical Mirror Analyzer (CMA).

The XSW experiments can be performed by either sweeping the photon energy or the sample angle relative to the incident X-ray beam. Controlling the angle of incidence in surface experiments is very demanding because of the need for vacuum-compatible high-resolution goniometers. On the other hand, XSW experiments which sweep the photon energy can be performed in the already existing EXAFS beam lines at synchrotron sources. For this reason, the experiments reported in this thesis were performed by sweeping the photon energy.

1.3.2 Reflectivity and the dynamical Bragg condition

The Bragg reflection of an X-ray beam by a crystal can be intuitively understood in terms of the constructive interference of the beams reflected by the crystal planes. This condition can be written in the following way [21]:

$$\mathbf{k}_H = \mathbf{k}_0 + \mathbf{H} \quad , \tag{1.1}$$

$$|\mathbf{k}_H| = |\mathbf{k}_0| \quad , \tag{1.2}$$

where $\mathbf{k}_0$ and $\mathbf{k}_H$ are the wave vector of the incident and reflected beams, and $\mathbf{H}$ is the corresponding Bragg crystal vector. Equations 1.1 and 1.2 are the so-called "kinematical" Bragg condition, and are equivalent to the Bragg law $\lambda = 2d_H \sin\theta_H$. To calculate the actual strength of the reflected beam, or reflectivity, it is necessary to take into account that the beam is reflected and transmitted up and down by each one of the atomic planes [20], as shown in the insert of Fig. 1.5. The treatment that takes the multiple reflections into account, including phase shifts upon scattering, is the so called "dynamical" approach. Equivalent to this approach, although much more concise and elegant, is directly solving Maxwell's equations for a system with a periodic dielectric function (see Chapter 4 and Appendix 1).

A consequence of the dynamical back-and-forth reflection of the X-ray beam is that the reflectivity is finite, not only at the exact Bragg condition, but in a finite area around it. The Du Mond diagram of Fig. 1.5 shows the (θ, λ) region (shadowed area) around the exact Bragg condition (central curve) in which the reflectivity is finite. The thick arrow in Fig. 1.5 indicates that the mode in which the experiments were performed was by keeping the angle fixed and sweeping the photon energy. Figure 1.6 shows the theoretical reflectivity as a function of energy for the (220) Bragg reflection of GaP for a fixed incident angle of 90^o. The intersection of the thick arrow of Fig. 1.5 with the outer (inner) curve corresponds to the low-energy (high-energy) side E_1 (E_2) of Fig. 1.6. Notice the finite range of energy in which the beam is reflected. This behavior is beyond what the kinetical approach (Eqs. 1.1 and 1.2) can explain because it predicts that, for a fixed angle, constructive interference (and finite reflectivity) is possible only for a single wavelength. The XSW technique makes heavy use of the details of the dynamical properties of the diffraction of X-rays by crystals. A dynamical discussion of the Bragg condition is provided in depth in Section 4.2.2.

1.3.3 The standing wave excitation spectrum

The standing wave is present in the range of strong reflectivity of Fig. 1.6. Also basic to the XSW technique is the experimental ability to control the position of the nodes of the electric field of the standing wave. This can be done by changing either the photon energy or the angle of incidence around the Bragg condition. A discussion of the change of the phase of the standing wave as we move around the Bragg condition is provided by Batterman et al. [20].

We call E_1 and E_2, defined in Fig. 1.6, the low- and high-energy sides of the reflectivity. At the low-energy side, the phase difference between the incident and reflected beams is such that the nodes of the electric field of the standing wave are situated at the planes of the atoms, as illustrated in the right side of Fig. 1.7. As we sweep the photon energy to the high-energy side, the phase difference changes in such a way that the nodes of the electric field of the standing wave move to the planes between the atoms (see the left side of Fig. 1.7). So, by sweeping the photon energy from E_1 to E_2, we can move the maximum of the electric field amplitude from between the atomic planes to the atomic planes, making a "search" for the atoms between the planes.

The behavior of the yield for the case of subtitutional impurities (marked with "S") is shown in Fig. 1.7. Because the standing wave extends into the vacuum, the following discussion also applies to adatoms at the surface. When the photon energy is at the low-energy side, these impurities see a node or minimum on the electric field amplitude, so the photoemission yield, Y(E), is minimum. As we move the photon energy to the high-energy side, the electric field amplitude seen by these atom increases, to finally reach a maximum when the photon energy is equal to E_2 (see the right side of Fig. 1.7). There, the photoemission yield reaches its maximum. The shape of the photoemission yield as the photon energy is swept is shown in Fig. 1.8. This shape would be the same had we chosen any other product of the excitation that is proportional to the number of core holes created, such as Auger electron yield or fluorescence yield. For the case of interstitial impurities, such as the one marked with "I" in Fig. 1.7, the corresponding yield, Y(E), is also shown in Fig. 1.8. The shape of Y(E) is very dependent on the position of the atom in question.

The excitation rate in the standing wave field of a monochromatic beam of energy E is as follows [22] (see Eq. 5.17):

$$Y(E) = 1 + \Re(E) + 2 f_c \sqrt{\Re(E)} \cos\left[\nu(E) - 2\pi \frac{\mathrm{D_c}}{\mathrm{d_H}} \right] \quad , \qquad (1.3)$$

where ν is the phase difference between the incident and reflected beam, and determines the position of the maximum and minimum of the electric field of the standing wave; $\Re$ is the intensity of the reflected beam with respect to the incident beam; $d_{\mathbf{H}} \equiv 1/|\mathbf{H}|$ is the interplanar distance; and $\mathbf{H}$ is the crystal vector defining the Bragg planes. The coherent distance (D_c) and the coherent fraction (f_c) depend on the atomic positions. In the simplest case, where every atom assumes equivalent positions in the crystal, D_c can be interpreted as the distance to the atomic planes. Equation 1.3 is fitted to the experimental data to find the best values for $D_c^{\mathbf{H}}$ and $f_c^{\mathbf{H}}$ (see Chapter 5).

Figure 1.9 displays XSW spectra for different values of the coherent distance. As can be seen, differences of 10% of the interplanar distance can be resolved just by eye inspection.

1.3.4 The distribution function

For more complicated situations, the general dependence of D_c and f_c on position is given in terms of a distribution function $f_{\mathbf{H}}(D)$, with D the dimension perpendicular to the planes (parallel to $\mathbf{H}$). The $f_{\mathbf{H}}(D)\,dD$ is the fraction of the atoms with a distance between D and $D + dD$ to its local crystal plane. Its integral over a Bragg interplanar distance is normalized to one. For example, if all the atoms are at a distance D_1 from the atomic planes, then $f_{\mathbf{H}}(D)$ is equal to a Dirac delta function around D_1. where D_c and f_c are the phase and amplitude of the Fourier integral of $f_{\mathrm{H}}(D)$ over a interplanar distance, with wave vector equal to the Bragg plane vector (see Section 5.1.2):

$$\int_0^{d_{\mathrm{H}}} dD\, f_{\mathrm{H}}(D) \exp\left\{-2\pi i \frac{D}{d_{\mathrm{H}}}\right\} = f_c^{\mathrm{H}} \exp\left\{-2\pi i \frac{D_c^{\mathrm{H}}}{d_{\mathrm{H}}}\right\} \quad . \tag{1.4}$$

In principle, it is possible to reconstruct the distribution function in real space from a large enough number of reflections, allowing us to transform Eq. 1.4 to its inverse. In practice, the systems of interest are simple enough to express the distribution function in terms of a finite and small number of parameters, such as the unknown coordinates of the adatoms. This allows Eq. 1.4 to relate the experimental values for D_c^{H} and f_c^{H} to the atomic coordinates of the adatoms. A detailed discussion of the distribution function is provided in Section 5.1.2.

1.4 Outline of the dissertation

The focus of this thesis is the geometric characterization of the structure formed by one monolayer of Bi on the (110) GaAs and GaP surfaces using the XSW technique. The experimental and analysis method employed for the two systems are identical, so much of the discussion will be done in parallel.

The information about the systems provided by previous STM and PES studies (Section 1.2), together with the two-site approximation (Section 2.1), is used to represent the systems with a simple distribution function (Section 2.3), so the problem is reduced to finding the free parameters of the distribution (Section 2.4). The problem is then attacked via XSW triangulation (Section 2.2) using three reflections: (220), (111), and $(11\bar{1})$. With these three reflections, there is enough information to determine the structure of the overlayer (Section 2.4) and to check the self-consistency of the two-site approximation (Section 2.6).

A experimental configuration for the (111) and $(11\bar{1})$ reflections is developed (Section 3.3) that allows the performance of all three reflection on a single sample, reducing the number of experimental variables, such as the degree of order. By using a back-reflection configuration for the (220) reflection (Section 3.3.1), and asymmetric configurations for the other two (Section 3.3.2), it is possible to perform the experiments with the same set of crystals in the monochromator, and without changing the orientation of the sample. There is an intrinsic problem with the (220) back-reflection (Section 3.4) because, in this configuration, the (200) and (020) Bragg conditions are also satisfied.

A method is developed to deal with the multireflection problem (Section 4.3). To this end, a new form of the wave equation for X-rays in crystals is derived (Section 4.2) that is simple enough to be applied to the problem. A computer program was developed to carry out the multireflection calculations (Appendix 2).

A method for fitting XSW data is developed (Section 5.2) that is more dependable, theoretically better justified, and faster than other methods traditionally used. It greatly improves the quality of the fits and self-consistency of the results (Section 6.4). A computer fitting program is constructed based on this method (Appendix 3). To develop this method, it was necessary to formalize the theoretical framework of the XSW theory (Section 5.1).

The experiments performed and data about the Bi/GaAs interface are presented (Section 6.1 and 6.4). The criteria used to average the data is based on the maximization of the correlation of the reflectivity (Section 6.3). The program that was developed and used to average the data is presented (Appendix 4). The results are shown to have remarkable reproducibility and self-consistency (Section 6.4). They determine that the structure is described by ECLS, confirming the suggestions from LEED experiments and TBTE calculations.

The experiments performed and data about the Bi/GaP interface are presented (Sections 7.1 and 7.2). A self-consistency test of the results shows that the two-site approximation is too simplistic for this system (Section 7.3). Nevertheless, the results discard every structure except ECLS (Sections 7.4 and 7.5).

The relaxation of P, with and without the Bi overlayer, is also studied with the XSW technique (Chapter 8), using a new experimental methodology that was developed so that the effect of the overlayer can be easily discriminated (Sections 8.5, 8.6). For the clean surface, the P atoms undergo a small rotation with center at the second layer Ga site. The effect of the Bi overlayer on P is a contraction of a larger magnitude in the direction of the bond to the second layer Ga site.

A summary is presented, together with the contributions of the thesis and future work (Chapter 9).

References

1. Workshop Working Group Reports of the Semiconductor Industry Association (1993).

2. J. Zegenhagen. "Surface structure determination with X-ray standing wave." Surface Science Reports **18**, 199 (1993) and references therein (see p. 256).

3. W.K. Ford, T. Guo, D.L Lessor, and C.B. Duke. "Dynamical low-energy electron-diffraction analysis of bismuth and antimony epitaxy on GaAs(110)." Physical Review B **42**, p. 8952 (1990).

4. W.K. Ford, T. Guo, K.J. Wan, and C.B. Duke. "Growth and atomic geometry of bismuth and antimony on InP(110) studied using low-energy electron diffraction." Physical Review B **45**, p. 11896 (1992).

5. T. Kendelewicz, J.C. Woicik, K.E. Miyano, A. Herrera-Gómez, P.L. Cowan, B.A. Karlin, C.E. Bouldin, P. Pianetta, and W.E. Spicer. "X-ray standing-wave study of monolayers of Sb on GaAs(110)." Physical Review B **46**, p. 7276 (1992).

6. T. Kendelewicz, J.C. Woicik, K.E. Miyano, P.L. Cowan, B.A. Karlin, C.E. Bouldin, P. Pianetta, and W.E. Spicer. "Synchrotron X-ray standing-wave study of Sb on GaAs(110) and InP(110)." Journal of Vacuum Science and Technology B **9**, p. 2290 (1991).

7. A.B. McLean, R.M. Feenstra, A. Taleb-Ibrahimi, and R. Ludeke. "Electronic and structural properties of a discommensurate monolayer system: GaAs(110)-(1×1) Bi." Physical. Review B **39**, p. 12925 (1989).

8. M. Prietsch, A. Samsavar, and R. Ludeke. "Structural and electronic properties of the Bi/GaP(110) interface." Physical Review B **43**, No. 14, p. 11850 (1991).

9. L. Pauling, "The Nature of the Chemical Bond," Cornell University Press, Ithaca, New York (1960).

10 P. Skeath, C.Y. Su, I. Lindau, and W.E. Spicer. "Column III and V elements on GaAs (110): bonding and adatom-adatom interaction." Journal of Vacuum Science and Technology **17**, p. 874 (1980).

11 C. Maani, A. McKinley, and R.H. Williams. "The absorption and electronic structure of antimony layers on clean cleaved indium phosphide (110) surfaces." Journal of Physics C **18**, p. 4975 (1985).

12 K.E. Miyano, T. Kendelewicz, R. Cao, C.J. Spindt, I. Lindau, W.E. Spicer, and J.C. Woicik. "Morphology and barrier-height development of Bi/InP(110) interfaces." Physical Review B **42**, p. 3017–23 (1990).

13. K.E. Miyano, R. Cao, T. Kendelewicz, A.K. Wahi, I. Lindau, and W.E. Spicer. "Photoemission spectroscopy of ordered overlayers on GaP (110)." Physica Scripta **41**, p. 973 (1990).

14. A.M. Green, M. Yamada, T. Kendelewicz, A. Herrera-Gómez, and W.E. Spicer. "In overlayers on Sb passivated GaAs." Journal of Vacuum Science and Technology B **10**, p. 1918 (1992).

15. M. Yamada, A.K. Wahi, T. Kendelewicz, and W.E. Spicer. "Fermi level pining on ideally terminated InP(110) surfaces." Physical Review B **45**, p. 3600 (1992).

16. M. Yamada, A.K. Wahi, P.L. Meissner, A. Herrera, T. Kendelewicz, and W.E. Spicer. "One monolayer of Sb or Bi used as a buffer layer preventing oxidation of InP." Applied Physics Letters **58**, p. 1413–15 (1991); Y. Meng, J.J. Joyce, M. Tang, J. Anderson, and G.J. Lapeyre. "Band bending model for the ideal Bi/InP(110) interface." Physical Review B **46**, p. 12818 (1992).

17. J.P. LaFemina, C.B. Duke, and C. Mailhiot. "New surface atomic structures for column V overlayers on the (110) surfaces of III-V compound semiconductors." Journal of Vacuum Science Technology B **8**, p. 888 (1990).

18. A.M. Bowler, J.C. Hermanson, J.P. LaFemina, C.B. Duke. "Surface atomic structure and bonding of GaAs(110)-p(1 × 1)—Bi (1 ML)." Journal of Vacuum Science Technology B **10**, p. 1953 (1992).

19. J.P. LaFemina. Private communication.

20. For examples, see: B.W. Batterman, H. Cole. "Dynamical diffraction of X-rays by perfect crystals." Review of Modern Physics **36**, No. 3, p. 681 (1964); R.W. James, "The Optical Principles of the Diffraction of X-Rays," Ox Bow Press, Woodbridge,

Connecticut (1947); and W.H. Zachariasen, "Theory of X-Ray Diffraction in Crystals," Dover Publications, Inc., New York (1945).

21. N.W Ashcroft and N.D. Mermin, "Solid State Physics," Saunders College, Philadelphia (1976).

22. D.P. Woodruff, D.L. Seymour, C.F. McConville, C.E. Riley, M.D. Crapper, and N.P. Prince. "A simple X-ray standing wave technique for surface structural determination—theory and an application." Surface Science **195**, p. 237 (1988).

III	IV	V
Al 1.26	Si 1.17	**P** **1.10**
Ga **1.26**	Ge 1.22	**As** **1.18**
In 1.44	Sn 1.40	Sb 1.36
Tl 1.47	Pb 1.46	**Bi** **1.46**

Table 1.1. The systems studied in this thesis are a monolayer of Bi on GaAs and on GaP. The elements are presented in Periodic Table order with the corresponding tetrahedral covalent radii.

	Bi/GaAs	Bi/GaP	Ideal (Sb/GaAs, Sb/InP, Bi/InP)
Main chemical components (PES)	2	2	2
Mismatch	20%	24%	< 15% (11, 7 and 15%)
Zigzag chains (STM)	√	√	√
Length of adatom chains (substrate surface unit cells)	5	3 and 4	indefinitely long
Width of vacancy rows (substrate surface unit cells)	1	3 and 2	no vacancy rows
LEED symmetry	(1×1) with an underlying (6×1)	(1×1) with an underlying (6×1)	(1×1)
Flat band condition (PES)	×	×	√
XSW structural determination	**this study**	**this study**	ECLS for all the cases
LEED structural determination	ECLS by a small margin		ECLS for all the cases
TBTE structural determination	ECLS by a small margin	not clear between EOTS and ECLS (unpublished)	ECLS for all the cases

Table 1.2. Comparison of the properties of the Bi/GaAs and Bi/GaP interfaces with the ideal cases.

	STM	EXAFS	LEED	XSW
Vertical resolution	4	× = none	2	1 = best
Horizontal resolution	3	×	2	1
Distance resolution	4	1	2	3
Chemically selective	3	1	×	1
Model independence	1	2	4	2
Adatom correlation independence	1	3	×	1
Not affected by vacancies	1	1	4	1
Analysis simplicity	1	3	4	2
Crystallinity independence	1	1	×	×

Table 1.3. Comparison between structural techniques.

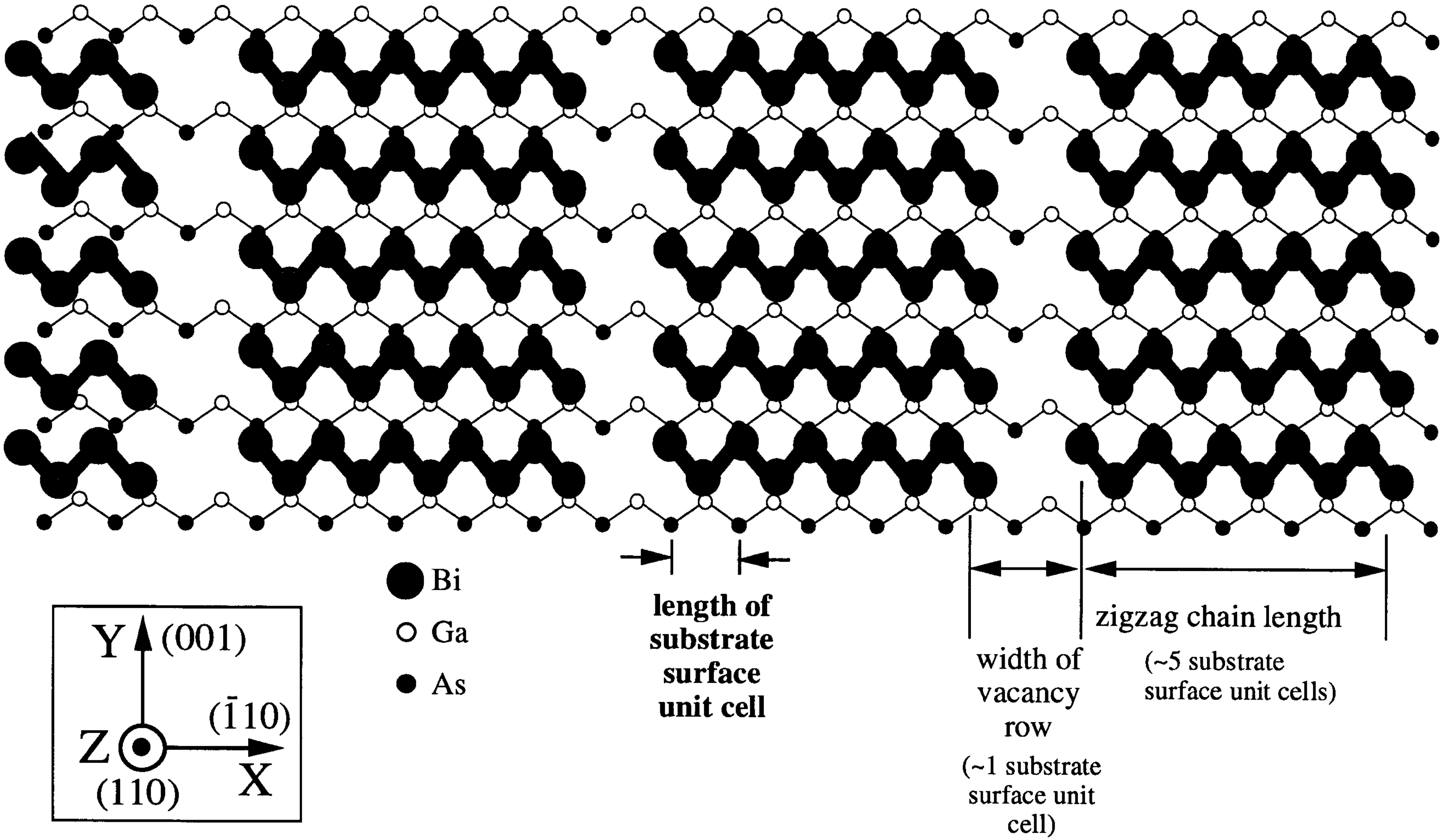

Figure 1.1. Schematics of the Bi/GaAs interface suggested by STM results [7]. Bismuth forms chains along the ($\bar{1}$10) direction of a length of five surface unit cells, interrupted by rows of vacancies of a width of one surface unit cell, and running along the (001) direction.

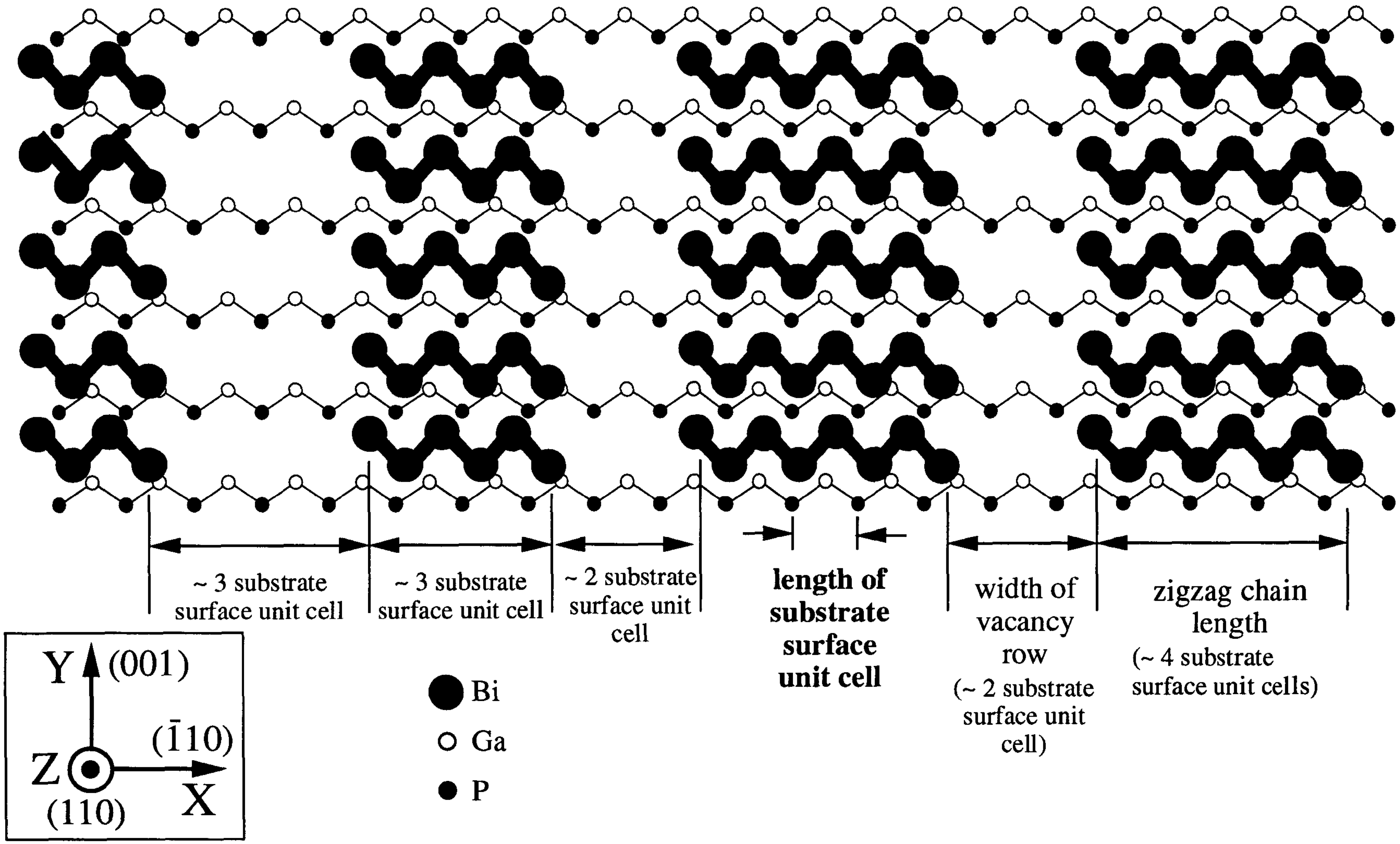

Figure 1.2. Schematics of the Bi/GaP interface suggested by STM results [8]. Bismuth forms chains along the $(\bar{1}10)$ direction of a length of three and four surface unit cells, interrupted by rows of vacancies of a width of two and three surface unit cells, and running along the (001) direction.

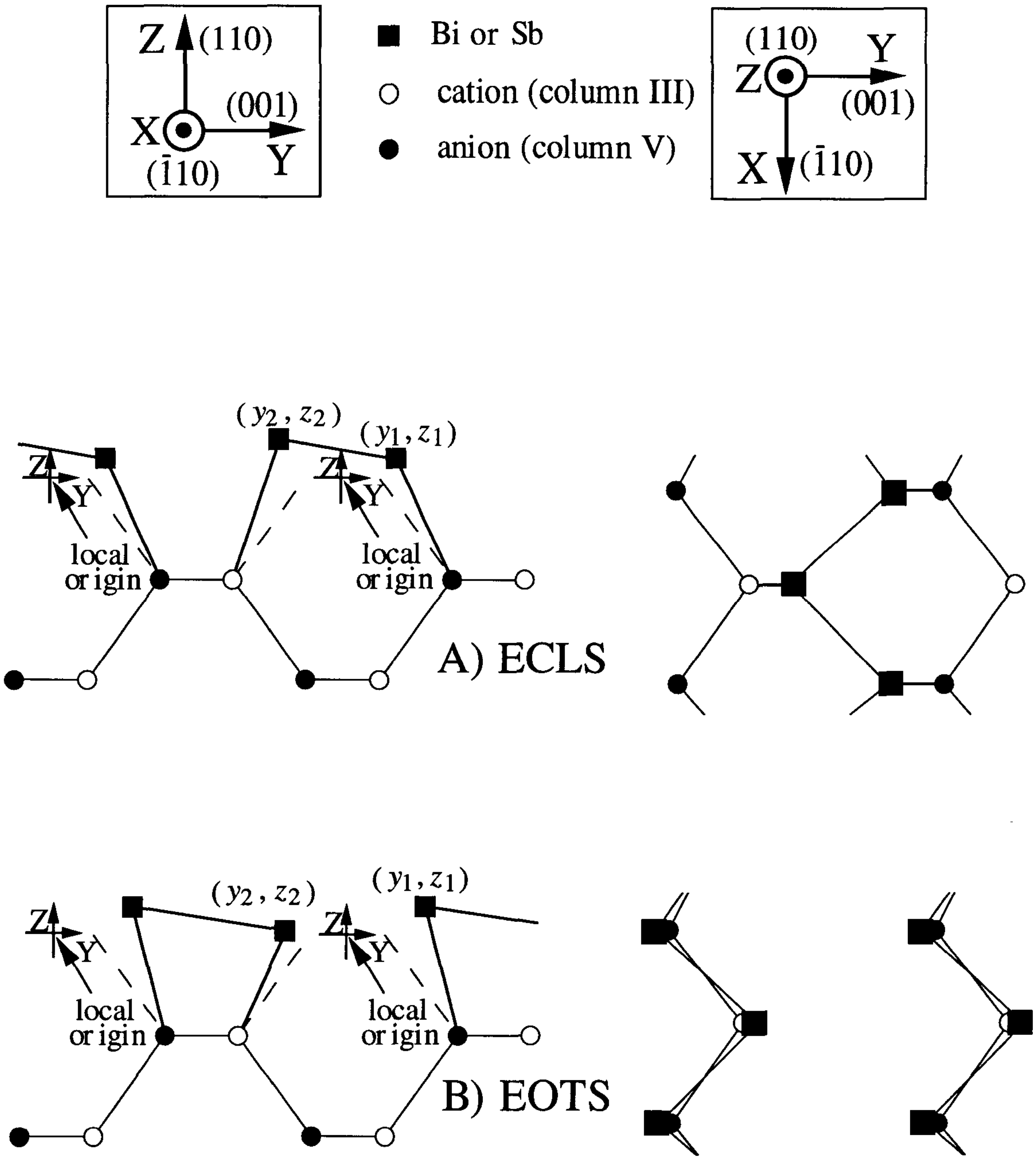

Figure 1.3. As shown by TBTE calculations [17], these structures minimize locally the energy of Column V overlayers (Sb or Bi) on III-V semiconductors.

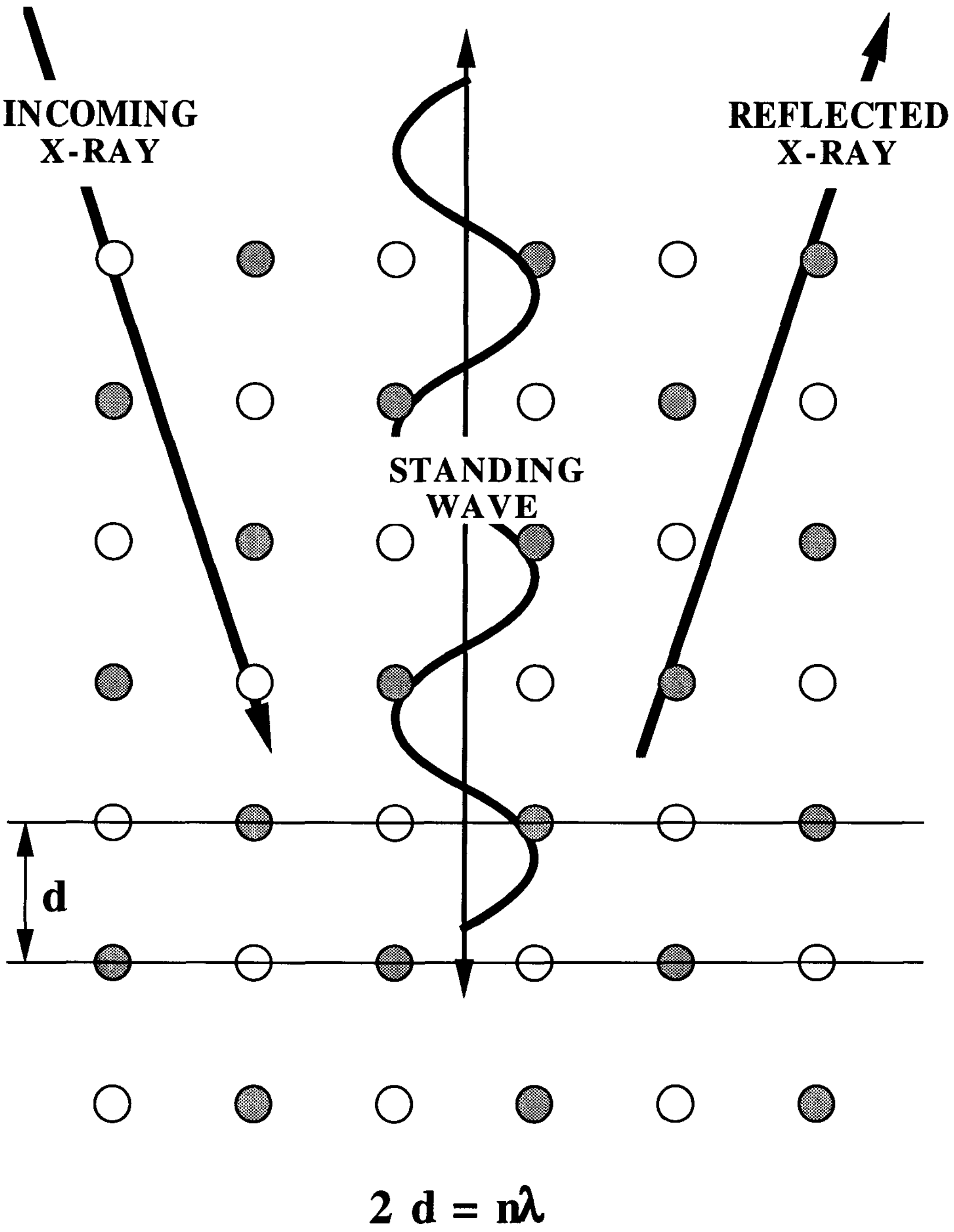

Figure 1.4. The interference of a Bragg reflected beam with the incident beam forms an X-ray standing wave with exactly the same periodicity as the Bragg planes.

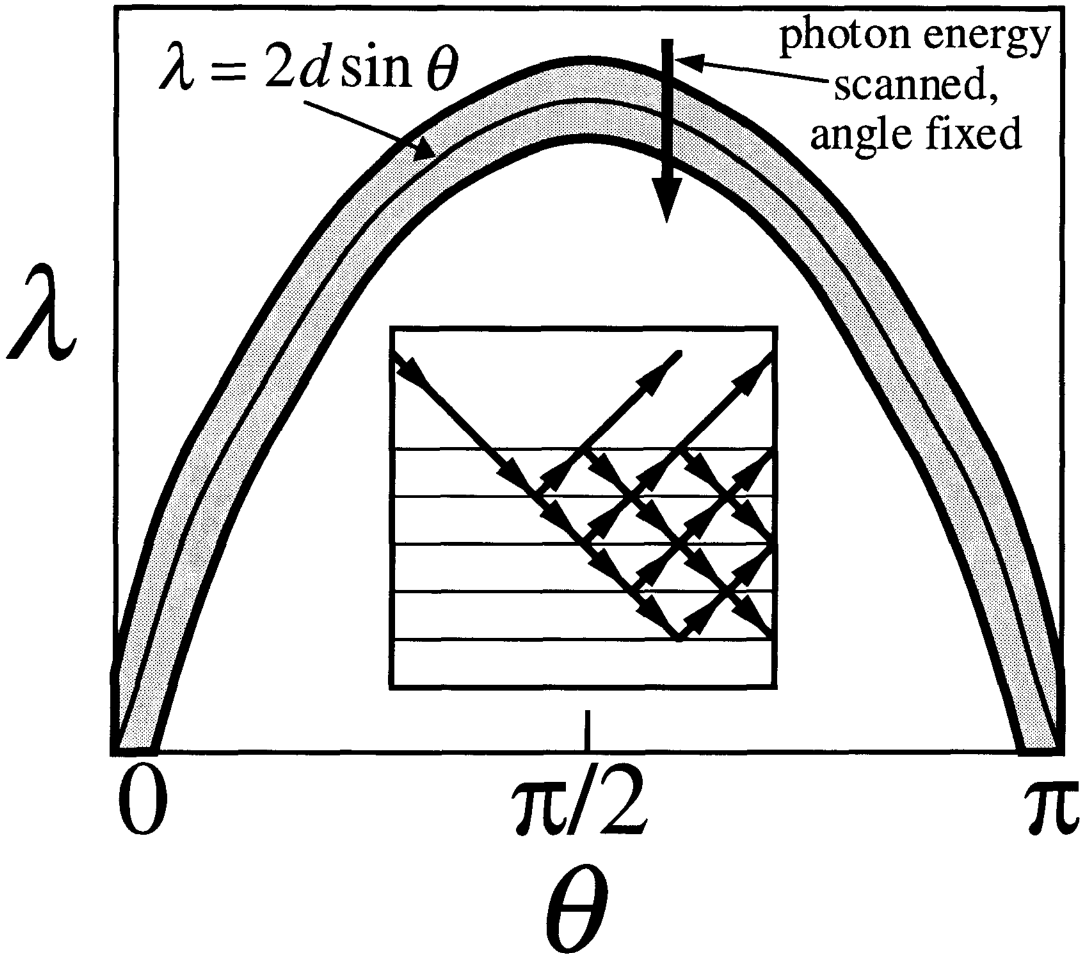

Figure 1.5. Du Mond diagram. The center curve corresponds exactly to the Bragg condition $\lambda=2d \sin\theta$. The reflectivity is close to unity in a finite region (shadowed) around the Bragg condition. The back and forth reflection of the incoming beam by every Bragg plane (see insert) is precisely that responsible for the finiteness of the region in which the incident beam is coupled to the reflected beam. The downward arrow indicates that the experiments are performed by sweeping the photon energy, keeping the angle fixed.

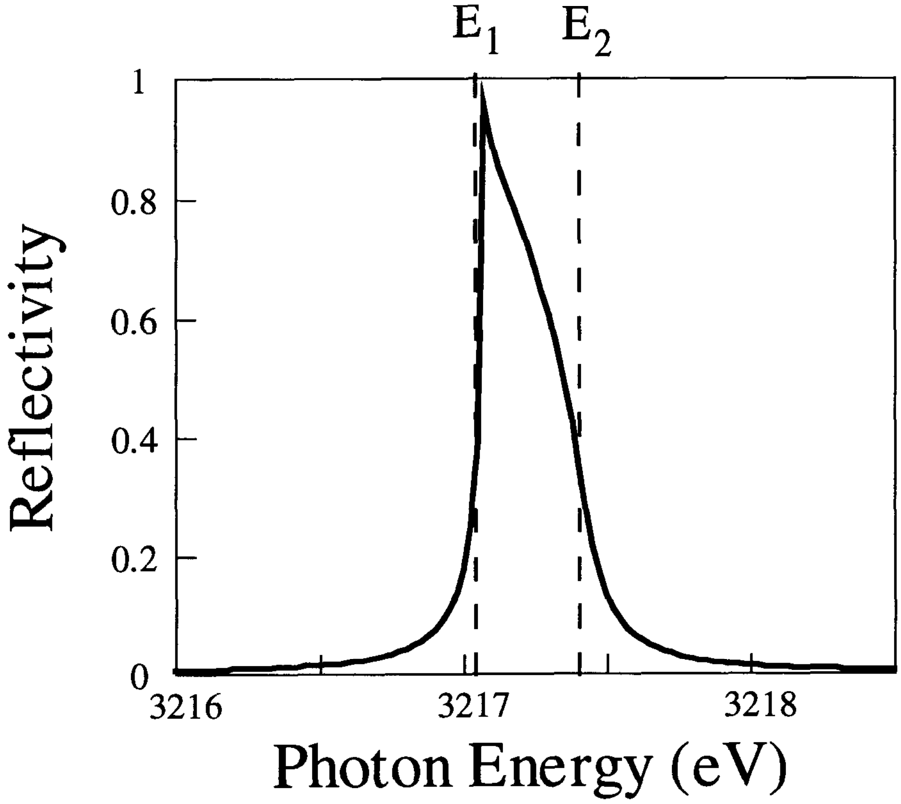

Figure 1.6. Theoretical reflectivity for the (220) reflection of GaP. The finite width is not due to temperature effects, but is inherent to Bragg reflections.

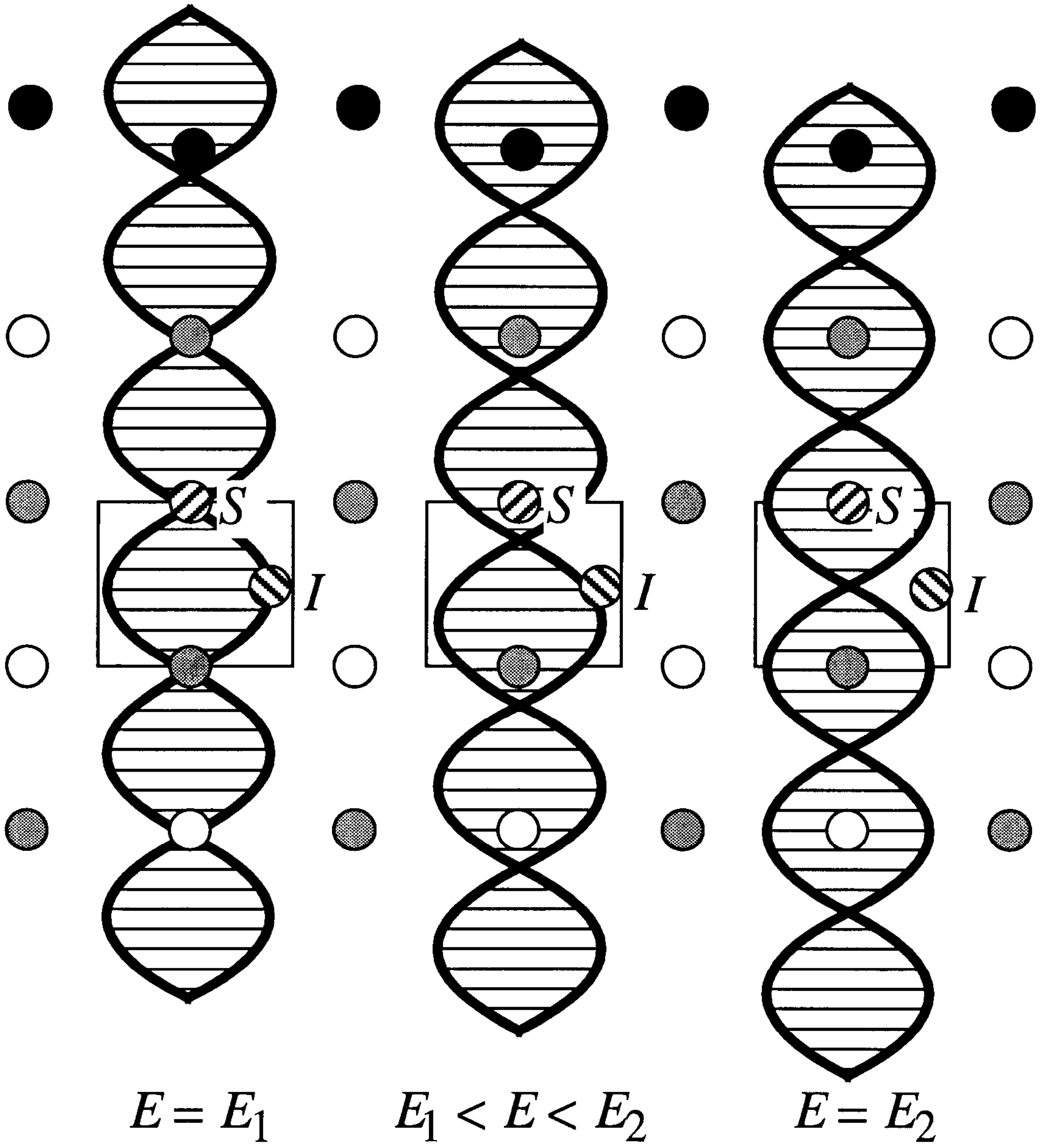

$E = E_1$ $E_1 < E < E_2$ $E = E_2$

▨ *Substitutional impurity*

▧ *Interstitial impurity*

● *Ad-atom*

Figure 1.7. Phase of the electric field standing wave for the three energies around the Bragg condition shown in Fig. 1.6.

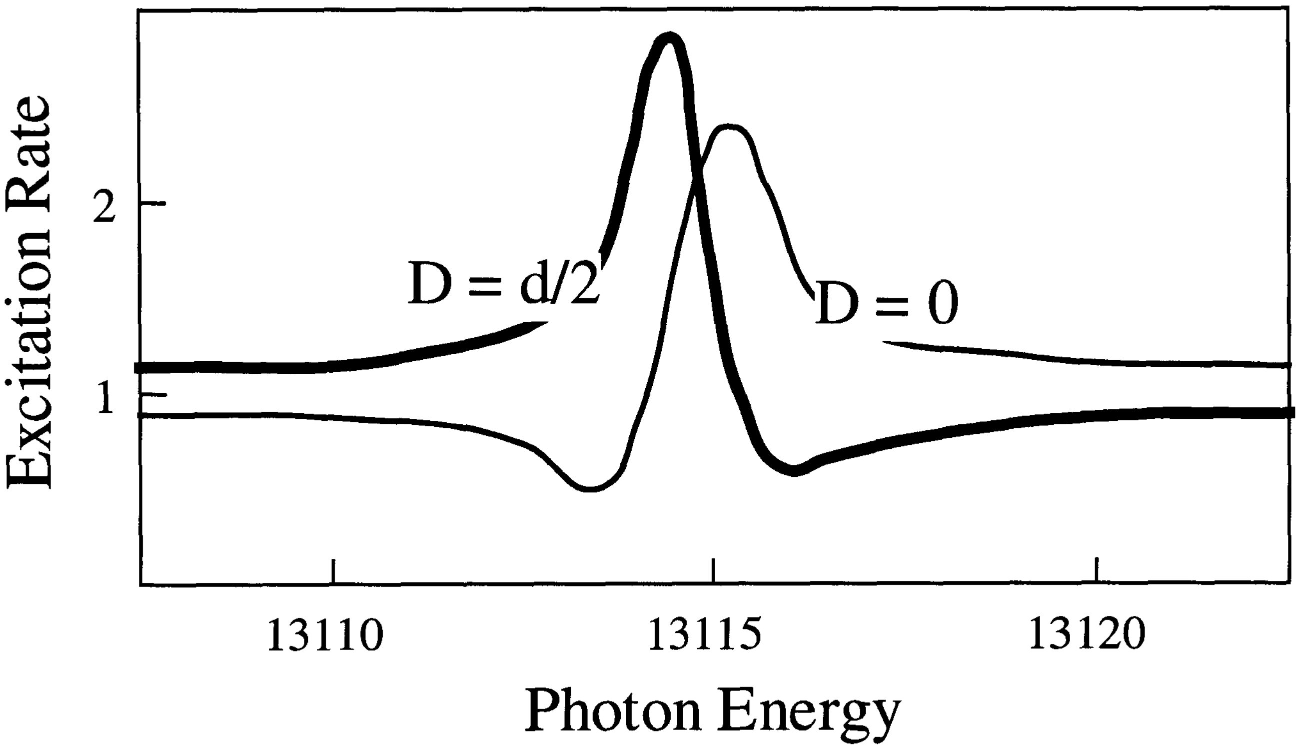

Figure 1.8. X-Ray Standing Wave spectra for atoms located at different distances from the Bragg planes. The excitation rate can be measured by monitoring photoelectrons, fluorescence yield, etc.

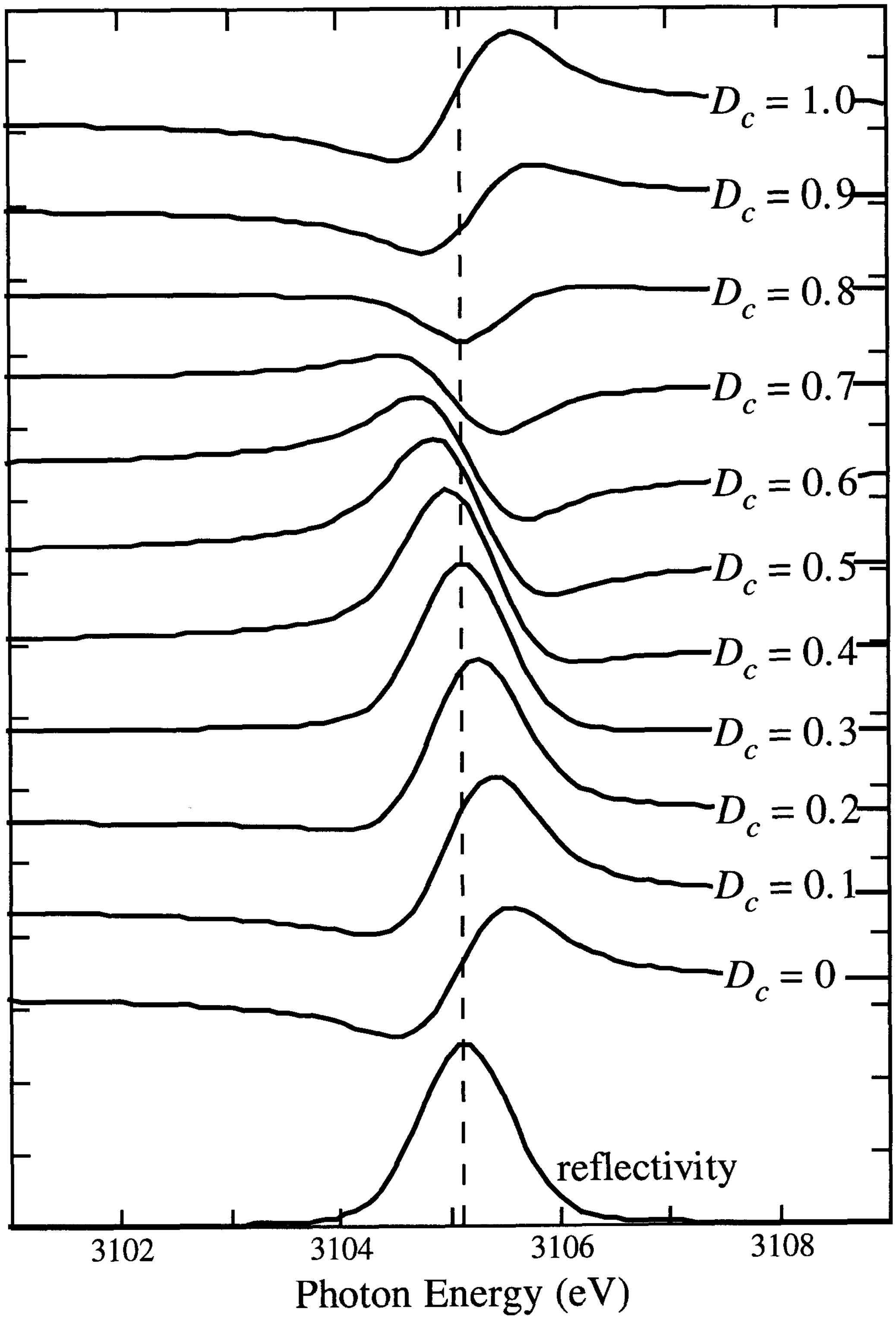

Figure 1.9. Calculated XSW spectrum for the (220) reflection of GaAs at 90°. The curves correspond to different values of the coherent distance; the coherent fraction was set to one. The files were broadened with a Gaussian of 0.8 eV FWHM. The bottom curve is the reflectivity. This figure shows that differences of 0.1 in the coherent distance can be resolved just by eye inspection.

Chapter 2. Methodology to Measure the Geometric structure of the Bi Overlayers

The lack of real periodicity of the Bi/GaAs and Bi/GaP systems (see Section 1.2.1) makes impossible their complete structural determination, so a level of simplification has to be chosen. On the other hand, ideal monolayers of the kind discussed in Section 1.2.1 are very simple because there are some restrictions imposed by symmetry. Some of these conditions are expected to be fulfilled only approximately on the more complex systems, in which the symmetry is broken by the presence of the vacancies (see Figs. 1.1 and 1.2). This is precisely the kind of approximations that are considered in Section 2.1 .

Once the problem, or level of simplification, is clearly defined, the next step is to recognize the experiments needed to obtain enough information to solve that problem. This is done in Section 2.2. The formalism used to connect the experimental results to the overlayer structure is discussed in the rest of the chapter.

2.1 Definition of the problem and the two-site approximation

As mentioned earlier, ideal overlayers contain two adatoms per substrate unit cell, one bonded to the cation (type 1) and the other to the anion (type 2). For this analysis, it is convenient to describe the position of the adatoms in terms of a new reference frame defined as follows: the X-axis runs along the $(\bar{1}10)$ direction, the Y-axis along the (001), and the Z-axis along the (110) direction (see Figs. 2.1 and 1.1). In the ideal systems, a complete determination of the geometrical structure of the overlayer requires the knowledge of six parameters, which are the coordinates of each one of the two adatoms. On the other hand, the (1×1) LEED symmetry and the crystal symmetry constrain the displacement along the X direction to be bulk-like; that is, the Bi adatoms have to lie on the $(\bar{1}10)$ atomic planes (see the right side of Fig. 1.3). The problem is thus reduced to finding the Y-Z coordinates of the two adatoms, resulting in four unknowns.

In contrast, the periodicity of the (nonideal) Bi/GaAs and Bi/GaP is much larger, and so is the number of parameters needed to completely determine the geometry of the overlayer. The objective of this work is to obtain information about the coordinates of the Bi adatoms in the Y-Z plane. The X direction, where the periodicity of the interfaces is longer, was not studied. The complexity of the problem would not allow the determination of the Y-Z coordinates for every adatom in the (6×1) unit cell, so an approximation was made in the modeling of the system by assuming that all the Bi atoms for each type have the same coordinates along the (001) and (110) (or Y and Z) directions. This is equivalent to saying that all the Bi atoms on the upper side of the chains—bonded to the anions (dark circles, Figs. 1.1 and 1.2)—have the same (y_1, z_1) coordinates, and all the Bi atoms on the lower side—bonded to the cations (white circles)—have the same (y_2, z_2) coordinates. Because the Bi atoms type 1 (or 2) close to the edge of the chain are not equivalent to those near the center, they do not necessarily have the same coordinates (as they would for ideal overlayers), so the result about the Y and Z coordinates for each kind of Bi should be understood as average values.

In these terms, the objective is to find the (y_1, z_1) and (y_2, z_2) coordinates of the Bi adatoms of type 1 and type 2. Due to the intrinsic and experimental difficulties of the problem, no attempt was made to obtain information about the relaxation in the X direction.

2.2 Reflections needed under the two-site model

Information about the Y-Z plane can be obtained by performing XSW experiments for reflections such that the corresponding crystal vector ($\mathbf{H}$) lies in that plane. This is because the coherent distance and coherent fraction depend only on the atomic coordinates parallel to $\mathbf{H}$ (see Eq. 5.13 and following discussion). The experimental results from such reflections are not affected by the dependence of the adatom distribution on the X direction.

We performed XSW experiments for three different Bragg planes defined by the crystal vectors (220), (111), and $(11\bar{1})$ (see Fig. 2.1). Those planes terminated with Ga are called (111), and those terminated with P are called $(11\bar{1})$. All these crystal vectors lie on the Y-Z plane, so the experimental data is completely independent of the adatom distribution on the X direction.

Under the two-site model described in the last section, these three reflections provide enough information to determine the Y-Z coordinates of the two Bi adatoms (see Section 2.4), and provide a means to check self-consistency (see Eq. 2.8).

2.3 The model for the distribution function

Before providing the model for the distribution function for the systems presented in this thesis, the simple but important case of an incoherent distribution will be discussed. For this case, the distribution function $[f_{\mathrm{H}}(D)]$ is uniform. (It is equal to $1/d_{\mathrm{H}}$ to ensure its normalization to 1, as required by the definition of Eq. 5.13.) An example of adatoms distributed randomly is a cluster, since the position of the adatoms forming a cluster keeps little or no coherence with the crystal (some degree of clustering is observed in similar systems [1]). Another possible source of disorder is the edge of substrate terraces, where the adatoms may be bonded in many different sites.

Some degree of disorder will be assumed for both the Bi/GaAs and Bi/GaP systems. Because all three reflections were performed using the same surface (see Chapter 3), the disorder will be assumed the same for every reflection. We are, then, considering two distinctive positions in the Y-Z plane, plus some degree of disorder. Besides thermal vibrations, the distribution function for reflections with crystal vector lying in this plane can be written:

$$f_{\mathbf{H}}(D) = \frac{(1-\phi)}{d_{\mathbf{H}}} + \frac{\phi}{2}\left[\delta\left(D-D_1^{\mathbf{H}}\right)+\delta\left(D-D_2^{\mathbf{H}}\right)\right] , \qquad (2.1)$$

where ϕ is the order parameter (so $1-\phi$ is the fraction of the adatoms with random positions), and $D_{1,2}^{\mathbf{H}}$ are the coordinates of the two Bi adatoms along the direction of $\mathbf{H}$. This form of the distribution guaranties its normalization to one, an equal population in sites 1 and 2, and a random part with density $(1-\phi)/d_{\mathbf{H}}$. The formalism of Eq. 2.1 is very convenient because it clearly defines the model that is being used. The $D_{1,2}^{\mathbf{H}}$ distances are not independent of each other because they have to triangulate properly (see Fig. 2.1).

The model of Eq. 2.1 has a large degree of generality; all the structures considered in tight-binding total-energy calculations (TBTE) on similar systems [2] correspond to the class represented by Eq. 2.1.

2.4 Structure determination under the two-site approximation

Now that the distribution function has been written in terms of the coordinates of the adatoms (Eq. 2.1), we can use Eq. 1.4 to relate the experimental values of the coherent distance and coherent fraction to the overlayer structure. When thermal vibrations are taken into account, the relations are as follows [3]:

$$D_c^{\mathbf{H}} = \frac{D_1^{\mathbf{H}}+D_2^{\mathbf{H}}}{2} , \qquad (2.2)$$

$$f_c^{\mathbf{H}} = e^{-M}\,\phi\,\cos\left(\pi\,\frac{D_1^{\mathbf{H}} - D_2^{\mathbf{H}}}{d_{\mathbf{H}}}\right), \tag{2.3}$$

where e^{-M} is the Debye-Waller factor [4], which accounts for the thermal vibrations. This factor appears because the evaluation of the coherent fraction involves exactly the same sum of phases that is used to calculate the scattering strength of X-rays [4].

When the origin is set between the ideal projected bulk positions, as illustrated in Fig. 2.1, Eqs. 2.2 and 2.3 read as follows:

$$D_c^{[220]} = \frac{1}{2}\left(z_1 + z_2\right), \tag{2.4.a}$$

$$D_c^{[111]} = \frac{1}{\sqrt{6}}\left(z_1 + z_2\right) + \frac{1}{2\sqrt{3}}\left(y_1 + y_2\right), \tag{2.4.b}$$

$$D_c^{[11\bar{1}]} = \frac{1}{\sqrt{6}}\left(z_1 + z_2\right) - \frac{1}{2\sqrt{3}}\left(y_1 + y_2\right), \tag{2.4.c}$$

and

$$f_c^{[220]} = e^{-M}\,\phi\cos\pi\,\frac{\sqrt{8}}{a}\left(z_1 - z_2\right), \tag{2.5.a}$$

$$f_c^{[111]} = e^{-M}\,\phi\cos\pi\left(\frac{\sqrt{2}}{a}\left(z_1 - z_2\right) + \frac{1}{a}\left(y_1 - y_2\right)\right), \tag{2.5.b}$$

$$f_c^{[11\bar{1}]} = e^{-M}\,\phi\,\cos\pi\left(\frac{\sqrt{2}}{a}\left(z_1 - z_2\right) - \frac{1}{a}\left(y_1 - y_2\right)\right), \tag{2.5.c}$$

where $\left(y_{1,2},\, z_{1,2}\right)$ are the coordinates of Bi of type 1 and 2 in the Y-Z plane. Solving for $z_1 + z_2$ and $y_1 + y_2$ is very direct from Eqs. 2.4. On the other hand, ϕ, $z_1 - z_2$, and $y_1 - y_2$ have to be found numerically from Eqs. 2.5.

Equations. 2.4 and 2.5 form a complete system from which the geometrical structure of the overlayer can be extracted.

2.5 Experimental estimation of the Debye-Waller factor

There is not much information in the literature about the value of this factor for surface atoms or overlayers, but, in any case, the bulk value should provide a good estimate for temperatures well below the melting and sublimation point. The bulk Debye-Waller factor can be experimentally determined from the standing wave signal from bulk crystal atoms.

One possible method of estimating e^{-M} is to use the total yield, which is the integrated photoemission yield, including secondary electrons and the low energy tail, and is overwhelmingly of bulk nature. The most direct way is to use the (220) reflection. The (220) planes are nonpolar, so the position of the bulk cation and anion atoms is the same relative to those planes. The distribution function of bulk atoms is, then, a delta function around its equilibrium position modified by thermal vibrations. The analog of Eq. 2.3 for this case is simply

$$f_c^{\mathbf{H}} = e^{-M} , \qquad \text{(bulk sensitive data)} . \tag{2.6}$$

Then the Debye-Waller factor for the (220) reflection is directly obtained from the coherent fraction of total yield (220) XSW data. By the use of this method, the values for e^{-M} are found to be indistinguishable from one. Because M goes as the square of $\mathbf{H}$, the Debye-Waller factor for the (111) (and $(11\bar{1})$) reflections is related to that of the (220) reflection as follows:

$$e^{-M}\Big|_{(111)} = \left(e^{-M}\Big|_{(220)}\right)^{3/8} . \tag{2.7}$$

Then, if e^{-M} is indistinguishable from one for the (220) reflection, it also is for the (111) and $(11\bar{1})$ reflections. The estimation of e^{-M} by other methods also produced a value of 1 within the experimental error.

Furthermore, the structural results would have been independent of the Debye-Waller factor, had the relation of Eq. 2.7 been linear (e^{-M} would be incorporated into ϕ in Eqs. 2.5).

2.6 Consistency checks for the two-site model

The method employed to obtain the structure has an intrinsic way to check the validity of approximating the Y-Z structure to two sites. The number of parameters to determine under the two-site model is five: the Y and Z coordinates of both site and the order parameter. On the other hand, the number of parameters determined experimentally was six (the coherent distance and the coherent fraction of each of the (220), (111), and

$(11\bar{1})$ reflections), resulting in six equations (Eqs. 2.4 and 2.5). The over-determination of the system imposes the following relation:

$$D_c^{[220]} = \sqrt{\frac{3}{8}} \left(D_c^{[111]} + D_c^{[11\bar{1}]} \right) , \qquad (2.8)$$

which is obtained by adding Eqs. 2.4.b and 2.4.c, and comparing with Eq. 2.4.a. Because $D_c^{[220]}$, $D_c^{[111]}$, and $D_c^{[11\bar{1}]}$ are obtained experimentally, Eq. 2.8 constitutes a consistency check for the two-site approximation.

Equation 2.8 can be seen as a simple triangulation of distances from different planes. This is because, under the two-site model, the coherent distances D_c^{H} are simple arithmetic averages of the actual distances D_1^{H} and D_2^{H} (see Eq. 2.2), so simple triangulation relation also hold for the coherent distances $D_c^{[220]}$, $D_c^{[111]}$, and $D_c^{[11\bar{1}]}$.

Extrinsic checks of the validity of the model is provided by, for example, the results for the Bi-Bi bond length, which is expected to be close to the sum of covalent radii, which has been proven valid for Sb on GaP [3], Sb on Ge [5], and Sb on Si [5].

References

1. T. Kendelewicz, J.C. Woicik, K.E. Miyano, A. Herrera-Gómez, P.L. Cowan, B.A. Karlin, C.E. Bouldin, P. Pianetta, and W.E. Spicer. "X-ray standing-wave study of monolayers of Sb on GaAs(110)." Physical Review B **46**, p. 7276 (1992).

2. J.P. LaFemina, C.B. Duke, and C. Mailhiot. "New surface atomic structures for column V overlayers on the (110) surfaces of III-V compound semiconductors." Journal of Vacuum Science & Technology B **8**, p. 888 (1990).

3. K.E. Miyano, T. Kendelewicz, J.C. Woicik, P.L. Cowan, C.E. Bouldin, B.A. Karlin, P. Pianetta, and W.E. Spicer. "Structural characterization of the (1 monolayer Sb)/GaP(110) interface using X-ray standing waves." Physical Review B **46**, No. 11, p. 6869 (1992).

4. R.W. James, "The Optical Principles of the Diffraction of X-Rays," Ox Bow Press, Woodbridge, Connecticut (1947).

5. T. Kendelewicz, J.C. Woicik, K.E. Miyano, A. Herrera-Gomez, P.L. Cowan, P. Pianetta, and W.E. Spicer. "Structure of Sb monolayers on Ge(111) 2×1:

a combined study using core-level photoemission, X-ray standing waves, and surface extended X-ray absorption fine structure." Journal of Vacuum Science & Technology B **11**, p. 1449-54 (1993); J.C. Woicik, T. Kendelewicz, K.E. Miyano, P.L. Cowan, C.E. Bouldin, B.A. Karlin, P. Pianetta, and W.E. Spicer. "Determination of the Sb/Si(111) interfacial structure by back-reflection X-ray standing waves and surface extended X-ray-absorption fine structure." Physical Review B **44**, p. 3475-8 (1991).

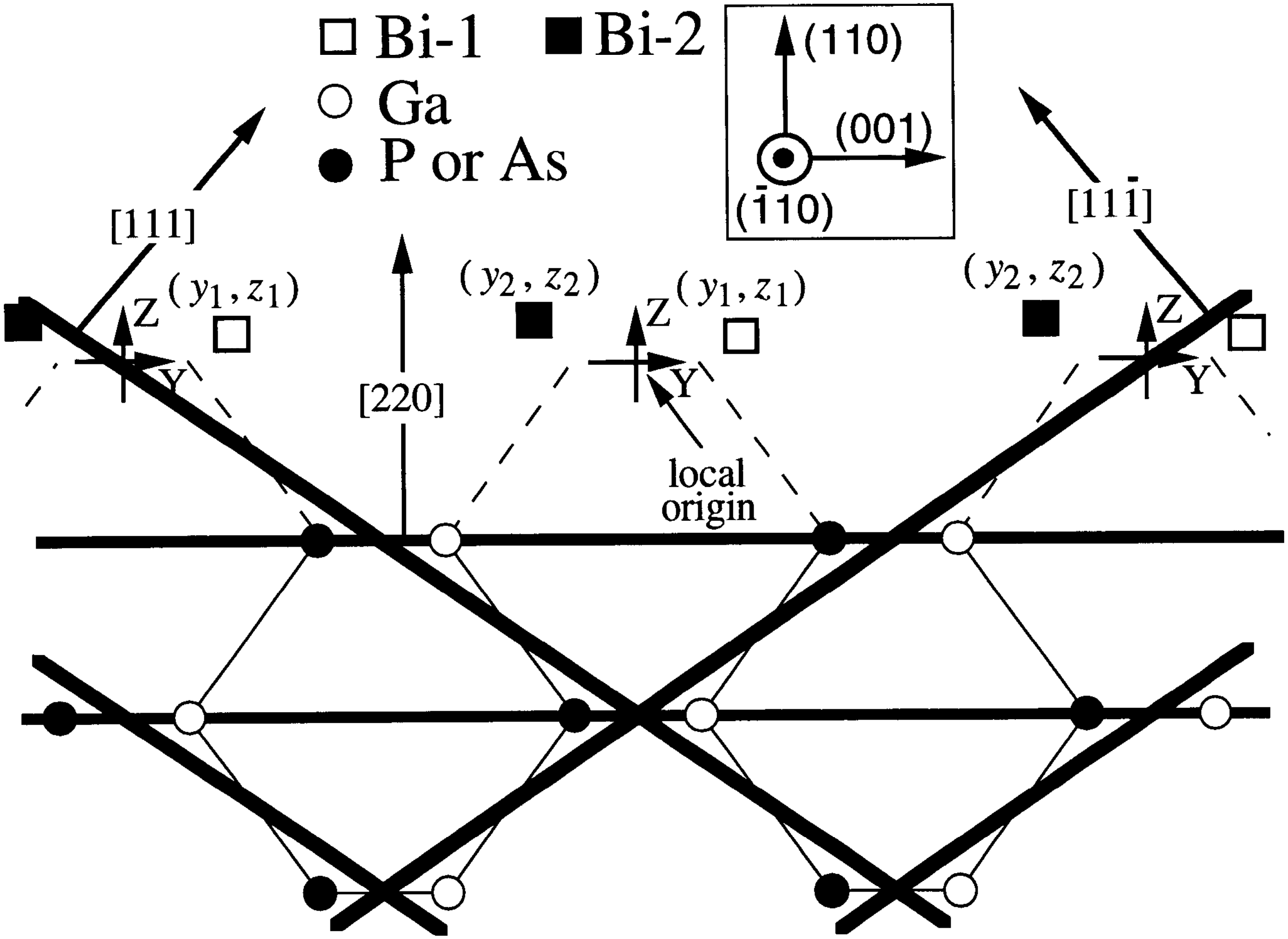

Figure 2.1. All (220), (111), and (11$\bar{1}$) reflections lie on the Y-Z plane defined in this figure. The origin is local to each unit cell.

Chapter 3. Experimental Configurations Used to Study the Bi Overlayer Structures

One underlying assumption of the last chapter, specifically of Eq. 2.1, is that the order parameter is the same for the different reflections. As mentioned, it was possible to make this simplification because the set of the three reflections was done, one at a time, on the same sample and for each one of the two systems (Bi/GaAs and Bi/GaP). This section describes the experimental configuration developed to allow performing all the reflections on the same sample.

3.1 Elements in the XSW experiments

As mentioned in the introduction, the XSW data were obtained by recording the photoemission yield from a core level of the element of interest with a energy discriminator CMA detector. Recorded simultaneously, but independently, were the reflectivity (which was recorded with a grid) and the total photoemission yield (which was recorded by measuring the total current leaving the sample). This is illustrated in Fig. 3.1. The reflectivity and total yield provide fiducial information on the energy calibration, energy resolution, and properties of the incident X-ray beam. As described in Chapter 5, this information is used heavily for the analysis of the XSW data.

3.2 Experiment Details

The experiments were performed on the X-24A beam line at the National Synchrotron Light Source (NSLS). Tuning of the beam photon energy was done by a double-crystal Si (111) monochromator. The Bi XSW data were recorded by monitoring the photoemission yield from the Bi $4d_{5/2}$ core level as the beam energy was swept around the corresponding Bragg condition. We also simultaneously, and independently, recorded the reflectivity (R) and total photoemission yield (TY). The TY is recorded by monitoring the current leaving the sample, which is connected to an electrical feedthrough.

The ultrahigh vacuum (UHV) system had base pressures in the low 10^{-10} Torr range. The chamber manipulator had three lineal and one angular degrees of freedom. The XSW spectra from Bi were obtained by recording photoemission yield with an angle integrated Cylindrical Mirror Analyzer (CMA). Since the Bi photoemission peak rides on the top of a background of inelastic electrons, the spectra from the background were also recorded, and subtracted from the elastic signal (see Section 6.2). The surface was prepared by cleaving an outgassed GaAs (GaP) crystal along the (110) face, followed by evaporation of approximately one monolayer of Bi, as measured by a quartz crystal oscillator. All the cleaves were mirror-like. The samples were next annealed at 325°C for 10 minutes to desorb any Bi in excess of one monolayer [1] and to enhance the interfacial order. Note that in the STM [2] experiments, the samples were not annealed, so we can expect much less clustering in our samples than that shown by the STM images; this is because annealing removes column V adatoms in excess of a monolayer [1].

3.3 Experimental configurations

The orientation of the sample with respect to the incoming beam and CMA was the same for every reflection. The experimental setup, including important elements of the monochromator and the position of the CMA detector, is depicted in Fig. 3.2. Figure 3.3 shows the configuration used for each reflection; that is, it shows the orientation of the sample, Bragg planes, and incident and reflected beams.

Performing the experiments in a nondispersive configuration as described in Chapter 8, which is very convenient for resolution [3], was out of the question because of the presence of the focusing mirror after the monochromator (see Fig. 3.2). Besides, it is not possible to perform all three reflections nondispersively using the same set of monochromator crystals, and changing monochromator crystals would prevent the use of the same surface for all three reflections due to the large changeover time and the sample finite life in vacuum. This section describes the configuration used for the different reflections.

3.3.1 The back-reflection configuration for the (220) experiment

The (220) reflection XSW experiment was performed in the back-reflection mode [4]. In this mode, the Bragg planes under study are perpendicular to the incoming X-ray beam, so the beam is back-reflected, and the reflectivity is recorded by the I_0 monitor (see Fig. 3.2), and appears on the top of the signal from the incident flux.

Figure 3.4 shows a Du Mond diagram corresponding to the back-reflection mode. The phase of the standing wave is constant along the lines within the broad stripe. The shaded rectangle corresponds to the (θ,λ)-zone illuminated by the incoming beam. In the ideal case, where the collimating mirror sends a perfectly parallel white X-ray to the monochromator, the height of the rectangle is equal to the width of the square of the reflectivity of the Si crystals. The focusing mirror sets the angular spread of the beam;

that is, it sets the width of the illuminated zone. This results in a illuminated zone of approximately rectangular shape. The arrows indicate that the experiments are performed by sweeping vertically; that is, by sweeping the nominal photon energy at a constant nominal angle.

It can be seen in Fig. 3.4 that the large angular dispersion introduced by the focusing mirror has only a small effect on the phase resolution. The phase resolution is ultimately what sets the experimental resolution. This is the property that makes advantageous the use of the back-reflection configuration.

3.3.2 The asymmetric-reflection configuration for the (111) and $(11\bar{1})$ experiments

Performing the (111) and $(11\bar{1})$ experiments in the back-reflection mode has many disadvantages, the most important being that it requires a change of crystals in the monochromator (for example, to InSb crystals) because the energy of the (111) and $(11\bar{1})$ back reflection is too low for the Si crystals—and, as mentioned, changing monochromator crystals would not allow the use of the same surface for the set of the three reflections. In fact, there would also not be an increase in resolution in the back-reflection configuration because the reflectivity from InSb crystals have a larger intrinsic width than the reflectivity from Si.

By performing the (111) and $(11\bar{1})$ XSW experiments in an asymmetric configuration (see Fig. 3.3), it was possible to use the same sample orientation as in the (220) reflection (see Fig. 3.2), and it was possible to use the same crystals in the monochromator. This configuration is called “asymmetric” because of the different angles made by the incoming and reflected beams with respect to the substrate surface (see Fig. 3.3).

Figure 3.5 shows a Du Mond diagram corresponding to the asymmetric reflection. The shaded rectangle corresponds to the (θ,λ)-zone illuminated by the incoming beam. The angular dispersion of the beam was reduced because the beam was intentionally unfocused. A comparison can be made with Fig. 8.2, which shows a Du Mond diagram for the case where there is no focusing mirror between the monochromator crystals and the sample, resembling a nondispersive configuration.

A general XSW expression, applicable to this nonsymmetric configuration, is derived in Appendix 1. An equivalent expression was later found in the literature.

3.4 The multireflection problem of the (220) back reflection configuration

When the (220) experiment is performed in the back-reflection configuration, the (200) and (020) reflections also satisfy the Bragg condition $\lambda = 2d_{\mathrm{H}} \sin \theta_{\mathrm{H}}$, where d_{H} is the interplanar distance and θ_{H} is the angle made by the beam to the Bragg planes. Even though the (200) and (020) interplanar distance is $\sqrt{2}$ times larger than that for the (220) reflection, the product $d_{\mathrm{H}} \sin \theta_{\mathrm{H}}$ stays constant because θ_{H} is 45° for the (200) and (020) reflections and 90° for the (220) reflection. The simultaneous fulfillment of the (220), (200), and (020) Bragg conditions is also illustrated by the Ewald construction of Fig. 3.6. A complete discussion of the multireflection problem is presented in Chapter 4, which shows the method in which the (220) back-reflection data should be analyzed.

This multireflection problem is important for wafers because the relative intensity of the (220), (200), and (020) reflections is a strong function of the cut angle of the wafer [5]. On the other hand, this experimental configuration has been widely used on cleaved surfaces [6], where no clear experimental observation of multireflections has been made.

In fact, in our case the (200) and (020) reflections can be neglected right away for the following reasons (see Chapter 4): The polarization of synchrotron radiation is in the plane of the synchrotron; then, for the orientation used for our experiments (see Fig. 3.3), the incident beam has a π polarization with respect to the (200) and (020) planes. On the other hand, as shown in Section 4.3.2, the (200) and (020) reflections are not coupled to the incident beam for π polarization. Furthermore, for the GaAs case, the (200) and (020) reflections are weak.

References

1 F. Schaffler, R. Ludeke, A. Taleb-Ibrahimi, G. Hughes, D. Rieger. "The role of order on the interface properties of Sb/GaAs(110)." Journal of Vacuum Science and Technology B **5**, p. 1048 (1987).

2. A.B. McLean, R.M. Feenstra, A. Taleb-Ibrahimi, and R. Ludeke. "Electronic and structural properties of a discommensurate monolayer system: GaAs(110)-(1 × 1) Bi." Physical Review B **39**, p. 12925 (1989); M. Prietsch, A. Samsavar, and R. Ludeke. "Structural and electronic properties of the Bi/GaP(110) interface." Physical Review B **43**, No. 14, p. 11850 (1991).

3. J. Zegenhagen. “Surface structure determination with X-ray standing wave.” Surface Science Reports **18**, 199 (1993) and references therein (see p. 256).

4. D.P. Woodruff, D.L. Seymour, C.F. McConville, C.E. Riley, M.D. Crapper, and N.P. Prince. “A simple X-ray standing wave technique for surface structural determination—theory and an application.” Surface Science **195**, p. 237 (1988).

5. G. Materlik. Private communication

6. T. Kendelewicz, J.C. Woicik, K.E. Miyano, A. Herrera-Gómez, P.L. Cowan, B.A. Karlin, C.E. Bouldin, P. Pianetta, and W.E. Spicer. “X-ray standing-wave study of monolayers of Sb on GaAs(110).” Physical Review B **46**, p. 7276 (1992); J.C. Woicik, T. Kendelewicz, K.E. Miyano, P.L. Cowan, C.E. Bouldin, B.A. Karlin, P. Pianetta and W.E. Spicer. “X-ray standing wave determination of the clean InP (110) surface reconstruction.” Physical Review Letters **68**, No. 3, p. 341 (1992); K.E. Miyano, T. Kendelewicz, J.C. Woicik, P.L. Cowan, C.E. Bouldin, B.A. Karlin, P. Pianetta and W.E. Spicer. “Structural characterization of the (1 monolayer Sb)/GaP(110) interface using X-ray standing waves.” Physical Review B **46**, No. 11, p. 6869 (1992).

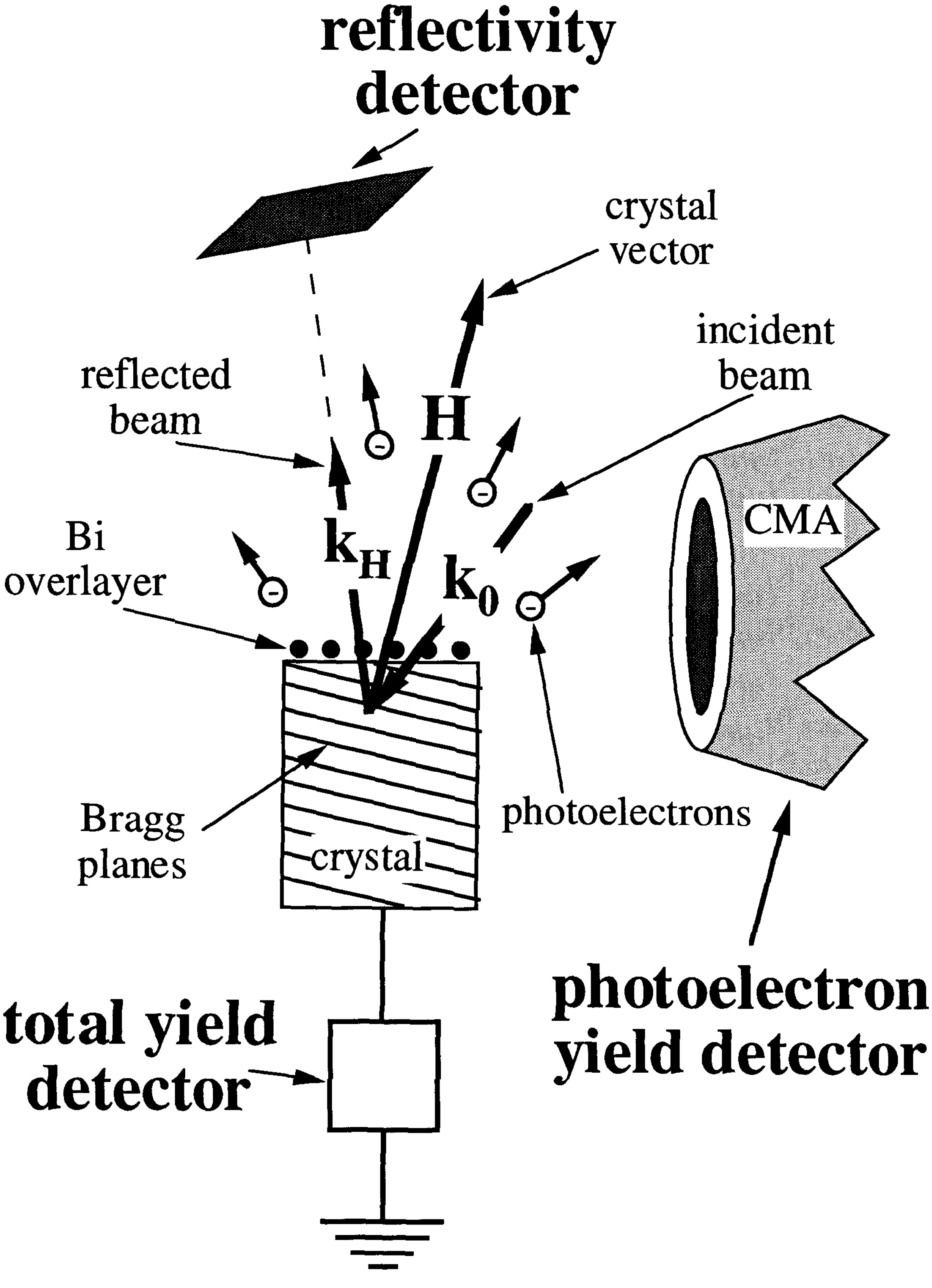

Figure 3.1. Three signals were recorded simultaneously, but independently, in the XSW experiments reported in this work: the Photoelectron Yield, with an energy discriminating CMA detector; the Reflectivity, with a grid; and the Total Photoemission Yield, by measuring the total current leaving the sample.

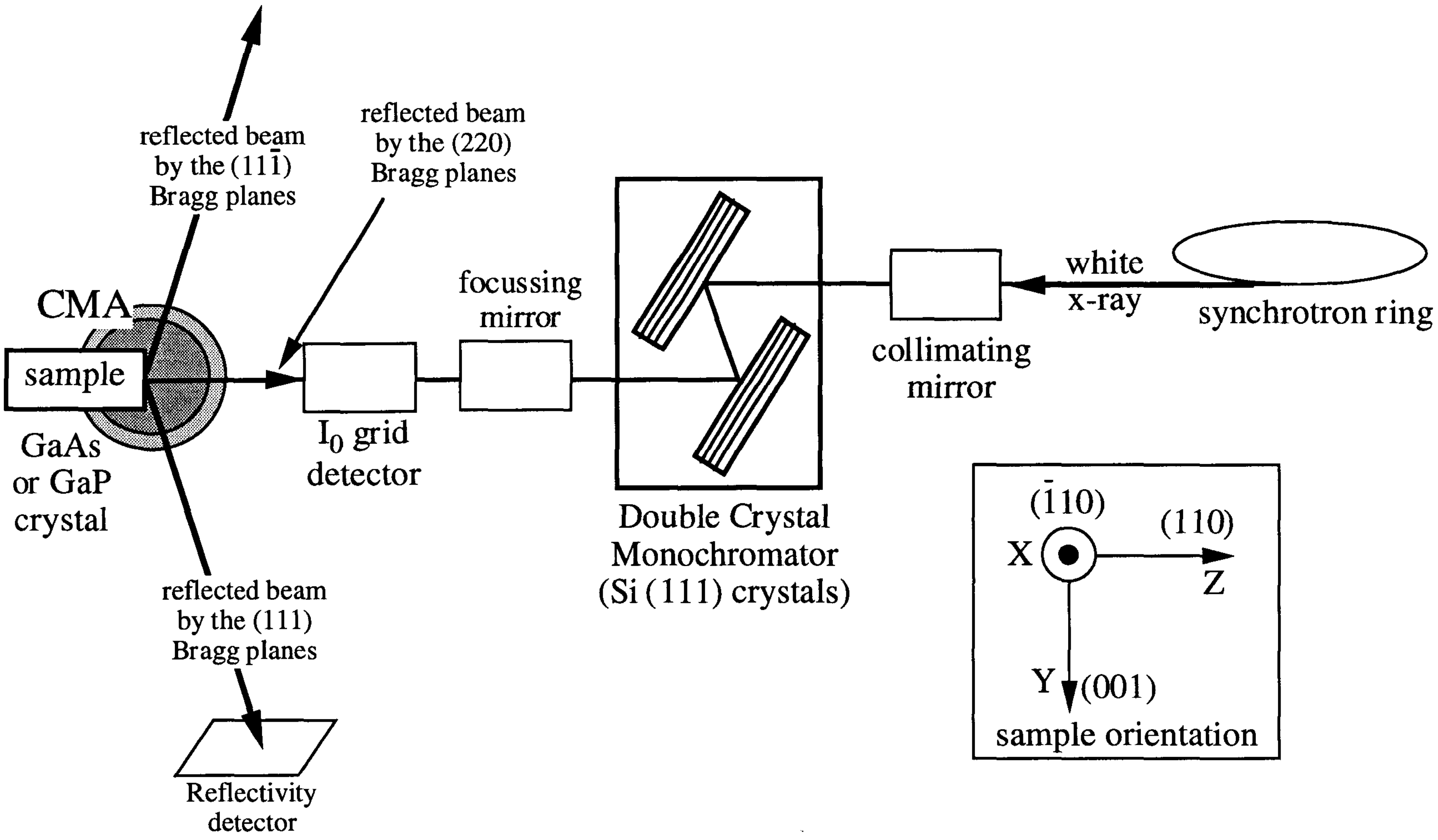

Figure 3.2. Experimental setup for the three reflections

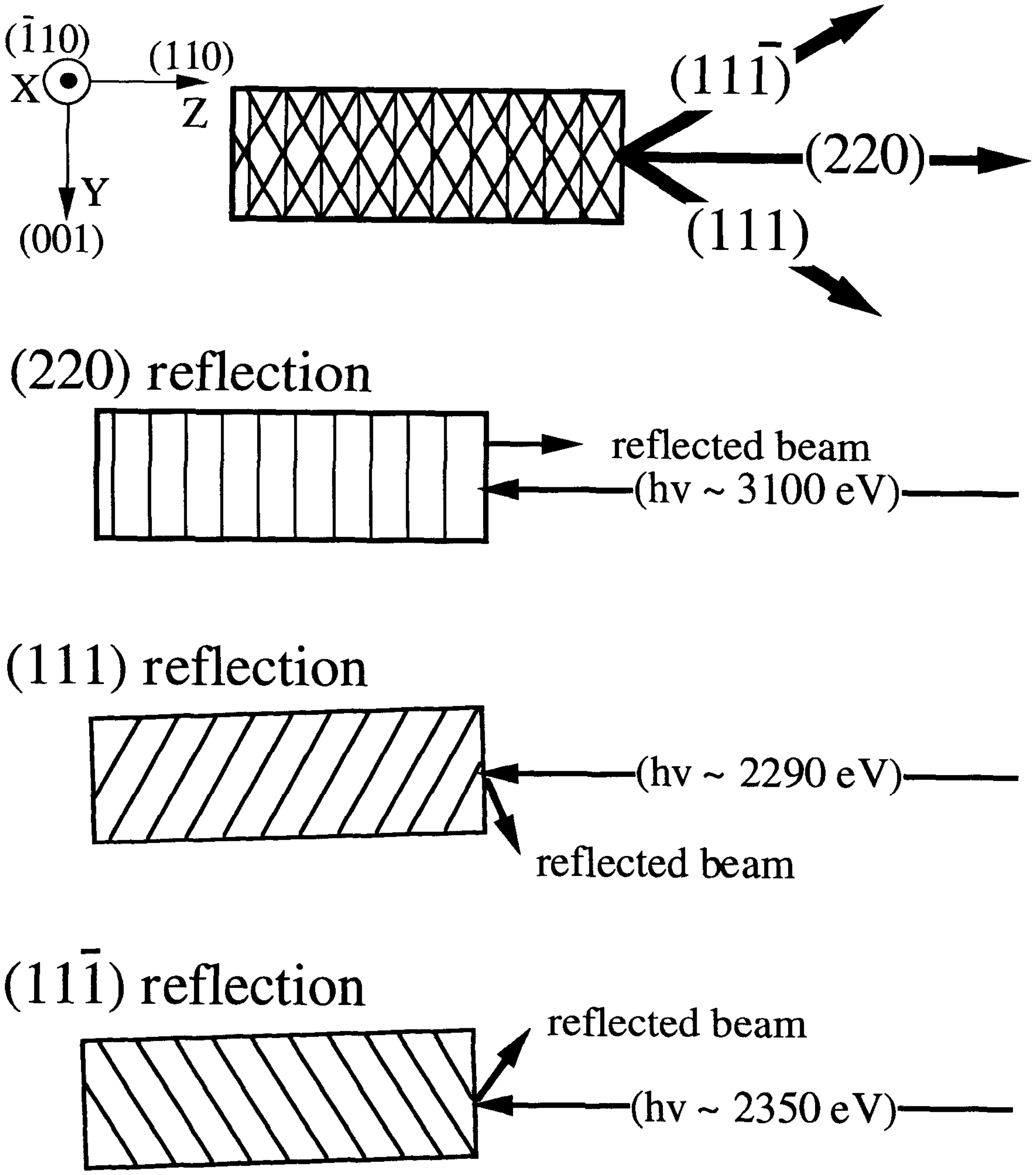

(220) reflection

(111) reflection

(11$\bar{1}$) reflection

Figure 3.3. The three reflections can be performed without moving the sample, just by moving the monochromator to the corresponding energy of each reflection. The (111) and (11$\bar{1}$) reflections do not occur at exactly the same energy because of a small angular tilt. The photon energies correspond to the GaAs experiments.

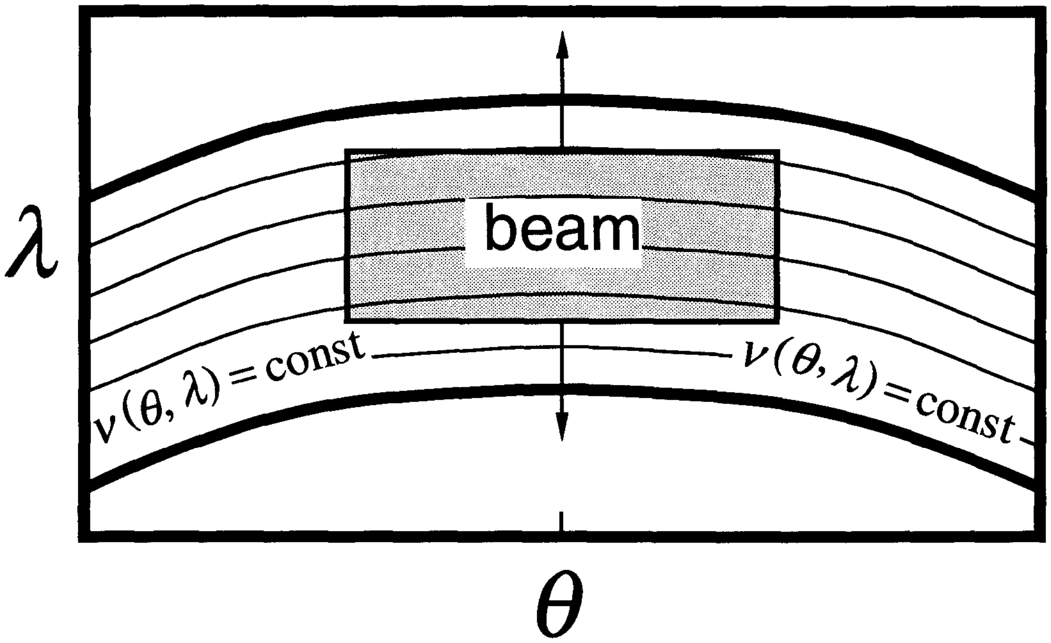

Figure 3.4. Du Mond diagram corresponding to the back-reflection configuration.

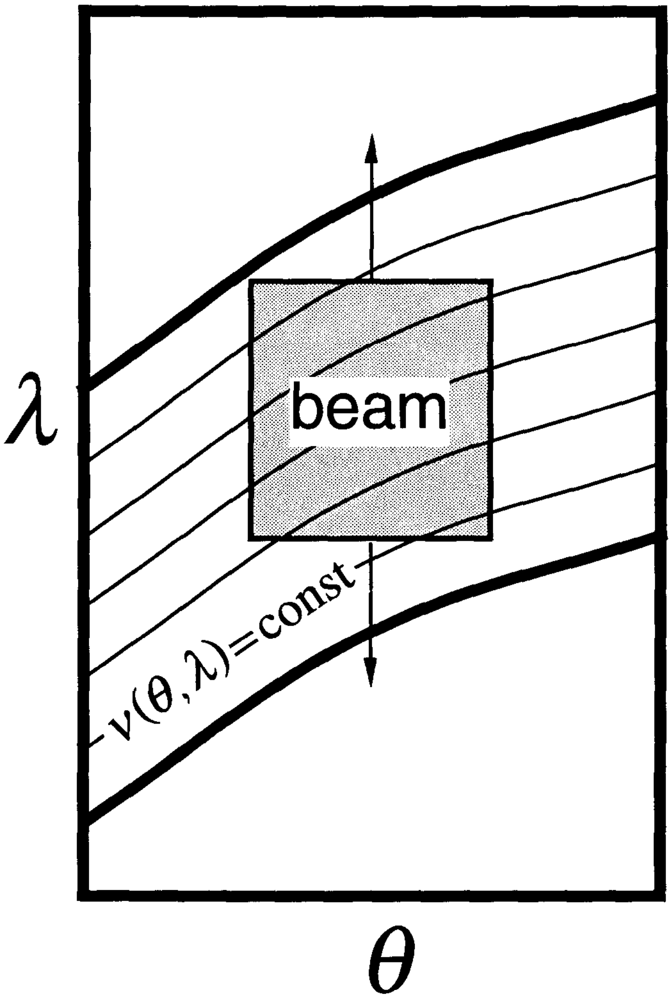

Figure 3.5. Du Mond Diagram corresponding to the asymmetric configuration.

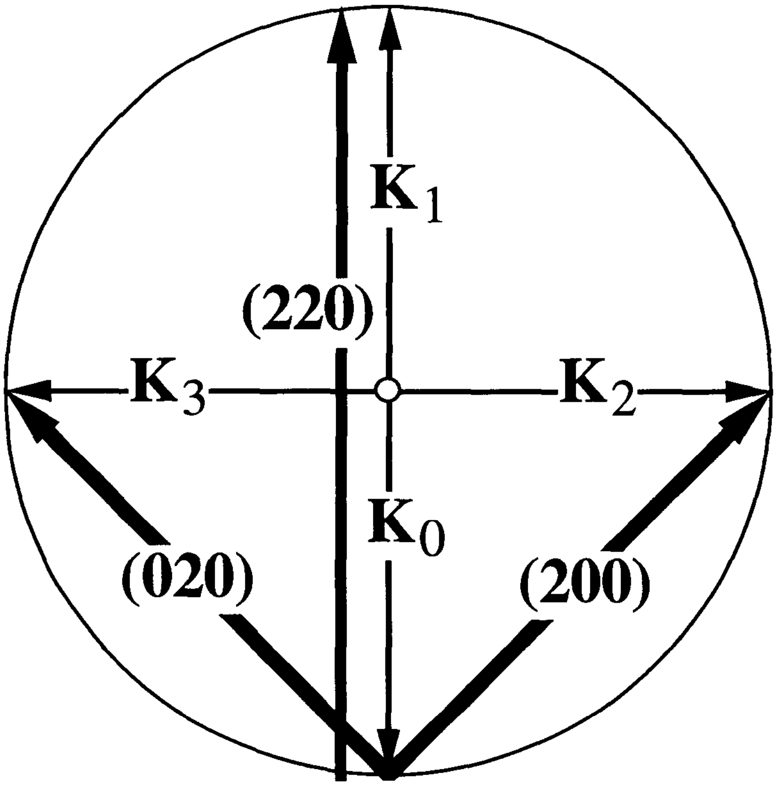

Figure 3.6. Ewald construction showing that the (200) and (020) Bragg conditions are simultaneously satisfied to the (220) Bragg condition in the back-reflection configuration.

Chapter 4. Study of the Multireflection Problem of the (220) Back-Reflection Configuration

4.1 The coupling of four beams

It was mentioned in Section 3.4 that performing the (220) experiment in the back-reflection mode has an intrinsic complication: the (200) and (020) reflections are excited simultaneously to the (220) reflection. The simultaneous fulfillment of the (220), (200), and (020) Bragg conditions is illustrated by the Ewald construction of Fig. 3.6. Illustrated in Fig. 4.1 are the four beams associated with each of the four wave vectors of Fig. 3.6. These four beams are coupled to each other because the beams bounce back and forth from each direction to the other three.

This problem is an important issue for experiments performed in wafers because the relative intensity of the (220), (200), and (020) reflections is a strong function of the cut angle of the wafer [1]. On the other hand, this experimental configuration has been widely used on cleaved surfaces [2], where no clear experimental observation of multireflection has been made.

Presented in this chapter are detailed calculations of the multireflection problem carried out in order to establish the way the (220) experimental data should be analyzed. To this end, it was necessary to develop a form of the wave equation of X-rays in crystals suitable for multireflection calculations. This new form (Eq. 4.12) is basically a simplification of the one existing in the literature [3]. Without the level of simplicity of Eq. 4.12, the multireflection discussion of this chapter would be practically impossible.

The great detail of these calculations may interrupt the flow of reading this thesis. Fortunately, the conclusions of this chapter are very simple, so the reader not interested in equations can skip Sections 4.2 and 4.3 and go directly to the summary in Section 4.4.

4.2 The wave equation of X-rays in crystals

This derivation is an extension and generalization of that presented by Batterman and Cole (B&C) in their 1964 classic paper [3]. The extension consists in showing that the longitudinal term of B&C's Eq. A12 cannot be neglected (as erroneously done by B&C), but has to be retained to correctly account for the polarization. In fact, that term can be nicely combined, leading to a simpler final expression (Eq. 4.12). This expression is the one needed to correctly carry out the multireflection calculations.

Up to Eq. 4.9, this derivation copies many elements from B&C, although it is done in a more general framework consistent with the discussion of Chapter 5. A purely formal advantage of the more general treatment is that the electromagnetic fields are not restrained to have, besides an overall exponential decay, the crystal periodicity (compare B&C's Eq. A1 to Eq. 4.4).

4.2.1 Derivation of the wave equation

The propagation of X-rays in crystals is governed by Maxwell's equations (as mentioned in Section 5.1.1, the calculation of the electric field is carried out classically). We start with the basic Maxwell's equations and a nonlocal in time relationship between the electric displacement and the electric field:

$$\nabla\times\mathbf{E}(\mathbf{r},t) = -\mu_0 \frac{\partial}{\partial t}\,\mathbf{H}(\mathbf{r},t) \quad , \tag{4.1}$$

$$\nabla\times\mathbf{H}(\mathbf{r},t) = \frac{\partial}{\partial t}\,\mathbf{D}(\mathbf{r},t) \;, \tag{4.2}$$

$$\mathbf{D}(\mathbf{r},t) = \int dt'\; \varepsilon(\mathbf{r},t')\;\mathbf{E}(\mathbf{r},t-t') \quad . \tag{4.3}$$

From these three equations, we can solve for the electric field. It will be done in Fourier space, so all the fields are expanded as follows:

$$\mathbf{A}(\mathbf{r},t) = \int d\mathbf{K}\,d\nu\,\mathbf{A}(\mathbf{K},\nu)\;\exp\{-2\pi i\,(\mathbf{K}\cdot\mathbf{r}-\nu\,t)\} \quad . \tag{4.4}$$

The dielectric function has the periodicity of the crystal, and is naturally expanded in terms of the structure factors:

$$\varepsilon(\mathbf{r},\nu) = \varepsilon_0\left(1-\Gamma\sum_{\mathbf{H}} F_{\mathbf{H}}(\nu)\;\exp\{-2\pi i\,\mathbf{H}\cdot\mathbf{r}\}\right) . \tag{4.5}$$

Here, $\mathbf{H}$ is a crystal vector and $F_{\mathbf{H}}$ is the unit cell structure factor on the direction of $\mathbf{H}$ and evaluated at the X-ray frequency. Γ is defined as follows:

$$\Gamma \equiv \frac{e^2}{4\pi\varepsilon_0 mc^2}\,\frac{\lambda^2}{\pi V} \quad ,$$

where $\lambda \equiv 1/k$ is the wave length in vacuum, m and e are the electron mass and charge, ε_0 is the vacuum dielectric constant, and V is the volume of the unit cell.

With these expansions, Eq. 4.1 reads as follows:

$$\begin{aligned} -2\pi i\int d\mathbf{K}d\nu\, \mathbf{K}\times\mathbf{E}(\mathbf{K},\nu)\ \exp\{-2\pi i\,(\mathbf{K}\cdot\mathbf{r}-\nu t)\} \\ = -2\pi i\nu\mu_0\int d\mathbf{K}d\nu\, \mathbf{H}(\mathbf{K},\nu)\ \exp\{-2\pi i\,(\mathbf{K}\cdot\mathbf{r}-\nu t)\}\ . \end{aligned}$$

From the lineal independence of the expansion we have:

$$\mathbf{K}\times\mathbf{E}(\mathbf{K},\nu) = \nu\mu_0\ \mathbf{H}(\mathbf{K},\nu) \quad . \tag{4.6}$$

In the same way, Eq. 4.2 results in:

$$\mathbf{K}\times\mathbf{H}(\mathbf{K},\nu) = -\nu\,\mathbf{D}(\mathbf{K},\nu) \quad . \tag{4.7}$$

From the convolution of Eq. 4.3, we get:

$$\mathbf{D}(\mathbf{r},\nu) = \varepsilon(\mathbf{r},\nu)\ \mathbf{E}(\mathbf{r},\nu)\ .$$

Expanding $\mathbf{D}(\mathbf{r},\nu)$ and $\mathbf{E}(\mathbf{r},\nu)$ in space, and using expansion 4.5, we get:

$$\begin{aligned} \int d\mathbf{K}\,\mathbf{D}(\mathbf{K},\nu)\exp\{-2\pi i\,\mathbf{K}\cdot\mathbf{r}\} \\ = \varepsilon_0\left(1-\Gamma\ \sum_{\mathbf{H}} F_{\mathbf{H}}(\nu)\exp\left\{-^{-2\pi i\,\mathbf{H}\cdot\mathbf{r}}\right\}\right)\int d\mathbf{K}\,\mathbf{E}(\mathbf{K},\nu)\ \exp\{-2\pi i\,\mathbf{K}\cdot\mathbf{r}\}\ . \end{aligned}$$

This equation can be conveniently simplified by performing the following changes of variable in this order:

$$(1)\quad \mathbf{H}\rightarrow -\mathbf{H}\ , \qquad (2)\quad \mathbf{K}-\mathbf{H}\rightarrow \mathbf{K}'\ , \qquad (3)\quad \mathbf{K}'\rightarrow\mathbf{K}\ .$$

This leads to:

$$\mathbf{D}(\mathbf{K},\nu) = \varepsilon_0\mathbf{E}(\mathbf{K},\nu)-\varepsilon_0\Gamma\sum_{\mathbf{H}} F_{\overline{\mathbf{H}}}(\nu)\,\mathbf{E}(\mathbf{K}+\mathbf{H},\nu) \quad . \tag{4.8}$$

Equations 4.6, 4.7, and 4.8 are the Fourier transform version of Eqs. 4.1, 4.2, and 4.3. To solve for $\mathbf{E}(\mathbf{K},\nu)$, we substitute equations 4.6 and 4.8 into 4.7 as follows:

$$\mathbf{K}\times\frac{1}{\mu_0 \nu}\,\mathbf{K}\times\mathbf{E}(\mathbf{K},\nu) = -\nu\varepsilon_0\left(\mathbf{E}(\mathbf{K},\nu)-\Gamma\sum_{\mathbf{H}} F_{\overline{\mathbf{H}}}(\nu)\,\mathbf{E}(\mathbf{K}+\mathbf{H},\nu)\right) ,$$

but

$$\nu^2\varepsilon_0\mu_0 = \frac{\nu^2}{c^2} \equiv k^2 ,$$

where $k^2 \equiv \mathbf{k}\cdot\mathbf{k}$, and $\mathbf{k}$ is the wave vector in vacuum. After very little algebra, we get:

$$\left[k^2(1-\Gamma F_0)-K^2\right]\mathbf{E}(\mathbf{K})-k^2\Gamma\sum_{\mathbf{H}\neq 0} F_{\overline{\mathbf{H}}}\,\mathbf{E}(\mathbf{K}+\mathbf{H})+\mathbf{K}\cdot\mathbf{E}(\mathbf{K})\,\mathbf{K}=0 , \quad (4.9)$$

where $K^2 \equiv \mathbf{K}\cdot\mathbf{K}$. For the sake of shortness, we have dropped the explicit dependence of the electric fields and structure factors on ν. This equation, which is equivalent to B&C's Eq. A.12, tells us that the radiation mode $(\mathbf{K}_0,\nu)$ is coupled to the radiation mode $(\mathbf{K}_1,\nu)$ only if $\mathbf{K}_1-\mathbf{K}_0$ is a crystal vector.

Up to Eq. 4.9, this derivation has been very similar to the one followed by B&C to get his equation A12. We extend the analysis by noticing that Eq. 4.9 can be nicely simplified. By dot multiplying Eq. 4.8 by $\mathbf{K}$ we get:

$$\mathbf{K}\cdot\mathbf{D}(\mathbf{K}) = \varepsilon_0\mathbf{K}\cdot\mathbf{E}(\mathbf{K})-\varepsilon_0\Gamma\sum_{\mathbf{H}} F_{\overline{\mathbf{H}}}\,\mathbf{K}\cdot\mathbf{E}(\mathbf{K}+\mathbf{H}) ,$$

but from Eq. 4.7, the first member is equal to zero, so we can write:

$$\mathbf{K}\cdot\mathbf{E}(\mathbf{K}) = \frac{\Gamma}{1-\Gamma F_0}\sum_{\mathbf{H}} F_{\overline{\mathbf{H}}}\,\mathbf{K}\cdot\mathbf{E}(\mathbf{K}+\mathbf{H}) .$$

Substituting into Eq. 4.9 we get:

$$\left[k^2(1-\Gamma F_0)-K^2\right]\mathbf{E}(\mathbf{K})$$
$$-k^2\Gamma\sum_{\mathbf{H}\neq 0} F_{\overline{\mathbf{H}}}\left[\mathbf{E}(\mathbf{K}+\mathbf{H}) - \frac{1}{k^2(1-\Gamma F_0)}\,\mathbf{K}\cdot\mathbf{E}(\mathbf{K}+\mathbf{H})\,\mathbf{K}\right]=0 . \quad (4.10)$$

The expression in the braket of the second term can be written:

$$\mathbf{E}(\mathbf{K}+\mathbf{H}) - \frac{K^2}{k^2(1-\Gamma F_0)}\ \hat{\mathbf{K}}\cdot\mathbf{E}(\mathbf{K}+\mathbf{H})\ \hat{\mathbf{K}} \tag{4.11}$$

where $\hat{\mathbf{K}}$ is the unitary vector in the direction of $\mathbf{K}$.

The ratio $K^2/k^2(1-\Gamma F_0)$ is very close to one for the following reason: We are interested oi those $\mathbf{K}$s for which $\mathbf{E}(\mathbf{K})$ is appreciable. From Eq. 4.10, $\mathbf{E}(\mathbf{K})$ can be large only if $\left[k^2(1-\Gamma F_0)-K^2\right]$ is of the order of $k^2\Gamma F_{\overline{\mathbf{H}}}$ (which is precisely the Bragg condition discussed in Section 4.2.2); but $\Gamma F_{\overline{\mathbf{H}}}$ is of the order of 10^{-5}.

Expression 4.11 can then be approximated to $\mathbf{E}(\mathbf{K}+\mathbf{H}) - \hat{\mathbf{K}}\cdot\mathbf{E}(\mathbf{K}+\mathbf{H})\ \hat{\mathbf{K}}$, which can be recognized as the component of $\mathbf{E}(\mathbf{K}+\mathbf{H})$ perpendicular to $\mathbf{K}$, and will be denominated $\mathbf{E}_{\perp\mathbf{K}}(\mathbf{K}+\mathbf{H})$. In this way, Eq. 4.10 reduces to:

$$\left[k^2(1-\Gamma F_0)-K^2\right]\mathbf{E}(\mathbf{K}) - k^2\Gamma \sum_{\mathbf{H}\neq 0} F_{\overline{\mathbf{H}}}\ \mathbf{E}_{\perp\mathbf{K}}(\mathbf{K}+\mathbf{H}) = 0 \quad . \tag{4.12}$$

This form of the wave equation of X-rays in crystals is simpler and more general than in the literature [3, 4], and allows for multireflection calculations.

4.2.2 Propagation of X-rays impinging a crystal and the dynamical Bragg condition

Consider the case where the radiation mode $(\mathbf{k}_0, \nu)$ is present in vacuum and impinging a crystal. The question to answer is which radiation modes inside the crystal will be excited.

From the boundary conditions, a radiation mode $(\mathbf{K}_0, \nu)$ is immediately excited with $\mathbf{K}_0 = \mathbf{k}_0 + q\mathbf{n}$, where $\mathbf{n}$ is a unit vector normal to the crystal surface; the constant q is small because the dielectric function of the crystal is very close to the vacuum dielectric function. Because the $\mathbf{E}(\mathbf{K}_0, \nu)$ is coupled to $\mathbf{E}(\mathbf{K}_0 + \mathbf{H}, \nu)$ for every $\mathbf{H}$, all the modes $(\mathbf{K}_0 + \mathbf{H}, \nu)$ for which

$$\left[k_0^2(1-\Gamma F_0) - (\mathbf{K}_0+\mathbf{H})\cdot(\mathbf{K}_0+\mathbf{H})\right] \sim k^2\Gamma F_{\overline{\mathbf{H}}} \tag{4.13}$$

will also be excited (see Eq. 4.12).

It is very important to notice that the condition for excitation of Eq. 4.13 is precisely the dynamical version of the Bragg condition. Say for example that, besides holding for $\mathbf{K} = \mathbf{K}_0$, the excitation condition (Eq. 4.13) holds for $\mathbf{K} = \mathbf{K}_0 + \mathbf{H}_1 \equiv \mathbf{K}_1$. We then have:

$$\left[k_0^2(1 - \Gamma F_0) - \mathbf{K}_0 \cdot \mathbf{K}_0\right] \sim k^2 \Gamma F_{\overline{\mathbf{H}}} \quad , \tag{4.14a}$$

$$\left[k_0^2(1 - \Gamma F_0) - \mathbf{K}_1 \cdot \mathbf{K}_1\right] \sim k^2 \Gamma F_{\overline{\mathbf{H}}} \quad . \tag{4.14b}$$

Again, because $\Gamma F_{\overline{\mathbf{H}}}$ is of the order of 10^{-5}, conditions 4.13 tell us that $\mathbf{K}_0$ and $\mathbf{K}_1$ have the same magnitude within a deviation of 10^{-5}. This means that for the mode $(\mathbf{K}_1, \nu)$ to be excited, $\mathbf{K}_1$ needs to satisfy the Bragg condition (see Eq. 1.2)—although not exactly, it must be within a deviation of 10^{-5}.

4.2.3 Propagation in the case of no Bragg condition met

Even though this case is very simple, it illustrates the methodology to solve more complex cases, such as the one treated in Appendix 1. Consider the case for which

$$\left[k_0^2(1 - \Gamma F_0) - (\mathbf{K}_0 + \mathbf{H}) \cdot (\mathbf{K}_0 + \mathbf{H})\right]$$

is not small for any $\mathbf{H}$ different from zero (in other words, no Bragg condition is met). Then, Eq. 4.12 reads as follows:

$$\left[k_0^2(1 - \Gamma F_0) - K_0^2\right] \mathbf{E}(\mathbf{K}_0) = 0 \quad . \tag{4.15}$$

This equation has a nontrivial solution if

$$\left[k_0^2(1 - \Gamma F_0) - K_0^2\right] = 0 \quad , \tag{4.16}$$

from which we obtain the familiar relation

$$K_0 = n\, k_0$$

where $n = \sqrt{1 - \Gamma F_0}$ is the index of refraction.

4.3 Solution to the wave equation in the multireflection case of the (220) back reflection configuration

4.3.1 The start-up equation

We apply Eq. 4.12 to the case in which the wave vector $\mathbf{k}_0$ of an incident X-ray is near the back-reflection condition of the (220) reflection. As mentioned in Section 4.1, the (200) and (020) reflections have also to be considered. The crystal vectors corresponding to those three reflections are the following:

$$\mathbf{H}_1 = H_1 \frac{1}{\sqrt{2}} (1,1,0) = \frac{\sqrt{8}}{a_L} \frac{1}{\sqrt{2}} (1,1,0) \quad ,$$

$$\mathbf{H}_2 = H_2(1,0,0) = \frac{2}{a_L} (1,0,0) \quad ,$$

$$\mathbf{H}_3 = H_3(0,1,0) = \frac{2}{a_L} (0,1,0) \quad ,$$

where a_L is the lattice constant. Equation 4.12 couples an infinite number of modes; however, as described in Section 4.2.2, only those modes satisfying a dynamical Bragg condition are not neglected. These modes, which are shown in Figs. 3.6 and 4.1, are: $\mathbf{K}_0$, $\mathbf{K}_1 \equiv \mathbf{K}_0 + \mathbf{H}_1$, $\mathbf{K}_2 \equiv \mathbf{K}_0 + \mathbf{H}_2$, and $\mathbf{K}_3 \equiv \mathbf{K}_0 + \mathbf{H}_3$.

Equation 4.12 applied for $\mathbf{K}$ equal to $\mathbf{K}_0$, $\mathbf{K}_1$, $\mathbf{K}_2$, and $\mathbf{K}_3$ results as follows:

$$\begin{aligned}&\left[k_0^2(1-\Gamma F_0)-K_0^2\right]\mathbf{E}(\mathbf{K}_0)\\ &\quad -k_0^2\Gamma\left[F_{\overline{\mathbf{H}}_1}\mathbf{E}_{\perp\mathbf{K}_0}(\mathbf{K}_1)+F_{\overline{\mathbf{H}}_2}\mathbf{E}_{\perp\mathbf{K}_0}(\mathbf{K}_2)+F_{\overline{\mathbf{H}}_3}\mathbf{E}_{\perp\mathbf{K}_0}(\mathbf{K}_3)\right]=0 \ ,\end{aligned} \tag{4.17a}$$

$$\begin{aligned}&\left[k_0^2(1-\Gamma F_0)-K_1^2\right]\mathbf{E}(\mathbf{K}_1)\\ &\quad -k_0^2\Gamma\left[F_{\mathbf{H}_1}\mathbf{E}_{\perp\mathbf{K}_1}(\mathbf{K}_0)+F_{\mathbf{H}_2}\mathbf{E}_{\perp\mathbf{K}_1}(\mathbf{K}_3)+F_{\mathbf{H}_3}\mathbf{E}_{\perp\mathbf{K}_1}(\mathbf{K}_2)\right]=0 \ ,\end{aligned} \tag{4.17b}$$

$$\begin{aligned}&\left[k_0^2(1-\Gamma F_0)-K_2^2\right]\ \mathbf{E}(\mathbf{K}_2)\\ &\quad -k_0^2\Gamma\left[F_{\mathbf{H}_4}\mathbf{E}_{\perp\mathbf{K}_2}(\mathbf{K}_3)+F_{\mathbf{H}_2}\mathbf{E}_{\perp\mathbf{K}_2}(\mathbf{K}_0)+F_{\overline{\mathbf{H}}_3}\mathbf{E}_{\perp\mathbf{K}_2}(\mathbf{K}_1)\right]=0 \ ,\end{aligned} \tag{4.17c}$$

$$\left[k_0^2(1-\Gamma F_0)-K_3^2\right]\mathbf{E}(\mathbf{K}_3)$$
$$-k_0^2\Gamma\left[F_{\overline{\mathbf{H}}_4}\mathbf{E}_{\perp\mathbf{K}_3}(\mathbf{K}_2)+F_{\overline{\mathbf{H}}_2}\mathbf{E}_{\perp\mathbf{K}_3}(\mathbf{K}_1)+F_{\mathbf{H}_3}\mathbf{E}_{\perp\mathbf{K}_3}(\mathbf{K}_0)\right]=0\ . \qquad (4.17d)$$

The terms included in the series are those for which $\mathbf{H}$ is such that $\mathbf{K}+\mathbf{H}$ is either $\mathbf{K}_0$, $\mathbf{K}_1$, $\mathbf{K}_2$, or $\mathbf{K}_3$. The crystal vectors that play a role are $\pm\mathbf{H}_1$, $\pm\mathbf{H}_2$, $\pm\mathbf{H}_3$, and $\pm\mathbf{H}_4$, where $\mathbf{H}_4 \equiv \mathbf{H}_2 - \mathbf{H}_3$. The presence of the crystal vector $\mathbf{H}_4$ is due to the reflection from $\mathbf{K}_2$ to $\mathbf{K}_3$ by the $(\bar{2}20)$ Bragg planes.

The polarization of the incident beam is either σ or π, and each case is considered separately. The simplest case is for the π polarization because the incident beam is not reflected by the (200) and (020) planes.

4.3.2 The π polarization

This is the simplest case because many of the terms can be neglected. For example, $\mathbf{E}_{\perp\mathbf{K}_0}(\mathbf{K}_2) \approx \mathbf{0}$ because $\mathbf{E}(\mathbf{K}_2)$ is almost parallel to $\mathbf{K}_0$ For this reason, the $\mathbf{K}_2$ and $\mathbf{K}_3$ modes are not coupled to the incident radiation $\mathbf{K}_0$. The system is reduced to the following two equations:

$$\left[k_0^2(1-\Gamma F_0)-K_0^2\right]\mathbf{E}(\mathbf{K}_0)-k_0^2\Gamma F_{\overline{\mathbf{H}}_1}\mathbf{E}_{\perp\mathbf{K}_0}(\mathbf{K}_1)=0\ , \qquad (4.18a)$$

$$\left[k_0^2(1-\Gamma F_0)-K_1^2\right]\mathbf{E}(\mathbf{K}_1)-k_0^2\Gamma F_{\mathbf{H}_1}\mathbf{E}_{\perp\mathbf{K}_1}(\mathbf{K}_0)=0\ . \qquad (4.18b)$$

This system is identical to the one solved in Appendix 1. The back-reflection configuration is just a particular case of the general solution presented in Appendix 1.

4.3.3 The σ polarization

4.3.3.1 The calculation method

For the σ polarization, $\mathbf{E}_{\perp\mathbf{K}_i}\left(\mathbf{K}_j\right) \approx \mathbf{E}\left(\mathbf{K}_j\right)$, so none of the terms of Eqs. 4.17 vanish. Equations. 4.17 can be slightly simplified because only three of the structure factors are different:

$$F_{\mathbf{H}_1} = F_{\overline{\mathbf{H}}_1} = F_{\mathbf{H}_4} = F_{\overline{\mathbf{H}}_4}\ \ (\equiv F_1)\ ,$$

$$F_{\mathbf{H}_2} = F_{\overline{\mathbf{H}}_2} = F_{\mathbf{H}_3} = F_{\overline{\mathbf{H}}_3}\ \ (\equiv F_2)\ .$$

It is convenient to express Eqs. 4.17 in matrix notation:

$$\begin{pmatrix} \Psi_0 & k_0^2\Gamma F_1 & k_0^2\Gamma F_2 & k_0^2\Gamma F_2 \\ k_0^2\Gamma F_1 & \Psi_1 & k_0^2\Gamma F_2 & k_0^2\Gamma F_2 \\ k_0^2\Gamma F_2 & k_0^2\Gamma F_2 & \Psi_2 & k_0^2\Gamma F_1 \\ k_0^2\Gamma F_2 & k_0^2\Gamma F_2 & k_0^2\Gamma F_1 & \Psi_3 \end{pmatrix} \begin{pmatrix} \mathbf{E}(\mathbf{K}_0) \\ \mathbf{E}(\mathbf{K}_1) \\ \mathbf{E}(\mathbf{K}_2) \\ \mathbf{E}(\mathbf{K}_3) \end{pmatrix} = 0 \quad , \tag{4.19}$$

where $\Psi_i \equiv k_0^2(1-\Gamma F_0)-K_i^2$.

To ensure continuity of phase fronts across the surface, the difference between the wave vector of the incident beam in vacuum ($\mathbf{k}_0$), with the wave vector of the beam propagating inside the crystal ($\mathbf{K}_0$), is a vector perpendicular to the surface

$$\mathbf{K}_0 = \mathbf{k}_0 - q\mathbf{n} \quad , \tag{4.20}$$

where $\mathbf{n}$ is a unitary vector normal to the surface. The parameter q is small (relative to $|\mathbf{k}_0|$) because the dielectric function of crystals in the X-ray frequency range differs only slightly from 1; q is found by solving Eq. 4.19.

To be able to consider deviations from the exact back-reflection, the incident vector $\mathbf{k}_0$ is allowed to make an angle (θ_0, ϕ_0) with the surface normal. Here, $\mathbf{k}_0$ can be expressed as follows:

$$\mathbf{k}_0 = -k_0(\cos\theta_0\,\mathbf{n} + \boldsymbol{\delta}) \quad , \tag{4.21}$$

where

$$\boldsymbol{\delta} = \alpha\,\frac{1}{\sqrt{2}}\,(1,-1,0) + \beta(0,0,1) \quad , \tag{4.22}$$

with $\alpha = \sin\theta_0\cos\phi_0$ and $\beta = \sin\theta_0\sin\phi_0$ This representation allows us to easily write every Ψ_i in terms of the parameter q and the angle of the incident beam, as follows:

$$\Psi_0 = K_0^2 - k_0^2(1-\Gamma F_0) \quad , \tag{4.23a}$$

$$\Psi_1 = H_1^2 + K_0^2 - 2k_0 H_1\cos\theta_1 - 2qH_1 - k_0^2(1-\Gamma F_0) \quad , \tag{4.23b}$$

$$\Psi_2 = H_2^2 + K_0^2 - 2k_0 H_2\cos\theta_2 - 2qH_2/\sqrt{2} - k_0^2(1-\Gamma F_0) \quad , \tag{4.23c}$$

$$\Psi_2 = H_3^2 + K_0^2 - 2k_0 H_2\cos\theta_3 - 2qH_3/\sqrt{2} - k_0^2(1-\Gamma F_0) \quad , \tag{4.23d}$$

where

$$K_0^2 = k_0^2 + q^2 + 2k_0 q \cos\theta_0 \quad ,$$

$$\theta_1 = \theta_2 \quad ,$$

$$\cos\theta_2 \equiv -\frac{\mathbf{H}_2 \cdot \mathbf{k}_0}{H_2 k_0} = \frac{1}{\sqrt{2}}\left(\cos\theta_0 + \alpha\right) \ ,$$

and

$$\cos\theta_3 \equiv -\frac{\mathbf{H}_3 \cdot \mathbf{k}_0}{H_3 k_0} = \frac{1}{\sqrt{2}}\left(\cos\theta_0 - \alpha\right) \quad .$$

From Eqs. 4.19, it is possible to express the intensities of the reflected beams in terms of the set of Ψ_i's:

$$\frac{\mathbf{E}(\mathbf{K}_1)}{\mathbf{E}(\mathbf{K}_0)} = \frac{\Psi_0 - k_0^2\ \Gamma F_1}{\Psi_1 - k_0^2\ \Gamma F_1} \quad ,$$

$$\frac{E(\mathbf{K}_2)}{E(\mathbf{K}_0)} = \frac{\Psi_0 F_1 - k_0^2 \Gamma F_2^2}{\Psi_2 F_2 - k_0^2 \Gamma F_1 F_2} + \frac{k_0^2 \Gamma F_1^2 - k_0^2 \Gamma F_2^2}{\Psi_2 F_3 - k_0^2 \Gamma F_1^2}\ \frac{E(\mathbf{K}_1)}{E(\mathbf{K}_0)} \quad ,$$

$$\frac{E(\mathbf{K}_3)}{E(\mathbf{K}_0)} = \frac{\Psi_2 - k_0^2 \Gamma F_1}{\Psi_3 - k_0^2 \Gamma F_1}\ \frac{E(\mathbf{K}_2)}{E(\mathbf{K}_0)} \quad .$$

A nontrivial solution of Eq. 4.19 requires the determinant of the 4×4 matrix to be zero.

$$\det\begin{pmatrix} \Psi_0 & k_0^2\Gamma F_1 & k_0^2\Gamma F_2 & k_0^2\Gamma F_2 \\ k_0^2\Gamma F_1 & \Psi_1 & k_0^2\Gamma F_2 & k_0^2\Gamma F_2 \\ k_0^2\Gamma F_2 & k_0^2\Gamma F_2 & \Psi_2 & k_0^2\Gamma F_1 \\ k_0^2\Gamma F_2 & k_0^2\Gamma F_2 & k_0^2\Gamma F_1 & \Psi_3 \end{pmatrix} = 0 \quad . \tag{4.24}$$

This constitutes an eighth-order equation for q. Here we make a point that the order of the equation is two times the number of waves. This is in contrast with the normal XSW case, which considers two waves but the equation to solve is quadratic (see Eq. A1.23). The reason for that is that the orientation of the back-reflection configuration does not allow some of the approximations used in Appendix 1. For example, parameter a of Eq. A1.24 would be zero for the (200) and (020) reflections.

The physical solution for q has to hold for each of the following conditions:

(1) It must ensure that the beam becomes extinct as it penetrates the crystal; the imaginary part of q has to be negative.

(2) The sum of the intensities of the reflected beams does not exceed the intensity of the incoming beam.

(3) The parameter q should be small, in the sense that the magnitude of the wave vector of the incoming beam in vacuum does not change too much as it enters the crystal; that is, K_0/k_0 should be of the order of 1.

These conditions allow us to discriminate the solution among the eight roots of Eq. 4.24.

The calculations were performed numerically. The computer program, which was written using MATHEMATICA, is provided in Appendix 2.

4.3.3.2 Results for the σ polarization case

Calculations were carried out for a range of angles around the exact back-reflection configuration, and for many atomic positions, and were compared to calculations where the (200) and (020) reflections are ignored. In all cases, the shape and intensity of the exactly calculated XSW spectrum were indistinguishable from those where the (200) and (020) reflections were ignored. The reason for this is that the intensity of the beams reflected by the (200) and (020) planes is relatively very small.

4.4 Conclusions of the multireflection study

The XSW theory is built under the assumption that only one Bragg condition is satisfied. A problem arises when the (220) reflection is performed in a back-reflection configuration because, for this particular orientation, the (200) and (020) Bragg conditions are also satisfied. Because the incident beam is reflected back and forth by the three sets of Bragg planes, the four waves of Fig. 4.1 are intrinsically coupled.

This problem is treated using Maxwell's equations. The results indicate that the intensity of the beam associated with the wave vectors $\mathbf{K}_2$ and $\mathbf{K}_3$ of Fig. 4.1 is zero for the π polarization, and neglectable for the σ polarization. Analysis of the XSW data obtained under this configuration can be performed as if only the (220) Bragg condition were satisfied.

References

1 G. Materlik. Private communication

2 T. Kendelewicz, J.C. Woicik, K.E. Miyano, A. Herrera-Gómez, P.L. Cowan, B.A. Karlin, C.E. Bouldin, P. Pianetta, and W.E. Spicer. "X-ray standing-wave study of monolayers of Sb on GaAs(110)." Physical Review B **46**, p. 7276 (1992); J.C. Woicik, T. Kendelewicz, K.E. Miyano, P.L. Cowan, C.E. Bouldin, B.A. Karlin, P. Pianetta and W.E. Spicer. "X-ray standing wave determination of the clean InP (110) surface reconstruction." Physical Review Letters **68**, No. 3, p. 341 (1992); K.E. Miyano, T. Kendelewicz, J.C. Woicik, P.L. Cowan, C.E. Bouldin, B.A. Karlin, P. Pianetta and W.E. Spicer. "Structural characterization of the (1 monolayer Sb)/GaP(110) interface using X-ray standing waves." Physical Review B **46**, No. 11, p. 6869 (1992).

3 B.W. Batterman and H. Cole. "Dynamical diffraction of X-rays by perfect crystals." Review of Modern Physics **36**, No. 3, p. 681 (1964).

4 C. Kittel, "Introduction to Solid State Physics," John Wiley & Sons, Inc., Fourth edition. New York, New York (1971).

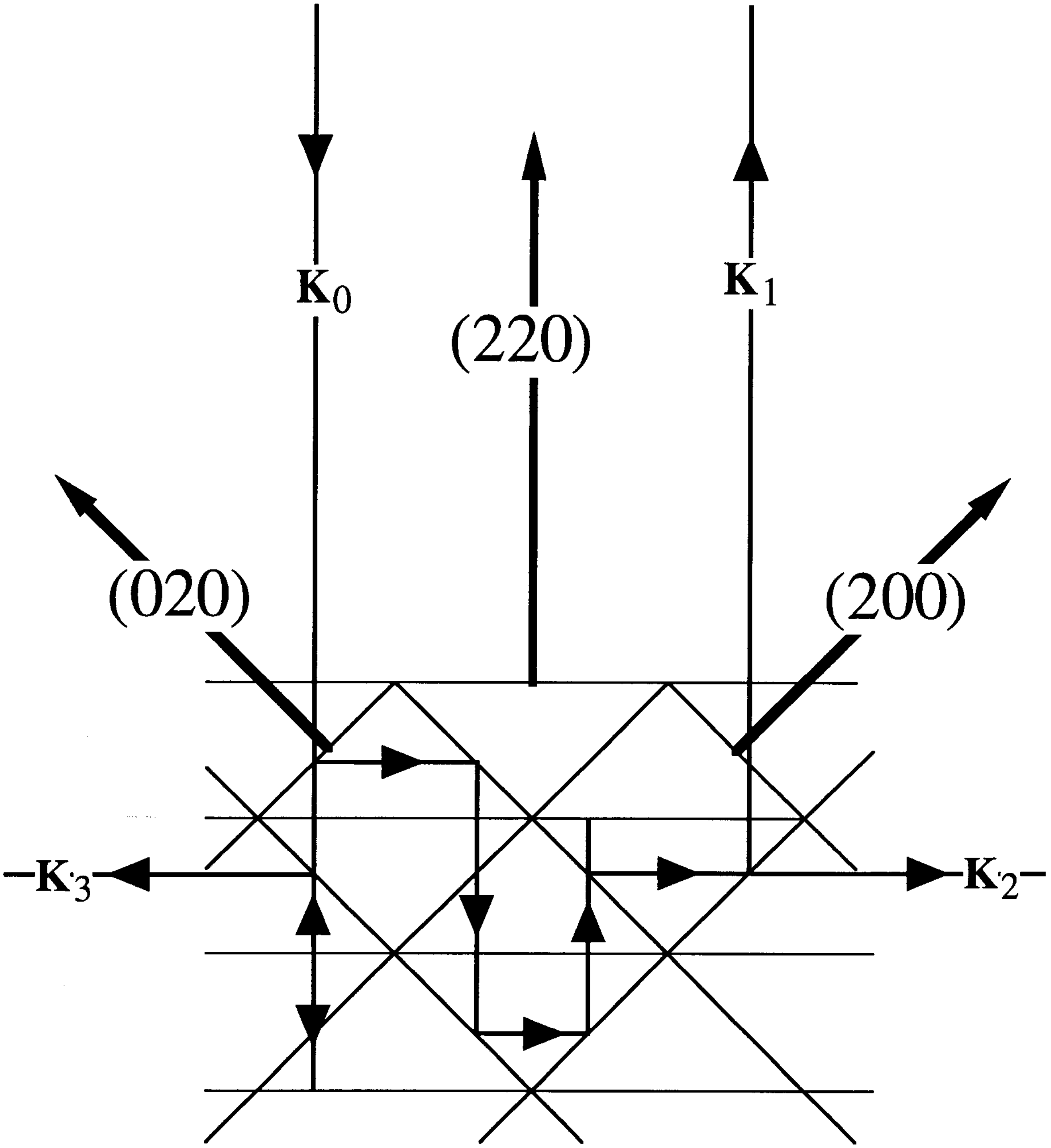

Figure 4.1. In the (220) back-reflection configuration, an incident wave is reflected back and forth by the (220), (200), and (020) crystal Bragg planes. This has as a result the coupling among the intensities of the four waves.

Chapter 5. The General XSW Expression and the Method of Extraction of D_c and f_c from the Experimental Data

As mentioned in Section 1.3.4, XSW spectra depend on the position of the atoms through the coherent distance (D_c) and coherent fraction (f_c). On the other hand, a real "monochromatized" X-ray beam has some degree of angular and frequency dispersion, which depend on the details of the experimental setup, such as the slit size, the shape of the mirrors, and the orbit of the electrons in the synchrotron ring. To fit XSW data, it is essential to account for the dispersion of the beam.

Under ideal experimental conditions, it is possible to obtain incident beams of enough uniformity to use the expected theoretical shape. On the other hand, as shown in previous studies, XSW experiments can very well be performed in nonspecialized XSW beamlines, as in those already existing for EXAFS studies, for which the incident beam is not perfectly characterized. This potentiality made possible the realization of the experiments presented in this thesis, and has prompted the proliferation of the use of the XSW technique in structural studies [1].

For the most common nonideal cases, a widespread method is to model the effects of the energy and angle dispersion of the incident beam with a single Gaussian broadening of the data; the parameters of the Gaussian are extracted from the reflectivity (or the total yield) and used to fit the XSW data [1]. For the data presented in this thesis, the Gaussian approximation was not good enough.

As shown in this chapter, a better approximation is to extract the characteristics of the incident beam from the reflectivity (or total yield) by deconvolution. To develop and present the ideas and approximations behind the deconvolution method, it was necessary to state formally some aspects of the framework of the XSW theory, a task that is done in Section 5.1. None of the ideas presented in Section 5.1 are new, but rather they were materialized from the general wisdom in the literature.

The advantages of the deconvolution method are that:

(1) It provides fits of much better quality.

(2) The results of the fits are more dependable. This is shown experimentally by fitting data for which the f_c and D_c are known.

(3) Theoretically, it is better justified.

(4) The fitting is a one step procedure, reducing the computer time by at least half.

5.1 The XSW expression for a dispersive incident beam

The purpose of this section is to provide a complete expression for the XSW signal (Eq. 5.16) and reflectivity (Eq. 5.19), taking into account the nonmonochromatic nature and angular divergence of the incident X-ray beam. These expressions shows that the XSW signal and reflectivity depend on the beam characteristics in the same way. The method of analysis presented in Section 5.2 makes heavy use of this fact.

The formalism employed produces additional benefits, such as a clear definition of the distribution function. This definition (Eq. 5.13) is used in Chapters 2, 6, 7, and 8 to properly interpret the experimental results. The equations are written in terms of the reflectance, for which an expression is derived in Appendix 1.

5.1.1 The excitation rate of electrons by Bragg-coupled X-ray beams

This section presents a formal expression for the electronic excitation rate by a real (non-monochromatic) incident X-ray beam. The XSW technique uses the coherent interference of X-rays to obtain structural information. It is emphasized that, although a spectrum of modes of radiation is present in the crystal, only those modes coupled by a Bragg condition are coherently added. The clear presentation of these concepts, which are not at all new, permits a more systematic discussion of the data analysis method employed in this dissertation.

The rate of electronic excitation of atoms in a crystal by an X-ray near a Bragg condition involves the destruction of a photon. To the knowledge of this author, a quantum electrodynamics solution to the problem of radiation diffracted by a crystal has not been presented in the literature (and it is not at all the objective of this work to resolve this problem). Nevertheless, the way that the problem has been treated in the literature implicitly combines quantum arguments with semiclassical and classical calculations. In this section, a formal XSW expression for a real beam is provided. As an aside, the quantum arguments behind the XSW theory are explicitly presented.

Incident X-ray radiation of wave vector $\mathbf{k}_0$ in vacuum propagates inside the crystal with a wave vector $\mathbf{K}_0 = \mathbf{K}_0(\mathbf{k}_0)$ slightly different from $\mathbf{k}_0$. It is well known that when $\mathbf{K}_0$ nearly satisfies a Bragg condition, the presence of the crystal induces the excitation of a mode of radiation with wave vector $\mathbf{K}_1 = \mathbf{K}_0 + \mathbf{H}$, with $\mathbf{H}$ the crystal vector corresponding to the reflecting Bragg planes. This means that the photons of the system are not simply planes waves, but have two parts corresponding to the incoming and reflected beams. The excitation of an electron by the destruction of a photon involves those two parts. The coherent interference of those parts is precisely what makes the XSW technique sensible to the atomic position.

Berman and Bedzyk (B&B) [2] presented an expression for the cross section ($d\sigma/d\Omega$) of the photoelectric excitation with the electromagnetic field treated classically. Using our nomenclature, we basically reproduce B&B's Eq. 2 as follows:

$$\frac{d\sigma}{d\Omega} \propto \left| \langle f | \left\{ E(\mathbf{K}_0) \exp(-2\pi i\, \mathbf{K}_0 \cdot \mathbf{r})\, \varepsilon_0 \cdot \nabla + E(\mathbf{K}_1) \exp(-2\pi i\, \mathbf{K}_1 \cdot \mathbf{r})\, \varepsilon_1 \cdot \nabla \right\} | i \rangle \right|^2 \quad (5.1)$$

where $\langle f|$ is the ejected electron defined by the solid angle Ω, $|i\rangle$ is the initial state of the electron, $\mathbf{r}$ is the vector position operator, ε_0 and ε_1 are the polarization vectors of the electric field, and $E(\mathbf{K})$ is the electric field intensity.

The dipole approximation is needed for the simplification of Eq. 5.1. Usually, the dipole approximation is stated as follows:

$$\exp(-2\pi\, i\, \mathbf{K} \cdot \mathbf{r}) \rightarrow 1 \qquad \text{("strong" dipole approximation)} \qquad (5.2)$$

It is important to stress that we cannot use the dipole approximation in its version given by Eq. 5.2 (as erroneously used by B&B), because we would be neglecting the dependence of the excitation rate on the atomic position. In fact, the approximation that has to be used to recover the XSW equations is the following:

$$\exp(-2\pi\, i\, \mathbf{K} \cdot \mathbf{r})\, |i\rangle \approx \exp(-2\pi\, i\, \mathbf{K} \cdot \mathbf{r}')\, |i\rangle \qquad \text{("weak" dipole approximation)} \qquad (5.3)$$

where $\mathbf{r}'$ (no longer an operator) is an averaged position of the electron in its initial state and will be taken as the atomic position. The approximation of Eq. 5.3 can be thought of as a weaker version of the dipole approximation. In most cases, when no interference is present, this approximation is equivalent to the strong dipole approximation because the phase disappears when the absolute value of the matrix element is calculated. When interference is important, as in the XSW case, the strong version cannot be used. The justification of Eq. 5.3, which is more difficult than in the optical case because the wavelength is of the order of the inter-atomic distance, is beyond the scope of this work. Expanding Eq. 5.1, and using the weaker approximation, we get:

$$\begin{aligned}\frac{d\sigma}{d\Omega} \propto\ & \left| E(\mathbf{K}_0) \right|^2 \left| \exp(-2\pi i\, \mathbf{K}_0 \cdot \mathbf{r}) \right| \left| \langle f | \boldsymbol{\varepsilon}_0 \cdot \nabla | i \rangle \right|^2 \\ & + \left| E(\mathbf{K}_1) \right|^2 \left| \exp(-2\pi i\, \mathbf{K}_1 \cdot \mathbf{r}) \right| \left| \langle f | \boldsymbol{\varepsilon}_1 \cdot \nabla | i \rangle \right|^2 \\ & + 2\mathrm{Re}\left\{ \exp(-2\pi i\, \mathbf{H} \cdot \mathbf{r})\ E(\mathbf{K}_1)\, E^*(\mathbf{K}_0)\, \langle i | \boldsymbol{\varepsilon}_0 \cdot \nabla | f \rangle \langle f | \boldsymbol{\varepsilon}_1 \cdot \nabla | i \rangle \right\}, \qquad (5.4)\end{aligned}$$

where we have dropped the prime on $\mathbf{r}'$. As nicely shown by B&B, the angular distribution of the photoelectron yield is described by Eq. 5.4. We are interested in the integrated yield, which is usually what is measured in the laboratory (a CMA detector, such as the one used in our experiments, measures angular integrated yield). The integrated excitation rate $w(\mathbf{r})$ of an electron of an atom positioned at $\mathbf{r}$, is obtained by adding over all solid angles, and results in [2]:

$$\begin{aligned} w(\mathbf{r}) \propto\ & \left|E(\mathbf{K}_0)\right|^2 \left| \exp(-2\pi i\, \mathbf{K}_0 \cdot \mathbf{r}) \right| + \left|E(\mathbf{K}_1)\right|^2 \left| \exp(-2\pi i\, \mathbf{K}_1 \cdot \mathbf{r}) \right| \\ & + 2\boldsymbol{\varepsilon}_0 \cdot \boldsymbol{\varepsilon}_1 \mathrm{Re}\left\{ \exp(-2\pi i\, \mathbf{H} \cdot \mathbf{r})\, E(\mathbf{K}_1)\, E^*(\mathbf{K}_0) \right\}. \qquad (5.5)\end{aligned}$$

Adding over all the incoming radiation, and ignoring changes in the matrix elements of Eq. 5.4 as $\mathbf{K}_0$ changes, we get:

$$\begin{aligned} w(\mathbf{r}) \sim \int d\mathbf{k}_0 \Big\{ & \left|E(\mathbf{K}_0)\right|^2 \left| \exp(-2\pi i\, \mathbf{K}_0 \cdot \mathbf{r}) \right| + \left|E(\mathbf{K}_1)\right|^2 \left| \exp(-2\pi i\, \mathbf{K}_1 \cdot \mathbf{r}) \right| \\ & + 2\boldsymbol{\varepsilon}_0 \cdot \boldsymbol{\varepsilon}_1\ \mathrm{Re}\left[\exp(-2\pi i\, \mathbf{H} \cdot \mathbf{r})\, E(\mathbf{K}_1)\, E^*(\mathbf{K}_0) \right] \Big\}, \qquad (5.6)\end{aligned}$$

where $\mathbf{E}(\mathbf{K}) = \boldsymbol{\varepsilon}\, E(\mathbf{K})$. In general, if many Bragg conditions are met simultaneously,

$$w(\mathbf{r}) \sim \int d\mathbf{k}_0 \left| \mathbf{E}(\mathbf{K}_0) \exp(-2\pi i\, \mathbf{K}_0 \cdot \mathbf{r}) + \sum_{\mathbf{H}} \mathbf{E}(\mathbf{K}_0 + \mathbf{H}) \exp\left(-2\pi i\, (\mathbf{K}_0 + \mathbf{H}) \cdot \mathbf{r}\right) \right|^2 . \qquad (5.7)$$

Equation 5.6 (or its generalization, Eq. 5.7) is basic to the XSW theory.

The most important conclusion is that $w(\mathbf{r})$ is not proportional to the square of the total electric field. Notice that some components of the electric field have been selectively grouped and added coherently, to then be added incoherently to the rest of the terms of the electric field. The integration on $\mathbf{k}_0$ is not over the whole wave vector space, but only over the incident part of the radiation (as stated earlier, the $\mathbf{K}_0$ is a function of $\mathbf{k}_0$).

The spatial modulation of the excitation rate is the result of the coherent interference of the incoming and Bragg reflected beams. The scale of interference is the interplanar distance, so, within an interplanar distance, there are fringes with large and fringes with small electric field. The rate of excitation of an electron depends on its average position $\mathbf{r}$.

In the literature (and of course in this thesis) the calculations of the electric field are carried out classically (see Chapter 4 and Appendix 1).

5.1.2 The general XSW expression and the definition of the distribution function

For the one-reflection case, the excitation rate of a core electron with average position $\mathbf{r}$ (due to all the incoming beam) is given by Eq. 5.6 and, with little algebra, can be written as:

$$w(\mathbf{r}) \propto \int d\mathbf{k}_0 \left|E(\mathbf{K}_0)\right|^2 C_{\mathbf{K}_0}(\mathbf{r}) \left\{1 + \left|\rho(\mathbf{k}_0)\right|^2 + 2\,|P| \operatorname{Re}\left[\rho(\mathbf{k}_0) e^{-2\pi i\, \mathbf{H}\cdot\mathbf{r}}\right]\right\} \tag{5.8}$$

where ρ is the reflectance defined:

$$\rho(\mathbf{k}_0) \equiv \frac{E(\mathbf{K}_1)}{E(\mathbf{K}_0)} \; . \tag{5.9}$$

An expression for the reflectance is derived in Appendix 1. The extinction factor $C_{\mathbf{K}_0}$ is defined as:

$$C_{\mathbf{K}_0}(\mathbf{r}) \equiv \left| \exp(-2\pi i\, \mathbf{K}_0 \cdot \mathbf{r}) \right| \; .$$

The equality

$$\left| \exp(-2\pi i\, \mathbf{K}_0 \cdot \mathbf{r}) \right| = \left| \exp(-2\pi i\, \mathbf{K}_1 \cdot \mathbf{r}) \right| \; ,$$

which can be shown by using Eq. A1.2, has been used in the derivation of Eq. 5.8.

The so-called extinction factor $C_{\mathbf{K}_0}$ is not equal to 1 because $\mathbf{K}_0$ has an imaginary part. This is precisely the factor that does not allow the incident beam to propagate too far inside the crystal, making possible the existence of the reflected beam. The extinction effect can be calculated through this factor. For both the overlayer and substrate relaxation studies included in this thesis, the extinction factor will not play any role because the signal comes from near the surface, and the extinction factor has no modulation along directions parallel to the surface—the direction of the imaginary part of $\mathbf{K}_0$ is normal to the surface (see Section A1.2), so the extinction fronts are parallel to the surface.

The first factor $\left|E(\mathbf{K}_0)\right|^2$ of Eq. 5.8 is proportional to the intensity (I) of the incident beam with wave vector $\mathbf{k}_0$. This intensity depends on the nominal frequency and angle set by the monochromator:

$$\left|E(\mathbf{K}_0)\right|^2 \propto I(\mathbf{k}_{00},\mathbf{k}_0)\ , \tag{5.10}$$

where the wave vector $\mathbf{k}_{00}$ correspond to the nominal energy (E) and angles (Ω) of the incident beam.

The last factor is the most interesting one because it is modulated between adjacent Bragg planes, and has exactly the spatial periodicity of the Bragg planes.

Experimentally, the signal comes from all the atoms of a given species in the sample, which means that it is necessary to multiply Eq. 5.8 by the density (f) and integrate over the sampled volume. It is also necessary to multiply by the probability of being detected (P_E), because it is less likely to detect an excitation deep in the crystal than near the surface. This probability plays no role for the overlayer case, because all the atoms are at the surface and have the same probability of being detected. On the other hand, it is important for the substrate relaxation studies presented in Chapter 8, because it is precisely what makes this type of studies possible. We then have:

$$Y(\mathrm{E}) \propto \iint d\mathbf{r}\, f(\mathbf{r}) P_E(\mathbf{r})\; d\mathbf{k}_0\, I(\mathrm{E},\mathbf{k}_0)\left\{1+\left|\rho(\mathbf{k}_0)\right|^2+2|P|\mathrm{Re}\left[\rho(\mathbf{k}_0)\exp(-2\pi i\,\mathbf{H}\cdot\mathbf{r})\right]\right\}, \tag{5.11}$$

where E is the nominal energy. The $I(\mathbf{k}_{00},\mathbf{k}_0)$ has been replaced by $I(\mathrm{E},\mathbf{k}_0)$ because in our experiments the nominal direction of incidence is kept constant, so the nominal angles Ω are obviated, characterizing the beam only through its nominal energy E.
Equation 5.11 can be rearranged as follows:

$$\begin{aligned} Y(\mathrm{E}) \propto & \left\{\int d\mathbf{r}\, f(\mathbf{r}) P_E(\mathbf{r})\right\} \int d\mathbf{k}_0\, I(\mathrm{E},\mathbf{k}_0) \\ & \times \left\{1+\left|\rho(\mathbf{k}_0)\right|^2+2\,|P|\ \mathrm{Re}\left[\rho(\mathbf{k}_0)\ \frac{\int d\mathbf{r}\, f(\mathbf{r}) P_E(\mathbf{r}) \exp(-2\pi\, i\,\mathbf{H}\cdot\mathbf{r})}{\int d\mathbf{r}\, f(\mathbf{r}) P_E(\mathbf{r})}\right]\right\}. \end{aligned} \tag{5.12}$$

It is natural to define a function, which is called Distribution Function, as:

$$f_{\mathrm{H}}(D) \equiv \frac{\int dr_1 dr_2 \sum_{\mathrm{n}} f(r_1,r_2,D+nd_{\mathrm{H}})\ P_E(r_1,r_2,D+nd_{\mathrm{H}})}{\int d\mathbf{r}\, f(\mathbf{r})P_E(\mathbf{r})}, \tag{5.13}$$

where $d_{\mathrm{H}} = 1/|\mathbf{H}|$ is the interplanar distance and the orientation of the reference frame was chosen in such a way that the third coordinate is parallel to $\mathbf{H}$. The distribution function $f_{\mathrm{H}}(D)$ can be viewed as the result of moving all the atoms within an interplanar Bragg distance d_{H}. It has the following properties:

$$\int_0^{d_{\mathrm{H}}} dD\, f_{\mathrm{H}}(D) \exp\left(-2\pi i\ \frac{D}{d_{\mathrm{H}}}\right) = \frac{\int d\mathbf{r}\, f(\mathbf{r})\ P_E(\mathbf{r}) \exp(-2\pi i\, \mathbf{H}\cdot\mathbf{r})}{\int d\mathbf{r}\, f(\mathbf{r})\ P_E(\mathbf{r})},$$

and

$$\int_0^{d_{\mathrm{H}}} dD\, f_{\mathrm{H}}(D) = 1 .$$

Then, Eq. 5.12 can be written:

$$\begin{aligned} Y(\mathrm{E}) \propto & \int d\mathbf{k}_0 I(\mathrm{E},\mathbf{k}_0) \\ & \times \left\{1+|\rho(\mathbf{k}_0)|^2 + 2|P|\mathrm{Re}\left[\rho(\mathbf{k}_0)\int_0^{d_{\mathrm{H}}} dD\, f_{\mathrm{H}}(D) \exp\left(-2\pi i\ \frac{\mathrm{D}}{d_{\mathrm{H}}}\right)\right]\right\}, \end{aligned} \tag{5.14}$$

where the constant first factor of Eq. 5.12 was dropped.

The coherent fraction (f_c) and the coherent distance (D_c) are defined in terms of the distribution function:

$$\int_0^{d_{\mathrm{H}}} dD\, f_{\mathrm{H}}(D) \exp\left(-2\pi i\ \frac{\mathrm{D}}{d_{\mathrm{H}}}\right) = f_c \exp\left(-2\pi i\ \frac{\mathrm{D_c}}{\mathrm{d_H}}\right). \tag{5.15}$$

Substituting Eq. 5.15 in Eq. 5.14, we obtain:

$$Y(\mathrm{E}) \propto \int d\mathbf{k}_0\, I(\mathrm{E},\mathbf{k}_0) \left\{1+|\rho(\mathbf{k}_0)|^2 + 2|P|\ f_c\ \mathrm{Re}\left[\rho(\mathbf{k}_0) \exp\left(-2\pi i\ \frac{\mathrm{D_c}}{\mathrm{d_H}}\right)\right]\right\}. \tag{5.16}$$

This, after important simplifications (see Section 5.2), is the expression that is used for the analysis. It usually is presented as [1]:

$$\frac{Y(E)}{Y_0} = 1+\Re(E)+2f_c\,|P|\,\sqrt{\Re(E)}\cos\left[\nu(E) - 2\pi\,\frac{\mathrm{D_c}}{\mathrm{d_H}}\right], \tag{5.17}$$

which corresponds to Eq. 5.16 for the monochromatic beam. Here $\Re$ and ν are the square of the absolute value and the phase of the reflectance.

It is useful to write the expressions in the opposite direction:

$$f_c = \left|\int_0^{d_\mathrm{H}} dD\, f_\mathrm{H}(D)\exp\left(-2\pi i\,\frac{\mathrm{D}}{d_\mathrm{H}}\right)\right|, \tag{5.18a}$$

and

$$D_c = \frac{d_\mathrm{H}}{2\pi}\arctan\frac{\int_0^{d_\mathrm{H}} dD\, f_\mathrm{H}(D)\sin 2\pi\,\frac{\mathrm{D}}{d_\mathrm{H}}}{\int_0^{d_\mathrm{H}} dD f_\mathrm{H}(D)\cos 2\pi\,\frac{\mathrm{D}}{d_\mathrm{H}}}, \tag{5.18b}$$

5.1.3 The reflectivity

The reflected beam is detected outside the crystal. We first discuss the case in which the reflected beam does not overlap with the incident beam at the site of the detection. The detection is made by measuring the total photoemission yield produced by the reflected beam on a grid or metal sheet. Applying the discussion of Section 5.1.1 to the case where only one beam is present, this yield (R) can be written:

$$R \propto \int d\mathbf{k}_0\, |E(\mathbf{K}_1)|^2\, |\exp(-2\pi i\,\mathbf{K}_1\cdot\mathbf{r})|\,\Big|_{\mathbf{r}=\text{surface}}\;.$$

The evaluation is done as the beam leaves the crystal sample (at $\mathbf{r}$ = surface) because no intensity is expected to be lost in vacuum; that is, the intensity of the reflected beam at the detector position is the same as when it leaves the crystal. Using Eqs. 5.9 and 5.10, this equation can be rewritten as follows:

$$R(\mathrm{E}) \propto \int d\mathbf{k}_0\, I(\mathrm{E},\mathbf{k}_0)\,|\,\rho(\mathbf{k}_0)\,|^2. \tag{5.19}$$

For the special case of exact back-reflection, in which the reflected beam overlaps with the incoming beam even at the detection point, the total photoemission yield of the grid detector (R) is as follows (see Eq. 5.16):

$$R(\mathrm{E}) \propto \int d\mathbf{k}_0\, I(\mathrm{E},\mathbf{k}_0)\left\{1+\left|\rho(\mathbf{k}_0)\right|^2+2\,|P|\,f_c^{\mathrm{grid}}\ \mathrm{Re}\left[\rho(\mathbf{k}_0)\exp\left(-2\pi i\ \frac{\mathrm{D}_c^{\mathrm{grid}}}{\mathrm{d_H}}\right)\right]\right\},$$

where the coherent fraction and coherent distance refers to the atomic distribution in the grid. Because the atoms in the grid do not have the periodicity of the standing wave, the coherent fraction of the grid is zero, so that this equation reduces to:

$$R(\mathrm{E}) \propto \int d\mathbf{k}_0\, I(\mathrm{E},\mathbf{k}_0)\ \left\{1+\left|\rho(\mathbf{k}_0)\right|^2\right\}.$$

The intensity of the incoming beam $\int d\mathbf{k}_0\, I(\mathrm{E},\mathbf{k}_0)$ can be subtracted, so that the expression is reduced to Eq. 5.19.

This shows that the reflectivity (Eq. 5.19) and the XSW signal (Eq. 5.16) are convoluted with the same function $I(\mathrm{E},\mathbf{k}_0)$. This conclusion is heavily used in Section 5.2 in the development of the fitting method.

5.2 The method of extraction of D_c and f_c from the experimental data

The objective is to extract the values of f_c and D_c by fitting Eq. 5.16 to the experimental data. In principle, this implies knowledge of the shape $I(\mathrm{E},\mathbf{k}_0)$ of the incident beam, which depends on the details of the experimental setup, such as the slit size, the shape of the mirrors, and the orbit of the electrons in the synchrotron ring. In practice, it is possible to make some (commonly used) approximations about $I(\mathrm{E},\mathbf{k}_0)$, which allows analysis even without an exact characterization of the incident beam.

In this section, a deconvolution method is presented that subtracts the effects of the characteristics of the X-ray beam on the shape of the XSW signal. In addition, the approximations about $I(\mathrm{E},\mathbf{k}_0)$ that are made by this and other traditional methods of XSW data fitting are clearly described using the formalism of Eq. 5.16.

The first approximation about $I(\mathrm{E},\mathbf{k}_0)$ is that the changes of its shape can be neglected when the nominal photon energy is scanned. In terms of Eq. 5.16, this approximation can be states as follows:

$$I(\mathbf{k}_{00},\mathbf{k}_0) \rightarrow I(\mathbf{k}_0-\mathbf{k}_{00}) \,. \tag{5.20}$$

In terms of the Du Mond diagram of Fig. 3.4 or 3.5, this means that the illuminated rectangle does not change shape as it moves up and down. This approximation is well justified because no appreciably change is expected over the range of energies of a XSW spectrum, which is less than 10 eV compared with typical absolute energies of the order of KeV.

Another important simplification can be made by noticing that small offsets in angle can be treated as an effective offset in energy. For small angular divergence, the only important dependence of the reflectance on the angles comes through the kinematical Bragg energy E_B (see Eqs. A1.28 and A1.29):

$$\mathrm{E}_B \equiv \frac{|\mathbf{H}_1|}{2\cos\chi} \,.$$

The change in E_B caused by the deviation of the angles from its nominal value can effectively be incorporated as part of the energy dispersion, so we have only to consider the energy dispersion of the beam. This can be seen as:

$$I(\mathbf{k}_0-\mathbf{k}_{00}) \rightarrow I(\mathrm{E}'-\mathrm{E}) \,, \tag{5.21}$$

where E' has incorporated not only the difference of energy between $\mathbf{k}_0$ and $\mathbf{k}_{00}$, but also the difference of E_B due to their difference angle.

By inspecting Eq. A1.28, it can be seen that angular effects other than the change in Bragg energy can be incorporated to some extent in Eq. 5.21.

These two approximations allow us to write Eq. 5.16 as a simple, one-dimensional convolution:

$$Y(\mathrm{E}) \propto \int d\mathrm{E}'\, I(\mathrm{E}'-\mathrm{E}) \left\{ 1+|\rho(\mathrm{E}')|^2 + 2|P|f_c \;\mathrm{Re}\left[\rho(\mathrm{E}')\exp\left(2\pi i\, \frac{\mathrm{D_c}}{\mathrm{d_H}}\right)\right]\right\} \,, \tag{5.22}$$

where we have made the change $\rho(\mathbf{k}_0) \rightarrow \rho(\mathrm{E}')$. In a similar way, the reflectivity can be written (see Eq. 5.19):

$$R(\mathrm{E}) \propto \int d\mathrm{E}' I(\mathrm{E}'-\mathrm{E})\, |\rho(\mathrm{E}')|^2 \,. \tag{5.23}$$

The reflectance ρ is known because it only depends on the parameters of the crystal (see Eq. A1.30).

Sometimes, although not always, $I(\mathrm{E}' - \mathrm{E})$ can be approximated to a Gaussian. A widely used method of analysis is to extract the width of the Gaussian and the peak center from Eq. 5.23, and to then substitute into Eq. 5.22.

In our analysis, we extract the function $I(\mathrm{E}' - \mathrm{E})$ by deconvolution (using Fourier analysis) of Eq. 5.23, and then substitute it in Eq. 5.22.

The total yield is also a XSW spectrum:

$$TY(\mathrm{E}) \propto \int d\mathrm{E}' I(\mathrm{E}' - \mathrm{E}) \left\{ 1 + |\rho(\mathrm{E}')|^2 + 2|P| f_c^{\mathrm{TY}} \,\mathrm{Re}\left[\rho(\mathrm{E}') \exp\left(-2\pi i \, \frac{\mathrm{D}_c^{\mathrm{TY}}}{\mathrm{d}_\mathrm{H}} \right) \right] \right\}, \quad (5.24)$$

If the coherent fraction and coherent distance of the total yield are known, it could also provide the function $I(\mathrm{E}' - \mathrm{E})$; then the function $I(\mathrm{E}' - \mathrm{E})$ can be resolved from both the reflectivity and the total yield spectra.

The FORTRAN program made to perform the analysis, which is called "SWDECONV", is presented in Appendix 3.

References

1. D.P. Woodruff, D.L. Seymour, C.F. McConville, C.E. Riley, M.D. Crapper, and N.P. Prince. "A simple X-ray standing wave technique for surface structural determination—theory and an application." Surface Science **195**, p. 237 (1988); T. Kendelewicz, J.C. Woicik, K.E. Miyano, A. Herrera-Gómez, P.L. Cowan, B.A. Karlin, C.E. Bouldin, P. Pianetta, and W.E. Spicer. "X-ray standing-wave study of monolayers of Sb on GaAs(110)." Physical Review B **46**, p. 7276 (1992); J.C. Woicik, T. Kendelewicz, K.E. Miyano, P.L. Cowan, C.E. Bouldin, B.A. Karlin, P. Pianetta, and W.E. Spicer. "X-ray standing wave determination of the clean InP (110) surface reconstruction." Physical Review Letters **68**, No. 3, p. 341 (1992); K.E. Miyano, T. Kendelewicz, J.C. Woicik, P.L. Cowan, C.E. Bouldin, B.A. Karlin, P. Pianetta, and W.E. Spicer. "Structural characterization of the (1 monolayer Sb)/GaP(110) interface using X-ray standing waves." Physical Review B **46**, No. 11, p. 6869 (1992); J. Zegenhagen. "Surface structure

determination with X-ray standing wave." Surface Science Reports **18**, 199 (1993) and references therein (see p. 256).

2. L.E. Berman, and M.J. Bedzyk. "Angular distribution of the photoelectron yield excited by two coherently coupled photon beams." Physical Review Letters **63**, p. 1172–75 (1989).

Chapter 6. Results of the Bi/GaAs Experiments

The experimental and theoretical methodology developed in the former chapters was applied to determine the geometrical structure of the system formed by one monolayer of Bi on the (110) GaAs cleaved surface. A preliminary study was published elsewhere [1].

6.1 Experiments performed

Two sets of (220), (111), and $(11\bar{1})$ XSW experiments were performed on two different samples, so two complete sets of data were obtained. The experimental setup and configurations were as described in Chapter 3.

Two $(11\bar{1})$ reflections were performed using configurations different from that described in Chapter 3. One $(11\bar{1})$ reflection was performed in the back-reflection mode using InSb (111) crystals in the monochromator. The other (111) reflection used the nondispersive configuration described in Chapter 8, with Si (111) monochromator crystals. In these two cases, the Bi signal was also obtained by monitoring the Bi 4d photoemission yield.

Some XSW spectra were acquired as well for bulk As. The purpose of this measurement was to discriminate between the (111) and $(11\bar{1})$ reflections. Because the position of bulk As relative to the planes is known, this also provides a check for experimental accuracy. The spectra were taken using either the As LMM Auger or As 3p photoemission lines.

6.2 The data collection procedure

As mentioned in Section 1.3.3, the excitation rate, and so the photoemission yield, is modulated as the photon energy is swept through the Bragg condition. Figure 6.1 displays the experimental reflectivity of the (111) reflection of GaAs (the data correspond to the (111) experiment performed using the nondispersive configuration of Chapter 8). The Bi 4d photoemission spectra were acquired for the photon energies indicated by the dashed lines of Fig. 6.1, and are displayed in Fig. 6.2. The modulation of the total Bi 4d photoemission signal with photon energy is very evident from the figure. The Bi 4d photopeak rides on the top of a background of secondary electrons. Also evident is the modulation of the height of the background with photon energy.

The data was obtained by using the fact that the height of the Bi peak ("Y" in Fig. 6.2) measured from the extrapolation of the background (dashed lines) is proportional to the total Bi signal (shadowed area). As the photon energy was swept through the Bragg condition, data was recorded with the CMA electron detector tuned to the Bi 4d peak (see Fig. 6.2), and with the CMA tuned to a higher electron energy corresponding to the background. The signal from the background files was then extrapolated to the energy corresponding to the Bi 4d peak, and subtracted from the peak files.

This extrapolation is done by multiplying the background signal by the appropriate factor. For this approach to be valid, a linear background with no structure is required, such as those in Fig. 8.2. Figure 8.3 displays Y—the difference between the Bi 4d peak signal and the extrapolated background signal (see Fig. 6.2)—as a function of photon energy, so the modulation corresponds solely to the Bi 4d photoemission signal. The dots on Fig. 6.3 correspond to the heights (Y) measured in the photoemission spectra of Fig. 6.2.

6.3 The averaging procedure

Many peak and background files were recorded in order to achieve good statistics. The files were then added or subtracted depending on whether they correspond to the peak or to the background. A problem arises because the energy of the incoming beam shifts gradually with time as the monochromator crystals change temperature due to the reduction of stored current in the synchrotron over time. When the shifting is not too strong to affect the energy scale, the problem can be solved by shifting the files by the "right" amount before adding. The right amount was found by maximizing the correlation between the reflectivity of the files. The shifts and interpolation needed were done with a computer program called "AVERAGE," which is presented in Appendix 4.

6.4 Data and fits

Figures 6.4 to 6.14 show the experimental data together with their theoretical fit. The fitting was done with the deconvolution method presented in Section 5.2. The reflectivity or the total yield is also plotted with the data depending on which one was used in the fitting calculations (not both the reflectivity and the total yield were recorded in all the reflections). The extracted values for the coherent distance and coherent fraction for all the reflections performed are displayed in Table 6.1. The coherent distances are in units of the corresponding interplanar distance d_H. The origin used is shown in Fig. 2.1. The uncertainties are chosen as the changes that produce twice the value of the minimum χ^2.

As it can be seen in Table 6.1, the reproducibility of the coherent distance is within 2%. When the coherent distances are expressed in units of the corresponding interplanar distance d_H, the consistency check of Eq. 2.8 reads as follows:

$$D_c^{[220]} = D_c^{[111]} + D_c^{[11\bar{1}]} \qquad \text{(interplanar units)}\,. \tag{6.1}$$

Both sets satisfy Eq. 6.1 within 7%, which is smaller than the combined uncertainties.

The reproducibility of the coherent fractions is also within a few percent, although some variation is expected from surface to surface because the order parameter (which directly affects their value, see Eq. 2.3) may vary even if the method of the surface preparation is the same. This is because the final degree of clustering may depend on the amount of Bi initially deposited, even if the sample is annealed to desorb excess Bi (see Section 3.2).

It is very reassuring that the As $(11\bar{1})$ coherent distance was within 2% of the expected value of 0.125. This accuracy is surprising because it was difficult to properly extrapolate the background corresponding to the As LMM data due to structure in the background produced by Bi core level peaks above the As LMM energy.

This remarkable quality of the fits, and the reproducibility and consistency of the whole data, were not at all apparent when the analysis was done assuming a Gaussian beam width as the monochromator response—the initial quality of the fits, self-consistency check, and coherent distance values for bulk As, formed a somewhat ugly panorama.

6.5 Structural results

It was mentioned in Chapter 2 that our XSW data provided information in the Y-Z plane (see Fig. 2.1). Equations 2.4 and 2.5 relate the coherent distances and coherent fractions to the atomic coordinates $(y_{1,2},\ z_{1,2})$. Solving for $z_1 + z_2$ and $y_1 + y_2$ is very direct from Eqs. 2.4. On the other hand, ϕ, $z_1 - z_2$, and $y_1 - y_2$ have to be found numerically from Eqs. 2.5. Equations 2.5 can be rearranged as follows:

$$\sin^2 \pi\, \frac{1}{a}\, (y_1 - y_2) \;=\; 1 - \frac{\left(f_c^{[111]} + f_c^{[11\bar{1}]}\right)^2}{2\phi\left(\phi + f_c^{[220]}\right)}\,, \tag{6.2a}$$

$$\sin^2 \pi\, \frac{1}{a}\, (y_1 - y_2) \;=\; \frac{\left(f_c^{[111]} - f_c^{[11\bar{1}]}\right)^2}{2\phi\left(\phi - f_c^{[220]}\right)}\,, \tag{6.2b}$$

$$\cos^2 \pi\, \frac{\sqrt{2}}{a}\, (z_1 - z_2) \;=\; \frac{1}{2}\left(\frac{f_c^{[220]}}{\phi} + 1\right), \tag{6.2c}$$

where the Debye-Waller factor has been ignored (see Sections 2.5 and 6.7). Figure 6.15 shows a graphical solution of Eqs. 6.2 for the first set. Equation 6.2a corresponds to curve A of Fig. 6.15, Eq. 6.2b to curve B, and Eq. 6.2c to curve C. Because the left sides of Eqs. 6.2a and 6.2b are identical, the intersection of curves A and B (the large dot in the figure) provides the solution for ϕ and for $(y_1 - y_2)$. The corresponding value of $(z_1 - z_2)$ is obtained by evaluating Eq. 6.2c at the solution value of ϕ (small dot). The parallel curves at each side of the main curves correspond to Eq. 6.2 for the most extreme combinations of the uncertainties on the coherent fractions. The shadow region corresponds to all allowed solutions. The uncertainties for ϕ, $(z_1 - z_2)$, and $(y_1 - y_2)$ were estimated using the extremes of the shadowed region.

The same method was used to solve for the second set of data, and both solutions are displayed in Table 6.2. The position of the Bi sites shown in Fig. 6.16 are scaled according to the solution of the first set (to the scale of the drawing of Fig. 6.16, the results of the two sets are indistinguishable). If no relaxation of the substrate atoms is considered, the results for the Ga-Bi and As-Bi bond length are 2.79 Å and 2.61 Å. These numbers are very close to 2.72 Å and 2.64 Å, which are the sum of covalent radii (see Table 1.1). On the other hand, results for the Bi–Bi distance (~ 2.68 Å, see Table 6.2) is short from twice the Bi covalent radii (2.92 Å).

6.6 Comparison to prior LEED and TBTE results

As it can be seen in Fig. 6.16, the XSW results locate the Bi adatoms close to those of the next layer of bulk GaAs, so our results determine that the structure of the Bi/GaAs interface is better described by ECLS (see the discussion of Section 7.4). Table 6.2 displays the results for the coordinates from each of the two sets of XSW data, and from prior LEED [2] experiments and TBTE [3] calculations. From these numbers, EOTS can be rejected right away. As mentioned in Section 1.2, both LEED and TBTE favor ECLS. Our results confirm that their assertions were correct. The comparison is, therefore, made with the ECLS version of the structures provided by the LEED and TBTE studies. Due to an inconsistency on the reported TBTE results, two values for the TBTE results on $(x_1 + x_2)/2$ are displayed. Uncertainties in the LEED results are not provided. It should be kept in mind that the XSW results are measured relative to the ideal bulk-lattice positions, and that the LEED and TBTE are measured relative to the positions of the last GaAs layer. This discrepancy should not introduce large differences between the XSW and LEED (or TBTE) results, because the position of the substrate atoms are very close to the ideal bulk [2, 3]. No experiment was performed that would provide information about the relaxation of the outermost Ga and As substrate atoms. The reason is that, although the relaxation of the substrate surface can be obtain from XSW using surface-sensitive Auger or photoemission peaks, there are no As or Ga surface sensitive peaks available for the range of photon energies used in the reflections.

The larger discrepancy between the XSW and LEED results is in the displacement parallel to the surface, where the sensitivity of LEED is smaller. For displacements perpendicular to the surface, the agreement is excellent. The overall comparison with the theoretical approach (TBTE) is poorer.

6.7 Discussion of the order parameter

The value for the order parameter ϕ (see Table 6.2) indicates that, for the surface used for the first (second) set of experiments, 35% (30%) of the Bi atoms were at incoherent positions. This value of disorder is larger than that obtained for Sb/GaAs, which is only ~10%. This is as expected because there is a larger mismatch between the Bi chains and the GaAs substrate (see Section 1.2.1). An even larger disorder of 42% is found for the Sb/GaP system [4]. If the disorder comes from clustering, the reproducibility in the amount of disorder may be an indication that annealing creates an equilibrium between the population in clusters and in a single monolayer. If the disorder comes from Bi on the substrate terrace edges, where Bi may reside at many positions, the reproducibility of the disorder may indicate that there is an equilibrium value of the density of terrace edges for cleaved surfaces.

On the other hand, it is possible that the low values for ϕ are not real, but result from using the two-site model. As mentioned in Section 1.2.1, STM images [5] show a missing Bi row approximately every six unit cells in the $(1\bar{1}0)$ direction, along with misfit dislocations. Our large value of disorder may thus come from the breakdown of our initial assumption, which considered only two distinct coherent positions. One of the effects of assuming that the adatoms have only two distinctive positions in the Y-Z plane, is to artificially lower the value of the order parameter. From Eqs. 2.1 and Eq. 5.15, we can write:

$$\phi = \frac{2f_c^{\mathrm{H}}/\mathrm{e}^{-M}}{\left|\exp\left(-2\pi i\,\frac{D_1^{\mathrm{H}}}{d_{\mathrm{H}}}\right)+\exp\left(-2\pi i\,\frac{D_2^{\mathrm{H}}}{d_{\mathrm{H}}}\right)\right|}\,.$$

The result for ϕ would be larger if more positions were considered.

As mentioned in Section 2.5, the Debye-Waller factor for the overlayer atoms are assumed to have the same value as that for the bulk atoms. If this is not the case, our results would have to be modified: the main effect would be an increase of the values for ϕ and $(y_1 - y_2)$. To get a quantitative idea of the extent of those changes, consider a value for the Bi Debye-Waller factor for the (220) reflection of 0.92 instead of 1. The new value for the order parameter would be 0.70 (in contrast to 0.65), and for $(y_1 - y_2)$ would be 1.88 Å (in contrast to 1.84 Å). The result for the Bi-Bi distance would be 2.75 Å (in contrast to 2.72 Å). The small dependence of the structure results on the Debye-Waller factor is because it is partially absorbed by ϕ in Eqs. 2.5. The factor e^{-M} is not completely incorporated in ϕ because of the nonlinearity of Eq. 2.7.

References

1 A. Herrera-Gómez, T. Kendelewicz, J.C. Woicik, K. Miyano, P. Pianetta, S. Southworth, P.L. Cowan, B.A. Karlin, and W.E. Spicer. "Determination of the geometrical configuration of Bi on GaAs (110) by X-ray standing wave triangulation." Journal of Vacuum Science and Technology A **11**, p. 2354 (1993).

2 W.K. Ford, T. Guo, D.L Lessor, and C.B. Duke. "Dynamical low-energy electron-diffraction analysis of bismuth and antimony epitaxy on GaAs(110)." Physical Review B **42**, p. 8952 (1990).

3 A.M. Bowler, J.C. Hermanson, J.P. LaFemina, C.B. Duke. "Surface atomic structure and bonding of GaAs(110)-p(1×1)—Bi (1 ML)." Journal of Vacuum Science and Technology B **10**, p. 1953 (1992).

4 K.E. Miyano, T. Kendelewicz, J.C. Woicik, P.L. Cowan, C.E. Bouldin, B.A. Karlin, P. Pianetta, and W.E. Spicer. "Structural characterization of the (1 monolayer Sb)/GaP(110) interface using X-ray standing waves." Physical Review B **46**, No. 11, p. 6869 (1992).

5 A.B. McLean, R.M. Feenstra, A. Taleb-Ibrahimi, and R. Ludeke. "Electronic and structural properties of a discommensurate monolayer system: GaAs(110)-(1×1) Bi." Physical Review B **39**, p. 12925 (1989).

			Configuration			
			Chapter 3		Back-Reflection	Nondispersive
			Surface #1	Surface #2	Surface #3	Surface #4
Bismuth (4d)	(220)	D_c	0.24±0.02	0.27±0.02		
		f_c	0.64±0.07	0.65±0.08		
		Peak (eV)	3104	3104		
	(111)	D_c	0.1±0.03	0.11±0.03		0.09±0.03
		f_c	0.37±0.06	0.51±0.08		0.33±0.04
		Peak (eV)	2346	2335		2364
	$(11\bar{1})$	D_c	0.06±0.03	0.07±0.04	0.06±0.03	
		f_c	0.31±0.05	0.29±0.06	0.30±0.0	
		Peak (eV)	2290	2288	1900	
Bulk Arsenic (LMM)	$(11\bar{1})$	D_c	0.123±0.03	0.142±0.02	0.141±0.02	
		f_c	0.84±0.16	0.89±0.12	0.85±0.09	
		Peak (eV)	2290	2288	1900	

Table 6.1. Bismuth XSW experiments performed on the Bi/GaAs interface, and results from the fits.

	XSW (First Set)	XSW (Second Set)	LEED (ECLS)	TBTE (ECLS)	TBTE (EOTS)
ϕ	0.65±0.08	0.70±0.14			
$\frac{z_1+z_2}{2}$ (Å)	0.47±0.04	0.53±0.04	0.52	0.56±0.2	0.82±0.2
$\frac{y_1+y_2}{2}$ (Å)	0.12±0.17	0.11±0.20	-0.16	−0.05±0.2 * 1.41 **	−3.04±0.2
$z_1 - z_2$ (Å)	-0.09±0.2	-0.24±0.2	-0.09	-0.11±0.2	+0.10±0.2
$y_1 - y_2$ (Å)	1.84±0.3	1.70±0.3	1.98	2.49±0.2	2.49±0.2
Bi-Bi (Å)	2.72±0.2	2.63±0.3	2.87	3.2	3.2

* Using reported bond length and angles.

** Using reported value of $d_{12,y}$. The discrepancy goes away if the definition of $d_{12,y}$ is changed by a/4 in Fig. 1(a) of reference [3].

Table 6.2 Bismuth coordinates determined by the XSW data. Results from other studies are also shown.

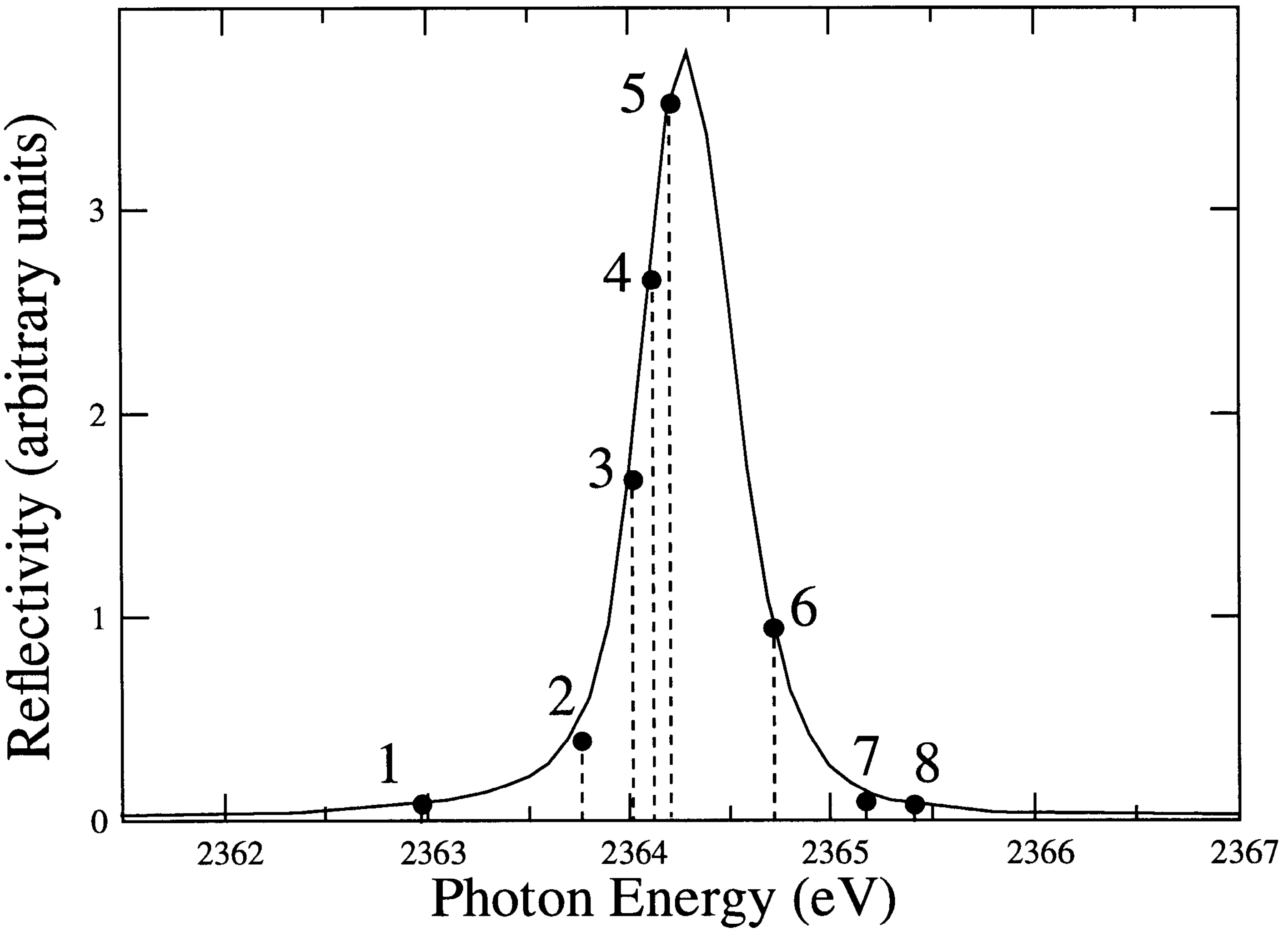

Figure 6.1. Experimental reflectivity of the (111) reflection of GaAs. Photoemission Bi 4d data were obtained for the energies corresponding to the points. The height of the points corresponds to the strength of the reflectivity, which was also recorded as the photoemission spectra were collected.

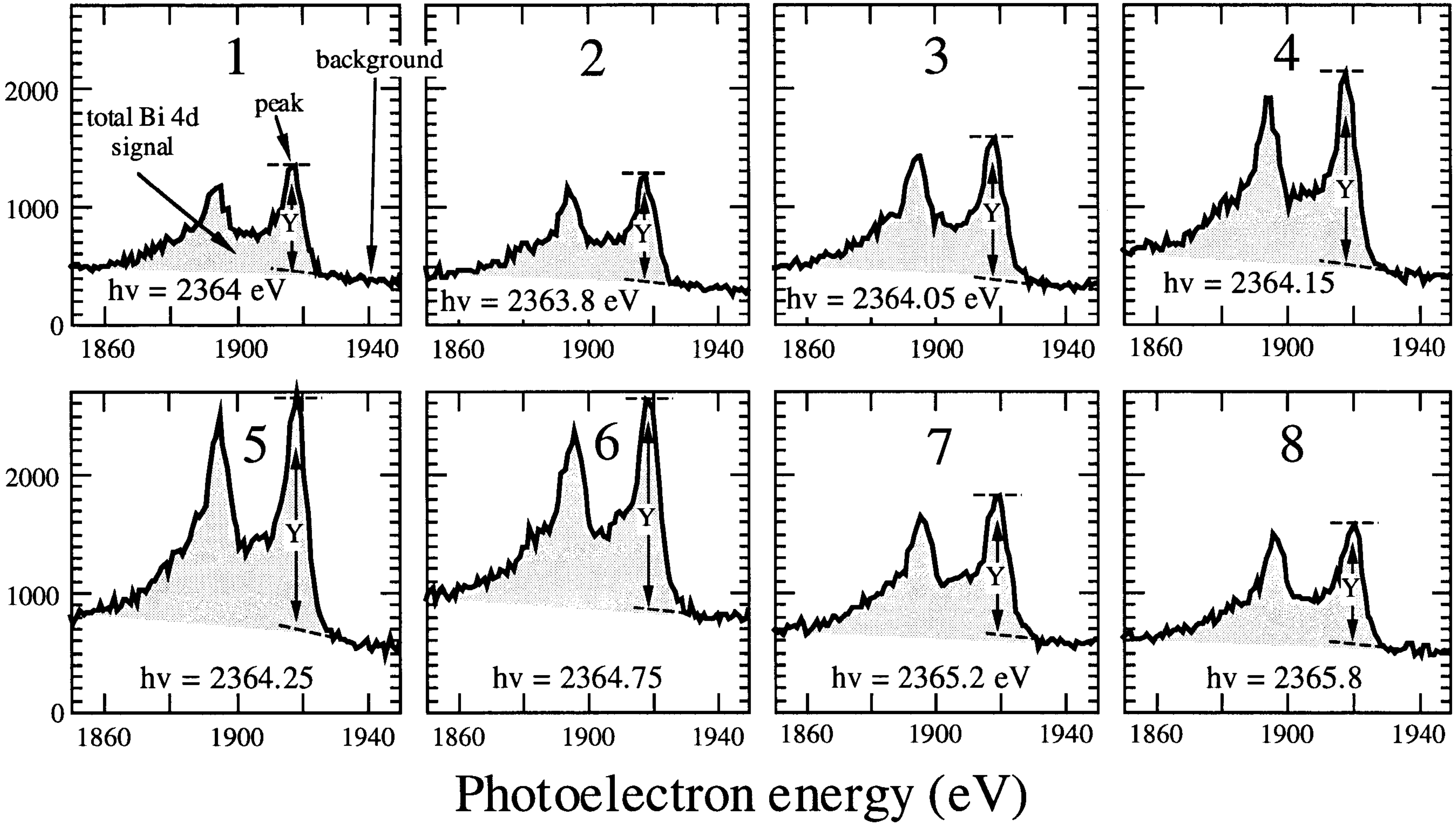

Figure 6.2. Bismuth 4d photoemission curves for one monolayer of Bi on GaAs. The photon energies are around the (111) GaAs Bragg condition, and correspond to the dots of Fig. 6.1. The difference (Y) between the photoemission yield from the peak (see spectrum #1) and the background on which it rides is proportional to the total Bi 4d signal. As can be seen, the background yield also has a modulation.

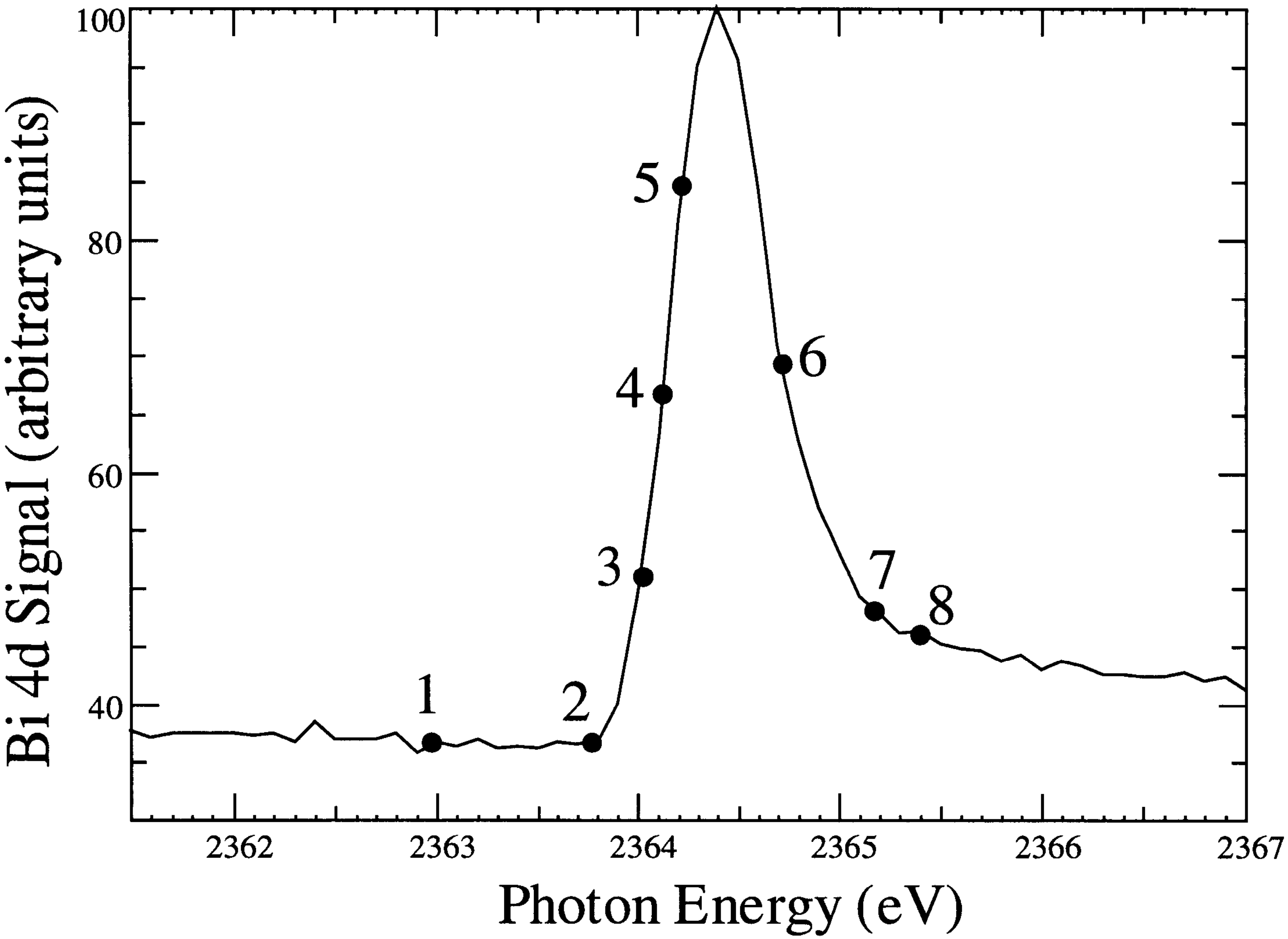

Figure 6.3. Bismuth 4d signal (Y) as the photon energy is scanned through the Bragg condition. As described in Fig. 6.2, Y is obtained by subtracting the photoemission yield of the background from the main peak. The dots correspond to the photon energies and heights (Y) of the photoemission spectra of Fig. 6.2.

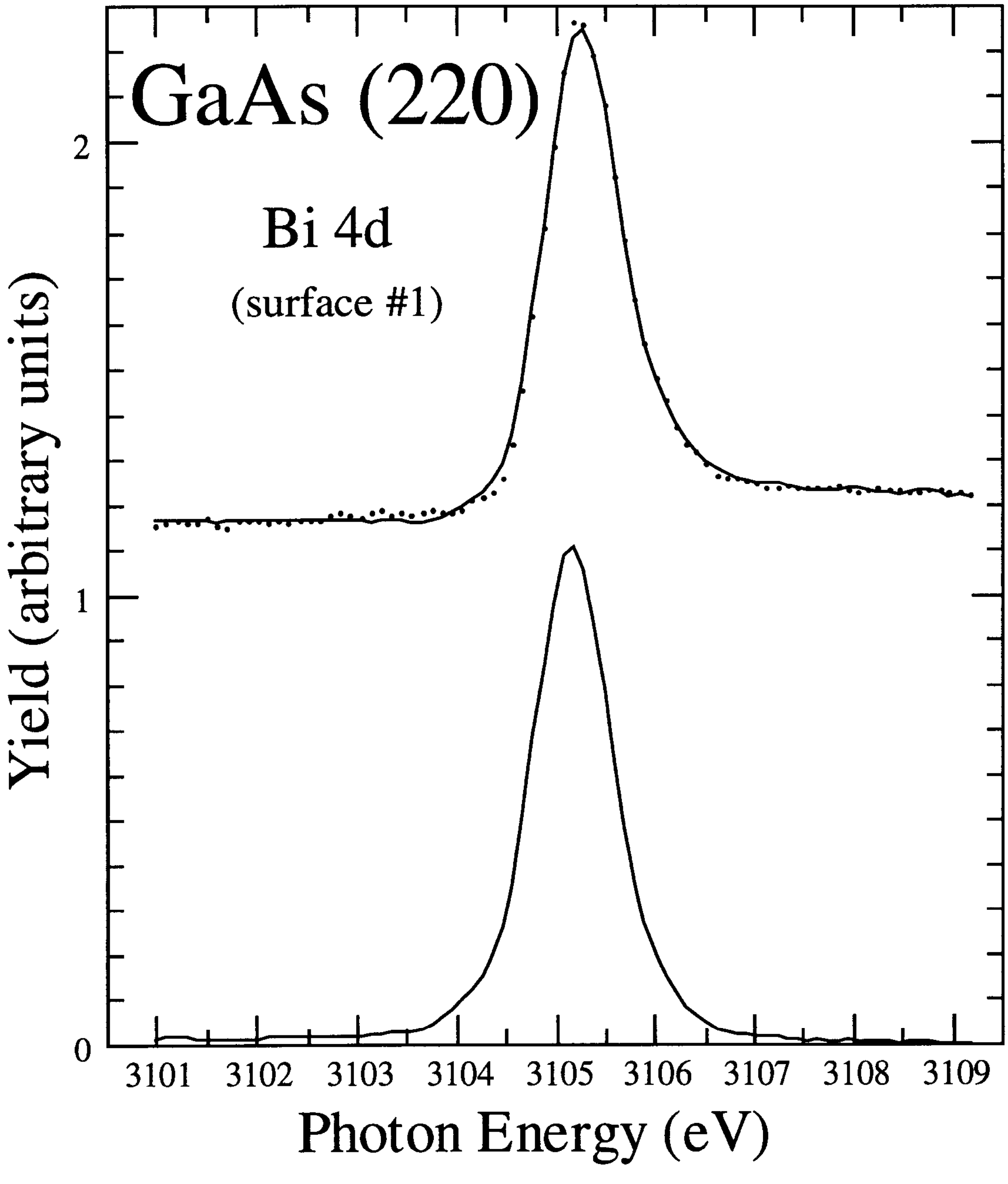

Figure 6.4. Bismuth 4d XSW data and theoretical fit for the (220) reflection of GaAs in the back-reflection configuration. The bottom curve is the reflectivity.

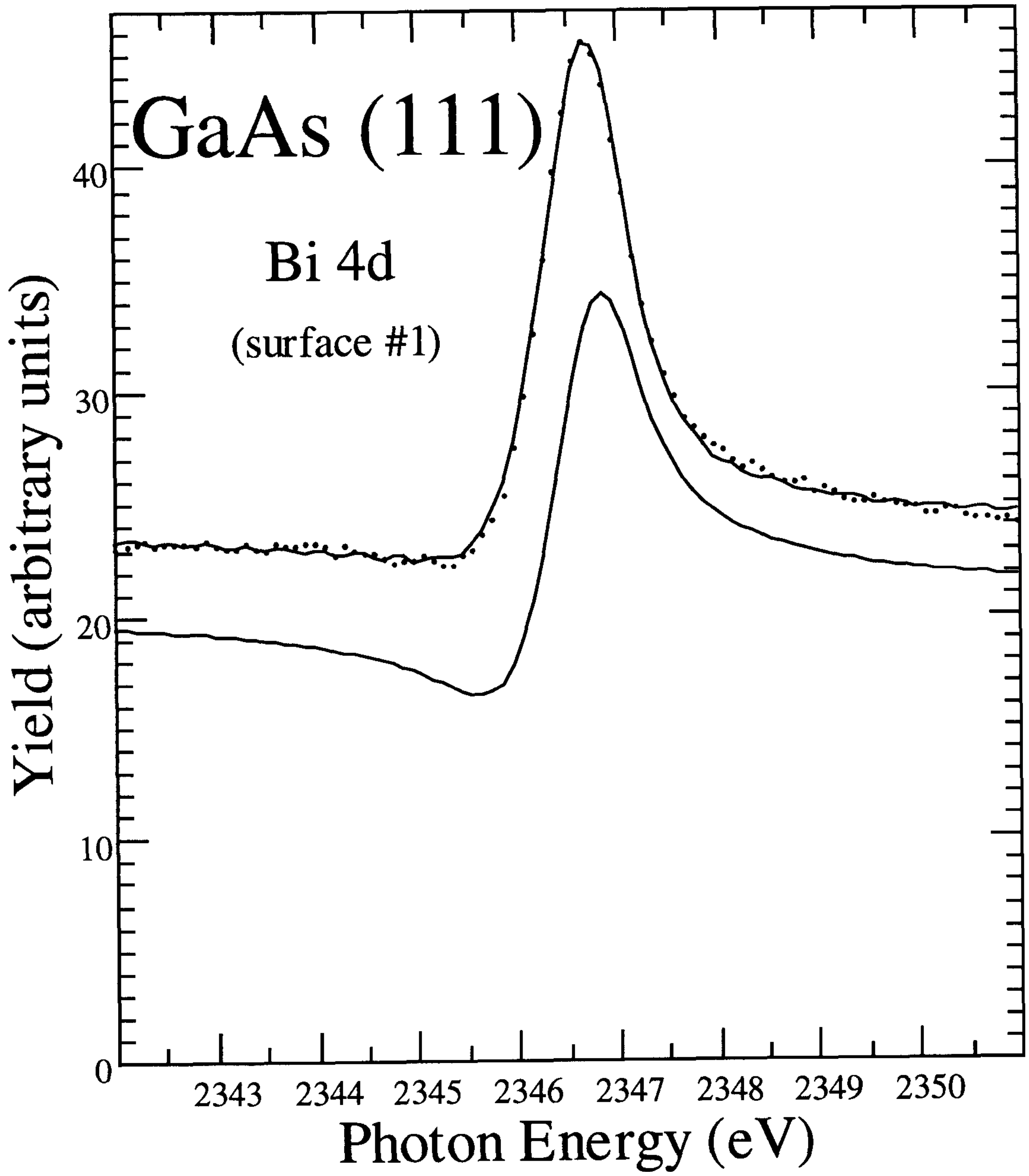

Figure 6.5. Bismuth 4d XSW data and theoretical fit for the (111) reflection of GaAs in the nonsymmetric configuration. The bottom curve is the total yield.

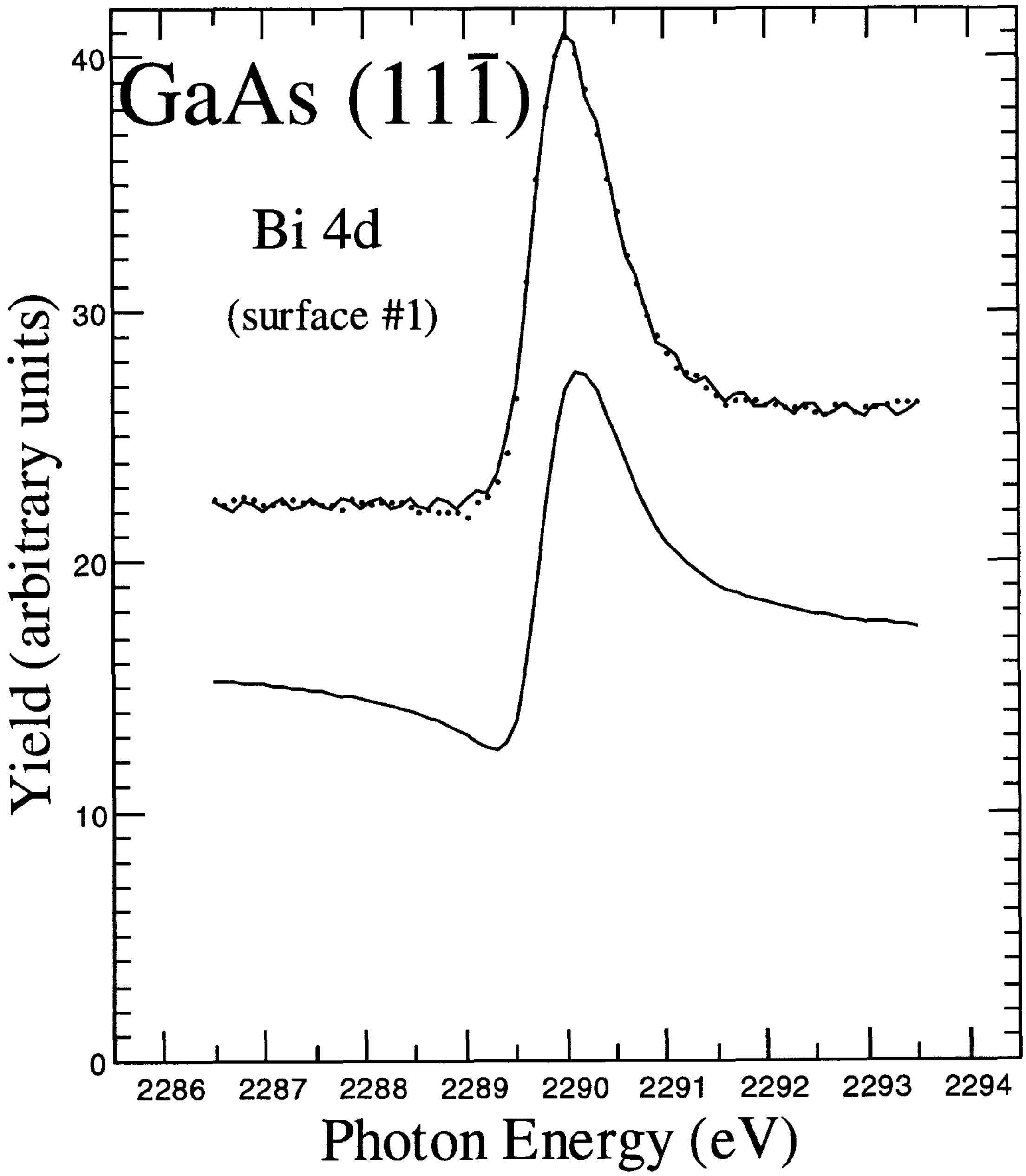

Figure 6.6. Bismuth 4d XSW data and theoretical fit for the (11$\bar{1}$) reflection of GaAs in the nonsymmetric configuration. The bottom curve is the total yield.

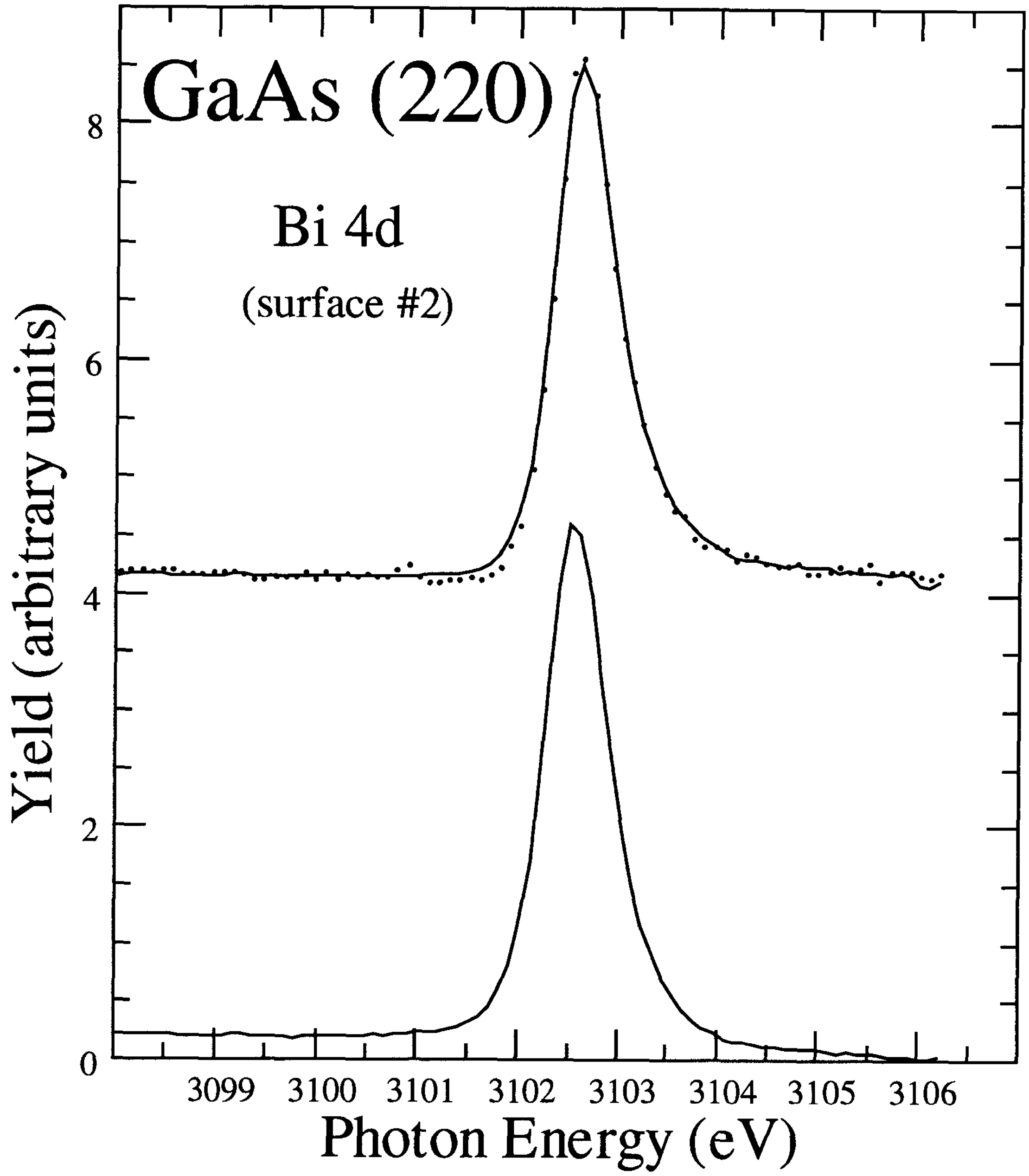

Figure 6.7. Bismuth 4d XSW data and theoretical fit for the (220) reflection of GaAs in the back-reflection configuration. The data correspond to surface #2 of Table 6.1. The bottom curve is the reflectivity.

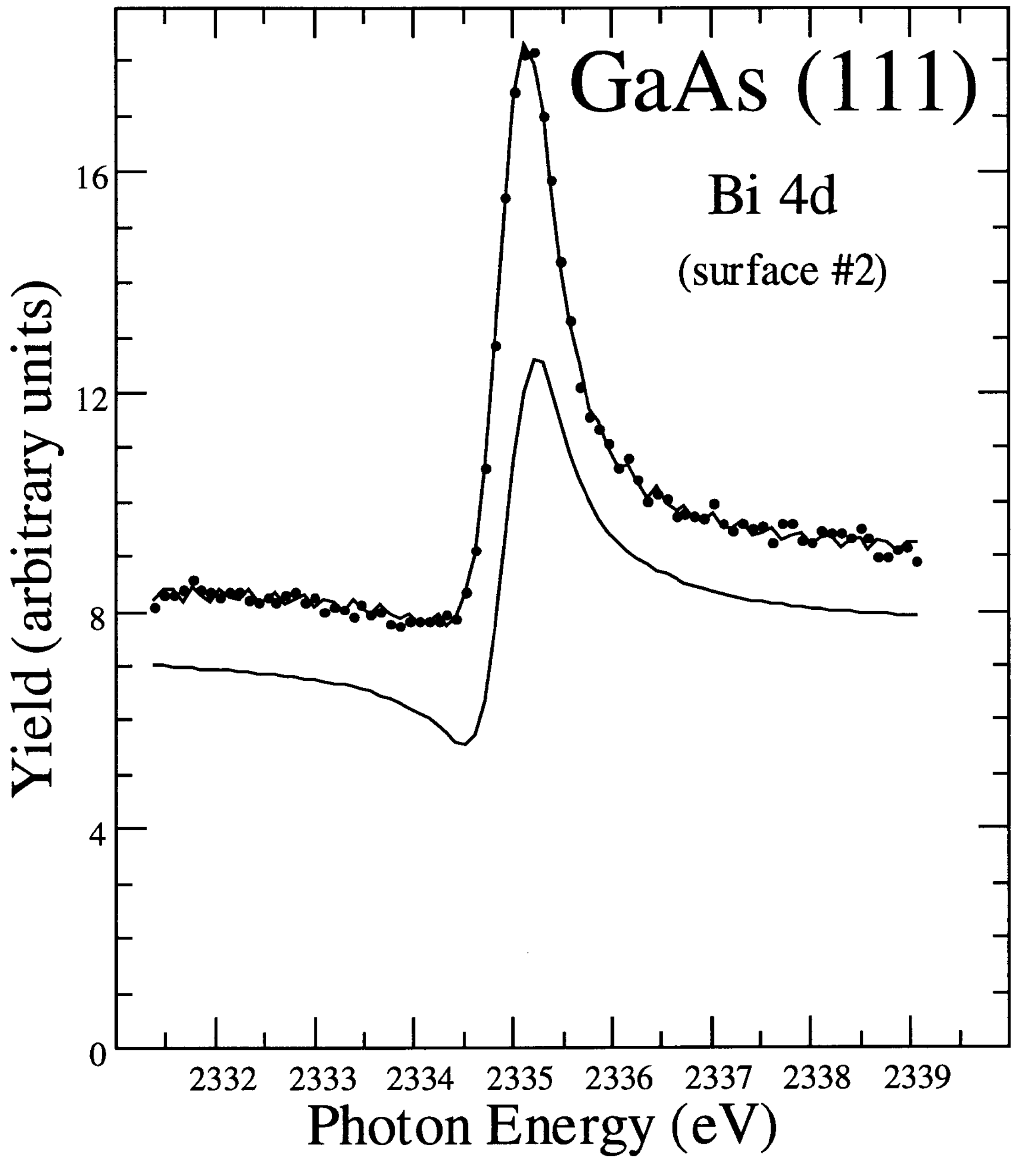

Figure 6.8. Bismuth 4d XSW data and theoretical fit for the (111) reflection of GaAs in the nonsymmetric configuration. The data correspond to surface #2 of Table 6.1. The bottom curve is the total yield.

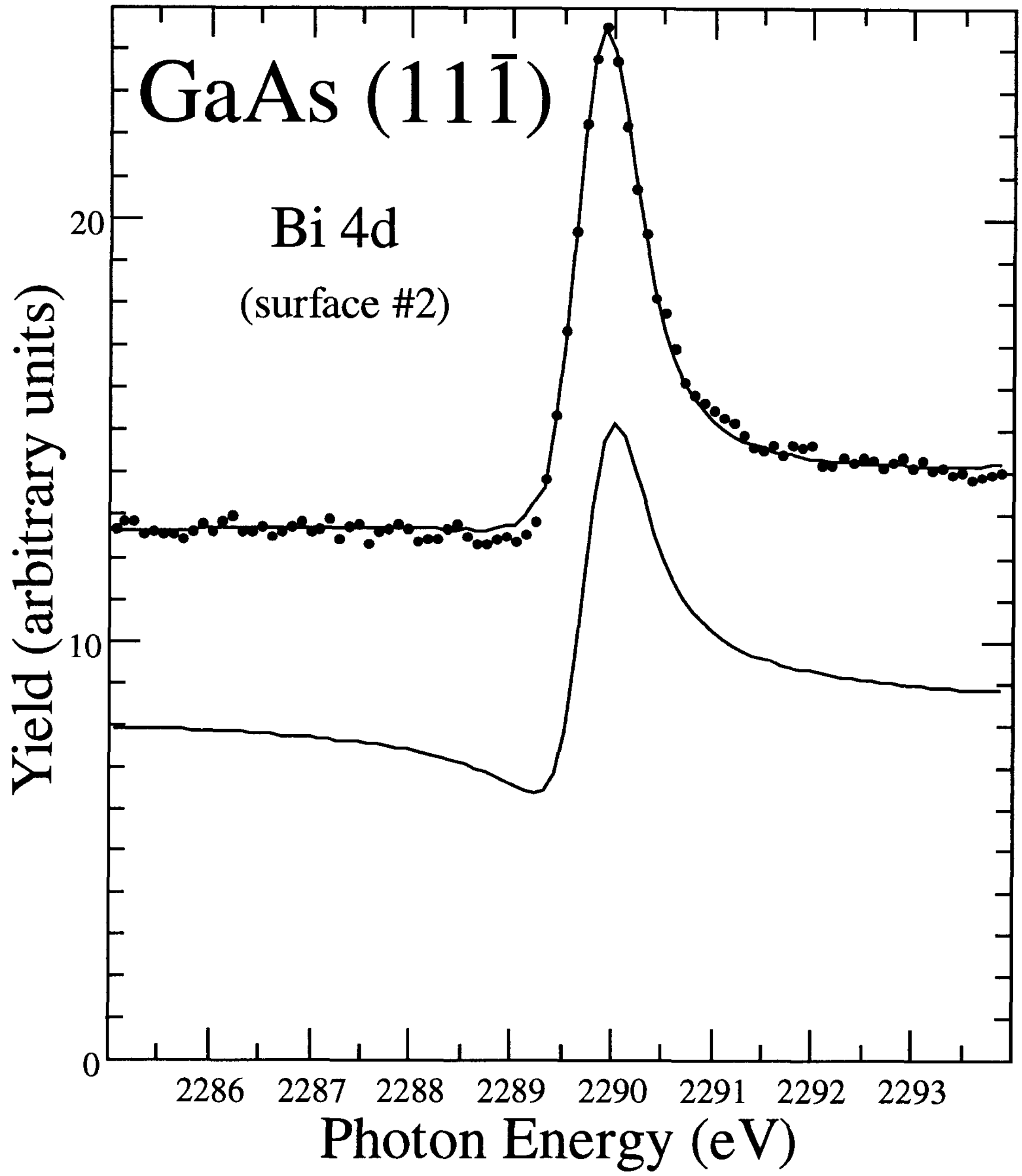

Figure 6.9. Bismuth 4d XSW data and theoretical fit for the (11$\bar{1}$) reflection of GaAs in the nonsymmetric configuration. The data correspond to surface #2 of Table 6.1. The bottom curve is the total yield.

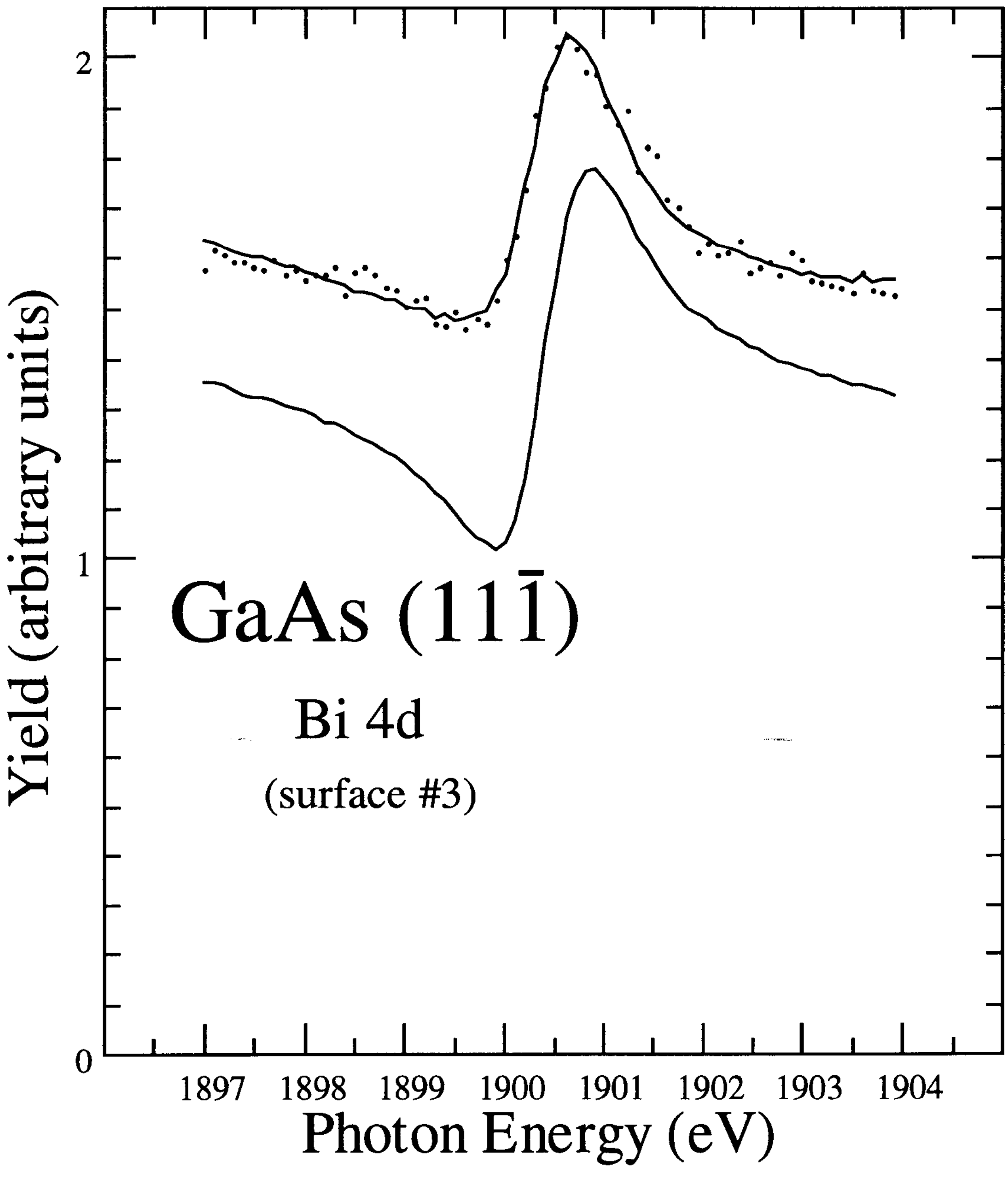

Figure 6.10. Bismuth 4d XSW data and theoretical fit for the (11$\bar{1}$) reflection of GaAs in the back-reflection configuration. The data correspond to surface #3 of Table 6.1. The bottom curve is the total yield.

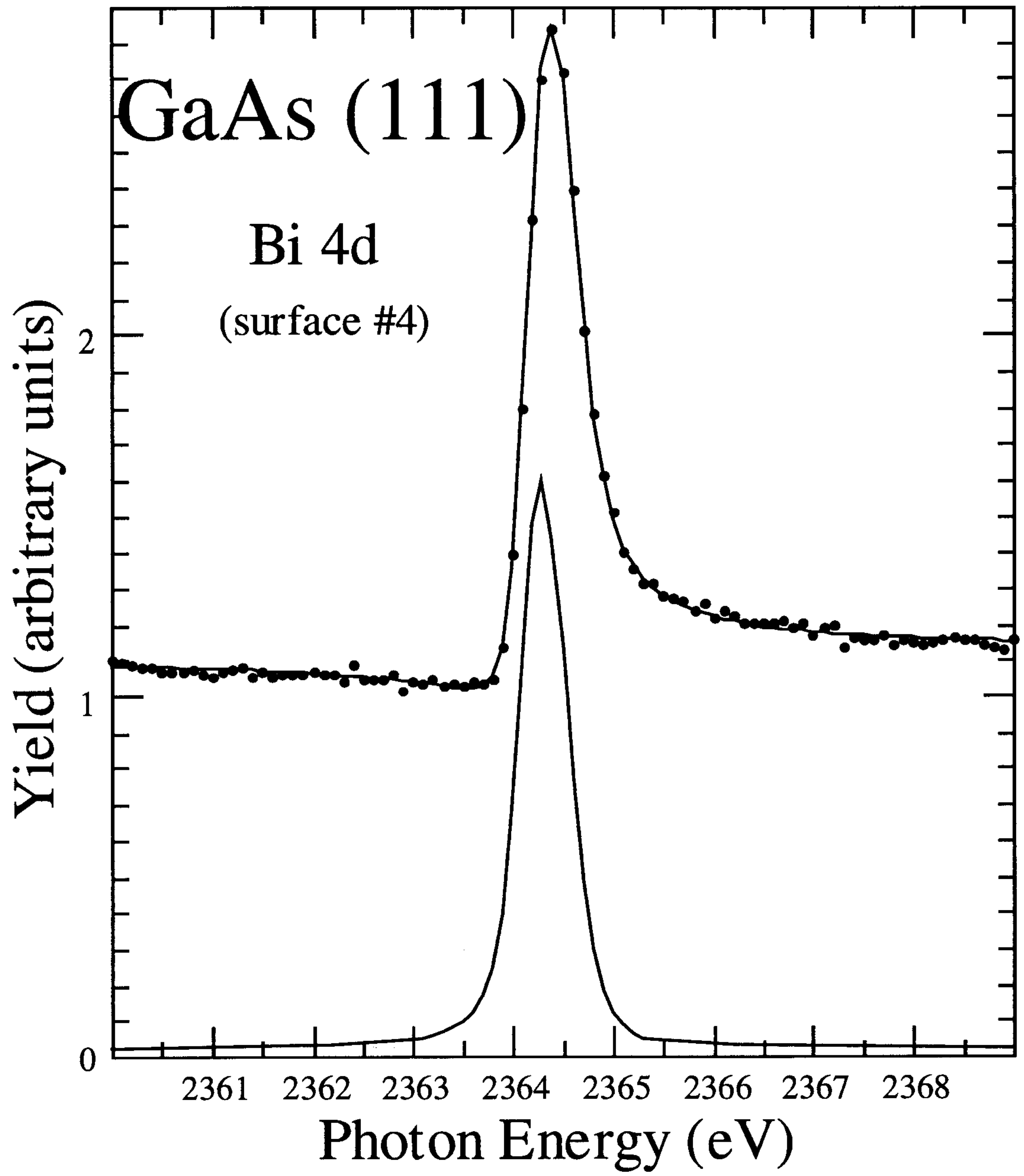

Figure 6.11. Bismuth 4d XSW data and theoretical fit for the (111) reflection of GaAs in the nondispersive configuration described in Chapter 8. The data correspond to surface #4 of Table 6.1. The bottom curve is the reflectivity.

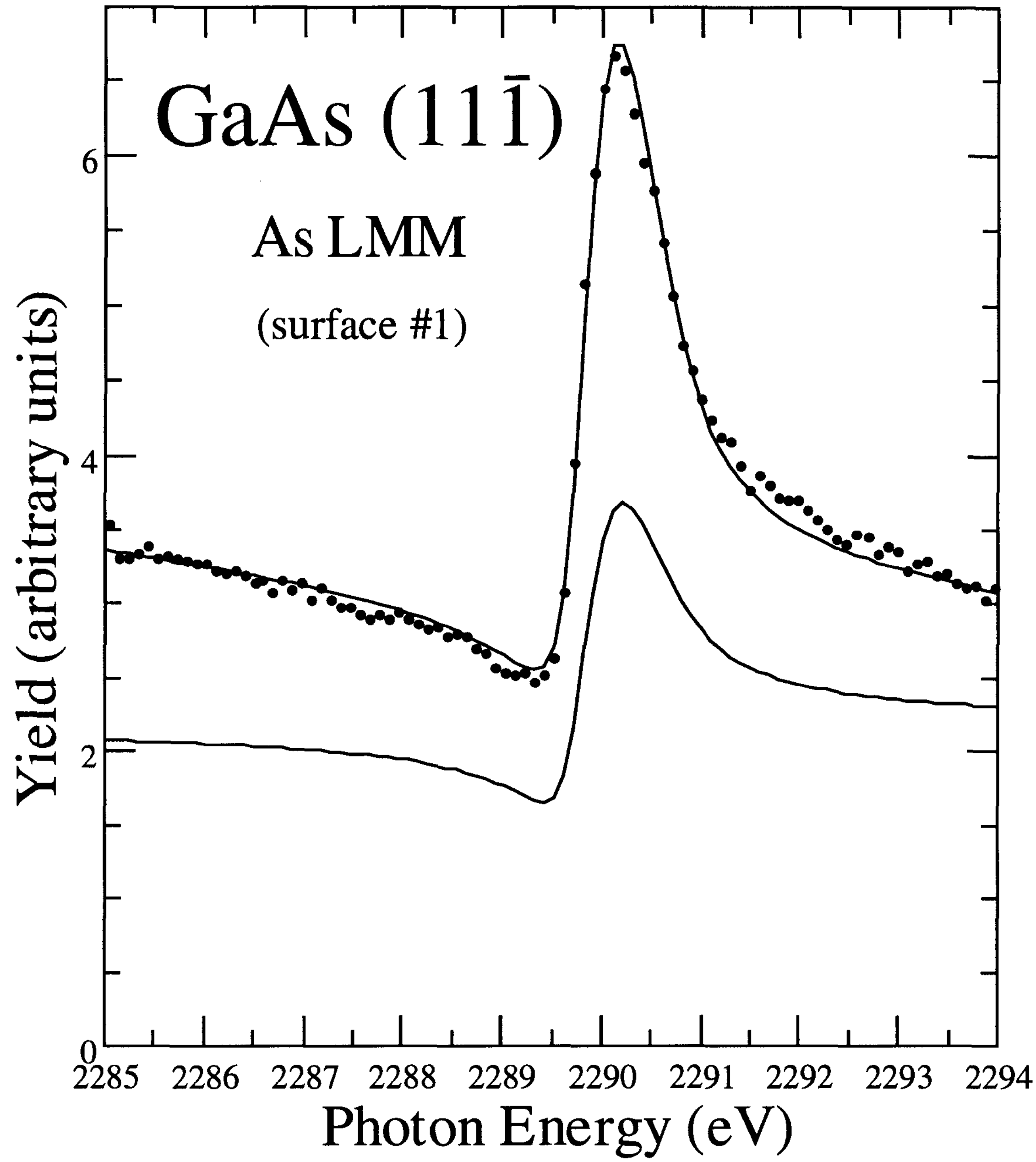

Figure 6.12. Arsenic LMM XSW data and theoretical fit for the (11$\bar{1}$) reflection of GaAs in the nonsymmetric configuration. The data correspond to surface #1 of Table 6.1. The bottom curve is the total yield.

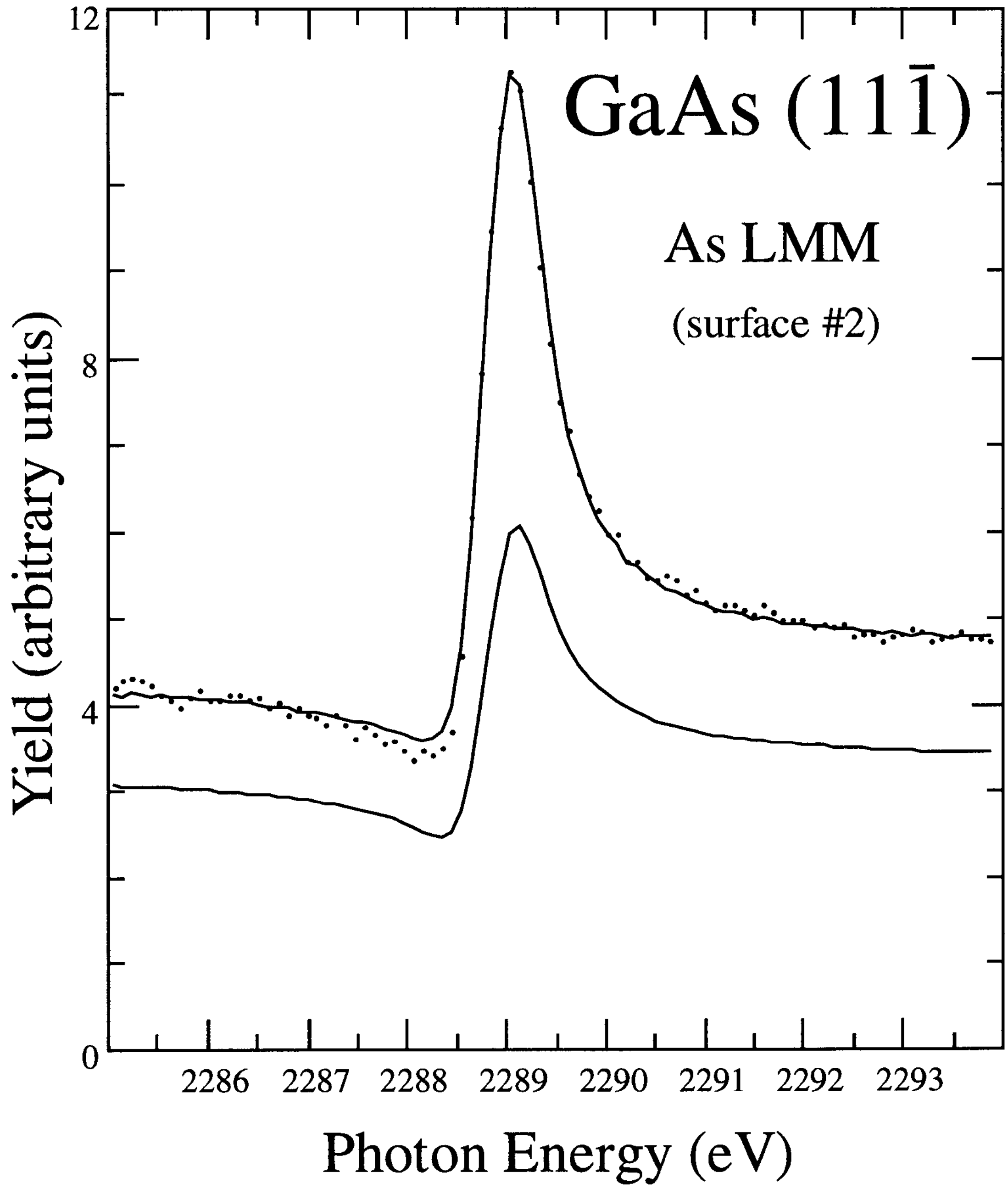

Figure 6.13. Arsenic LMM XSW data and theoretical fit for the (11$\bar{1}$) reflection of GaAs in the nonsymmetric configuration. The data correspond to surface #2 of Table 6.1. The bottom curve is the total yield.

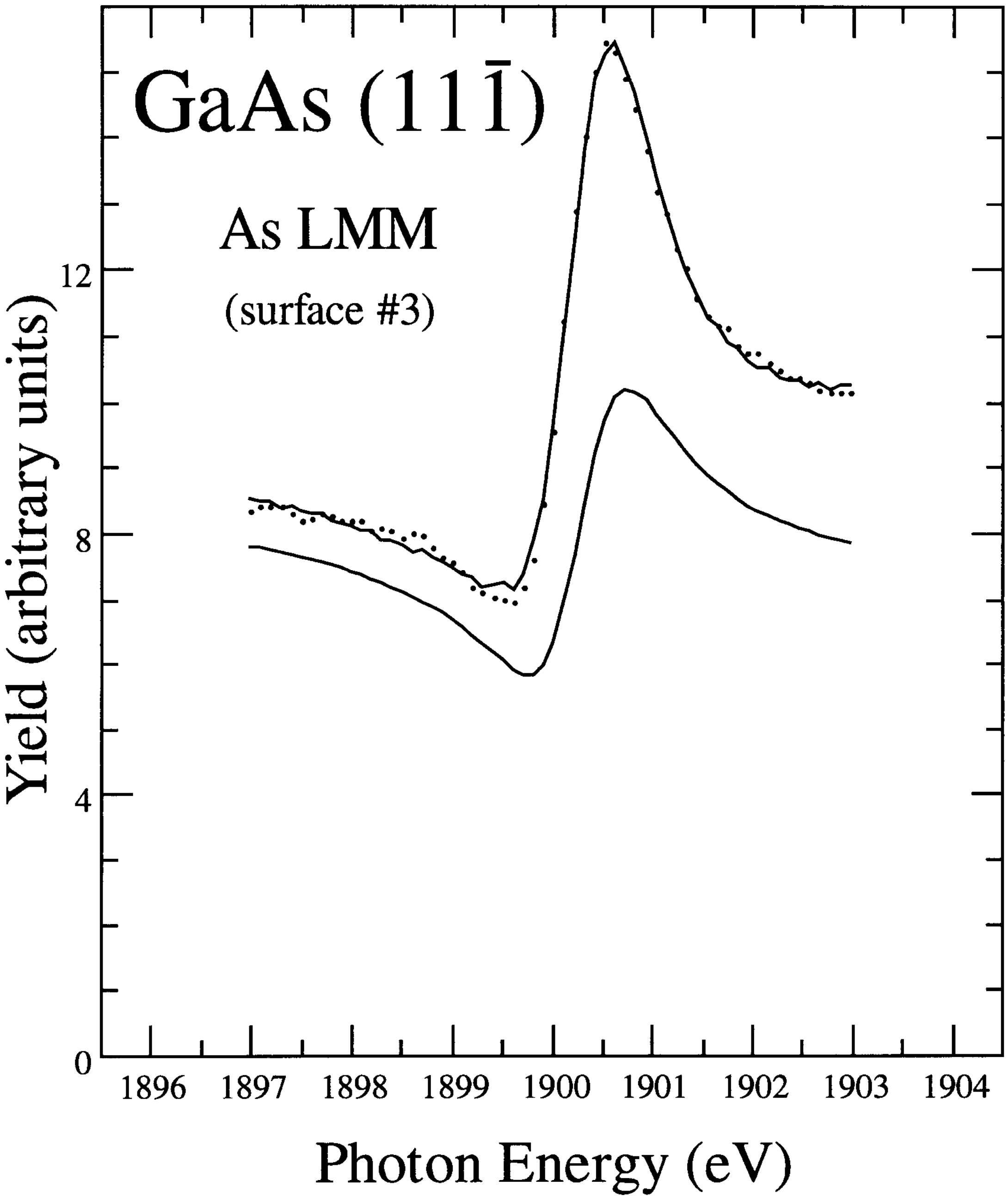

Figure 6.14. Arsenic LMM XSW data and theoretical fit for the (11$\bar{1}$) reflection of GaAs in the back-reflection configuration. The data correspond to surface #3 of Table 6.1. The bottom curve is the total yield.

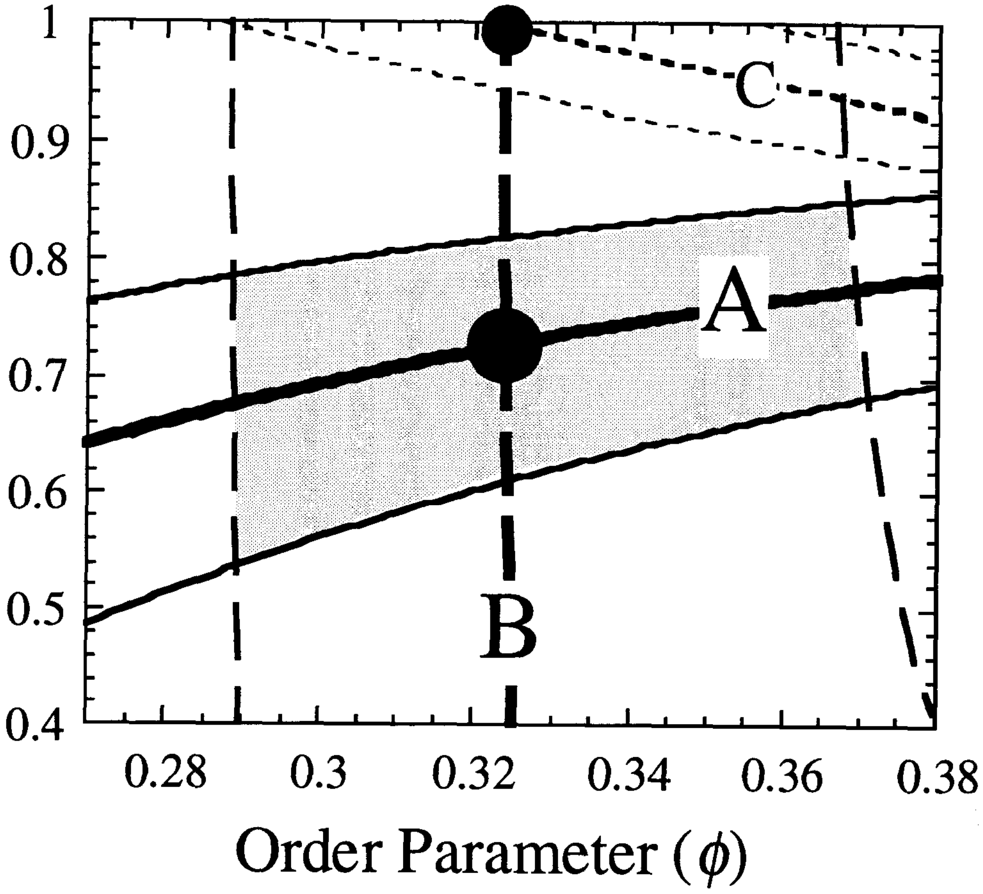

Figure 6.15. Graphical solution of Eqs. 6.2.

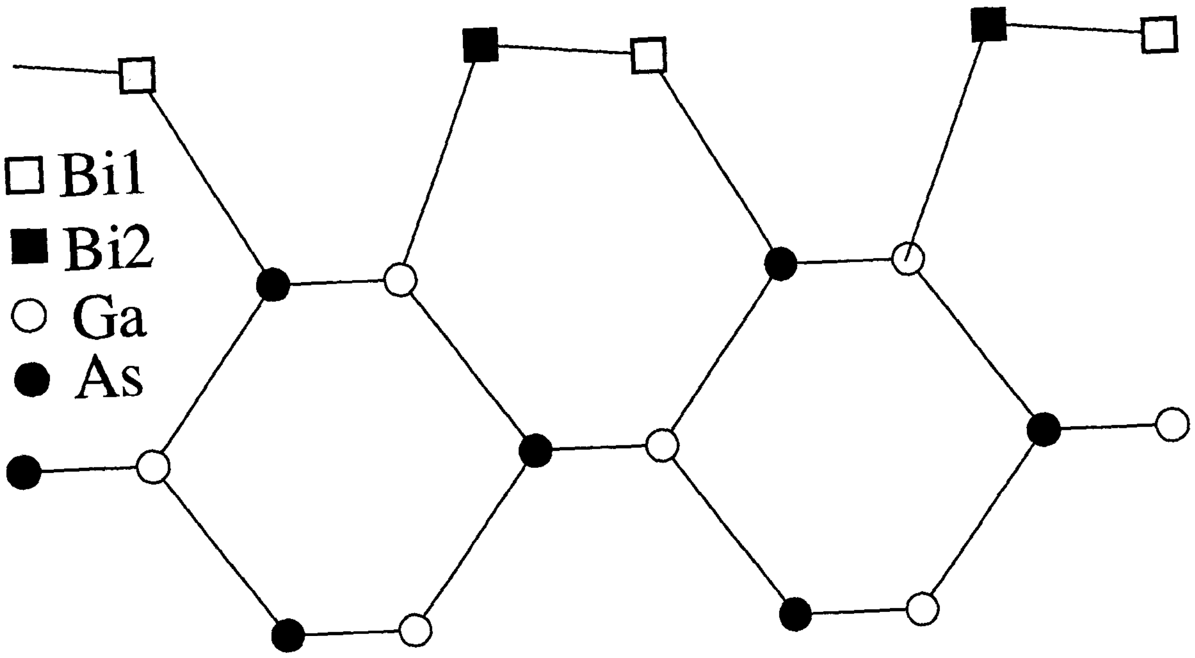

Figure 6.16. Position of the Bi atoms on the GaAs surface scaled to our results.

Chapter 7. Results of the Bi/GaP Experiments

The experimental and theoretical methodology developed in the former chapters was applied to determine the geometrical structure of the system formed by one monolayer of Bi on the (110) GaP cleaved surface.

7.1 Experiments performed

One complete set of (220), (111), and $(11\bar{1})$ XSW experiments was performed on a single surface, using the experimental setup and configurations described in Chapter 3. An extra (111) reflection was performed on another surface, using a back reflection mode with InSb (111) crystals in the monochromator; the Bi signal was obtained by monitoring the Bi 4d photoemission yield.

7.2 Data and fits

The averaging of the data was done as described in Section 6.2. Figures 7.1 to 7.4 show the experimental data together with its theoretical fit. The fittings were done with the deconvolution method presented in Section 5.2. The reflectivity or the total yield is also plotted with the data depending on which one was used in the fitting calculations (not both the reflectivity and the total yield were recorded in all the reflections). As it can be seen, the quality of the fits is excellent. The extracted values for the coherent distance and coherent fraction for all the reflections performed are displayed in Table 7.1. The coherent distances are in units of the corresponding interplanar distance d_H. The origin used is shown in Fig. 2.1. The uncertainties are chosen to be those changes that will produce twice the value of the minimum χ^2.

As seen in Table 7.1, the reproducibility of the coherent distance for the (111) reflection, which was the only one measured twice on different samples, is excellent. The reproducibility of the coherent fraction is also within a few percent, although some variation is expected from surface to surface for the reasons discussed in Section 6.4.

7.3 The failure of the two-site model consistency check

As discussed in Section 2.6, the method employed provides a consistency check for the two-site approximation (see Eq. 2.8 or Eq. 6.1) that is basically the proper triangulation of the average distance to the three Bragg planes. From Table 7.1, it can be seen that this consistency check is failed by Bi on GaP by 19%, which is beyond the experimental error.

This implies that the two-site model is too simplistic to describe the structure of the overlayer. The presence of more than two sites is a consequence of the break of the symmetry by the vacancies. The Bi atoms at the edge and center of the chains take positions that cannot be approximated as equivalent.

The degree of failure of the consistency check (19%) is probably a good estimation of the nonequivalence among the Bi atoms in a chain. A more precise interpretation would require considering a model with at least four sites.

As mentioned in Section 2.6, there are other extrinsic consistency checks, such as the Bi–Bi bond length. Our result for the Bi–Bi bond length is 2.31±0.32 Å, which is well short of the expected value of 2.92 Å (its covalent radius is 1.46 Å [1]). This difference cannot be explained by the expansion of the chains with respect to the substrate found by the STM study [2], which sees an approximately 7% lack of registry. The failure of the Bi–Bi bond length consistency check is not surprising because, as has been shown, the two-site model cannot correctly describe the structure.

7.4 ECLS versus EOTS

Even though the Bi/GaAs system cannot be described with two sites, it is of interest to establish which one of the two-site structural models proposed by the TBTE calculations is closer to the actual geometry. The Bi atomic positions for the ECLS and EOTS models are shown in Fig. 7.5. Also displayed are the (220), (111), and $(11\bar{1})$ Bragg planes, so the position of the adatoms with respect to these planes can be clearly appreciated.

The average position (see Fig. 7.5) for ECLS is much closer to the origin than that for EOTS (the origin was set at the intersection of the atomic planes, see Fig. 2.1). Atomic coordinates for the ECLS and EOTS were estimated using as bond lengths the sum of covalent radii. The corresponding coherent fraction and coherent distance for each reflection were calculated using Eqs. 2.4 and 2.5, and are displayed in Table 7.1. From the values of the coherent distance, EOTS can be discarded right away. For the same reason, the p^3 and EOCS structures, which are also considered in references [3, 4], can be dismissed.

The experimental results also have a serious disagreement with ECLS, the only candidate left alive. The tilt for ECLS is such that the adatom bonded to Ga is higher than the one bonded to P (see Fig. 7.5). However, the fact that the $(11\bar{1})$ experimental coherent fraction is larger than that for the (111) reflection (beyond the experimental error) indicates a tilt in the opposite direction (see Fig. 7.7).

7.5 Structural results

Because of the 19% failure of the self-consistency check of the two-site approximation, the structural results (see Table 7.2) that were obtained using the two-site model should be understood as qualitative. We solved for the atomic coordinates $\left(y_{1,2}, z_{1,2}\right)$ with the method described in Section 6.5. Figure 7.6 shows a graphical solution of Eqs. 6.2 for the Bi/GaP results. As in the Bi/GaAs case, the parallel curves at each side of the main curves correspond to Eq. 6.2 for the most extreme combinations of the uncertainties on the coherent fractions. The shadow region corresponds to all allowed solutions. The uncertainties for ϕ, $(z_1 - z_2)$, and $(y_1 - y_2)$ were estimated using the extremes of the shadowed region.

To the knowledge of the author, there are no other published structural studies of the Bi/GaP interface, so no comparison to other techniques will be made.

The position of the Bi sites shown in Fig. 7.7 are scaled according to our results. This figure shows that the Bi1-Bi2 tilt angle is opposite to that for the Bi/GaAs case (see Fig. 6.16).

References

1 L. Pauling, "The Nature of the Chemical Bond," Cornell University Press, Ithaca, New York (1960).

2 M. Prietsch, A. Samsavar, and R. Ludeke. "Structural and electronic properties of the Bi/GaP(110) interface." Physical Review B **43**, No. 14, p. 11850 (1991).

3 J.P. LaFemina, C.B. Duke, and C. Mailhiot. "New surface atomic structures for column V overlayers on the (110) surfaces of III-V compound semiconductors." Journal of Vacuum Science and Technology B **8**, p. 888 (1990).

4 G.P. Srivastava. "Atomic geometry, electronic states and bonding at the GaP(110)-Sb (1ML) interface." Journal of Physics: Condensed Matter **5** p. 4695, (1993).

		Complete Set	Back-Reflection	ECLS	EOTS
(220)	D_c	0.29±0.04		0.29	0.40
	f_c	0.67±0.14		0.70	0.70
	Peak (eV)	3220			
(111)	D_c	0.02±0.02	0.0±0.02	0.13	0.68
	f_c	0.46±0.04	0.38±0.04	0.37	0.27
	Peak (eV)	2410	1975		
$(11\bar{1})$	D_c	0.08±0.03		0.16	0.72
	f_c	0.61±0.08		0.28	0.37
	Peak (eV)	2430			

Table 7.1. Experiments performed and fitting results of the Bi data for the Bi/GaP surface. Also shown are the approximated coherent distance and coherent fraction expected for the ECLS and EOTS models.

ϕ	$\frac{z_1+z_2}{2}$ (Å)	$\frac{y_1+y_2}{2}$ (Å)	z_1-z_2 (Å)	y_1-y_2 (Å)	Bi–Bi (Å)
0.71±0.18	0.55±0.07	-0.15±0.15	+0.21±0.2	1.25±0.45	2.31±0.2

Table 7.2. Bi coordinates determined by the XSW results.

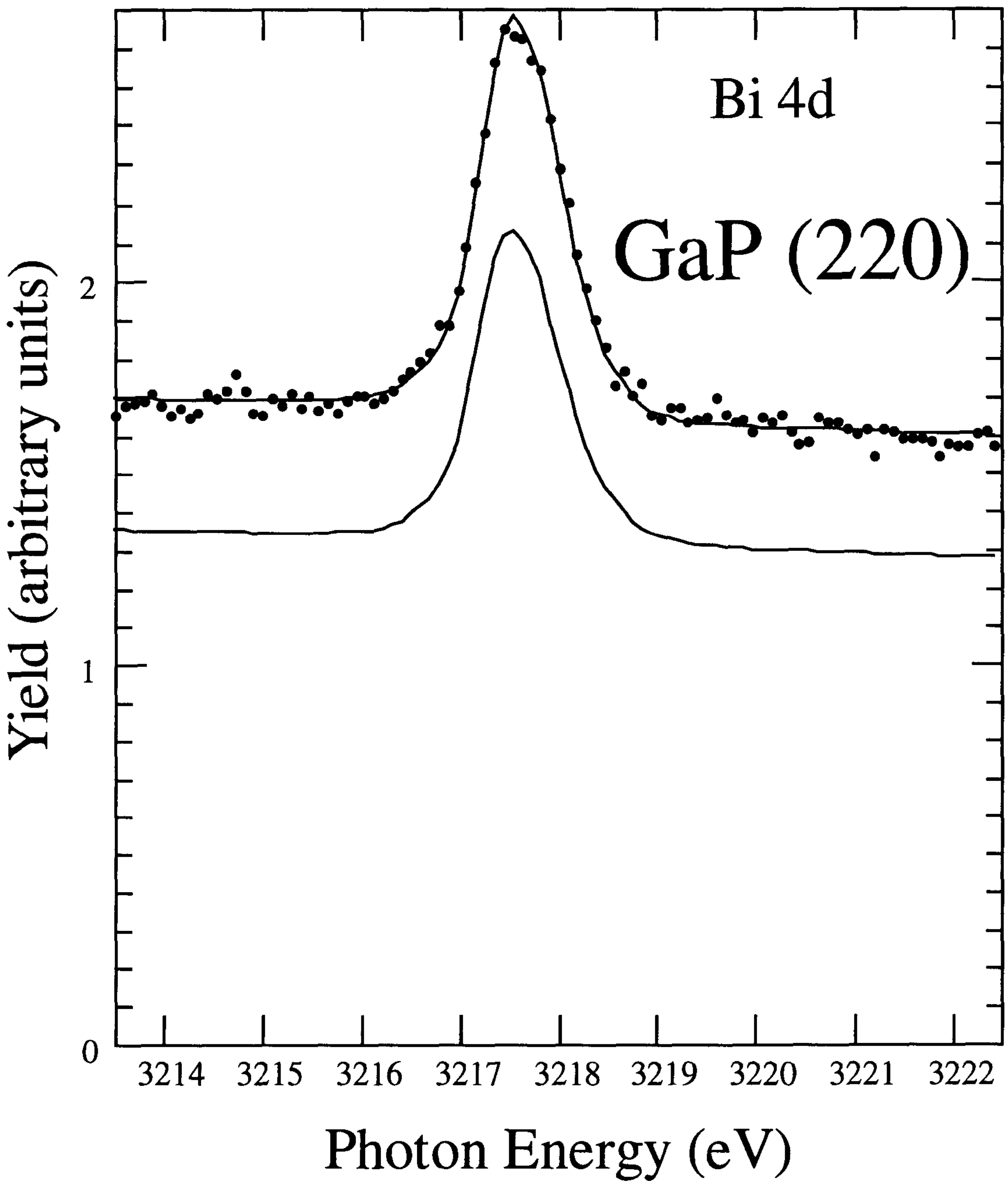

Figure 7.1. Bismuth 4d XSW data and theoretical fit for the (220) reflection of GaP in the back-reflection configuration. The bottom curve is the reflectivity.

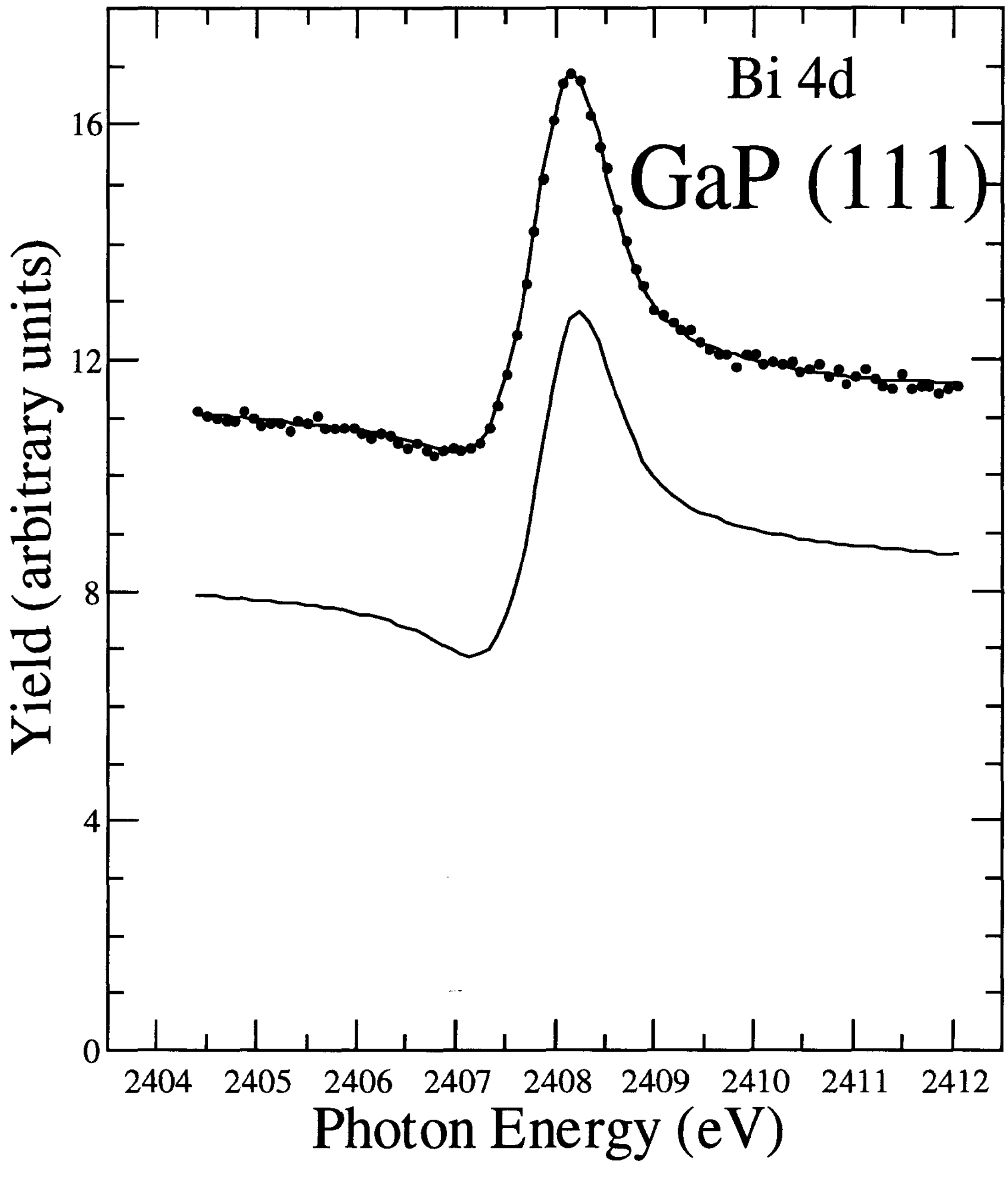

Figure 7.2. Bismuth 4d XSW data and theoretical fit for the (111) reflection of GaP in the nonsymmetric configuration. The bottom curve is the total yield.

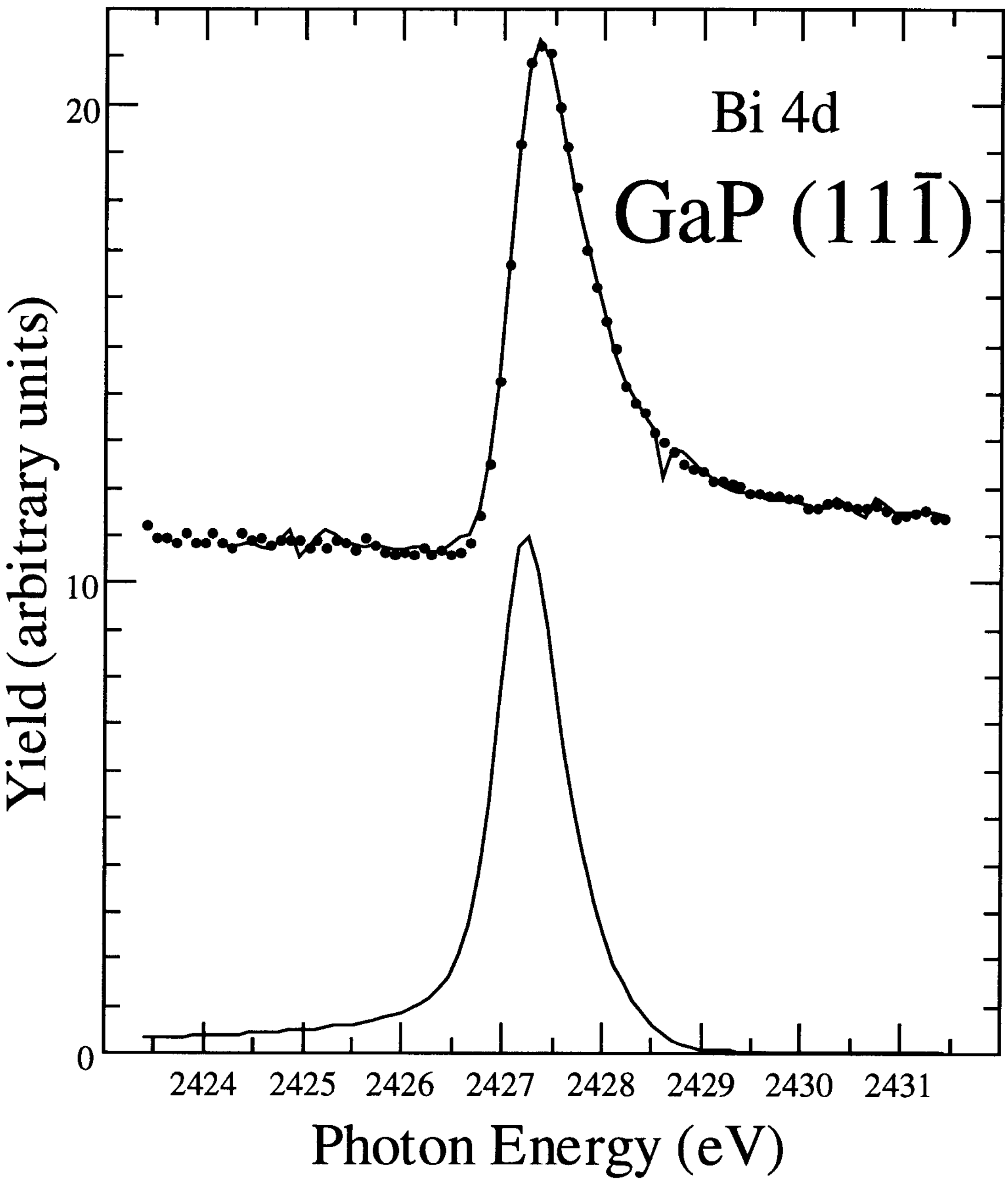

Figure 7.3. Bismuth 4d XSW data and theoretical fit for the (11$\bar{1}$) reflection of GaP in the nonsymmetric configuration. The bottom curve is the reflectivity.

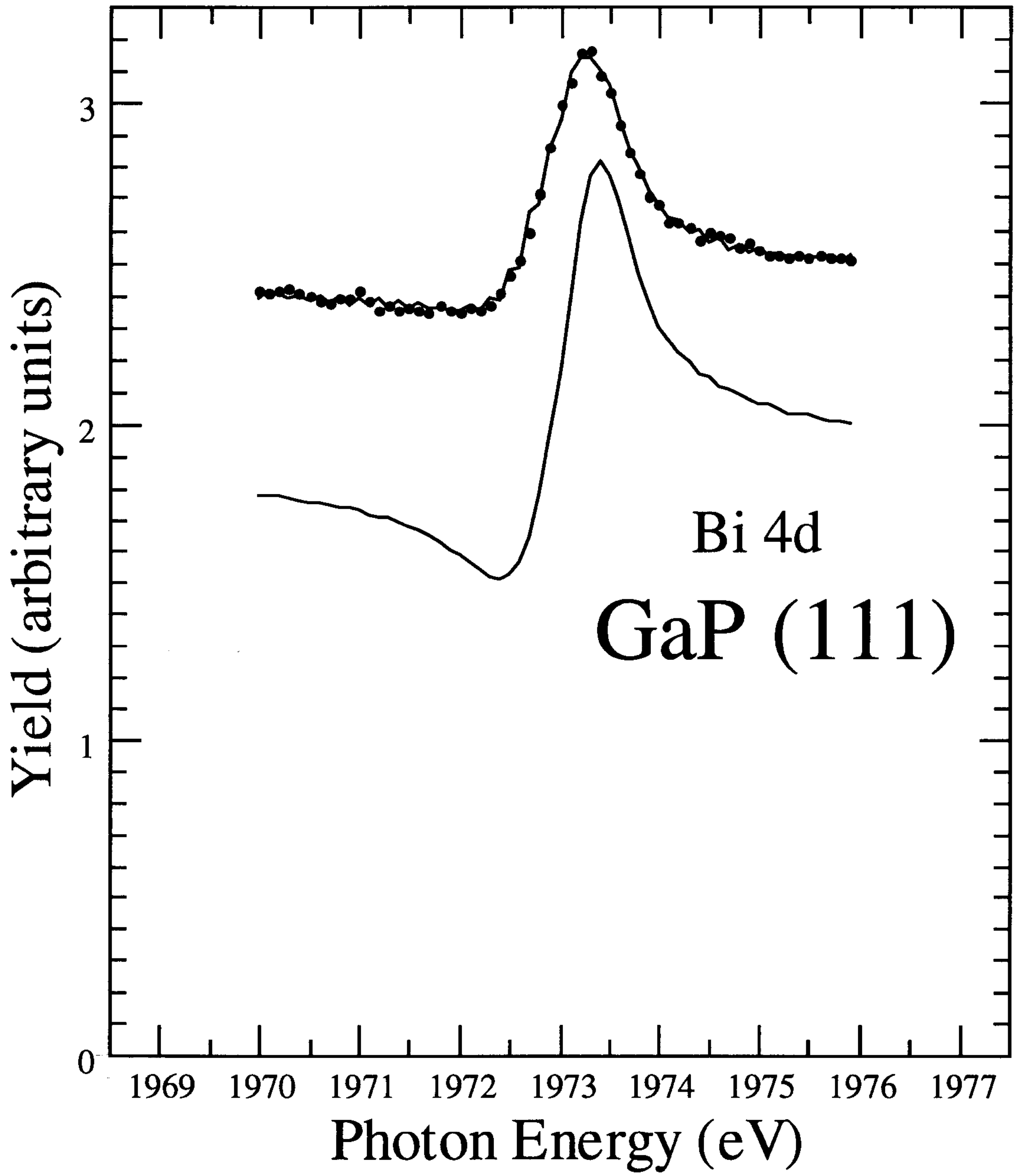

Figure 7.4. Bismuth 4d XSW data and theoretical fit for the (111) reflection of GaP in a back-reflection configuration. The bottom curve is the total yield.

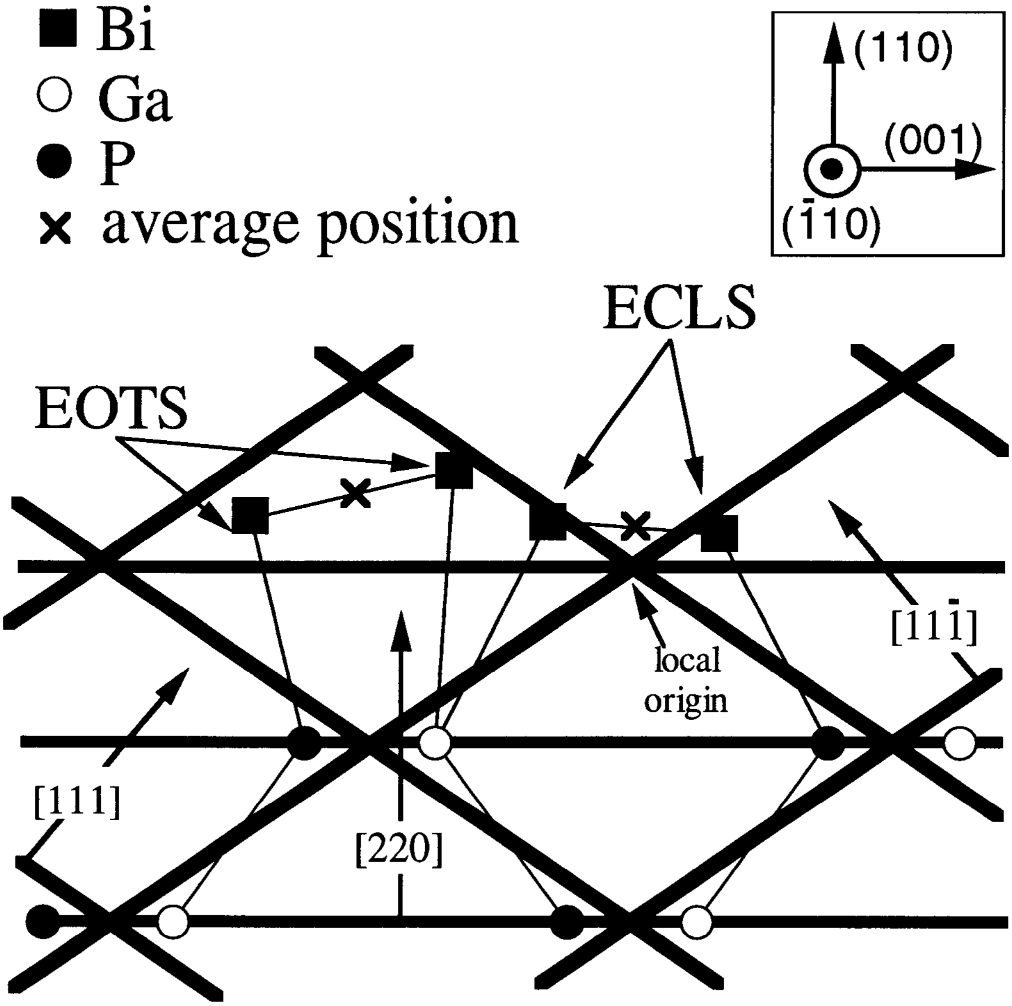

Figure 7.5. Position of the Bi atoms with respect to the (220), (111), and (11$\bar{1}$) Bragg planes for the ECLS and EOTS models. The origin is set at the intersection of the Bragg planes. As can be seen, the average adatom position for ECLS is closer to the origin for all reflections. The average position is defined as the intermediate point between nearest adatoms.

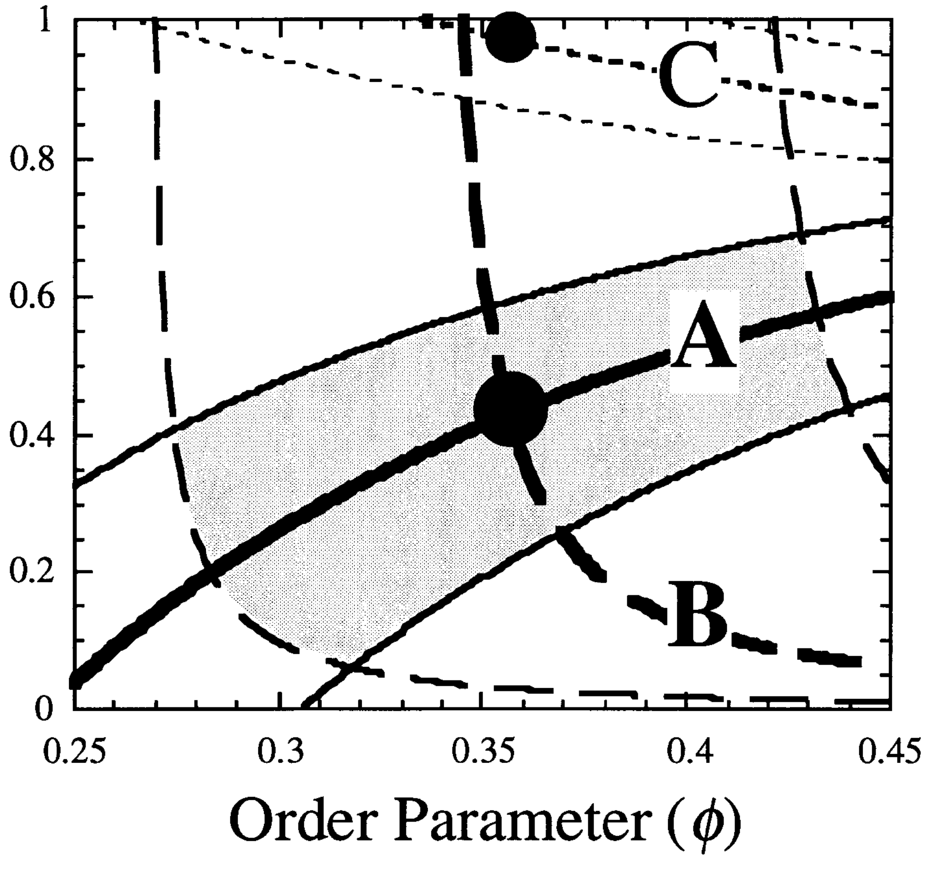

Figure 7.6. Graphical solution of Eqs. 6.2 for the experimental results of Bi on GaP of Table 7.1.

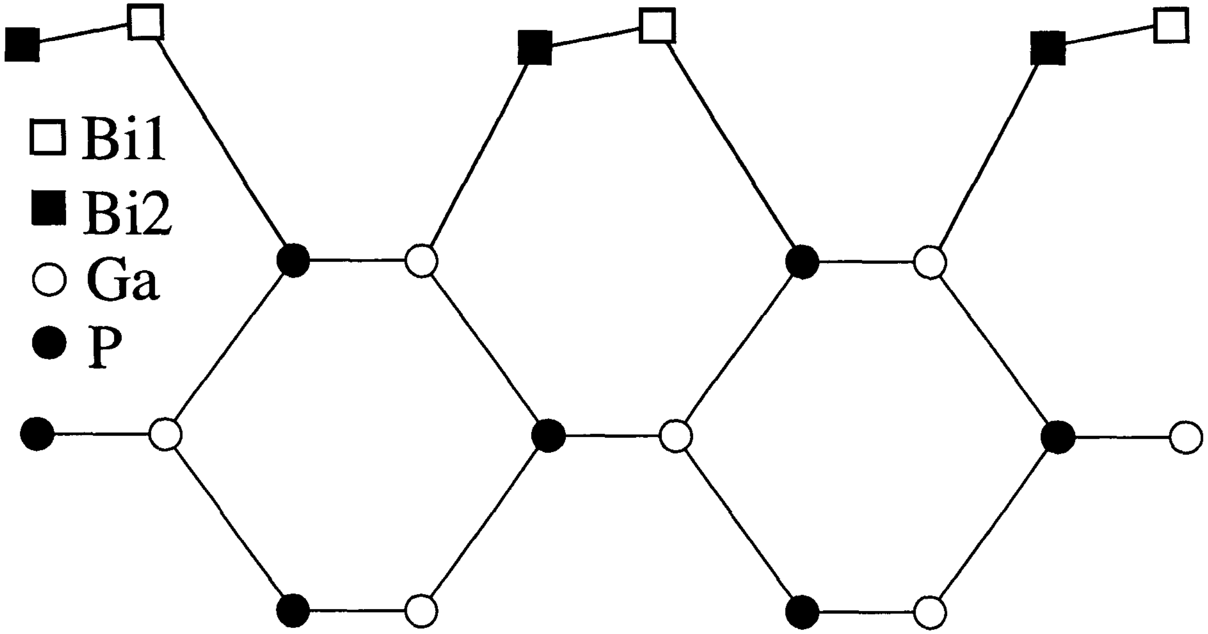

Figure 7.7. Position of the Bi atoms on the GaP surface scaled to our results. Because of the failure of the self-consistency check of the two-site model, these results should be understood as qualitative.

Chapter 8. Phosphorus Relaxation for the Clean and Bi-Covered (110) GaP Surface

8.1 Introduction

A complete study of the interface requires the determination of the deformation of the substrate induced by the overlayer. To study relaxation of substrate atoms, it is necessary to use surface-sensitive photoemitted electrons. By performing XSW experiments for the (200) reflection in a back-reflection configuration—and for the (111) and $(11\bar{1})$ reflections with an asymmetrical configuration similar to that used in the Bi experiments—it was possible to study the relaxation of P for the clean and Bi covered GaP (110) surface.

The reproducibility and dependability of the results were enhanced by comparing surface-sensitive data, which contain information of the surface reconstruction, with bulk-sensitive data, for which the structure is known. In this way, most systematic errors could be eliminated.

XSW relaxation studies in the (110) direction of the clean InP (110) surface, have been published elsewhere [1] using a different methodology.

8.2 Definition of the problem

The position of bulk atoms in a perfect crystal are periodic, only perturbed by temperature vibrations. The termination of a crystal induces deformation, which is larger close to the surface. To completely determine experimentally the deformation of a crystal, and how it changes due to the presence of an overlayer, is an extremely difficult problem because it implies the isolation of the signal coming from a given depth; so, again, a level of simplification has to be chosen. This study will consider that only the last substrate layer deviates from the ideal lattice positions, and also that the deformation is the same for all the surface P atoms.

Studies of the relaxation of the last layer using the XSW technique are possible due to the availability of surface-sensitivity photoemission signals. Electrons that have been photoexcited inside a solid to energies between 50 and 200 eV have very little chance to escape without suffering any collision with valence or core electrons [2]. Electrons that have participated in electron-electron scattering events may escape and contribute to the secondary tail signal, with a different energy from the unscattered electrons. Most of the electrons contributing to the photoemission peak signal come from near the surface. For electrons exited to energies between 50 and 200 eV, the contribution to the photoemission peak signal from the atoms located in the surface layer is appreciable (around 40–50%—see Section 8.6.3), which is why they are called surface-sensitive photopeaks. The rest of the signal (50–60%) comes from atoms located beyond the surface layer. The surface-sensitive photopeak used to measure the relaxation of P was P 1s. No surface-sensitive photopeaks was available for Ga for the photon energies used in the experiments.

Because the P 1s signal recorded has contributions from P at the surface layer (40–50%) and from the rest of the P in the crystal (50–60%), two positions—the relaxed surface and the bulk—have to be considered in the distribution function.

8.3 Experimental methodology

8.3.1 Experiments details

The experiments were performed on the 3-3 beam line at the Stanford Synchrotron Radiation Laboratory (SSRL). Tuning of the beam photon energy was done by a double crystal Si (111) monochromator. The P XSW data were recorded by monitoring the photoemission yield from the P 1s core level, and the KLL Auger line as the beam energy was swept around the corresponding Bragg condition. We also, simultaneously and independently, recorded the reflectivity (R) and the total photoemission yield (TY). The TY is recorded by monitoring the current leaving the sample, which was connected to an electrical feedthrough.

The UHV systems had base pressures in the low 10^{-10} Torr range. The chamber manipulator had three linear and one angular degrees of freedom. The XSW spectra from P were obtained by recording photoemission yield with an angle integrated Cylindrical Mirror Analyzer (CMA). Since the P photoemission peak rides on the top of a background of inelastic electrons, the spectra from the background were also recorded and subtracted from the elastic signal (see Section 6.2). Clean surfaces were prepared by cleaving an outgassed GaP crystal along the (110) face. The Bi-covered surfaces were prepared by evaporation of approximately one monolayer of Bi as measured by a quartz crystal oscillator. All the cleaves were mirror-like. The Bi-covered samples were next annealed at 325°C for 10 minutes to desorb any Bi in excess of one monolayer [3], and to enhance the interfacial order.

8.3.2 Experimental configurations

The experimental setup for every reflection, including important elements of the monochromator, is depicted in Fig. 8.1.

8.3.2.1 Configuration for the (111) and $(11\bar{1})$ reflections

Figure 8.1 shows the configuration used for the (111) and $(11\bar{1})$ reflections; that is, it shows the orientation of the sample (see the top-left of Fig. 8.1), the direction of the reflected beam, and the position of the CMA detector. Notice that this configuration has many similarities to the one used for Bi, described in Section 3.3.2. There are, however, some major differences. The 3-3 SSRL beamline (where the P experiments were performed) does not have a collimating mirror (compare Fig. 8.1 with Fig. 3.2), and the focusing mirror is placed before the monochromator, so that there is no mirror between the monochromator and the sample.

This asymmetric configuration is close to being nondispersive because the Si (111) diffracting planes of the monochromator are close to parallel to the GaP (111) [or $(11\bar{1})$] Bragg planes; they are not exactly parallel because of the difference in lattice constant between Si and GaP. Nondispersive reflections have the property that the angular divergence of the beam combines with the energy dispersion in such a way that the phase resolution is maximized. This can be seen in the Du Mond diagram of Fig. 8.2. The resolution of the experiments performed with this configuration was excellent.

Even though this is not a completely nondispersive configuration, we will call it "nondispersive" to distinguish it from the other nonsymmetric configuration described in Chapter 3.

8.3.2.2 Configuration for the (200) reflection

Figure 8.3 shows the configuration used for the (200) reflection. Figure 8.4 shows the shape of the incoming beam in a Du Mond diagram. As for the nondispersive configuration, the (θ, λ) region illuminated by the beam is inclined because the crystals in the monochromator are Si (111). The resolution of the (200) experiments was also excellent, although not as good as for the (111) and $(11\bar{1})$ reflections. This is despite the fact that the photon energy for the (200) reflection is smaller. The reason for this can be seen by comparing the number of phase lines crossed by the illuminated region of Figs. 8.2 and 8.4.

8.4 Experiments performed

The experiments performed are shown in Table 8.1. The averaging of the data was done with the method described in Section 6.3. Table 8.1 also shows the final kinetic energy of the photoelectrons. The P 1s experiments are surface sensitive because the energy of the P 1s photoemitted electrons lies in the 50-200 eV range, where the escape depth is the smallest. Bulk-sensitive data for P were also obtained using the P KLL Auger emission. The P KLL and P 1s data were taken one after the other, without changing any detail of the experimental setup. This makes very meaningful the comparison between both results, and enhances the dependability of the analysis.

Figures 8.5 to 8.19 show the experimental data together with the best fits. The analysis was done with the method described in Section 5.2. The reflectivity is also plotted with the data, and was used in all cases in the fitting calculations. Once again, the quality of the fits is excellent.

8.5 Data analysis results and "corrected" coherent distances for the P 1s data

Also shown in Table 8.1 are the extracted values for the coherent distance and coherent fraction. The origin was chosen at the ideal P site, so that the nominal value for the coherent distance of the bulk experiments is zero. The reproducibility of the P KLL results for the coherent distance is remarkable. The values are within 2% of the nominal value of zero and, in most cases, are within 0.7%.

The coherent distances for the P 1s experiments are very close to zero, which alone implies small relaxation. Nevertheless, the P 1s coherent distances are consistently larger than the coherent distance of P KLL for the clean surface. The opposite is observed for the P 1s coherent distances in the presence of the Bi overlayer, which are consistently smaller than those corresponding to P KLL. This implies expansion in the clean surface case, and contraction in the Bi covered case.

Errors on the values used for the structure factors may introduce errors comparable to the values of the P 1s coherent distance. Notice that the photon energy is within 200 eV of the P 1s edge. The atomic structure factors vary strongly around an absorption edge and also are affected by EXAFS effects, so the closer they are to an absorption edge, the less reliable their theoretical values.

Those, and other systematic errors, are canceled by comparison with the results for the bulk data. The difference between the coherent distance of the P 1s experiments and the coherent distance of the P KLL experiments is shown as "corr D_c" in Table 8.1. This difference is believed to better represent the coherent distance of the surface sensitive experiments. Table 8.2 summarizes the average of the corrected values of the P 1s coherent distance that were used in the calculations of the relaxation.

The values of the P 1s coherent fraction are consistently smaller than those for P KLL, as expected. It will become apparent that the coherent fractions are not really needed, and so they will not be used for the relaxation calculations.

8.6 Structural determination

8.6.1 The distribution function

As discussed in Section 8.2, we are considering two positions, although with different populations. Ignoring thermal vibrations, the distribution function can be written:

$$f_{\mathrm{H}}(D) = \zeta\,\delta\!\left(D - D_S^{\mathrm{H}}\right) + (1-\zeta)\,\delta\!\left(D - D_B^{\mathrm{H}}\right), \tag{8.1}$$

where ζ is the fraction of the signal coming from the outermost P atoms, and D_S^{H} and D_B^{H} are the distances of the surface and bulk atoms to the local Bragg planes.

It is possible to obtain information about D_S^{H} because for the surface sensitive experiments a significant fraction (40–50%) of the signal comes from the outermost P atoms, so ζ is not zero.

Because the bulk P position D_B^{H} is known, the problem has been reduced to finding D_S^{H}. This can be done independently for each reflection performed. To find the three dimensional components of the relaxation, three noncoplanar reflections are needed. The experiments performed involve noncoplanar Bragg vectors [the (200), (111), and $(11\bar{1})$ vectors are not in the same plane].

8.6.2 Connection of the experimental results with the structure parameters

The parameters of the distribution function (Eq. 8.1) are related to the coherent distance and coherent fraction results by Eqs. 5.18. By performing the integrals, we obtain:

$$f_c^{\mathbf{H}} = \left| (1-\zeta)\,\exp\left(-\,2\pi i\frac{D_B^{\mathbf{H}}}{d_{\mathbf{H}}}\right) + \zeta\,\exp\left(-\,2\pi i\frac{D_S^{\mathbf{H}}}{d_{\mathbf{H}}}\right)\right| , \tag{8.2}$$

and

$$D_c^{\mathbf{H}} = \frac{d_{\mathbf{H}}}{2\pi}\arctan\frac{(1-\zeta)\,\sin\left(2\pi\frac{D_B^{\mathbf{H}}}{d_{\mathbf{H}}}\right) + \zeta\,\sin\left(2\pi\frac{D_S^{\mathbf{H}}}{d_{\mathbf{H}}}\right)}{(1-\zeta)\,\cos\left(2\pi\frac{D_B^{\mathbf{H}}}{d_{\mathbf{H}}}\right) + \zeta\cos\left(2\pi\frac{D_S^{\mathbf{H}}}{d_{\mathbf{H}}}\right)} . \tag{8.3}$$

Equations 8.2 and 8.3 form a complete set for each reflection $\mathbf{H}$, and can be inverted to obtain the values of ζ and $D_S^{\mathbf{H}}$ from the experimental values of the coherent fraction ($f_c^{\mathbf{H}}$) and coherent distance ($D_c^{\mathbf{H}}$). However, the uncertainty for ζ and $D_S^{\mathbf{H}}$ evaluated using Eqs. 8.2 and 8.3 is very large because of the large uncertainties on the coherent fraction.

An alternative method is to estimate ζ using tabulated values of the escape depth (there is extensive literature about the escape depth of electrons as a function of kinetic energy [4]). The value for ζ can be used in Eq. 8.3 to estimate $D_S^{\mathbf{H}}$. Equation 8.3 only involves the coherent distance, for which the uncertainty is much smaller than for the coherent fraction. Figures 8.21, 8.22, and 8.23 will show that a generous range for ζ does not introduce too much uncertainty on $D_S^{\mathbf{H}}$.

Equation 8.3 can be rearranged as follows:

$$\zeta = \frac{\tan 2\pi D_c^{\mathbf{H}}}{\left[1-\cos\left(2\pi\,\frac{D_S^{\mathbf{H}}}{d_{\mathbf{H}}}\right)\right]\tan 2\pi D_c^{\mathbf{H}} + \sin\left(2\pi\,\frac{D_S^{\mathbf{H}}}{d_{\mathbf{H}}}\right)} . \tag{8.4}$$

The origin has been chosen such that $D_B^{\mathbf{H}} \equiv 0$.This form is more convenient for plotting purposes.

8.6.3 Evaluation of the fraction of the photoemission signal coming from the outermost P atoms

As mentioned in Section 5.1.2, substrate relaxation studies are possible if the escape probability of the electrons collected is such that a nonneglectable fraction comes from the surface layer. As shown by Lindau et al. [4], for most materials (GaP included), the escape length of electrons with energy between 50 and 200 eV is only 5 to 10 Å, so that a large enough fraction of the signal comes from the outermost layer. For the energy corresponding to the reflections described below, the energy of electrons coming from the P 1s core level is inside the 50–200 eV range, so it was possible to perform experiments to measure the P relaxation.

The photodetector is set to collect electrons that have not, or almost not, lost any energy (no electron-electron collision). It was shown by Spicer et al. [5] that an excellent approximation to the probability of escaping without any electron-electron collision is the following:

$$P_E(\mathbf{r}) = \exp\left(-\frac{\mathbf{r}\cdot\mathbf{n}}{\lambda(E)\,\cos\,\theta}\right), \tag{8.5}$$

where θ is the detection angle with respect to the normal of the crystal, and λ is the escape depth. The origin is set at the surface to make $\mathbf{r}\cdot\mathbf{n}$ the distance from the generation of the photoelectron to the surface. The total signal is proportional to the following series:

$$\text{total signal} \propto \sum_{j=0}^{\infty} \exp\left(-j\,\frac{d_{(220)}}{\lambda(E)\,\cos\theta}\right) = \frac{1}{1-\,\exp\left(-\,\frac{d_{(220)}}{\lambda(E)\,\cos\theta}\right)},$$

where $d_{(220)} = a_l/\sqrt{8}$ is the (220) interplanar distance. This distance plays a role because it is the separation of the different layers of P atoms parallel to the surface. For the surface signal, only the term with $j = 0$ is kept, so that we have:

$$\text{surface signal} \propto 1\ ,$$

and the fraction of surface signal is given by:

$$\frac{\text{surface signal}}{\text{total signal}} = 1-\,\exp\left(\frac{d_{(220)}}{\lambda(E)\,\cos\theta}\right). \tag{8.6}$$

This expression have been integrated for the angle of acceptance of the CMA (42.3±6°) for the sample orientations used in the nondispersive configuration—where the sample faces the beam (see Fig 8.1)—and for the orientation used for the (200) reflection—where the sample makes a 45° angle with the incoming beam (see Fig. 8.3). The integration is calculated as follows:

$$\zeta = \frac{\int d\Omega \left[1 - \exp\left(-\frac{d_{(220)}}{\lambda(E)\ \cos\theta} \right) \right]}{\int d\Omega} . \qquad (8.7)$$

An important point is that Eq. 8.7 is valid regardless of whether the substrate surface is covered.

It can be seen in Fig. 8.20 that the surface sensitivites ζ for the sample orientations corresponding to the three reflections (which are calculated using Eq. 8.7) are very close to each other for all values of the escape depth λ. The escape depth for the range of photoelectron energies of the surface-sensitive experiments is between 5 and 10 Å [4]. From the curves of Fig. 8.20, the corresponding ranges for ζ are $0.39 < \zeta < 0.6$ for the (111) and $(11\bar{1})$ reflections, and $0.36 < \zeta < 0.55$ for the (200) reflection. These estimations are used in conjunction with Eq. 8.4 to calculate the surface displacements D_S^{H} (see Figs. 8.21, 8.22, and 8.23).

8.7 Structure results

8.7.1 Determination of the coordinates of the relaxation

Figures 8.21, 8.22, and 8.23 show Eq. 8.4 plotted for the values of the coherent distances of Table 8.2. Using the range of values of the fraction of the signal coming from the outermost P atoms found in the previous section, a range for the reconstruction D_S^{H} is found. These values are displayed in Table 8.3.

The coordinates of the relaxation can be obtained by triangulating the results of Table 8.3. If the values of D_S^{H} are expressed in interplanar units, the Y coordinate of the relaxation is as follows:

$$Y = \frac{D_S^{(111)} - D_S^{(11\bar{1})}}{2} a_l , \qquad (8.8)$$

where a_l is the lattice constant.

The (1×1) symmetry shown by the LEED pattern [6] symmetry implies that the P relaxation in the X direction is zero. This results in an overdetermination of the system, so the Z coordinate can be found in two ways. The first is:

$$Z = \frac{D_S^{(111)} + D_S^{(11\bar{1})}}{\sqrt{8}} a_l , \tag{8.9}$$

and the second is using the (200) result:

$$Z = \frac{D_S^{(200)}}{\sqrt{2}} a_l . \tag{8.10}$$

The Z coordinate of the P relaxation for the clean surface was calculated using both Eqs. 8.9 and 8.10. It is surprising that the two independent methods coincide within 0.1%. Using Eq. 8.9, the result is Z=0.065 Å. Using Eq. 8.10, the result is Z=0.066 Å. It was not possible to do this consistency check for the covered surface experiments because no P 1s XSW data for the $(11\bar{1})$ reflection for the Bi covered surface were recorded.

Table 8.4 displays the relaxation coordinates calculated from Eqs. 8.8, 8.9, and 8.10. Figure 8.24 shows the P relaxation scaled to our results. For the clean surface the relaxation is a small counterclockwise rotation, and for the covered surface, it is a contraction in the direction of the bond to the second layer.

8.7.2 Comparison to other techniques

Also displayed in Table 8.4 are the results from LEED [6] experiments and first principles pseudopotential (FPP) [7] calculations for the relaxation of P for the clean GaP (110) surface. No comparison could be made for the covered surface because, to the knowledge of the author, no study of the relaxation of the GaP surface in the presence of a Bi overlayer has been published.

The XSW results compare to the LEED results for the displacement perpendicular to the surface (Z), although the agreement is not as good for the displacement parallel to the surface (Y), which is where the LEED resolution is poorer.

References

1. J.C. Woicik, T. Kendelewicz, K.E. Miyano, P.L. Cowan, C.E. Bouldin, B.A. Karlin, P. Pianetta, and W.E. Spicer. "X-ray standing wave determination of the clean InP (110) surface reconstruction." Physics Review Letters **68**, No. 3, p. 341 (1992).

2. W.E. Spicer and F. Wooten. "Photoemission and photomultipliers." Proceedings of the IEEE **51**, p. 1119 (1963).

3. F. Schaffler, R. Ludeke, A. Taleb-Ibrahimi, G. Hughes, and D. Rieger. "The role of order on the interface properties of Sb/GaAs(110)." Journal of Vacuum Science and Technology B **5**, p. 1048 (1987).

4. I. Lindau and W.E. Spicer. "The probing depth in photoemission and Auger-electron spectroscopy." Journal of Electron Spectroscopy and Related Phenomena **3**, p. 409-413 (1974).

5. W.E. Spicer. "Photoemissive, photoconductivity, and optical absorption studies of alkali-antimony compounds." Physical Review **112**, p. 114 (1958).

6. C.B. Duke, A. Paton, W.K. Ford, A. Kahn, and J. Carelli. "Dynamical analysis of low-energy-electron-diffraction intensities from GaP(110)." Physical Review B **24**, p. 562 (1981).

7. G.P. Srivastava. "Atomic geometry, electronic states and bonding at the GaP(110)–Sb (1ML) interface." Journal of Physics: Condensed Matter **5** p. 4695, (1993).

			Clean Surface		With a Bi Monolayer	
			P KLL	P 1s	P KLL	P 1s
(200)	Surface # 1	D_c	0.02	0.022		
		Corr D_c	—	**+0.002**		
		f_c	0.96±0.1	0.95±0.1		
		E (eV)	1850	125		
	Surface # 2	D_c	0.015	0.025		
		Corr D_c	—	**+0.010**		
		f_c	1.07±0.14	0.92±0.08		
		E (eV)	1850	125		
	Surface # 3	D_c	0.007	0.019	−0.005	−0.02
		Corr D_c	—	**+0.012**	—	**−0.015**
		f_c	0.87±0.06	0.84±0.08	0.86±0.07	0.84±0.14
		E (eV)	1850	125	1850	125
(111)	Surface # 1	D_c	0.001	0.004		−0.007
		Corr D_c	—	**+0.003**		**−0.008**
		f_c	1.00±0.04	0.99±0.05		0.97±0.1
		E (eV)	1850	170		170
	Surface # 2	D_c	0.001	0.007		
		Corr D_c	—	**+0.006**		
		f_c	0.998±0.03	1.01±0.06		
		E (eV)	1850	170		
$(11\bar{1})$	Surface # 4	D_c	−0.004	0.008		
		Corr D_c	—	**+0.012**		
		f_c	0.94±0.1	0.934±0.08		
		E (eV)	1850	165		

Table 8.1. Fitting results of the experimental data.

	Clean Surface	With Bi
(200)	+0.008	−0.015
(111)	+0.004	−0.008
$(11\bar{1})$	+0.012	

Table 8.2. Averaged values of the corrected coherent distance ($D_c^{\mathbf{H}}$) for the P 1s XSW data in interplanar units.

	Clean Surface	With Bi
(200)	+0.017±0.003	−0.032±0.007
(111)	+0.009±0.002	−0.017±0.003
$(11\bar{1})$	+0.025±0.005	

Table 8.3. Results for the P surface reconstruction ($D_S^{\mathbf{H}}$) from Figs. 8.21, 8.22, and 8.23 in interplanar units.

	Clean Surface			With B
	XSW	LEED	FPP	XSW
Y (Å)	−0.045	−0.225	−0.126	−0.185
Z (Å)	0.065	0.09	0	−0.121

Table 8.4 Relaxation of P (from the ideal position) determined by our data. Results m other studies are also shown.

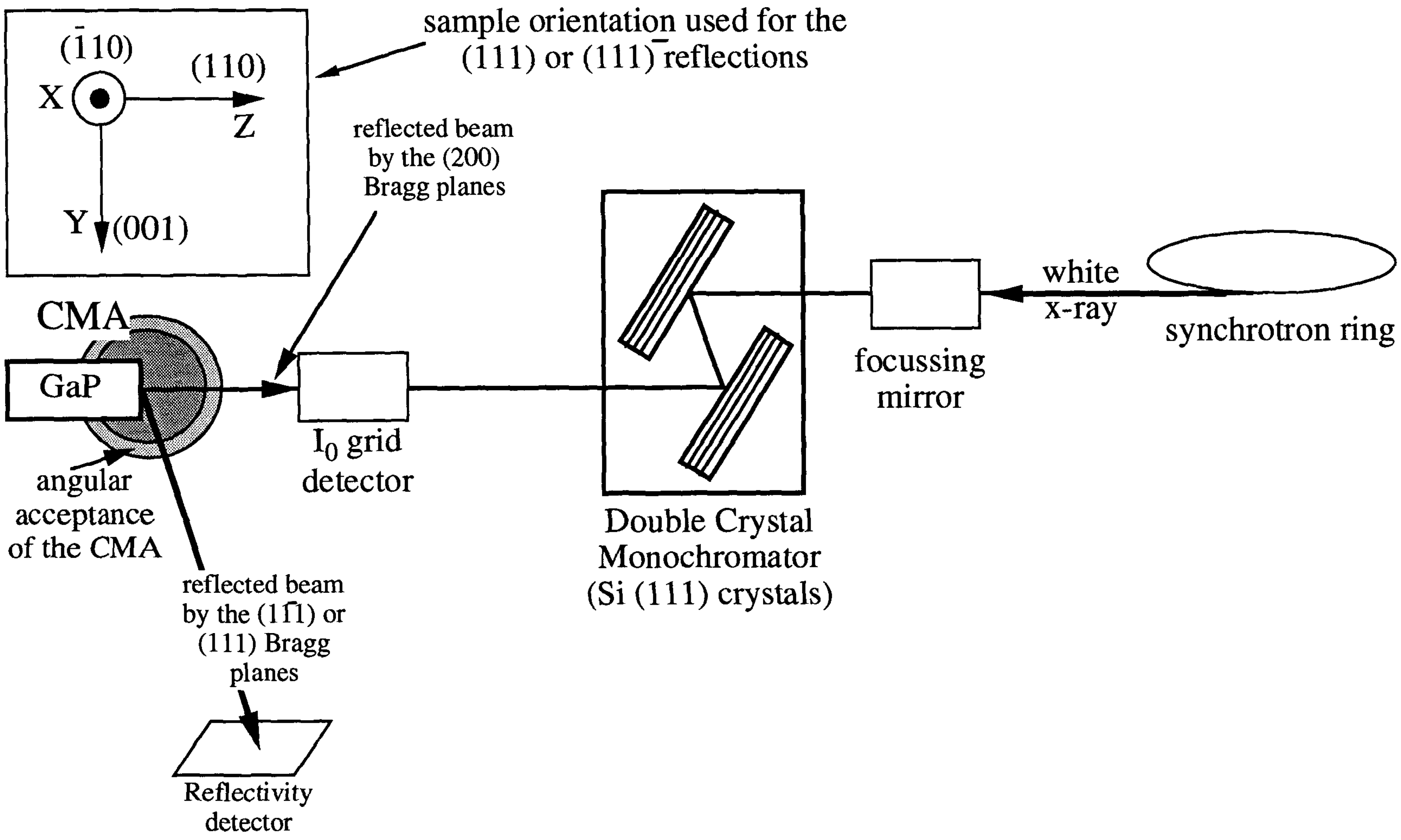

Figure 8.1. Experimental setup. The orientation of the sample for the nondispersive reflections is also shown.

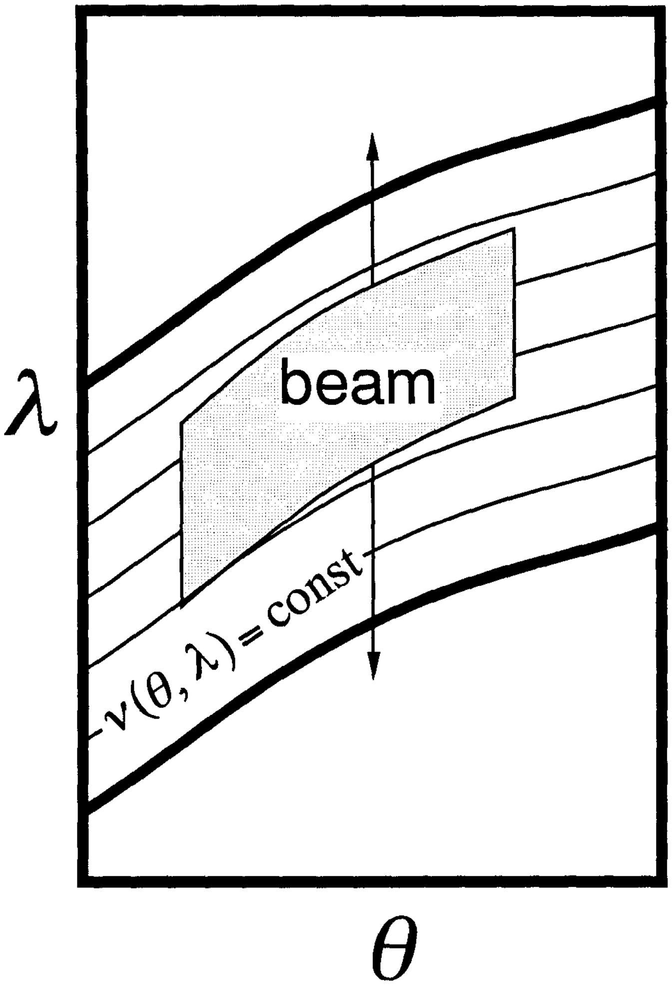

Figure 8.2. Du Mond diagram for the asymmetric configuration performed on beamline 3-3 of SSRL, which is close to being nondispersive.

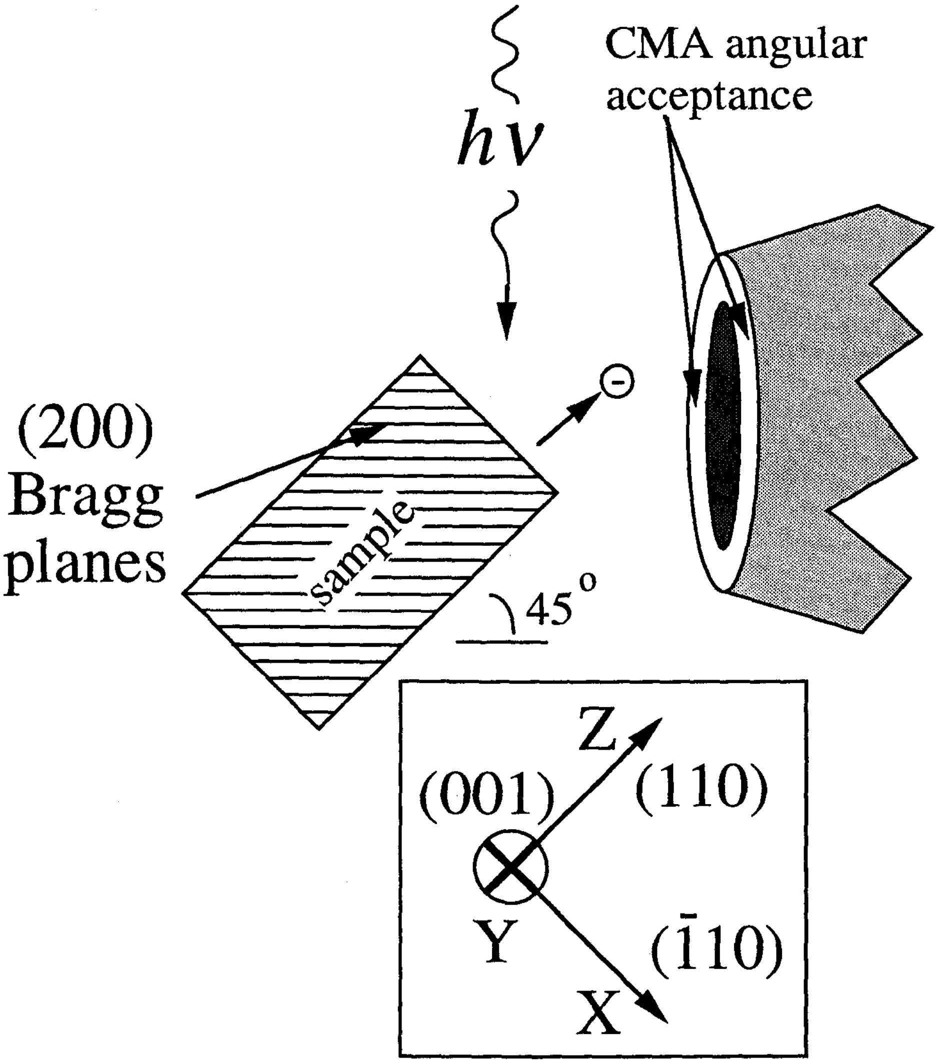

Figure 8.3. Configuration for the (200) reflection.

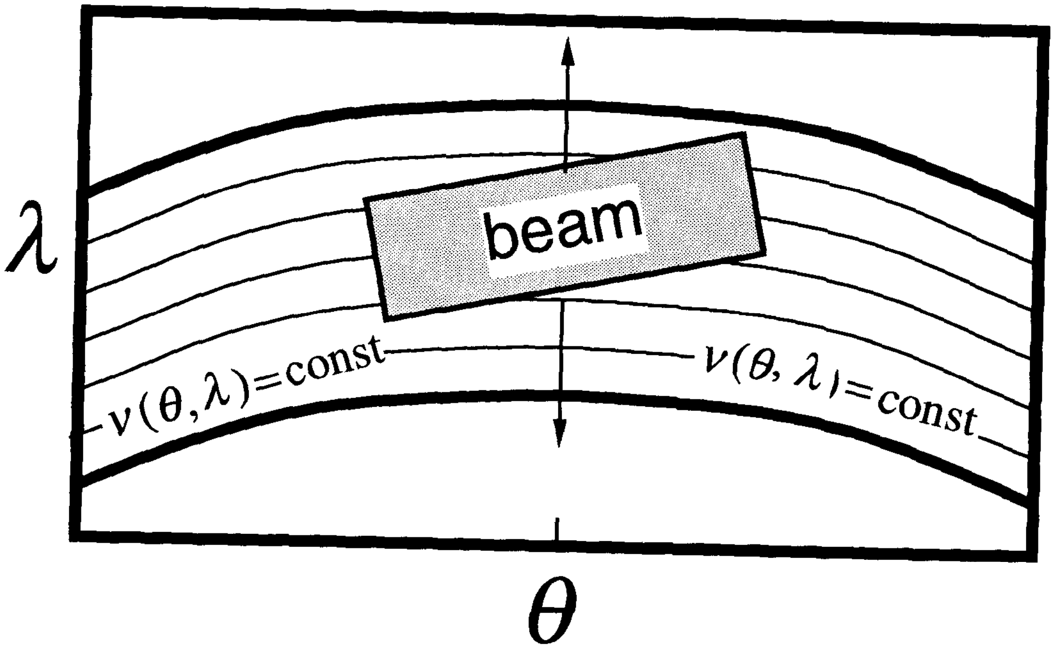

Figure 8.4. Du Mond diagram for the (200) reflection.

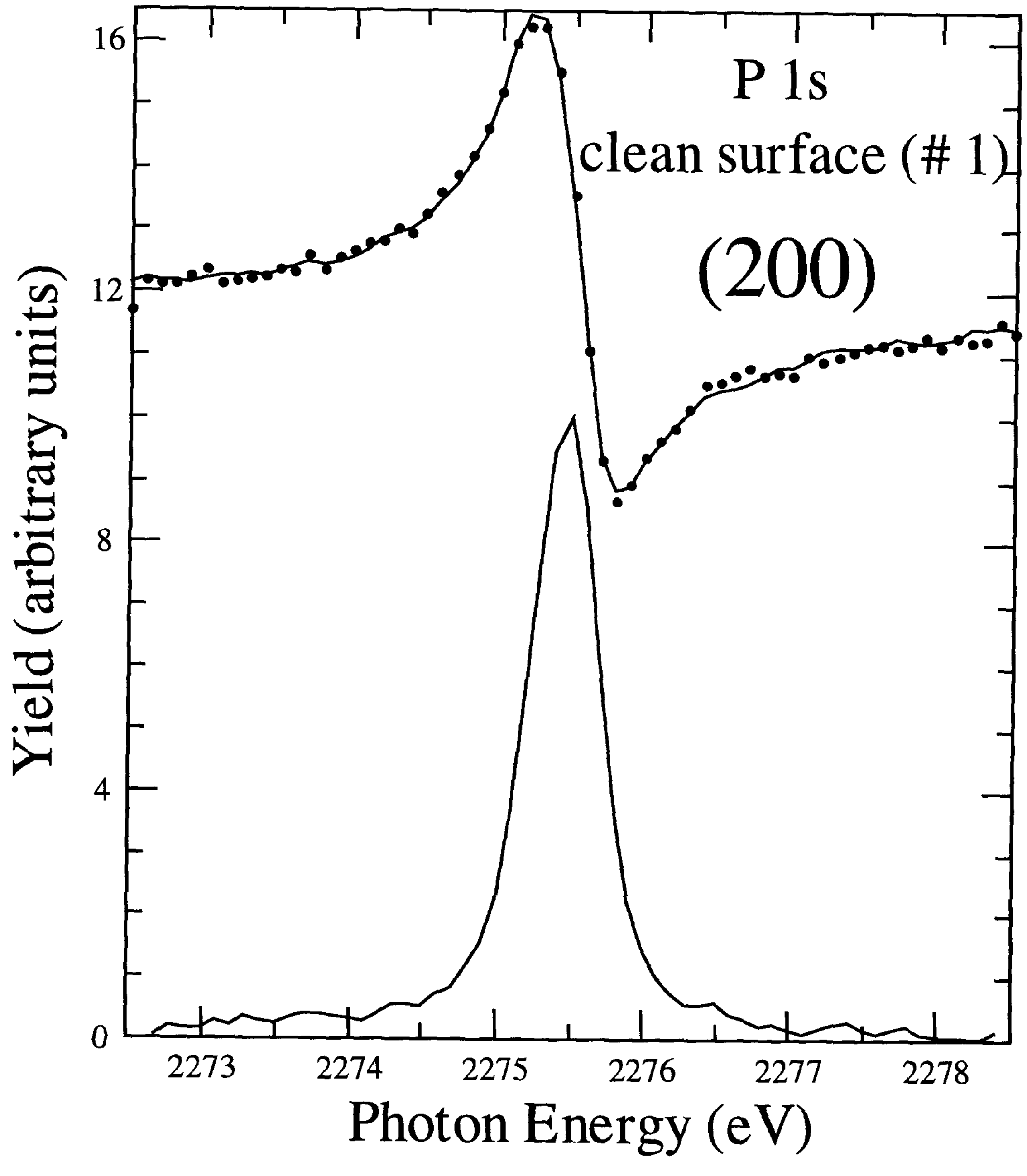

Figure 8.5. Phosphorus 1s XSW data and theoretical fit for the (200) reflection for a clean surface (#1). The bottom curve is the reflectivity.

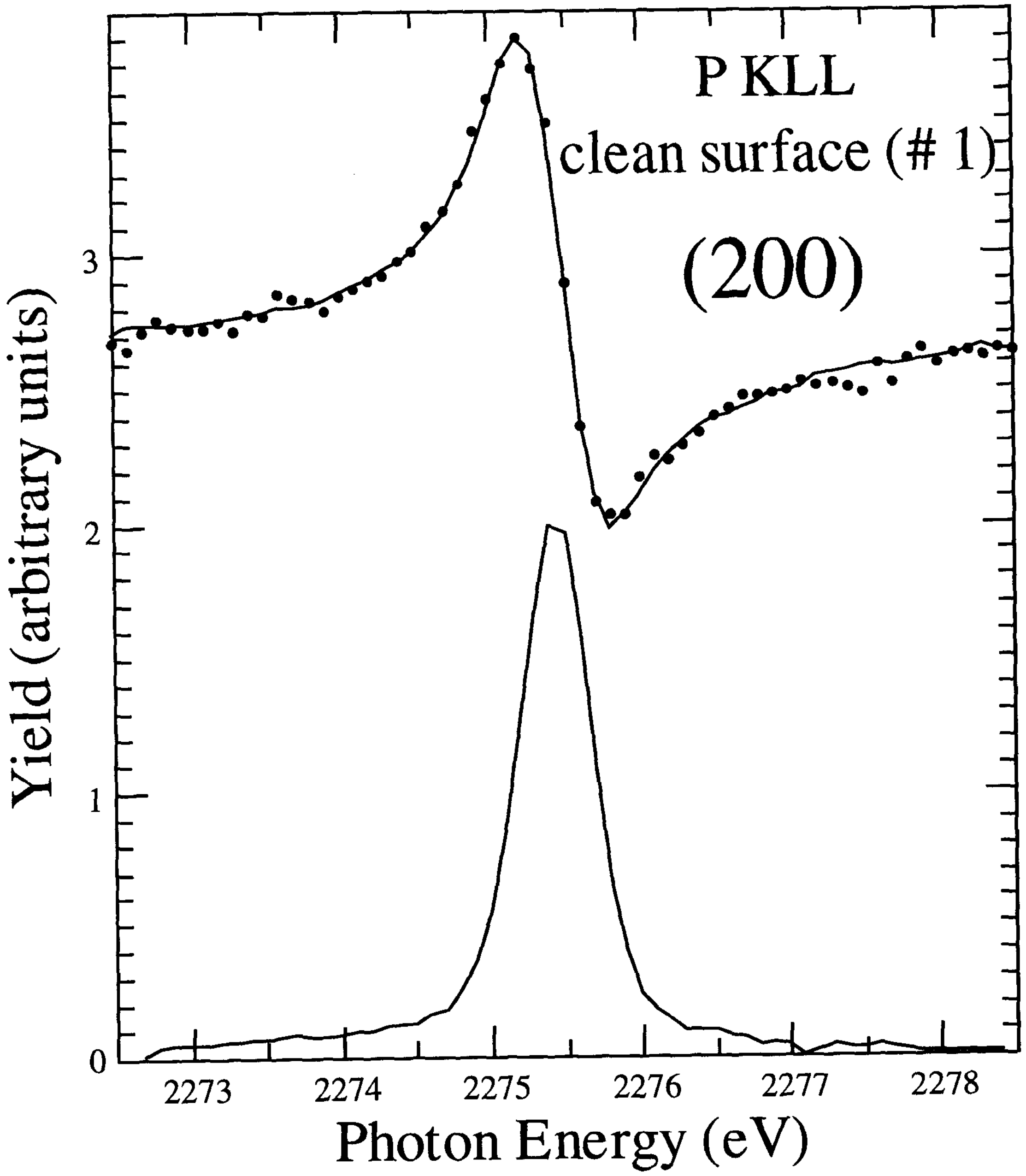

Figure 8.6. Phosphorus KLL XSW data and theoretical fit for the (200) reflection for a clean surface (#1). The bottom curve is the reflectivity.

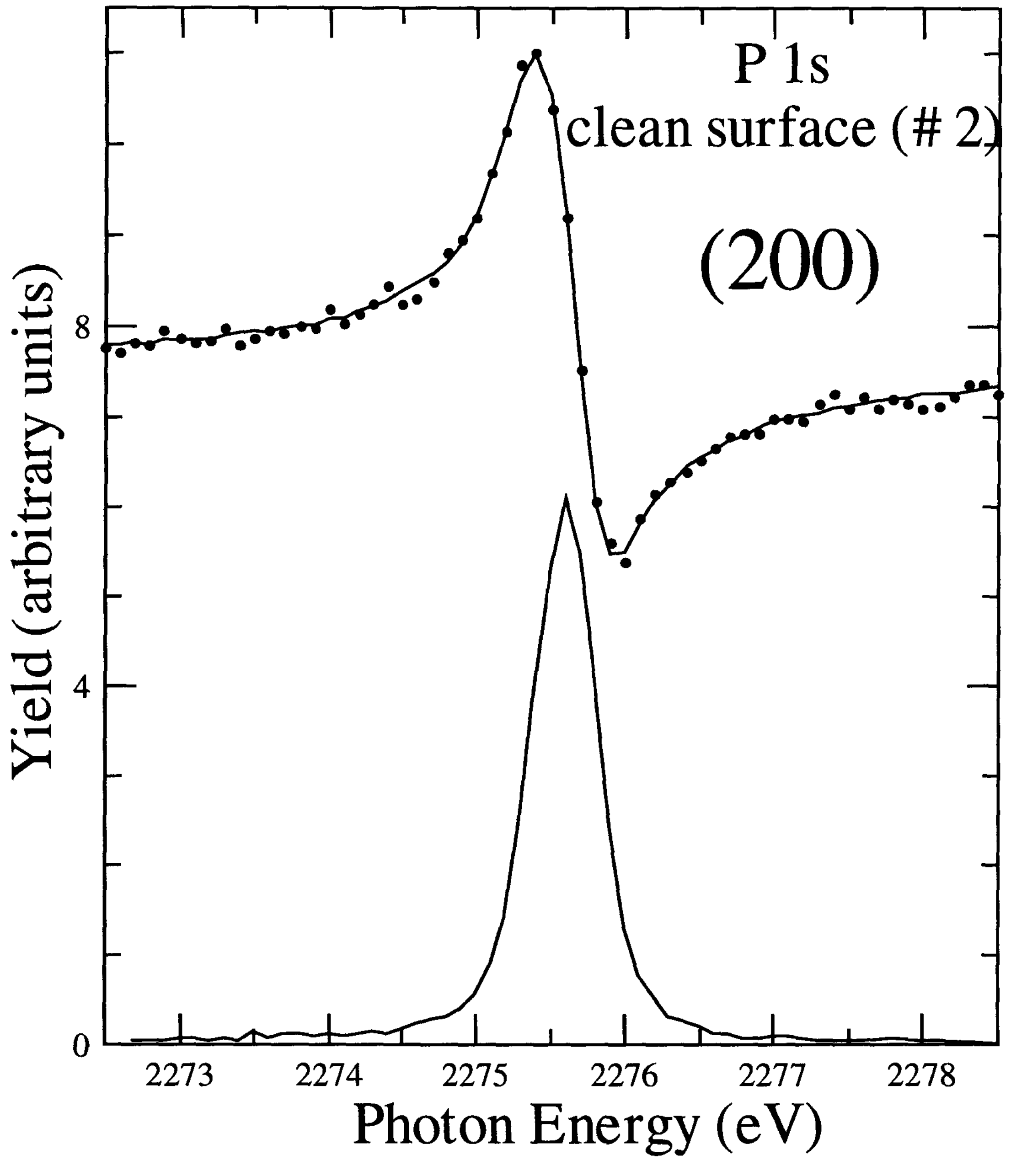

Figure 8.7. Phosphorus 1s XSW data and theoretical fit for the (200) reflection for a clean surface (#2). The bottom curve is the reflectivity.

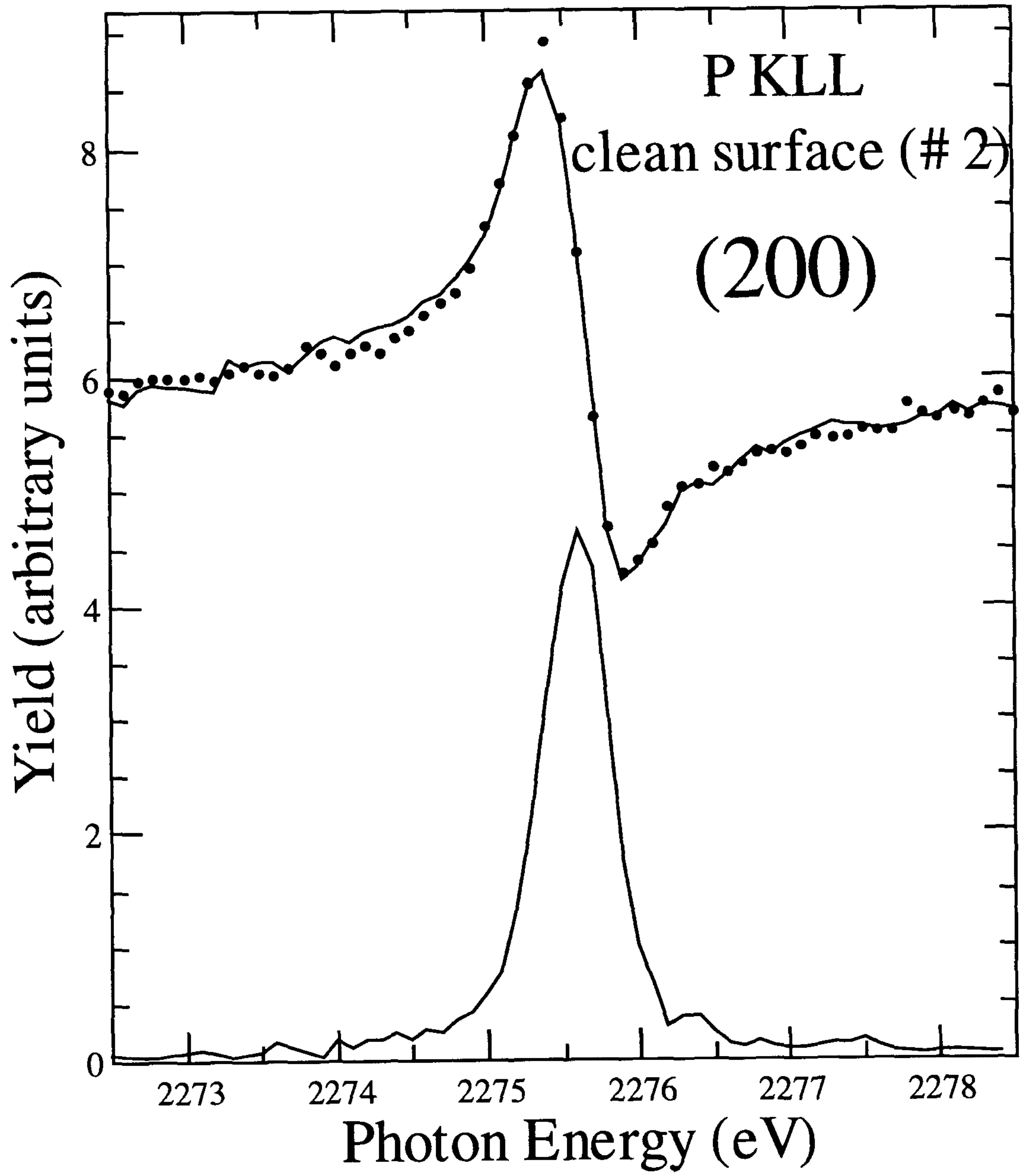

Figure 8.8. Phosphorus KLL XSW data and theoretical fit for the (200) reflection for a clean surface (#2). The bottom curve is the reflectivity.

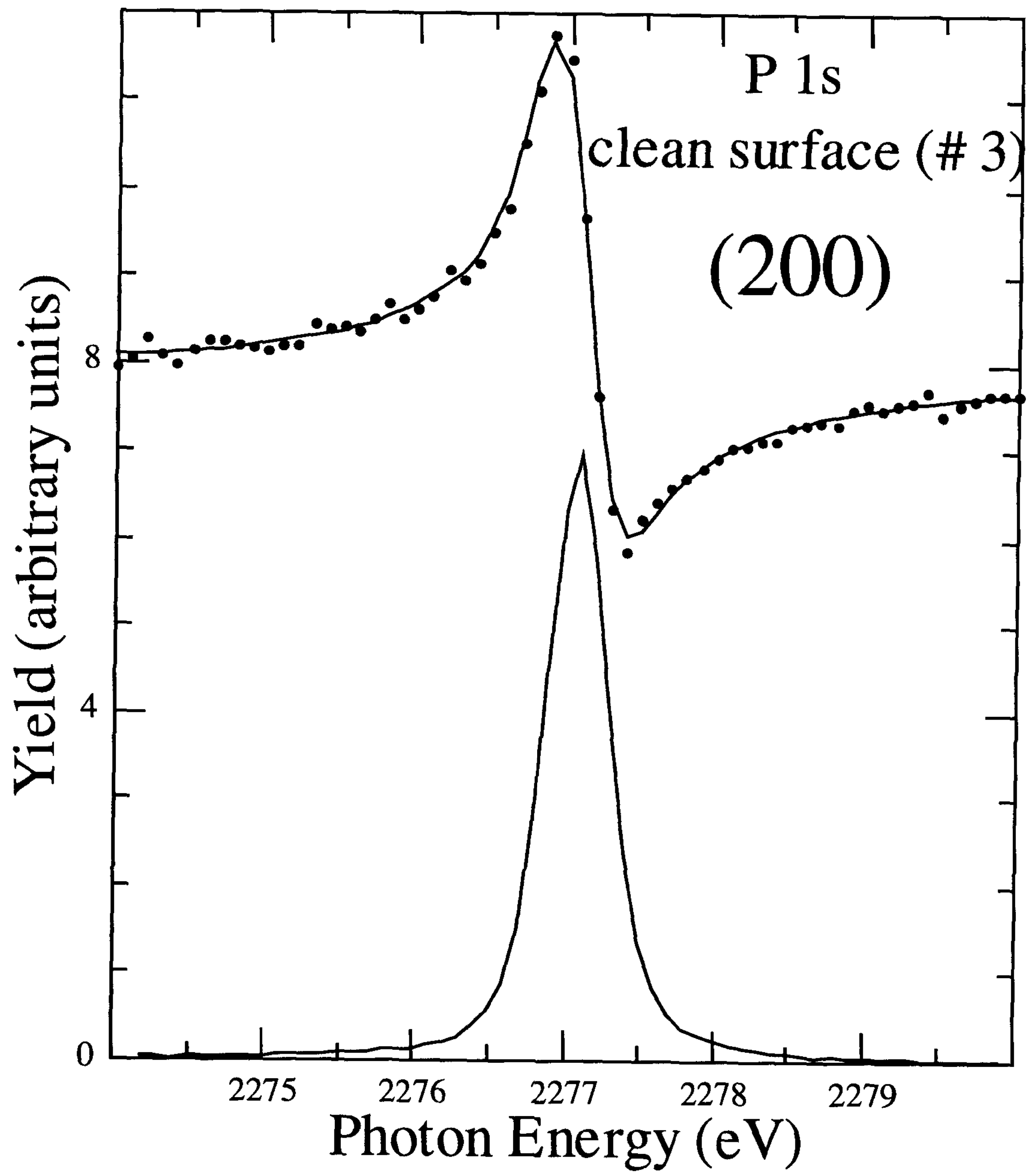

Figure 8.9. Phosphorus 1s XSW data and theoretical fit for the (200) reflection for a clean surface (#3). The bottom curve is the reflectivity.

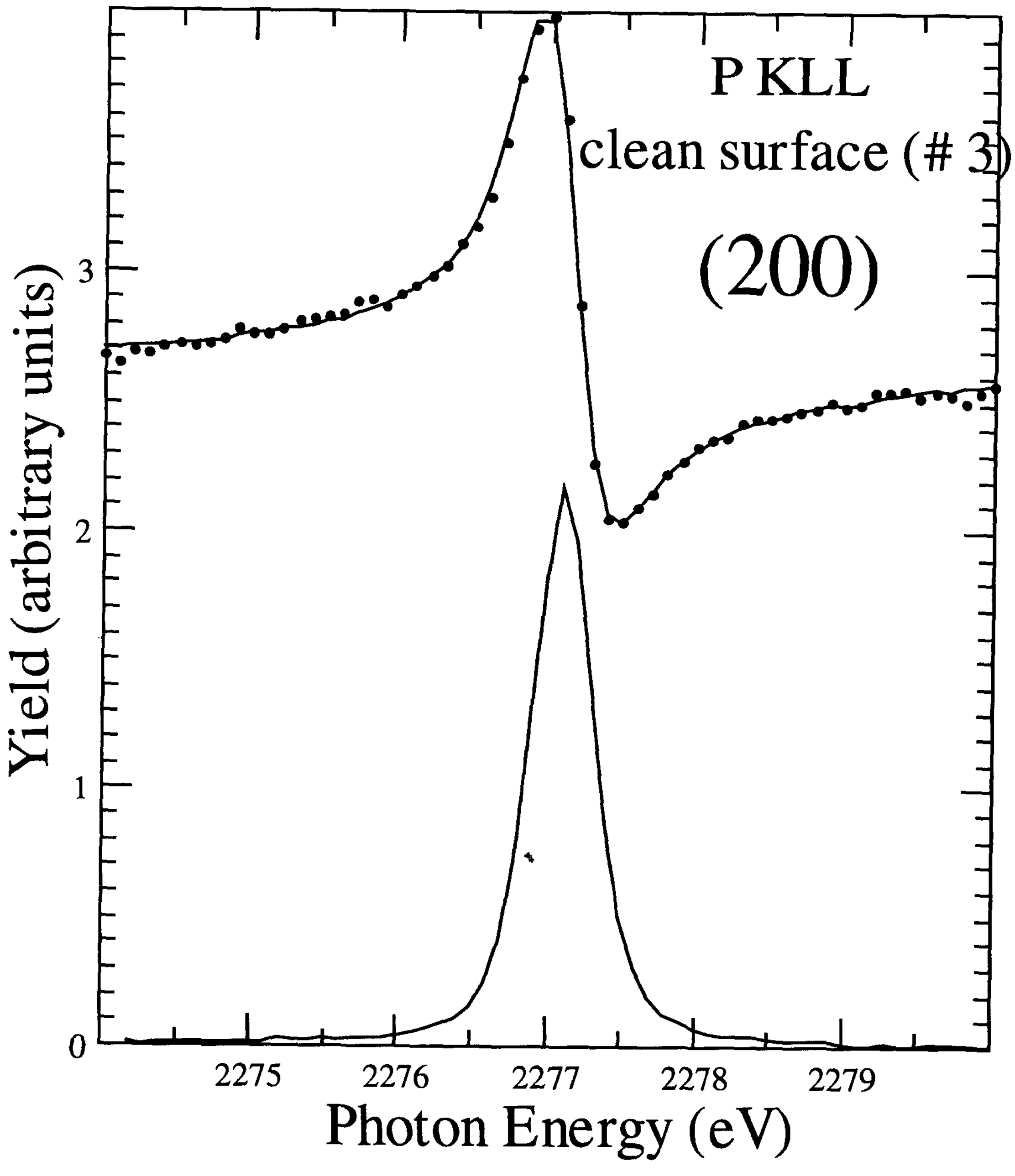

Figure 8.10. Phosphorus KLL XSW data and theoretical fit for the (200) reflection for a clean surface (#3). The bottom curve is the reflectivity.

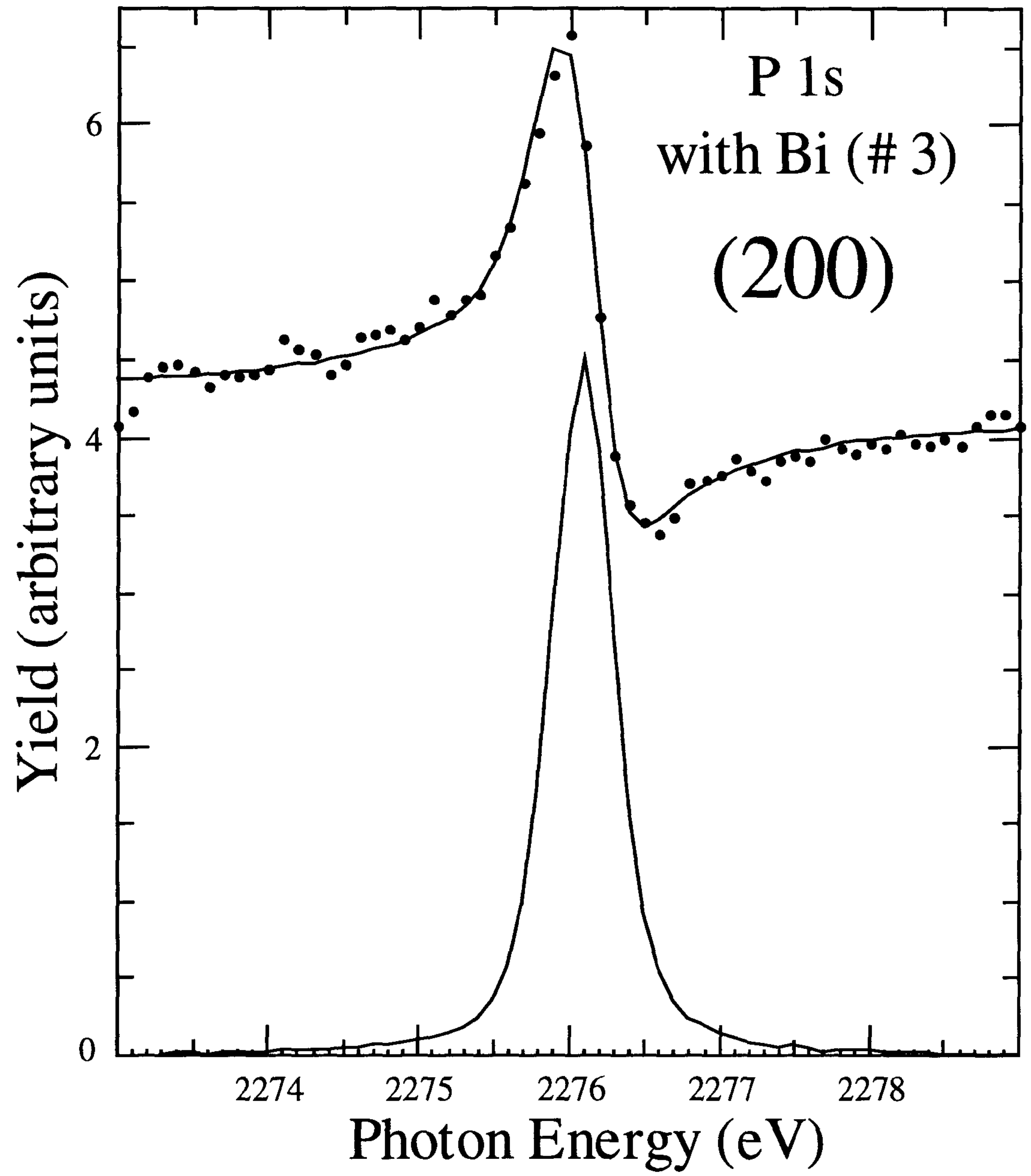

Figure 8.11. Phosphorus 1s XSW data and theoretical fit for the (200) reflection for a Bi-covered surface (#3). The bottom curve is the reflectivity.

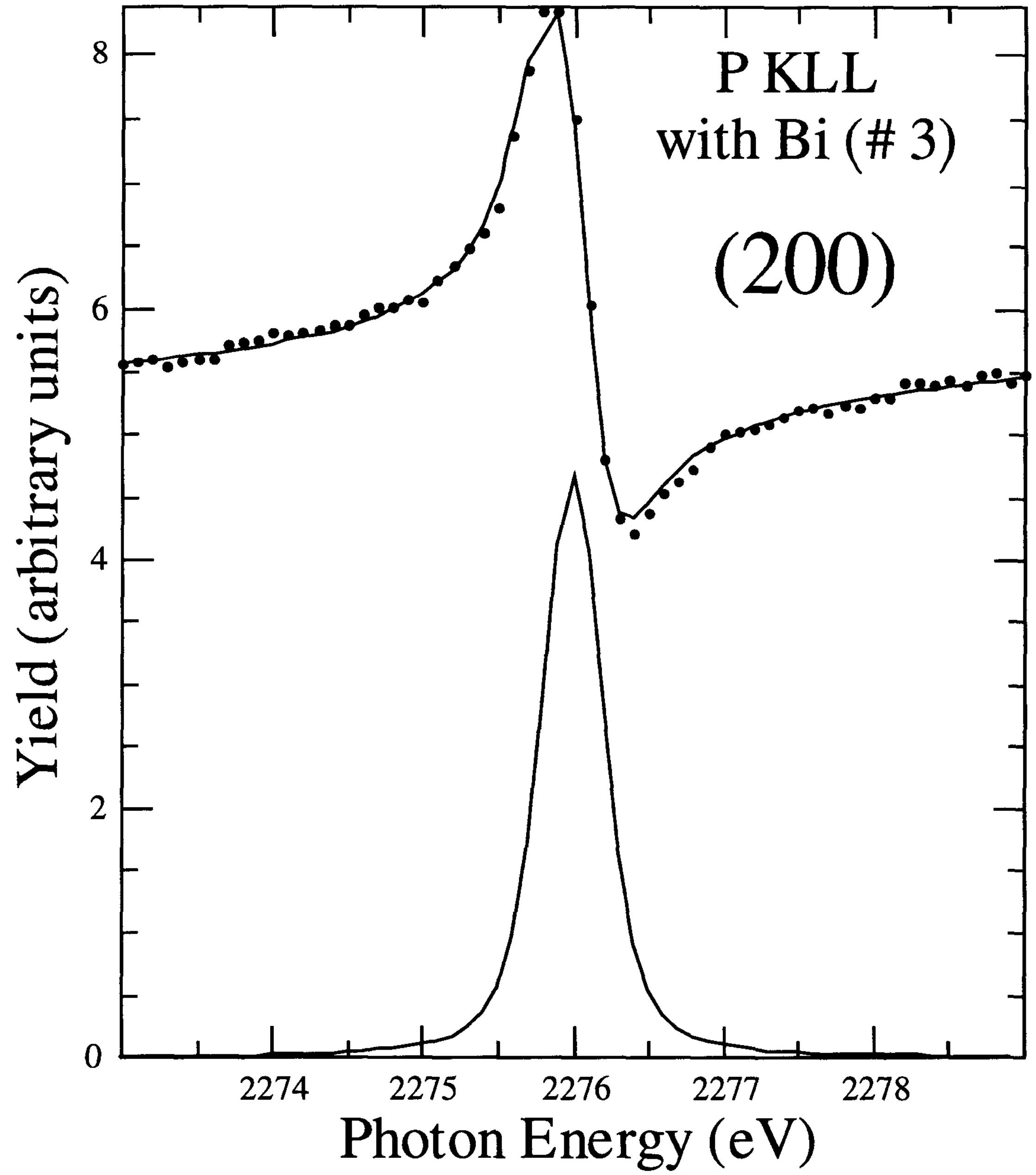

Figure 8.12. Phosphorus 1s XSW data and theoretical fit for the (200) reflection for a Bi-covered surface (#3). The bottom curve is the reflectivity.

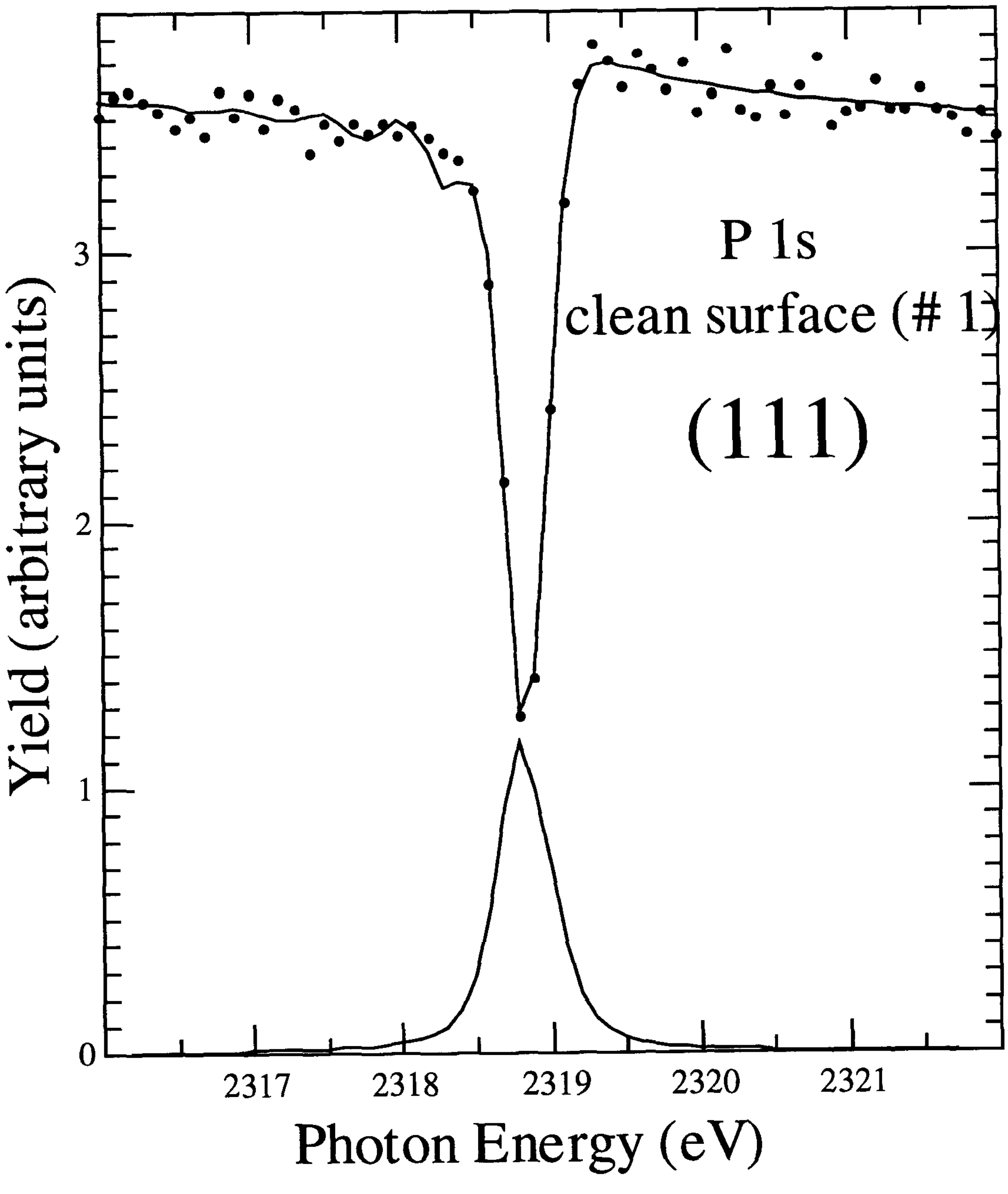

Figure 8.13. Phosphorus 1s XSW data and theoretical fit for the (111) reflection for a clean surface (#1). The bottom curve is the reflectivity.

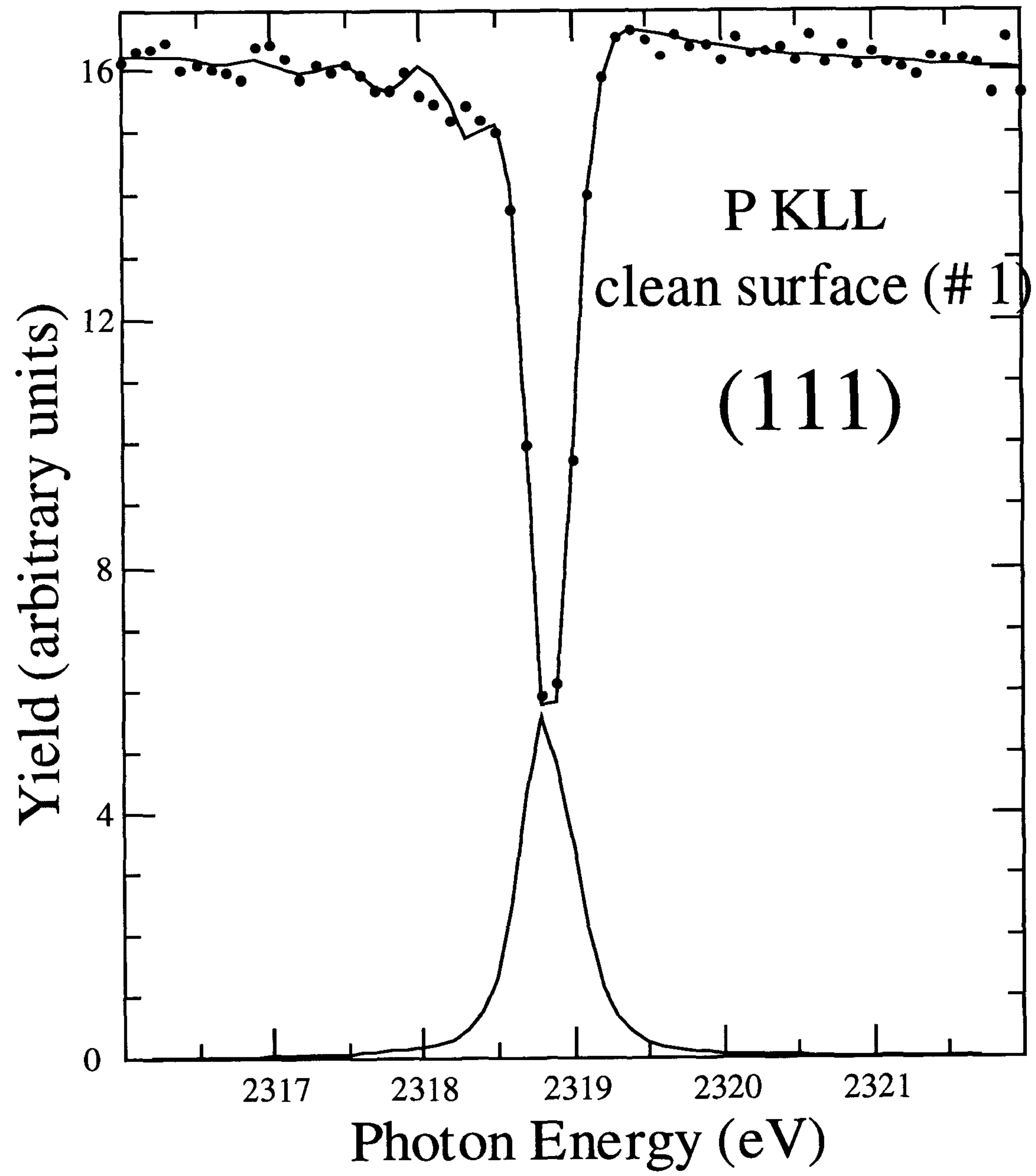

Figure 8.14. Phosphorus KLL XSW data and theoretical fit for the (111) reflection for a clean surface (#1). The bottom curve is the reflectivity.

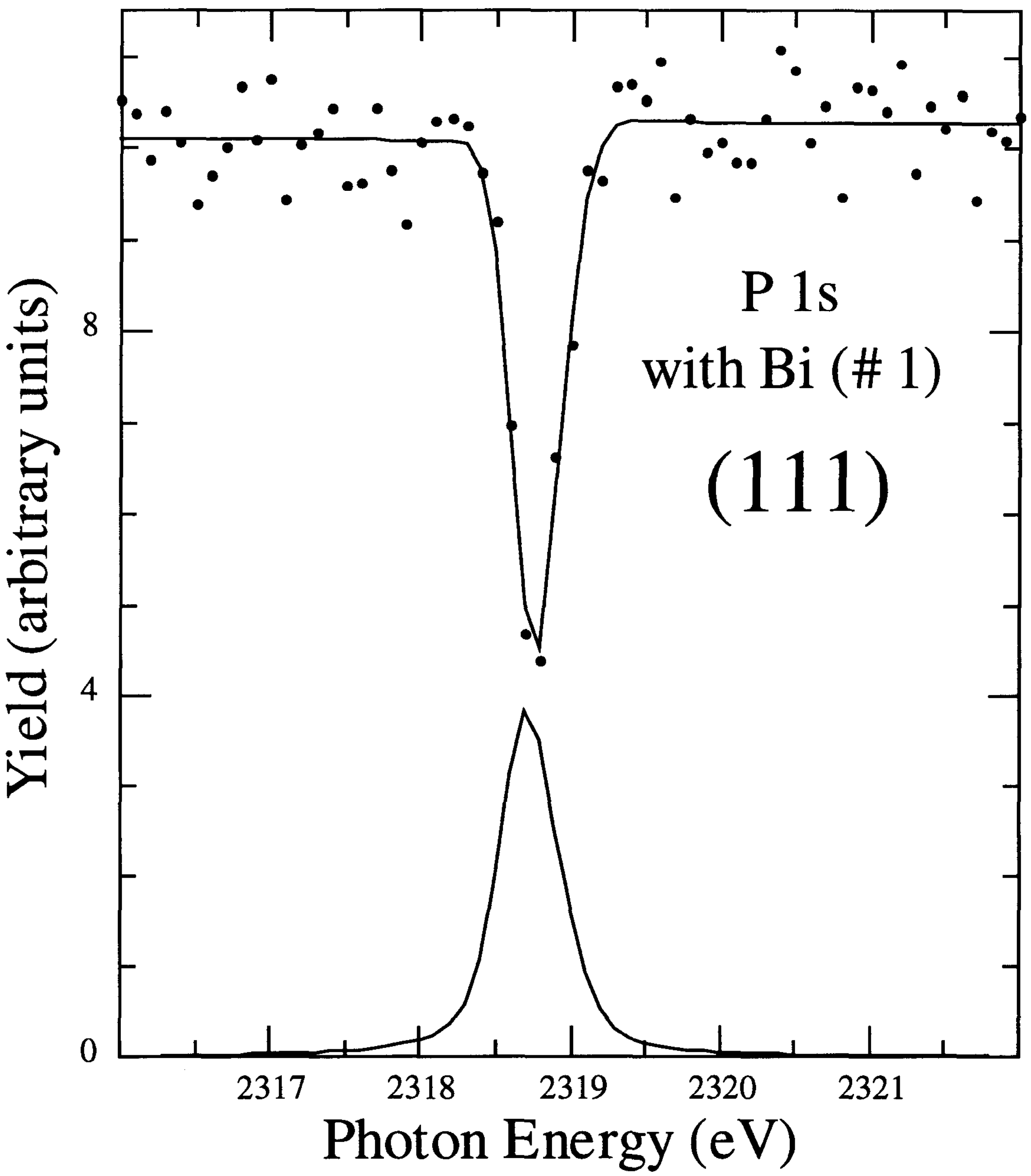

Figure 8.15. Phosphorus 1s XSW data and theoretical fit for the (111) reflection for a Bi-covered surface (#1). The bottom curve is the reflectivity.

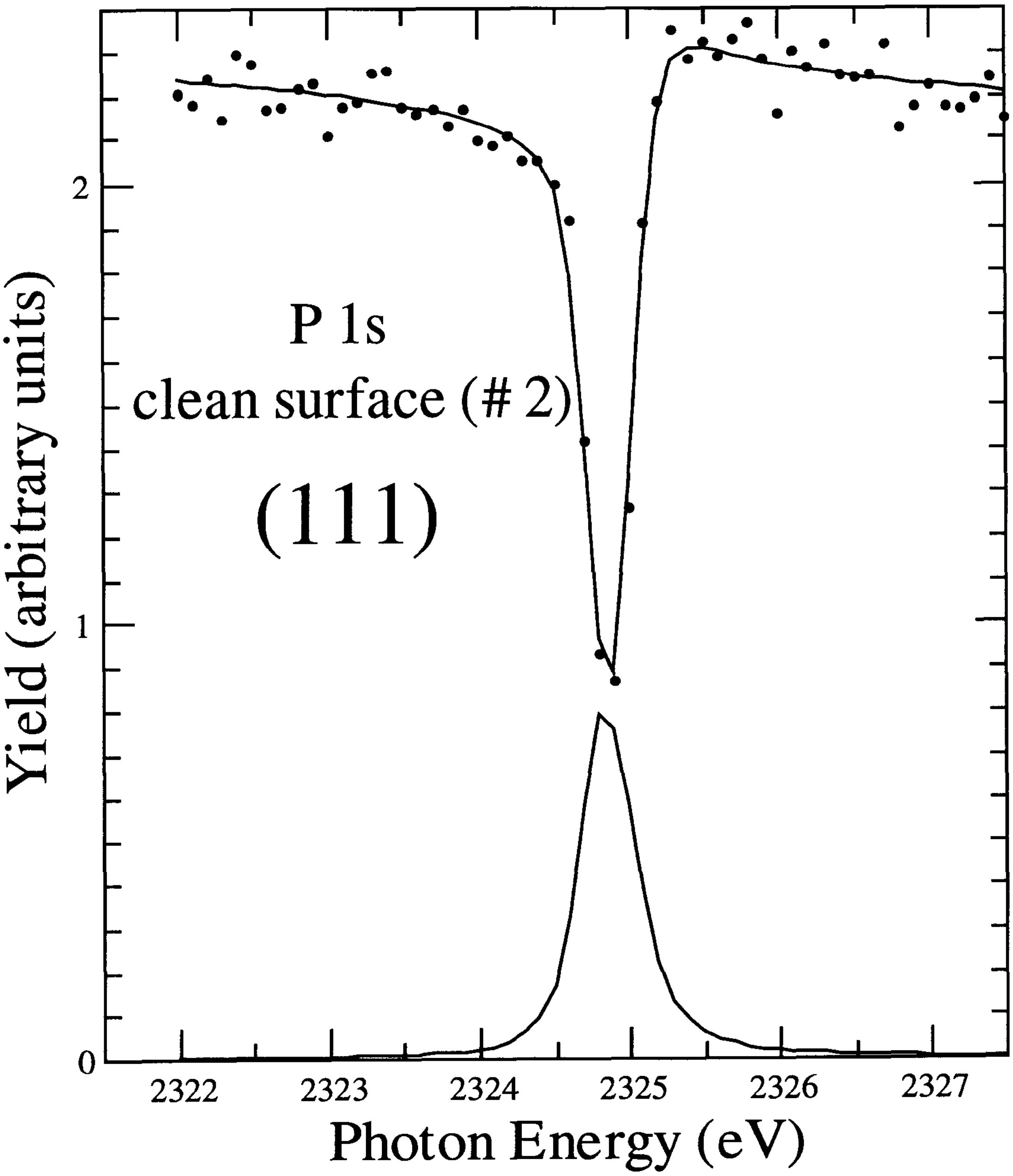

Figure 8.16. Phosphorus 1s XSW data and theoretical fit for the (111) reflection for a clean surface (#2). The bottom curve is the reflectivity.

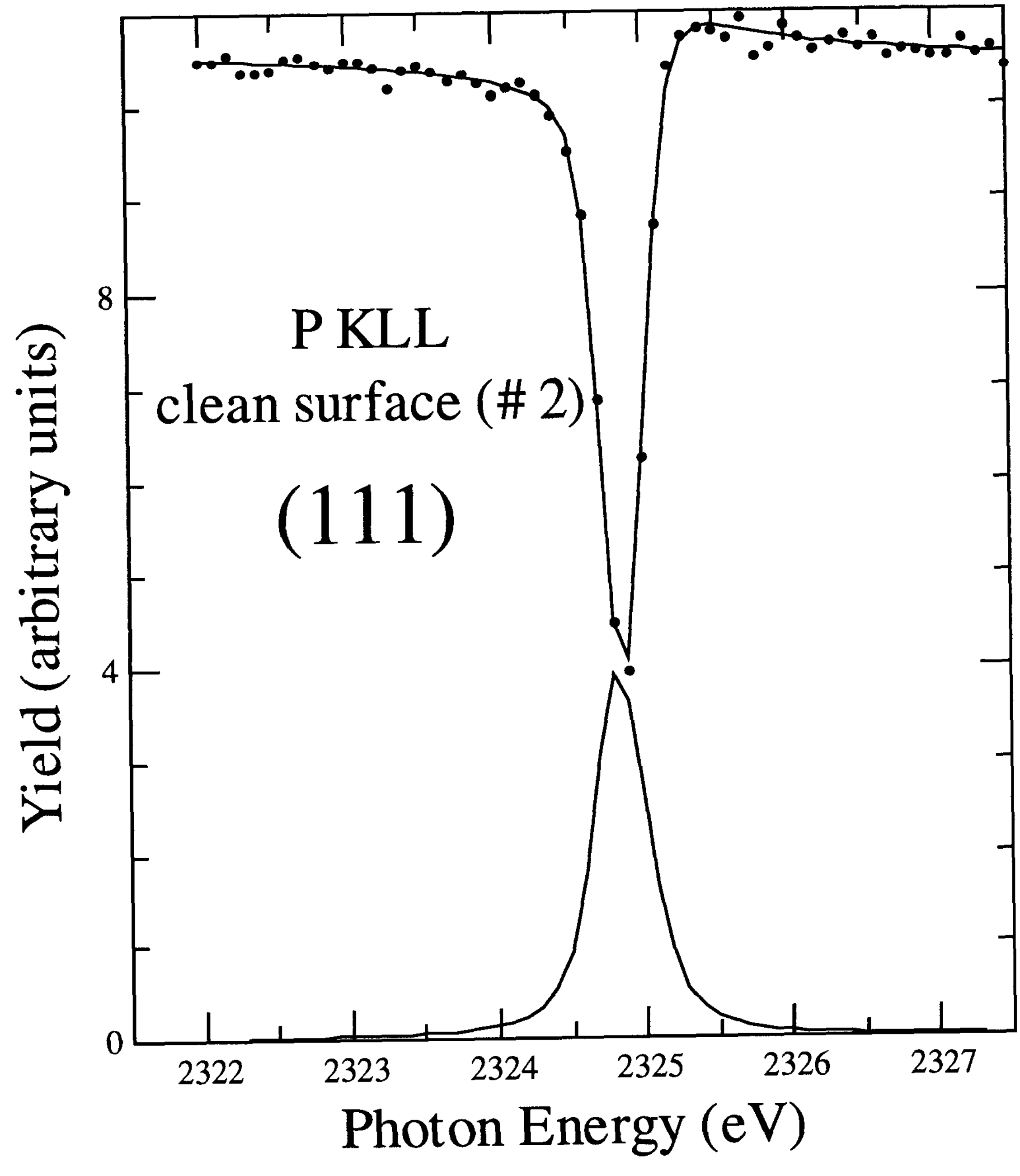

Figure 8.17. Phosphorus KLL XSW data and theoretical fit for the (200) reflection for a clean surface (#2). The bottom curve is the reflectivity.

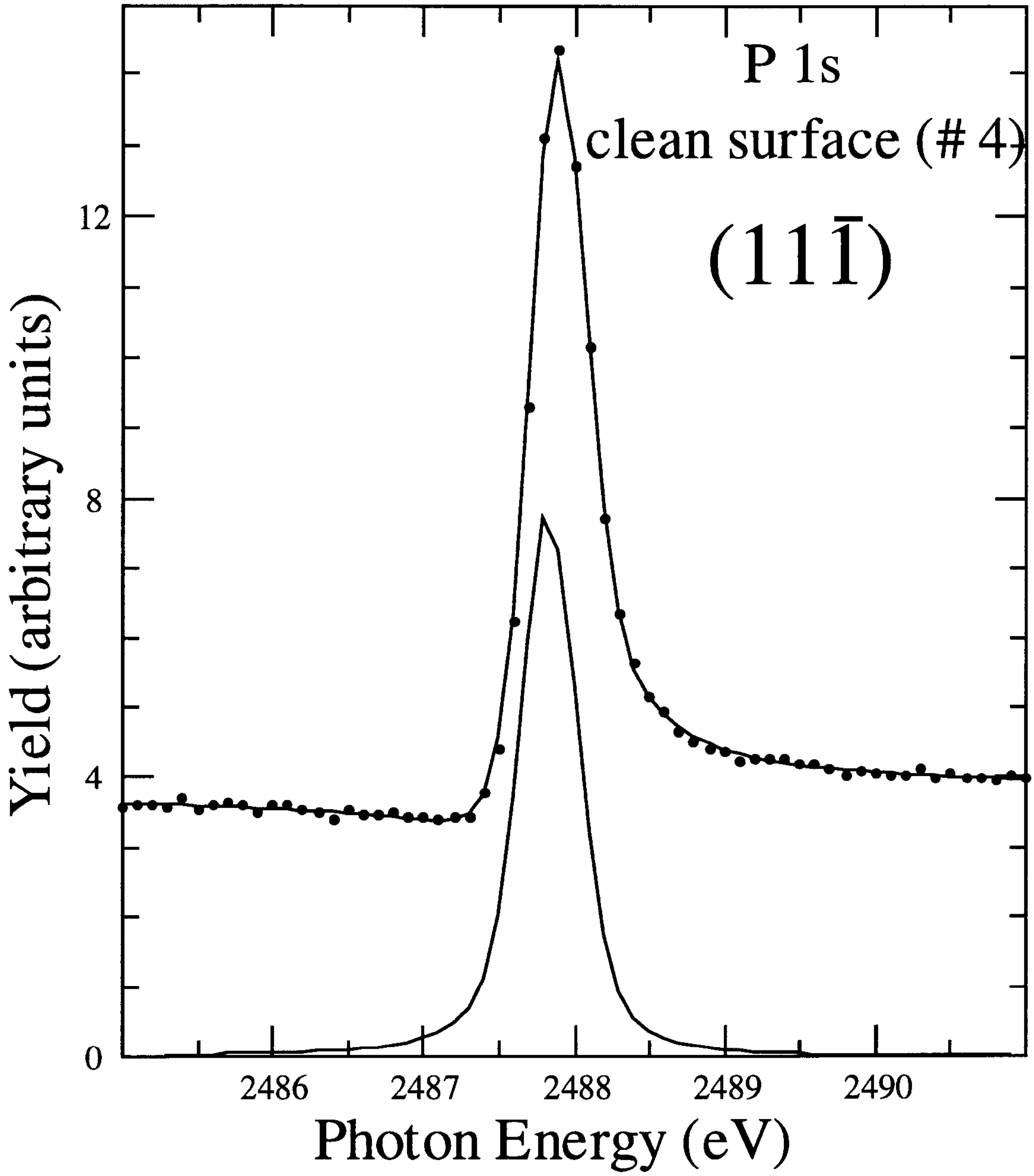

Figure 8.18. Phosphorus 1s XSW data and theoretical fit for the (11$\bar{1}$) reflection for a clean surface (# 4). The bottom curve is the reflectivity.

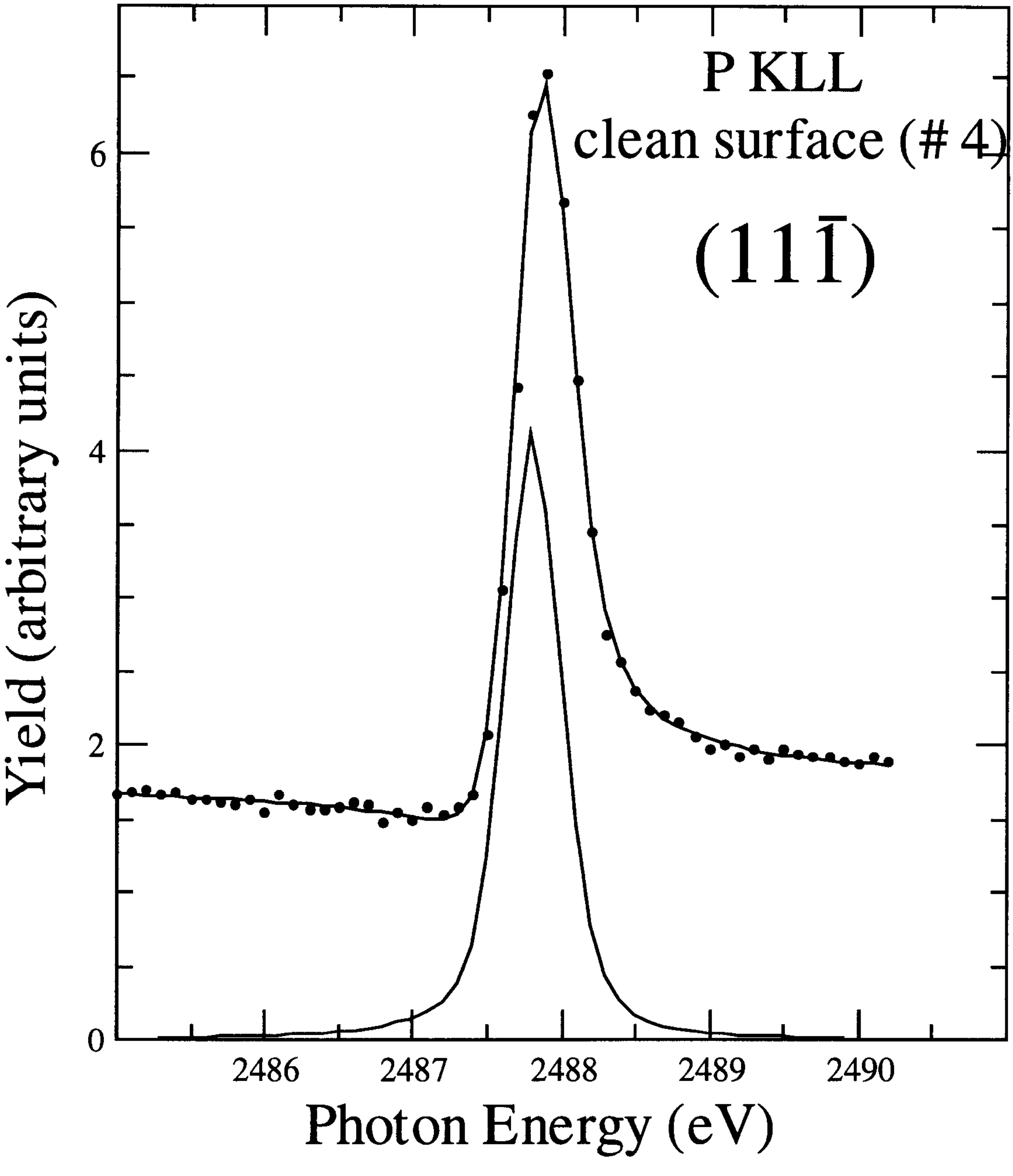

Figure 8.19. Phosphorus KLL XSW data and theoretical fit for the (11$\bar{1}$) reflection for a clean surface (# 4). The bottom curve is the reflectivity.

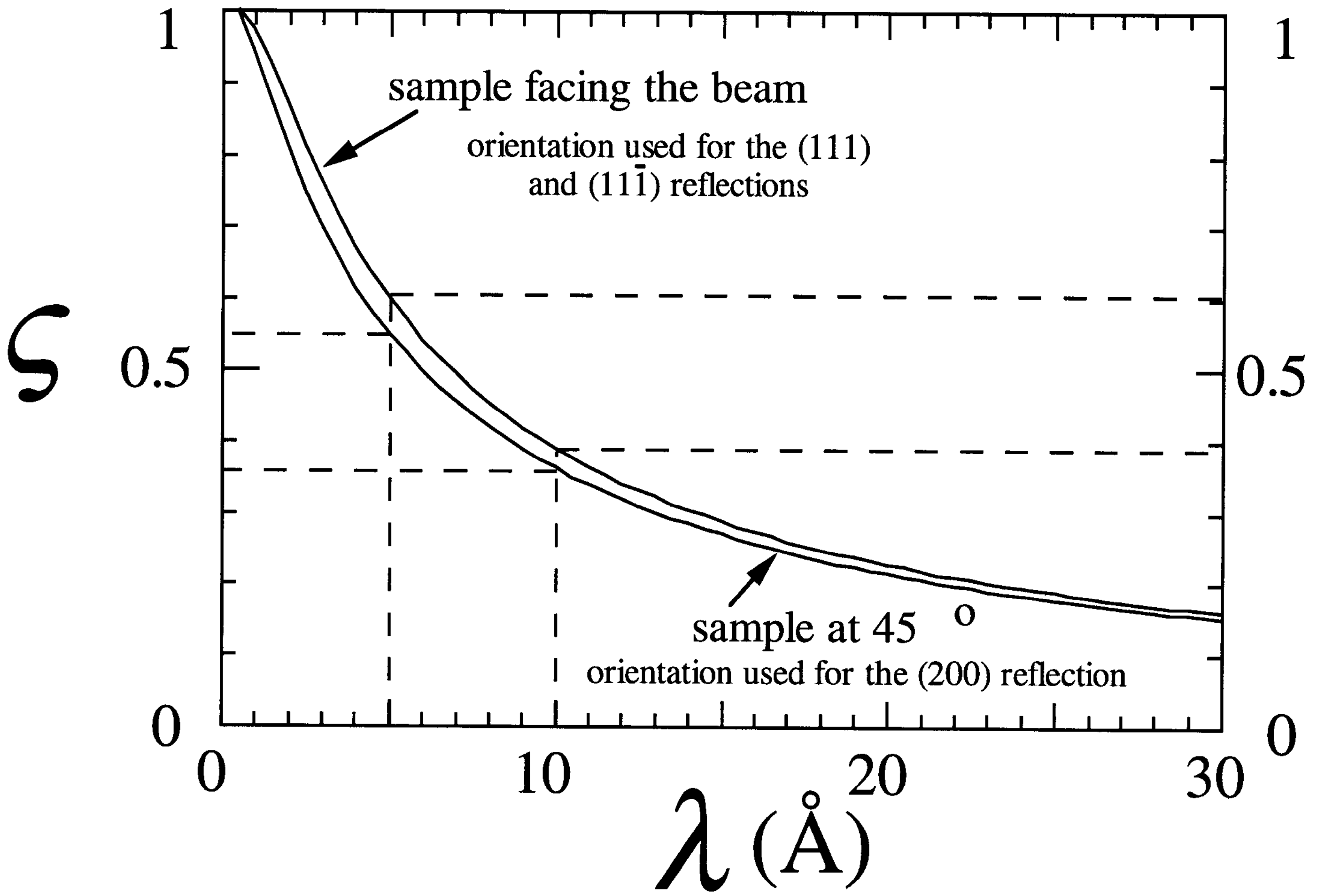

Figure 8.20. Fraction of the signal coming from the outermost substrate layer as a function of escape depth. The calculation have been done by integration of Eq. 8.7 for the angle acceptance of the CMA, for the sample orientations corresponding to the different reflections.

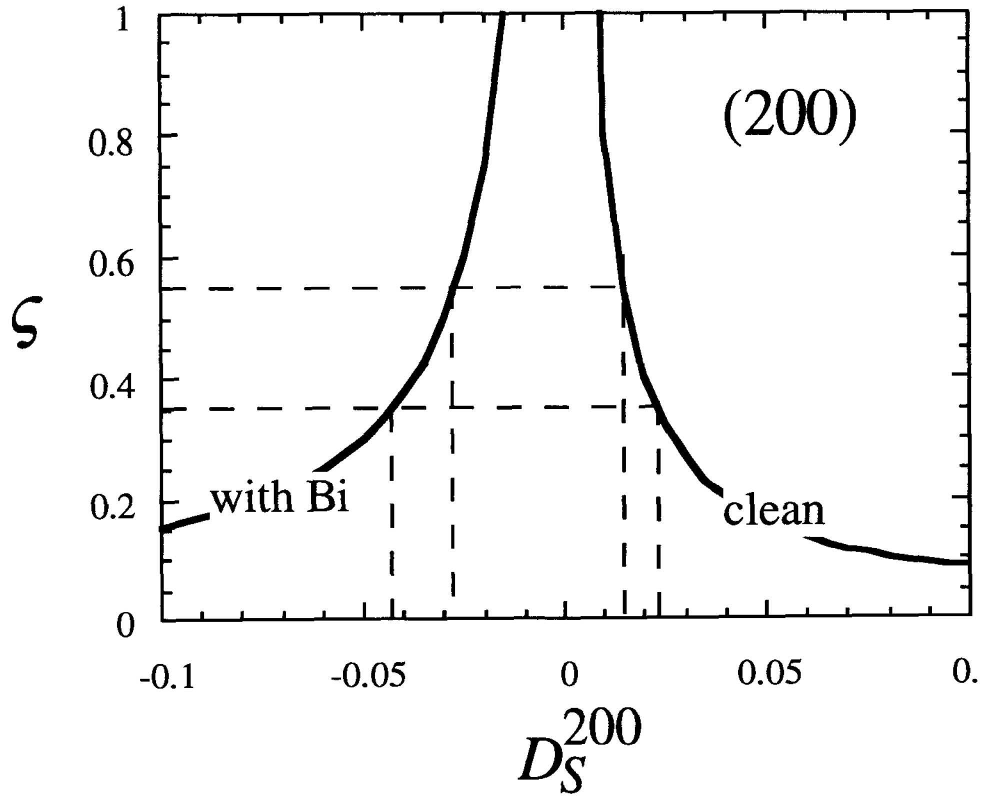

Figure 8.21. Graphical solution of Eq. 8.4 using the (200) coherent distance of Table 2. The phosphorus displacement is in interplanar units. The fraction of the signal coming from the outermost P atoms is calculated from Fig. 8.20.

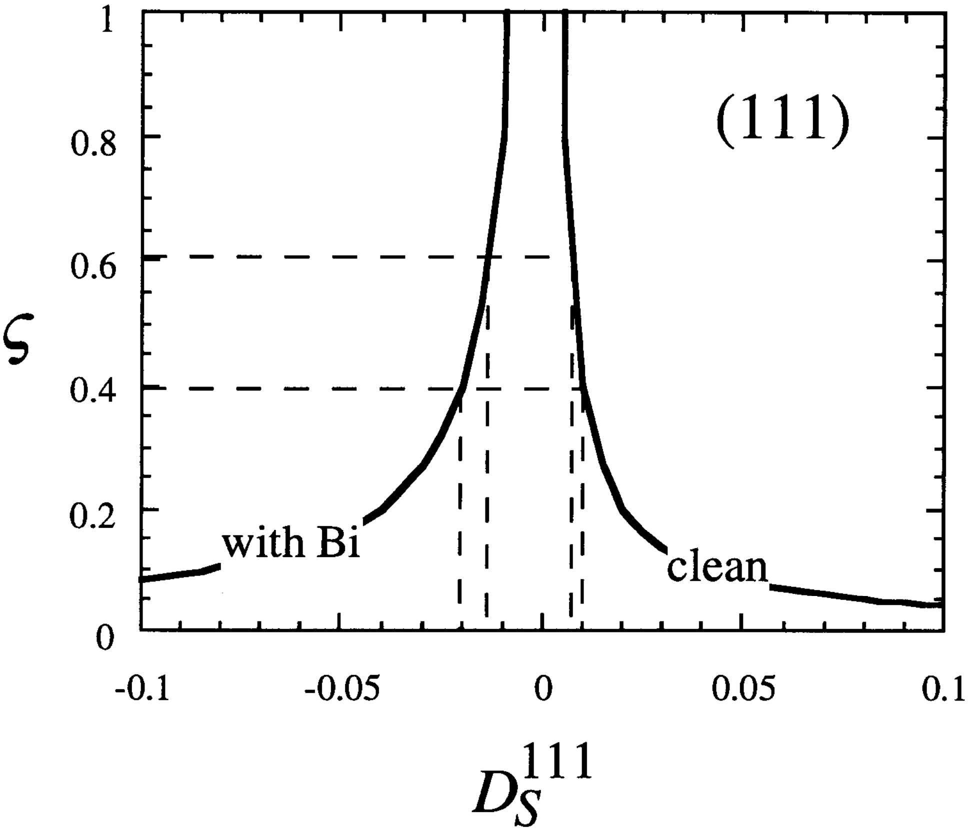

Figure 8.22. Graphical solution of Eq. 8.4 using the (111) coherent distance of Table 2. The phosphorus displacement is in interplanar units. The fraction of the signal coming from the outermost P atoms is calculated from Fig. 8.20.

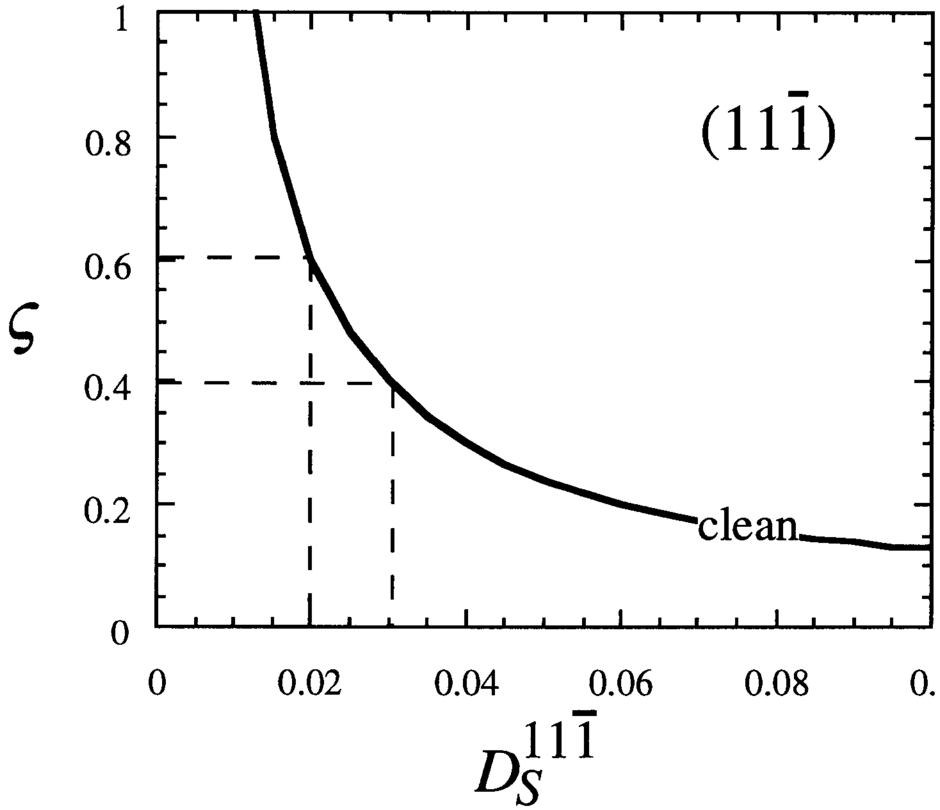

Figure 8.23. Graphical solution of Eq. 8.4 using the (11$\bar{1}$) coherent distance of Table 2. The phosphorus displacement is in interplanar units. The fraction of the signal coming from the outermost P atoms is calculated from Fig. 8.20.

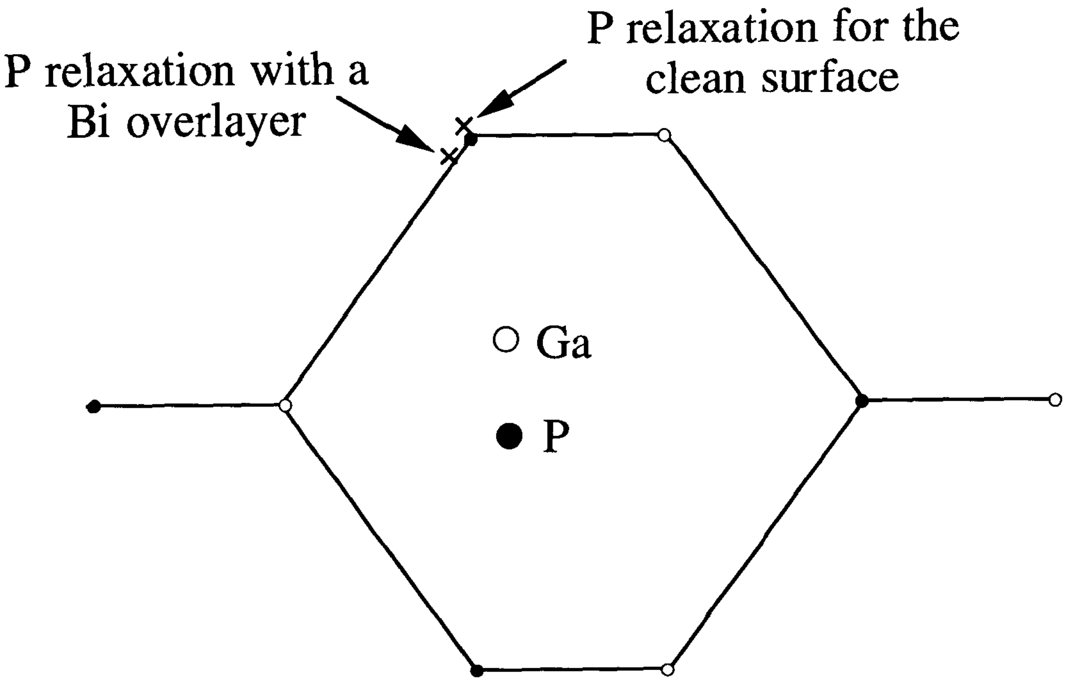

Figure 8.24. Relaxation of the outermost P atoms for the clean and Bi-covered (110) GaP surface scaled to our results.

Chapter 9. Conclusions

9.1 Summary

The central point of this thesis was the determination of the Bi geometric structure in the systems formed by one monolayer of Bi on the (110) cleaved surfaces of GaAs and GaP. The relaxation of P in the clean and covered GaP (110) surface was also studied.

The experimental and analytical method employed to study the Bi structure is identical for the Bi/GaAs and Bi/GaP systems, so much of the discussion about those systems was done in parallel. First of all, the level of simplification in which the problem of the overlayer structure were to be treated was clearly defined. Based on previous STM and PES studies, and comparing with other V/III-V interfaces, the two-site approximation in the Y-Z plane was used for both systems. The X direction, which is where the periodicity of the interfaces is more complex, was not studied. Three reflections [(220), (111), and $(11\bar{1})$] are required to triangulate two positions in the Y-Z plane, and to provided an intrinsic self-consistency check of the two-site approximation.

A new experimental configuration for the (111) and $(11\bar{1})$ reflections was developed that allowed performance of all three reflections on the same sample. Using the same surface was imperative to reduce the number of experimental variables, so that three reflections would indeed be enough to solve for the two positions in the Y-Z plane.

The back-reflection configuration used for the (220) reflection has an intrinsic multireflection problem because the (200) and (020) reflections are simultaneously satisfied to the (220) reflection. It was shown that the way to perform the analysis is to simply ignore the (200) and (020) reflections. This is in contrast to wafers, where there is a finite angle between the surface and the (220) planes, so that these two reflections cannot be ignored. To attack the multireflection problem, it was necessary to derive a simple enough wave equation for X-rays in crystals, to develop a method to deal with multireflections, and to create a program that could numerically solve the equations involved.

To analyze the experimental data, it was necessary to develop a more general fitting method, because the traditional Gaussian method was not accurate enough for our data. The new method is more dependable, theoretically better justified, and faster than other methods traditionally used. It greatly improves the quality of the fits and self-consistency of the results. Also needed was the creation of a computer-fitting program based on this method.

Changes of the temperature of the monochromator crystals creates a continuous shifting of the beam energy, so that consecutive experiments are shifted from one another. A criteria had to be developed to estimate the corrections to be done to the files before averaging. A computer averaging program was developed to perform these shifts based on the maximization of the correlation of the reflectivity.

The results for Bi on GaAs have remarkable reproducibility and self-consistency. They determine that the structure is described by ECLS, confirming the suggestions from LEED experiments and TBTE calculations that the structure is ECLS type. The self-consistency of the results about the Bi/GaP interface shows that the two-site approximation is an oversimplification. Nevertheless, the results indicate that the structure also resembles ECLS.

The method developed to measure the position of P surface atoms for GaP can be indistinguishably applied to the clean and Bi-covered GaP surface, so the effect of the Bi overlayer on the substrate relaxation can be clearly discriminated. For the clean surface, the P relaxation is in the form of a small outwards rotation with axis centered at the position of the second-layer Ga atom. The effect of the Bi overlayer on the P relaxation is a contraction towards the position of the second-layer Ga atom.

9.2 Contributions of this Dissertation

- This unique XSW study determined the position of two adatom sites in two dimensions, and the relaxation of the substrate surface —clean and covered—in three dimensions. The structure of the Bi overlayer on the (110) GaAs and GaP surfaces was determined under the two-site approximation in the Y-Z plane (Chapters 6 and 7). The relaxation of P for the clean GaP surface, as well as with the presence of a Bi overlayer, was determined in three dimensions (Chapter 8).

- The reflections required to triangulate two positions in the Y-Z plane were recognized. This also provided an intrinsic self-consistency check of the results (Chapter 2).

- An experimental method was developed that would allow the experiments for each of the three reflection to be performed onto a single surface (Chapter 3).

- A fundamental problem of the widely used (220) back-reflection configuration (also used in this work) consisting of multiple reflections was discussed in depth. The method to analyze the data that is taken in this configuration was established (Chapter 4).

- A simpler form of the wave equation for X-rays in crystals was derived that is suitable for the multireflection calculations (Chapter 4).

- A method was developed to deal with the multireflection problem suitable for numerical calculations (Chapter 4). A computer program was developed to carry out the calculations (Appendix 2).

- An analysis method was developed that greatly improves the quality and reliability of the fits (Chapter 5). A computer program that uses the new method was developed to carry out the fitting calculations (Appendix 3). A formalism was developed that included the dispersion of the X-ray beam and allowed a systematic discussion of the analysis method. As a side result, a formal definition of the distribution function was introduced (Chapter 5).

- The averaging of the data was done by first shifting the data to maximize the correlation of the reflectivity (Chapter 6). A computer program was developed to calculate this shift and to average the data (Appendix 4).

9.3 Future Work

9.3.1 Determination of other V/III-V structures

The methodology presented in this dissertation is ready to be applied to similar systems of interest.

9.3.2 Substrate relaxation

As mentioned in Chapters 6 and 8, the relaxation of Ga and As could not be measured in any of the GaAs and GaP cases because the photon energies used did not produce surface-sensitive Ga or As photopeaks. Those experiments can be done, however, if the angle is such that the Bragg energy of the reflections is above the K edge of Ga (As). At these energies ($\sim$ 11 KeV), it is necessary to use a nondispersive configuration in order to have satisfactory resolution.

Appendix 1. The Reflectance as a Function of Energy

Batterman and Cole (B&C), in their classical 1964 paper [1], provided a detailed derivation of the XSW expression for the case in which the incident photon energy is kept fixed and the angle is scanned through the Bragg condition. However, in the experiments presented in this dissertation, the angle of incidence of the X-ray beam is kept constant and the photon energy is scanned through the Bragg condition. The appropriate expression for the reflectance (defined in Chapter 5) that is used in the analysis of data obtained with this experimental mode are derived in Section A1.2.

The method of derivation has many elements that are used in Chapter 4 to solve the (220) back-reflection multireflection problem. It is very systematic, so it paves the way for further generalizations, and it also fits into the general framework of this thesis. Equivalent equations were later found in the literature [2]. The formulas derived in Section A1.2 are extensively used in the analysis of the experimental data (see Chapter 5). Section A1.1 provides the basic formulas for the discussion of Section A1.2.

A1.1 The dispersion relation and its simplification

The discussion of this section—the derivation of the dispersion equation of X-rays in crystals near a Bragg condition—takes many elements from the B&C paper. An equivalent dispersion equation was already derived by B&C. The present derivation is more correct and general, because it does not neglect the longitudinal term of B&C's Eq. A12 (as erroneously done by B&C). This B&C error is happily annulled by a second one, so that their final result is correct. Both derivations merge in Eq. A1.5, and are identical from there to the end of Section A1.1 (this section).

In the Bragg case, there is a crystal vector $\mathbf{H}_1$ for which

$$\left[k_0^2(1-\Gamma F_0)-(\mathbf{K}_0+\mathbf{H}_1)\cdot(\mathbf{K}_0+\mathbf{H}_1)\right]$$

is small (see Section 4.2.2). Then, in addition to $(\mathbf{K}_0, \nu)$, the radiation mode $(\mathbf{K}_0+\mathbf{H}_1, \nu)$ is also excited; all the other terms in the series of Eq. 4.12 can be neglected. Equation 4.12 for $\mathbf{K}=\mathbf{K}_0$ reads:

$$\left[k_0^2(1-\Gamma F_0)-K_0^2\right]\mathbf{E}(\mathbf{K}_0)-k_0^2\,\Gamma F_{\overline{\mathbf{H}}_1}\mathbf{E}_{\perp\mathbf{K}_0}(\mathbf{K}_1) \;=\; 0 \;, \qquad \text{(A1.1)}$$

where we have written

$$\mathbf{K}_1 \equiv \mathbf{K}_0 + \mathbf{H}_1 \quad . \tag{A1.2}$$

When Eq. 4.12 is applied to $\mathbf{K} = \mathbf{K}_1$, the term that survives in the series is for $\mathbf{H} = \overline{\mathbf{H}}_1$, so we get:

$$\left[k_0^2(1-\Gamma F_0) - K_1^2\right] \mathbf{E}(\mathbf{K}_1) - k_0^2\, \Gamma F_{\mathbf{H}_1} \mathbf{E}_{\perp\mathbf{K}_1}(\mathbf{K}_0) = 0 \quad . \tag{A1.3}$$

Besides Eqs. A1.1 and A1.3, there is no other $\mathbf{K}$ for which Eq. 4.12 involves any of the $(\mathbf{K}_0, \nu)$ and $(\mathbf{K}_1, \nu)$ modes.

To consider the system formed by Eqs. A1.1 and A1.3 as complete, we need to get the relations between $\mathbf{E}_{\perp\mathbf{K}_0}(\mathbf{K}_1)$ and $\mathbf{E}(\mathbf{K}_1)$, and between $\mathbf{E}_{\perp\mathbf{K}_1}(\mathbf{K}_0)$ and $\mathbf{E}(\mathbf{K}_0)$. This is done very conveniently by discussing each polarization separately. The fact that $\mathbf{E}_{\perp\mathbf{K}_0}(\mathbf{K}_1)$ and $\mathbf{E}(\mathbf{K}_0)$ are along the same direction (see Eq. A1.1), as well as $\mathbf{E}_{\perp\mathbf{K}_1}(\mathbf{K}_0)$ and $\mathbf{E}(\mathbf{K}_1)$ (see Eq. A1.3), is used to obtain the following scalar relations:

$$\left.\begin{aligned} E_{\perp\mathbf{K}_0}(\mathbf{K}_1) &= E(\mathbf{K}_1) \\ &\text{and} \\ E_{\perp\mathbf{K}_1}(\mathbf{K}_0) &= E(\mathbf{K}_0) \end{aligned}\right\rangle \sigma \text{ polarization} , \tag{A1.4a}$$

$$\left.\begin{aligned} E_{\perp\mathbf{K}_0}(\mathbf{K}_1) &= E(\mathbf{K}_1)\,|\sin 2\chi| \\ &\text{and} \\ E_{\perp\mathbf{K}_1}(\mathbf{K}_0) &= E(\mathbf{K}_0)\,|\sin 2\chi| \end{aligned}\right\rangle \pi \text{ polarization} , \tag{A1.4b}$$

where χ is the angle between $\mathbf{k}_0$ and $\overline{\mathbf{H}}_1$. It is important to stress that Eqs. A1.4 cannot be obtained from Eq. 4.9 (which is equivalent to B&C Eq. A12) by neglecting the last term, but that the complete derivation provided by Eq. 4.12 is essential.

As in B&C's paper, we define P as 1 for the σ polarization, and $\sin 2\chi$ for the π polarization, so that we can rewrite Eqs. A1.1 and A1.3 as:

$$\left[k_0^2(1-\Gamma F_0) - K_0^2\right] E(\mathbf{K}_0) - k_0^2\, \Gamma F_{\overline{\mathbf{H}}_1} P\, E(\mathbf{K}_1) = 0 \quad , \tag{A1.5a}$$

$$\left[k_0^2(1-\Gamma F_0) - K_1^2\right] E(\mathbf{K}_1) - k_0^2\, \Gamma F_{\mathbf{H}_1} P\, E(\mathbf{K}_0) = 0 \quad . \tag{A1.5b}$$

reflection. Similarly, the dispersion relation is obtained by noticing that the system has a nontrivial solution if the determinant is zero:

$$\begin{vmatrix} k_0^2(1-\Gamma F_0)-K_0^2 & P\,k_0^2\,\Gamma F_{\bar{H}_1} \\ P\,k_0^2\,\Gamma F_{H_1} & k_0^2(1-\Gamma F_0)-K_1^2 \end{vmatrix} = 0\ . \tag{A1.6}$$

Equation A1.6 is the analog to Eq. 4.16, although solving A1.6 is far more complicated than solving Eq. 4.16. After some simplifications are done, the solution of Eq. A1.6 is presented in the following section (Section A1.2). This forth-order equation can be reduced to quadratic by the following approximations (see B&C's Eq. 18):

$$\begin{aligned} k_0^2(1-\Gamma F_0)-K_0^2 &= \left[k_0\sqrt{1-\Gamma F_0}\,-K_0\right]\left[k_0\sqrt{1-\Gamma F_0}\,+K_0\right] \\ &\approx \left[k_0\sqrt{1-\Gamma F_0}\,-K_0\right]\,2\,k_0 \\ &\approx \left[k_0(1-1/2\,\Gamma F_0)\,-K_0\right]\,2\,k_0 \end{aligned} \tag{A1.7}$$

and

$$\begin{aligned} k_0^2(1-\Gamma F_0)-K_1^2 &= \left[k_0\sqrt{1-\Gamma F_0}-K_1\right]\left[k_0\sqrt{1-\Gamma F_0}+K_1\right] \\ &\approx \left[k_0\sqrt{1-\Gamma F_0}-K_1\right]\,2\,k_0 \\ &\approx \left[k_0(1-1/2\,\Gamma F_0)-K_1\right]\,2\,k_0 \end{aligned} \tag{A1.8}$$

Approximating $\left[k_0\sqrt{1-\Gamma F_0}+K_0\right]$ (and $\left[k_0\sqrt{1-\Gamma F_0}+K_1\right]$) to $2\,k_0$ is very well justified because its ratio differs from one in 10^{-5}. It is also convenient to introduce the following abbreviations:

$$\xi_0 \equiv K_0-k_0\left(1-\frac{1}{2}\,\Gamma F_0\right)\ , \tag{A1.9a}$$

$$\xi_1 \equiv K_1-k_0\left(1-\frac{1}{2}\,\Gamma F_0\right)\ . \tag{A1.9b}$$

Using the approximations of Eqs. A1.7 and A1.8, and the definitions of Eqs. A1.9, Eqs. A1.5 read:

$$2k_0\xi_0 E(\mathbf{K}_0)+k_0^2\,\Gamma F_{\overline{\mathbf{H}}_1} P\,E(\mathbf{K}_1) \;=\; 0\ , \tag{A1.10a}$$

$$2k_0\xi_1 E(\mathbf{K}_1)+k_0^2\,\Gamma F_{\mathbf{H}_1} P\,E(\mathbf{K}_0) \;=\; 0\ , \tag{A1.10b}$$

and Eq. A1.6 reduces to:

$$\xi_0\,\xi_1-\frac{1}{4}\,P^2k_0^2\,\Gamma^2\,F_{\mathbf{H}_1}\,F_{\overline{\mathbf{H}}_1} \;=\; 0\ , \tag{A1.11}$$

which is equivalent to B&C's Eq. 21.

A1.2 Derivation of the expression of the reflectance

This discussion consists of basically solving the dispersion relation, Eq. A1.11. The geometry is defined in terms of the angles between the incident beam, the crystal surface, and the Bragg planes (shown in Fig. A1.1) and can be written:

$$\cos\alpha \;=\; \mathbf{n}\cdot\hat{\mathbf{H}}_1, \tag{A1.12a}$$

$$\cos\gamma \;=\; \hat{\mathbf{k}}_0\cdot\overline{\mathbf{n}}\ , \tag{A1.12b}$$

$$\cos\chi \;=\; \hat{\mathbf{k}}_0\cdot\left(-\hat{\mathbf{H}}_1\right)\ , \tag{A1.12c}$$

where $\hat{\mathbf{H}}_1$ is the unitary vector in the direction of $\mathbf{H}_1$, $\mathbf{n}$ is the unitary vector normal to the surface, and $\hat{\mathbf{k}}_0$ is the unitary vector in the direction of $\mathbf{k}_0$.

We now express K_0 and K_1 in terms of the angles and $\mathbf{k}_0$. As discussed in Section 4.3.1, from the boundary conditions, $\mathbf{K}_0$ differs from $\mathbf{k}_0$ in a vector perpendicular to the surface:

$$\mathbf{K}_0 \;=\; \mathbf{k}_0+q\mathbf{n}\ ; \tag{A1.13}$$

then

$$K_0 \;\equiv\; \sqrt{\mathbf{K}_0\cdot\mathbf{K}_0} \;=\; \sqrt{k_0^2+2q\mathbf{k}_0\cdot\mathbf{n}+q^2}\ \ .$$

Here, q is small because, for X-rays, the dielectric function of the crystal is nearly equal to the dielectric function of vacuum. Expanding the square root and ignoring square terms in q, we get:

$$K_0 = k_0 - q\cos\gamma \ . \tag{A1.14}$$

From Eq. A1.9a we get

$$\xi_0 = k_0 - q\cos\gamma - k_0\left(1 - \frac{1}{2}\ \Gamma F_0\right) = -q\cos\gamma + \frac{1}{2}\ \Gamma F_0 k_0 \quad .\text{(A1.15)}$$

To obtain K_1, it is useful to divide $\mathbf{k}_0$ into two parts:

$$\mathbf{k}_0 = (k_0' + \Delta k)\,\hat{\mathbf{k}}_0 \ , \tag{A1.16}$$

where

$$k_0' \equiv \frac{H_1}{2\cos\chi} \tag{A1.17}$$

and Δk is defined by $\Delta k \equiv k_0 - k_0'$. Notice that Δk is very small because, as stated in Section 4.2.2, $\mathbf{k}_0$ very nearly satisfies the kinematical Bragg condition (within a deviation of 10^{-4}), and k_0' is defined to exactly satisfy the Bragg condition. With these definitions, we can write:

$$\mathbf{K}_1 \equiv \mathbf{K}_0 + \mathbf{H}_1 = (k_0' + \Delta k)\,\hat{\mathbf{k}}_0 + q\mathbf{n} + \mathbf{H}_1 \ ,$$

with $\mathbf{k}_0' \equiv k_0'\hat{\mathbf{k}}_0$,

$$\mathbf{K}_1 = (\mathbf{k}_0' + \mathbf{H}_1) + \Delta k\hat{\mathbf{k}}_0 + q\mathbf{n} \tag{A1.18a}$$

or

$$\mathbf{K}_1 = \mathbf{k}_1' + \Delta k\hat{\mathbf{k}}_0 + q\mathbf{n} \tag{A1.18b}$$

where $\mathbf{k}_1' \equiv \mathbf{k}_0' + \mathbf{H}_1$. Notice that the magnitude of $\mathbf{k}_1'$ is equal to k_0'; that is, the vectors $\mathbf{k}_0'$ and $\mathbf{k}_1'$ exactly satisfy the Bragg condition:

$$k_1' = k_0' \ . \tag{A1.19}$$

From $K_1 \equiv \sqrt{\mathbf{K}_1 \cdot \mathbf{K}_1}$, expanding the square root and ignoring the quadratic terms in Δk and q, we get:

$$K_1 = k_1' + \frac{1}{k_1'}\, \mathbf{k}_1' \cdot \Delta k \hat{\mathbf{k}}_0 + \frac{1}{k_1'}\, \mathbf{k}_1' \cdot q\mathbf{n} = k_1' + \frac{1}{k_1'}\left(\mathbf{k}_0' + \mathbf{H}_1\right) \cdot \Delta k \hat{\mathbf{k}}_0 + \frac{1}{k_1'}\left(\mathbf{k}_0' + \mathbf{H}_1\right) \cdot q\mathbf{n} \ .$$

Performing the dot products, we get:

$$K_1 = k_1' + \frac{1}{k_1'}\left(k_0' - H_1 \cos\chi\right)\Delta k + \frac{1}{k_1'}\left(-k_0' \cos\gamma + H_1 \cos\alpha\right) q \ .$$

Using Eqs. A1.17 and A1.19, we get:

$$K_1 = k_1' + \left(1 - 2\cos^2\chi\right)\Delta k + \left(-\cos\gamma + 2\cos\chi \, \cos\alpha\right) q \ ,$$

but $k_1' + \Delta k = k_0$; then

$$K_1 = k_0 - 2\cos^2\chi \, \Delta k + -q\cos\gamma + 2q\cos\chi \, \cos\alpha \ . \qquad \text{(A1.20)}$$

Substituting into Eq. A1.9b, we get:

$$\xi_1 = -2\cos^2\chi \, \Delta k - q\cos\gamma + 2q\cos\chi \, \cos\alpha + \frac{1}{2}\, \Gamma F_0 k_0 \ . \qquad \text{(A1.21)}$$

Using Eq. A1.15 to express q in terms of ξ_0, and substituting into Eq. A1.21, gives us:

$$\xi_1 = \left(1 - 2\,\frac{\cos\chi \, \cos\alpha}{\cos\gamma}\right) \xi_0 - 2\cos^2\chi \, \Delta k + \frac{\cos\chi \, \cos\alpha}{\cos\gamma}\, \Gamma F_0 k_0 \ . \qquad \text{(A1.22)}$$

Substituting Eq. A1.22 into Eq. A1.11, we get a quadratic equation for ξ_0:

$$\left(2\,\frac{\cos\chi \, \cos\alpha}{\cos\gamma} - 1\right)\xi_0^2 + \left(2\cos^2\chi \, \Delta k - \frac{\cos\chi \, \cos\alpha}{\cos\gamma}\, \Gamma F_0 k_0\right) + \frac{1}{4}\, P^2 k_0^2 \, \Gamma^2 F_{\mathbf{H}_1} F_{\bar{\mathbf{H}}_1} = 0 \ .$$

(A1.23)

The following definitions simplify the notation:

$$a \equiv 2\,\frac{\cos\chi \, \cos\alpha}{\cos\gamma} - 1 \qquad \text{(A1.24)}$$

and

$$b \equiv 2\cos^2\chi\,\Delta k - \frac{\cos\chi\,\cos\alpha}{\cos\gamma}\,\Gamma F_0 k_0 \ . \tag{A1.25}$$

The solution of Eq. A1.23 can be written in terms of these abbreviations:

$$\xi_0 = \frac{1}{2a}\left(-b \pm \sqrt{b^2 - aP^2k_0^2\,\Gamma^2\,F_{\mathbf{H}_1}\,F_{\overline{\mathbf{H}}_1}}\right) \tag{.A1.26}$$

The reflectance, defined in Eq. 5.9, can be obtained from Eq. A1.10a and definition A1.9a:

$$\rho(\mathbf{k}_0) \equiv \frac{E(\mathbf{K}_1)}{E(\mathbf{K}_0)} = -\frac{2\xi_0}{k_0\,\Gamma F_{\overline{\mathbf{H}}_1} P} \ . \tag{A1.27}$$

A more convenient abbreviation, very similar to that of Eq. A1.25, is the following:

$$\eta \equiv \frac{b}{\sqrt{a}\,\sqrt{F_{\mathbf{H}_1}F_{\overline{\mathbf{H}}_1}}\;k_0\Gamma} = \frac{2\cos^2\chi\,\dfrac{\mathrm{E}-\mathrm{E}_B}{\mathrm{E}} - \dfrac{a+1}{2}\,\Gamma F_0}{\sqrt{a}\,\sqrt{F_{\mathbf{H}_1}F_{\overline{\mathbf{H}}_1}}\;\Gamma} \ , \tag{A1.28}$$

where

$$\mathrm{E}_B \equiv \frac{|\mathbf{H}_1|}{2\cos\chi} \ . \tag{A1.29}$$

E_B can be recognized as the kinematical Bragg energy.

Finally, we obtain for the reflectance:

$$\rho(\mathbf{k}_0) = \frac{1}{\sqrt{a}}\sqrt{\frac{F_{\mathbf{H}_1}}{F_{\overline{\mathbf{H}}_1}}}\left(\eta \pm \sqrt{\eta^2 - 1}\right) . \tag{A1.30}$$

The angles for each configuration are used to calculate a (see Fig. A1.1). This is the expression for the reflectance that is used in Chapter 5 for the analysis of the data.

References

1. B.W. Batterman and H. Cole. "Dynamical diffraction of X-rays by perfect crystals." Review of Modern Physics **36**, p. 681 (1964).

2. W.H. Zachariasen. "Theory of X-Ray Diffraction in Crystals." Dover Publications, Inc., New York (1945).

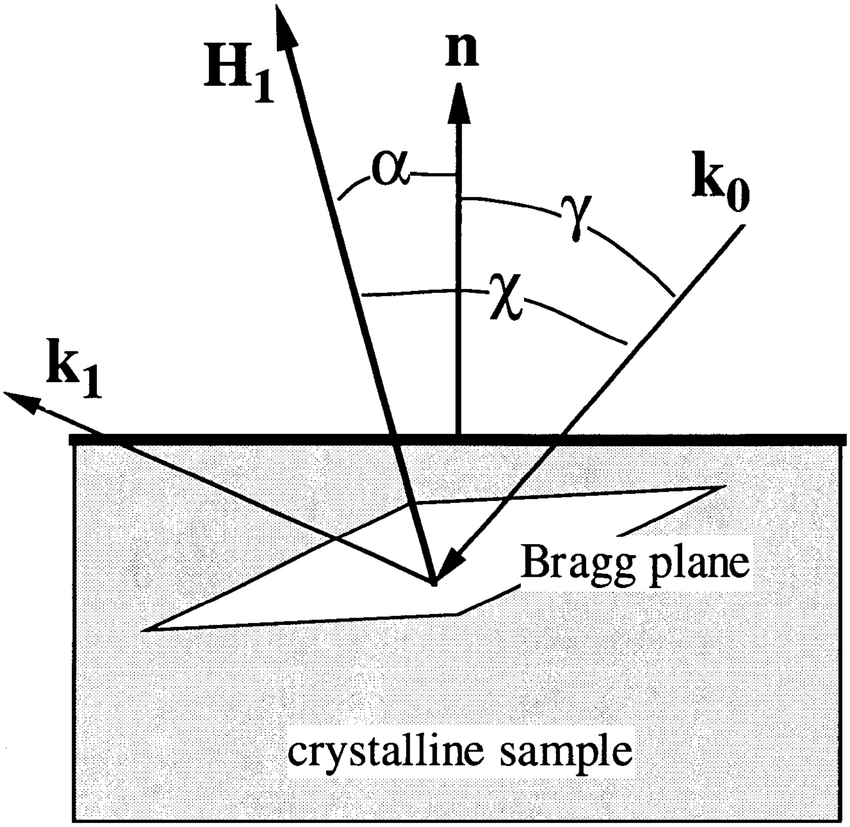

Figure A1.1. Angles that define the orientation of the sample and Bragg planes with respect to the incoming beam.

Appendix 2.   Program “MULTIREFL”

This MATHEMATICA program was used for the multireflection calculations of Chapter 4.

```
GetRoot[ener_,teta_,fi_]:=
 Block[  {m,j,gamma,k1,sol,
         i,ii,
         sw,
         d1,d2,
          r1,r2,ref1,ref2,ref3,ref,
           xxsi0,xxsi1,xxsi2,xxsi3,xsi0,xsi1,xsi2,xsi3,
            kk0sq,k0sq,h1,h2,h3,h4,f0,f1,f2,f3,f4,
         costeta2,costeta3,teta1,alfa,
         q,qq,
         ret},
     xxsi0=Array[el1,{8}];
     xxsi1=Array[el2,{8}];
     xxsi2=Array[el3,{8}];
     xxsi3=Array[el3,{8}];
     kk0sq=Array[el4,{8}];
     qq=Array[el5,{8}];
     ref1=Array[el6,{8}];
     ref2=Array[el7,{8}];
     ref3=Array[el8,{8}];
     ref=Array[el9,{5,8}];
     m=Array[el10,{4,4}];
     sw=Array[el11,{10}];
     ret=Array[el12,13];
          j = 0;
          gamma=27.276/ener^2;
          k = ener/1974;
          f0= (56.54+I 7.01) gamma;
          f1= (39.19+I 7.01) gamma;
          f2= (23.03+I 2.09) gamma;
          f3= f2;
```

```
            f4= f1;
            h1=2 N[Pi,5] /(5.8686/Sqrt[8]);
            h2=2 N[Pi,5] /(5.8686/2);
            h3=h2;
            alfa  = Sin[teta] Cos[fi];
            teta1 = teta;
            costeta2 =  1/Sqrt[2] (Cos[teta] + alfa) ;
            costeta3 =  1/Sqrt[2] (Cos[teta] - alfa) ;
            k1    = h1/( 2 Cos[teta1] );
   k0sq := k^2 + 2 k q Cos[teta] + q^2;
   xsi0 := k0sq - k^2 (1-f0);
   xsi1 := h1^2 + k0sq -2 k h1 Cos[teta1]
                  - 2 h1 q - k^2 (1-f0);
   xsi2 := h2^2 + k0sq -2 k h2 costeta2
                  - 2 h2 q/Sqrt[2] - k^2 (1-f0);
   xsi3 := h3^2 + k0sq -2 k h3 costeta3
                  - 2 h3 q/Sqrt[2] - k^2 (1-f0);
m:={
   {  xsi0   , k^2 f1   , k^2 f2   , k^2 f3   },
   { k^2 f1   ,    xsi1  , k^2 f3   , k^2 f2   },
   { k^2 f2   , k^2 f3   ,    xsi2  , k^2 f4   },
   { k^2 f3   , k^2 f2   , k^2 f4   ,    xsi3  }

                                                         };
    sol = N[Solve[Det[m]==0,q]];
     For[i=1,i<=8,i++,
  qq[[i]] = sol[[i,1]][[2]];
  kk0sq[[i]] = k^2 + 2 k qq[[i]] Cos[teta] + qq[[i]]^2;
xxsi0[[i]] = kk0sq[[i]] - k^2 (1-f0);
xxsi1[[i]] = h1^2 + kk0sq[[i]] - 2 k h1 Cos[teta1] - 2 h1 qq[[i]]
             - k^2 (1-f0) ;
xxsi2[[i]] = h2^2 + kk0sq[[i]] - 2 k h2 costeta2
             - 2 h2 qq[[i]]/Sqrt[2] - k^2 (1-f0) ;
xxsi3[[i]] = h3^2 + kk0sq[[i]] - 2 k h3 costeta3
             - 2 h3 qq[[i]]/Sqrt[2] - k^2 (1-f0) ;
ref1[[i]] = (k^2 f1 - xxsi0[[i]])/( k^2 f1 - xxsi1[[i]] );
ref2[[i]] = (k^2 f2 f3 - xxsi0[[i]] f4) / ( k^2 f2 f4 - xxsi2[[i]] f3)
```

```
   + ref1[[i]] (k^2 f3 f3 - k^2 f1 f4)/(k^2 f2 f4 - xxsi2[[i]] f3) ;
ref3[[i]] = (k^2 f4 - xxsi2[[i]])/( k^2 f4 - xxsi3[[i]] ) ref2[[i]];
 If[    N[ ( Abs[ref1[[i]]] )^2+( Abs[ref2[[i]]] )^2+
          ( Abs[ref3[[i]]] )^2 ]          <=     1.01
         && N[Im[qq[[i]]]] <=0
         && N[Abs[Re[Sqrt[kk0sq[[i]]]]/k1-1]] <.2 ,
 ( r1=Abs[ ref1[[i]] ]^2;
   For[ii=1,ii<=10,ii++,
      d1=Exp[ I 2 N[Pi,5] (ii-1)/10 ];
   sw[[ii]]=Abs [ (ref1[[i]] + ref2[[i]]
                  + ref3[[i]]) d1 + 1 ]^2  ];
     r2=Abs[ ref2[[i]] ]^2;
 ),
     j++ ];
   ];
    ret = {r1,r2,sw[[1]],sw[[2]],sw[[3]],sw[[4]],sw[[5]],
               sw[[6]],sw[[7]],sw[[8]],sw[[9]],sw[[10]],j};
   Return[ret];
]


Wresults[iimax_,ijmax_,ikmax_]:=
 Block[ {ii,ij,ik,
        ffil,file,
        yz,
        eninit},
  yz=Array[el,13];
  ffil=Array[el2,13];
  For[i=1, i<=13, i++,
   file=StringJoin["file",ToString[i]];
   ffil[[i]] = OpenWrite[file]   ];
  enrange = 12;
  eninit = 2984;
  tetarange = N[Pi,5]/90;
  firange = N[Pi,5]/2;
For[ii=1,ii<=iimax+1,ii++,
```

```
For[i=1, i<=13,i++,
WriteString[ffil[[i]], N[eninit+(ii-1)/iimax enrange],"\t" ] ];
  For[ij=1,ij<=ijmax,ij++,
     For[ik=1,ik<=ikmax,ik++,
 yz = N[GetRoot[eninit+(ii-1)/iimax enrange,
        tetarange (ij-1)/ijmax, firange (ik-1)/ikmax] ];
         For[i=1, i<=13,i++,
         WriteString[ffil[[i]], InputForm[yz[[i]]],"\t" ] ];
     ];
  ];
    For[i=1, i<=13,i++, WriteString[ffil[[i]], "\n" ] ];
];
    For[i=1, i<=13,i++, Close[ ffil[[i]] ] ];
  Return[ii,ij,ik];
         ]
```

Appendix 3 Program "SWDECONV"

This FORTRAN program was used to fit the XSW data, and is based on the theory developed in Chapter 5.

```
C THIS PROGRAM GENERATES THE STANDING WAVE AROUND THE BRAGG
CONDITION
      PROGRAM GENERATOR
      IMPLICIT NONE
C
      REAL ENERO,EXTRA
      REAL GAMMA,A,PLANE,DEPTH,COSRATIO
      COMPLEX FH,FMINH,FO
      COMPLEX FGA(2049)
      INTEGER*4 NUMP,ITER
      LOGICAL SYMMETRIC
      COMMON ENERO,EXTRA
      COMMON GAMMA,A,PLANE,DEPTH,COSRATIO
      COMMON FH,FMINH,FO
      COMMON FGA(2049)
      COMMON NUMP,ITER
      COMMON SYMMETRIC
C
      REAL GAR(5)
      INTEGER*4 J
C
      REAL DELZ,CFRAC
      REAL ENERGY(260), IOEXP(260)
      REAL SWEXP(260), SWCAL(260)
      REAL CHI
      REAL DELDELZ, DELCFRAC
      CHARACTER*255 INFO
      CHARACTER*255 DATA, PARAMFILE
      INTEGER*4 I
      CHARACTER*255 OUTFILE
```

```
        REAL IOINTERP(2049), EINTERP(2049)
        REAL IMAX
        CHARACTER OSCKILL
        CHARACTER BKCORRECT
        INTEGER CHANNEL, TYCHANNEL, REFCHANNEL, LARGERCHANNEL
        REAL TYEXP(260)
        REAL DCTY,FCTY
        CHARACTER*2 TYORREF
        INTEGER*4 FILENUMBER
        CHARACTER CH
C
        FILENUMBER = 0
        OPEN (UNIT=5,STATUS='OLD',FILE='AUTOMATIC' )
        READ(5,*) CH
C
10     WRITE(9,*) 'PARAMETERS FILE? INP[220] ,DATAFILE? (I PUT .TXT)'
      READ(5,*,END=900,ERR=900) PARAMFILE,DATA,
     &      TYORREF,CHANNEL,TYCHANNEL,REFCHANNEL
       IF( TYORREF .NE. 'RE' .AND. TYORREF .NE. 'TY' ) THEN
       PAUSE 'TY OR RE?'
       GOTO 900
      END IF
        DATA = TRIM(DATA)//'.TXT'
        WRITE(9,*) 'DATA FILE ',DATA
C
        OPEN (UNIT=10,STATUS='OLD',FILE=TRIM(DATA) )
        OPEN  (UNIT=2,STATUS='OLD',FILE='RESULTS',POSITION='APPEND')
C
      WRITE(2,15) TRIM(PARAMFILE),TRIM(DATA)
15     FORMAT(/,'PARAMFILE,DATAFILE ',2(A20))
C
        WRITE(9,*) 'CHANNEL ', CHANNEL
        LARGERCHANNEL = MAX0( CHANNEL, TYCHANNEL, REFCHANNEL )
C
        IF( TYORREF .EQ. 'RE' ) THEN
         IMAX = 0.
```

```
       DO 20, I=1,260
        READ(10,*,END = 21) (GAR(J), J=1,LARGERCHANNEL )
        ENERGY(I) = GAR(1)
        IOEXP(I) = GAR(REFCHANNEL)
        SWEXP(I) = GAR(CHANNEL)
         IF(IOEXP(I) .GT. IMAX) THEN
          IMAX = IOEXP(I)
          ENERO = ENERGY(I)        !FIRST GUESS FOR ENERO
         END IF
20     CONTINUE
21     NUMP = I - 1
      ELSE IF( TYORREF .EQ. 'TY' ) THEN
       IMAX = 0.
       DO 30, I=1,260
        READ(10,*,END = 31) (GAR(J), J=1,LARGERCHANNEL )
        ENERGY(I) = GAR(1)
        IOEXP(I) = GAR(REFCHANNEL)
        SWEXP(I) = GAR(CHANNEL)
        TYEXP(I) = GAR(TYCHANNEL)
         IF(TYEXP(I) .GT. IMAX) THEN
          IMAX = TYEXP(I)
          ENERO = ENERGY(I)        !FIRST GUESS FOR ENERO
         END IF
30     CONTINUE
31     NUMP = I - 1
      END IF
      CLOSE(10)
C
   CALL GETPARAM(PARAMFILE,DELZ,CFRAC,OSCKILL,BKCORRECT,DCTY,FCTY)
      !PARAMETERS AND THE FIRST GUESS FOR DELZ
C
CX    CALL AXESFOR(IOEXP,ENERGY,NUMP)
CX    CALL DIBUJA(IOEXP,ENERGY,NUMP)
CX    WRITE(9,*) 'JUST READ DATA'
CX    PAUSE 'JUST READ DATA'
C
```

```
      IF( TYORREF .EQ. 'RE' ) THEN
     IF((BKCORRECT .EQ. 'N') .OR. (BKCORRECT .EQ. 'n')) THEN
       CONTINUE
    ELSE IF( BKCORRECT .EQ. '1' ) THEN
       CALL CORRECTIO(ENERGY,IOEXP,NUMP)
    ELSE IF( BKCORRECT .EQ. '2' ) THEN
    CALL TWOCORRECTIO(ENERGY,IOEXP,NUMP)
      ELSE
       WRITE(9,*) 'CORRECT BK OR NOT? PLEASE ABORT '
       PAUSE 'CORRECT BK OR NOT? PLEASE ABORT '
      END IF
      END IF
C
      CALL GETFGA(ENERGY,IOEXP,TYEXP,DCTY,FCTY,TYORREF)
C
C NOW DO THE JOB
    CALL GETCFRAC(DELZ,CFRAC,ENERGY,SWEXP,CHI,SWCAL,DATA,OSCKILL)
    FILENUMBER = FILENUMBER + 1
C
      WRITE(2,400) DCTY, FCTY, DELZ, CFRAC, ENERO, CHI
400   FORMAT ( 'SwExtDeconOsc.FOR','     DCTY ',G12.6,'   FCTY ',
   &  G12.6,/,'DELZ, CFRAC, ENERO, CHI ',5(G12.6) )
      WRITE(2,410) BKCORRECT, OSCKILL, CHANNEL, TYORREF, TYCHANNEL
410   FORMAT ('BG CORRECTION: ',A1,'  KILL OSC? ',A1,'  SWCHANNEL ',I1,
   &        '  TYORREF ',A2,'  TYCHANNEL ',I1)
C
      WRITE(OUTFILE,420) FILENUMBER
420   FORMAT( I2 )
      OUTFILE = 'sw'//TRIM(OUTFILE)//'.TXT'
      CALL PUTINFILE(SWCAL,ENERGY,OUTFILE,NUMP)
C
      IF( TYORREF .EQ. 'RE' ) THEN
       WRITE(OUTFILE,420) FILENUMBER
       OUTFILE = 'REF'//TRIM(OUTFILE)//'.TXT'
       CALL PUTINFILE(IOEXP,ENERGY,OUTFILE,NUMP)
      END IF
```

```
C
      CALL UNCDELZ(DELZ,CFRAC,ENERGY,SWEXP,CHI,DELDELZ)
      CALL UNCCFRAC(DELZ,CFRAC,ENERGY,SWEXP,CHI,DELCFRAC)
      WRITE(2,500) DELDELZ, DELCFRAC
500   FORMAT ( 'DELDELZ,DELCFRAC ',2(G12.6) )
C
      CLOSE(2)
      GOTO 10
900   CONTINUE
      CLOSE(5)
      PAUSE 'DONE'
      STOP
      END
C-----------------------------------------------------------------------
      SUBROUTINE TWOCORRECTIO(ENERGY,IOEXP,NUMP)
      IMPLICIT NONE
      REAL ENERGY(260), IOEXP(260)
      INTEGER*4 NUMP
C
      INTEGER*4 I
      INTEGER*4 FIRSTS, LASTS
      REAL M, BO
      REAL X(260), Y(260)
C
      FIRSTS = 5
      LASTS = 5
C
      DO 10, I=1, FIRSTS
       X(I) = ENERGY(I)
       Y(I) = IOEXP(I)
10    CONTINUE
C
      DO 15, I = 1, LASTS
       X(FIRSTS + I) = ENERGY(NUMP - LASTS + I)
       Y(FIRSTS + I) = IOEXP(NUMP - LASTS + I)
15    CONTINUE
```

```
C
       CALL GETSLOPE(X,Y,M,BO,FIRSTS+LASTS)
       DO 20, I = 1, NUMP
     IOEXP(I)= IOEXP(I) / ( M*( ENERGY(I)-X(1) ) + BO ) - 1.
20     CONTINUE
C
       RETURN
       END
C------------------------------------------------------------------------
       SUBROUTINE GETSLOPE(X,Y,M,BO,NUMP)
       REAL X(260), Y(260)
       REAL M,BO
       INTEGER*4 NUMP
C
       IMPLICIT NONE
       REAL AN(2), B(2), C(2)
       INTEGER*4 I
C
       DO 5, I=1,2
       AN(I) = 0.
       B(I) = 0.
5      C(I) = 0.
C
       DO 10, I=1, NUMP
        AN(1) = AN(1) + ( X(I)-X(1) )**2
        AN(2) = AN(2) + X(I)-X(1)
        B(1) = B(1) + X(I)-X(1)
        B(2) = B(2) + 1.
        C(1) = C(1) + Y(I)*( X(I)-X(1) )
     C(2) = C(2) + Y(I)
10     CONTINUE
C
       M = ( C(1)*B(2) - C(2)*B(1) ) / ( AN(1)*B(2) - AN(2)*B(1) )
       BO = ( AN(1)*C(2) - AN(2)*C(1) ) / ( AN(1)*B(2) - AN(2)*B(1) )
C
       RETURN
```

```
      END
C-----------------------------------------------------------------------
      SUBROUTINE CORRECTIO(ENERGY,IOEXP,NUMP)
      IMPLICIT NONE
      REAL ENERGY(260), IOEXP(260)
      INTEGER*4 NUMP
C
      INTEGER*4 I
      INTEGER*4 INIT, FINAL
      REAL M, BO
C
      INIT = NUMP - 8
      FINAL = NUMP
      CALL GETLINE(ENERGY,IOEXP,INIT,FINAL,M,BO,NUMP)
      DO 20, I = 1, NUMP
    IOEXP(I)= IOEXP(I) / ( M*( ENERGY(I)-ENERGY(INIT) ) + BO )
   &  - 1.
20    CONTINUE
C
      RETURN
      END
C-----------------------------------------------------------------------
      SUBROUTINE GETFGA(ENERGY,IOEXP,TYEXP,DCTY,FCTY,TYORREF)
      IMPLICIT NONE
      REAL ENERGY(260),IOEXP(260),TYEXP(260)
      REAL DCTY,FCTY
      CHARACTER*2 TYORREF
C
      REAL ENERO,EXTRA
      REAL GAMMA,A,PLANE,DEPTH,COSRATIO
      COMPLEX FH,FMINH,FO
      COMPLEX FGA(2049)
      INTEGER*4 NUMP,ITER
      LOGICAL SYMMETRIC
      COMMON ENERO,EXTRA
      COMMON GAMMA,A,PLANE,DEPTH,COSRATIO
```

```
      COMMON FH,FMINH,FO
      COMMON FGA(2049)
      COMMON NUMP,ITER
      COMMON SYMMETRIC
C
      INTEGER*4 I,J
      REAL REFLFUNCTION, SWFUNCTION
      REAL STEP
      CHARACTER*255 OUTFILE
C
      COMPLEX FIOCAL(2049), FIOINTE(2049)
      REAL ENER
      REAL DELTA
      REAL IOINTERP(2049),EINTERP(2049)
C
     STEP = (ENERGY(NUMP)-ENERGY(1)+2.*EXTRA)/(ITER-1.)
C
      IF( TYORREF .EQ. 'TY' ) THEN
       CALL GETINTERP(ENERGY,TYEXP,IOINTERP)
      ELSE
       CALL GETINTERP(ENERGY,IOEXP,IOINTERP)
      END IF
C
      ENER = ENERGY(1) - EXTRA
       DO 6, I=1,ITER
        IF( TYORREF .EQ. 'TY' ) THEN
         FIOCAL(I) = CMPLX(SWFUNCTION(DCTY,FCTY,ENER),0.)
        ELSE
         FIOCAL(I) = CMPLX(REFLFUNCTION(ENER),0.)
        END IF
        FIOINTE(I) = CMPLX(IOINTERP(I),0.)
        ENER = ENER + STEP
6      CONTINUE
C
      CALL FOUR1(FIOINTE,ITER,1)
      CALL FOUR1(FIOCAL,ITER,1)
```

```
C
        DO 15, J=2,ITER - 1
         IF( CABS( FIOCAL(J) ) .LT. 1.E-10 ) FIOCAL(J) =
   &          ( FIOCAL(J-1) + FIOCAL(J+1) ) / 2.
15      CONTINUE
        DO 20, I=1,ITER
         FGA(I) = FIOINTE(I) / FIOCAL(I) / ITER
20      CONTINUE
C
        RETURN
        END
C--------------------------------------------------------------------------
        SUBROUTINE GETINTERP(ENERGY,IOEXP,IOINTERP)
        IMPLICIT NONE
        REAL ENERGY(260), IOEXP(260)
        REAL IOINTERP(2049)
C
        REAL ENERO,EXTRA
        REAL GAMMA,A,PLANE,DEPTH,COSRATIO
        COMPLEX FH,FMINH,FO
        COMPLEX FGA(2049)
        INTEGER*4 NUMP,ITER
        LOGICAL SYMMETRIC
        COMMON ENERO,EXTRA
        COMMON GAMMA,A,PLANE,DEPTH,COSRATIO
        COMMON FH,FMINH,FO
        COMMON FGA(2049)
        COMMON NUMP,ITER
        COMMON SYMMETRIC
C
        INTEGER*4 I,K
        REAL STEP
        REAL STEX, DELTA
        REAL M,B
        INTEGER*4 INIT, FINAL
C
```

```
    STEP = (ENERGY(NUMP)-ENERGY(1)+2.*EXTRA)/(ITER-1.)
    STEX = ( ENERGY(NUMP)-ENERGY(1) )/(NUMP-1.)
C
      INIT = 1
      FINAL = 3
      CALL GETLINE(ENERGY,IOEXP,INIT,FINAL,M,B,NUMP)
      WRITE(9,*) 'FIRST M,B ',M,B
      INIT = 1
      FINAL = INT(EXTRA/STEP)
      DO 10, I=INIT,FINAL
       IOINTERP(I) = M * ( - EXTRA + (I-1)*STEP ) + B
10    CONTINUE
C
    INIT = INT(EXTRA/STEP)+1
    FINAL = INT((EXTRA+ENERGY(NUMP)-ENERGY(1))/STEP)
      DO 20, I=INIT,FINAL
       K = INT( ( (I-1)*STEP-EXTRA )/STEX ) + 1
       DELTA = ( (I-1)*STEP-EXTRA )/STEX + 1 - K
CX     IOINTERP(I) = 0.
CX      WRITE(9,*) 'K,DELTA ',K,DELTA
       IOINTERP(I) = IOEXP(K) * (1. - DELTA) + IOEXP(K+1) * DELTA
20    CONTINUE
C
      INIT = NUMP - 2
      FINAL = NUMP
C
CX    WRITE(9,*) 'STEP,STEX,EXTRA ',STEP,STEX,EXTRA
CX    WRITE(9,*) 'INIT,FINAL,NUMP ',INIT,FINAL,NUMP
CX    PAUSE
C
      CALL GETLINE(ENERGY,IOEXP,INIT,FINAL,M,B,NUMP)
CX    WRITE(9,*) 'M,B ',M,B
    INIT = INT((EXTRA+ENERGY(NUMP)-ENERGY(1))/STEP)+1
    FINAL = ITER
      DO 30, I=INIT,FINAL
       IOINTERP(I) = M * ( 2.*STEX + (I-INIT)*STEP ) + B
```

```
30     CONTINUE
C
       RETURN
       END
C-------------------------------------------------------------------------
       SUBROUTINE GETLINE(ENERGY,EXPDAT,INIT,FINAL,M,BO,NUMP)
       REAL ENERGY(260), EXPDAT(260)
       REAL M,BO
       INTEGER*4 INIT,FINAL
C
       IMPLICIT NONE
       REAL AN(2), B(2), C(2)
       INTEGER*4 I
C
       DO 5, I=1,2
       AN(I) = 0.
       B(I) = 0.
5      C(I) = 0.
C
       DO 10, I=INIT, FINAL
        AN(1) = AN(1) + ( ENERGY(I)-ENERGY(INIT) )**2
        AN(2) = AN(2) + ENERGY(I)-ENERGY(INIT)
        B(1) = B(1) + ENERGY(I)-ENERGY(INIT)
        B(2) = B(2) + 1.
        C(1) = C(1) + EXPDAT(I)*( ENERGY(I)-ENERGY(INIT) )
      C(2) = C(2) + EXPDAT(I)
10     CONTINUE
C
       M = ( C(1)*B(2) - C(2)*B(1) ) / ( AN(1)*B(2) - AN(2)*B(1) )
       BO = ( AN(1)*C(2) - AN(2)*C(1) ) / ( AN(1)*B(2) - AN(2)*B(1) )
C
       RETURN
       END
C-------------------------------------------------------------------------
       SUBROUTINE UNCDELZ(DELZ,CFRAC,ENERGY,SWEXP,CHI,DELDELZ)
       IMPLICIT NONE
```

```
      REAL ENERGY(260), SWEXP(260)
      REAL CHI, DELDELZ, DELZ, CFRAC
C
      REAL ENERO,EXTRA
      REAL GAMMA,A,PLANE,DEPTH,COSRATIO
      COMPLEX FH,FMINH,FO
      COMPLEX FGA(2049)
      INTEGER*4 NUMP,ITER
      LOGICAL SYMMETRIC
      COMMON ENERO,EXTRA
      COMMON GAMMA,A,PLANE,DEPTH,COSRATIO
      COMMON FH,FMINH,FO
      COMMON FGA(2049)
      COMMON NUMP,ITER
      COMMON SYMMETRIC
C
      REAL DELZ1, DELZ2, CHI1, CHI2
      CHARACTER*255 INFO
      REAL SWCAL(260), SWCONV(260)
      INTEGER*4 I
      DELZ2 = DELZ
      DELZ1 = DELZ
      I = 0
C
10    DELZ1 = DELZ1 - 0.01
      I = I + 1
      IF(I .GT. 100) THEN
       DELDELZ = 1.
       RETURN
      END IF
      CALL CONVOLVE(ENERGY,DELZ1,CFRAC,SWCONV)
      CALL PUTBACKG(ENERGY,SWEXP,SWCONV,NUMP)
      CALL GETCHI(SWCONV,SWEXP,CHI1,NUMP)
      WRITE(INFO,15) I,DELZ,DELZ1
15    FORMAT( 'I,DELZ,DELZ1 ',I4,2(G12.6),'        ' )
      CALL LETRERO(INFO,15)
```

```
      WRITE(INFO,16) CHI,CHI1
16    FORMAT( 'CHI,CHI1 ',2(G12.6),'        ' )
      CALL LETRERO(INFO,16)
      IF ( CHI1 .LT. (2.*CHI) ) GOTO 10
      CALL DIBUJA(SWCONV,ENERGY,NUMP)
C
      I = 0
20    DELZ2 = DELZ2 + 0.01
      I = I + 1
      IF(I .GT. 100) THEN
       DELDELZ = 1.
       RETURN
      END IF
       CALL CONVOLVE(ENERGY,DELZ2,CFRAC,SWCONV)
       CALL PUTBACKG(ENERGY,SWEXP,SWCONV,NUMP)
       CALL GETCHI(SWCONV,SWEXP,CHI2,NUMP)
      WRITE(INFO,25) I,DELZ,DELZ2
25    FORMAT( 'I,DELZ,DELZ2 ',I4,2(G12.6),'        ' )
      CALL LETRERO(INFO,18)
      WRITE(INFO,26) CHI,CHI2
26    FORMAT( 'CHI,CHI2 ',2(G12.6),'        ' )
      CALL LETRERO(INFO,19)
      IF ( CHI2 .LT. (2.*CHI) ) GOTO 20
C
      DELDELZ = AMAX1(DELZ-DELZ1, DELZ2-DELZ)
      WRITE(INFO,*) 'DELZ1, DELZ, DELZ2 ',DELZ1, DELZ, DELZ
      CALL LETRERO(INFO,20)
    WRITE(INFO,*) 'DEL1,DEL2,DELDELZ ',DELZ-DELZ1,
  &           DELZ2-DELZ,DELDELZ
      CALL LETRERO(INFO,21)
C
      RETURN
      END
C-----------------------------------------------------------------------
      SUBROUTINE UNCCFRAC(DELZ,CFRAC,ENERGY,SWEXP,CHI,DELCFRAC)
      IMPLICIT NONE
```

```
      REAL ENERGY(260), SWEXP(260)
      REAL CHI, DELCFRAC, DELZ, CFRAC
C
      REAL ENERO,EXTRA
      REAL GAMMA,A,PLANE,DEPTH,COSRATIO
      COMPLEX FH,FMINH,FO
      COMPLEX FGA(2049)
      INTEGER*4 NUMP,ITER
      LOGICAL SYMMETRIC
      COMMON ENERO,EXTRA
      COMMON GAMMA,A,PLANE,DEPTH,COSRATIO
      COMMON FH,FMINH,FO
      COMMON FGA(2049)
      COMMON NUMP,ITER
      COMMON SYMMETRIC
C
      REAL CFRAC1, CFRAC2, CHI1, CHI2
      CHARACTER*255 INFO
      REAL SWCAL(260), SWCONV(260)
      INTEGER*4 I
      CFRAC2 = CFRAC
      CFRAC1 = CFRAC
      I = 0
C
10    CFRAC1 = CFRAC1 / 1.01
      I = I + 1
      IF(I .GT. 100) THEN
       DELCFRAC = 1.
       RETURN
      END IF
       CALL CONVOLVE(ENERGY,DELZ,CFRAC1,SWCONV)
       CALL PUTBACKG(ENERGY,SWEXP,SWCONV,NUMP)
       CALL GETCHI(SWCONV,SWEXP,CHI1,NUMP)
      WRITE(INFO,15) I,CFRAC,CFRAC1
15    FORMAT( 'I,CFRAC,CFRAC1 ',I4,2(G12.6),'        ' )
      CALL LETRERO(INFO,5)
```

```
      WRITE(INFO,16) CHI,CHI1
16    FORMAT( 'CHI,CHI1 ',2(G12.6),'        ' )
      CALL LETRERO(INFO,6)
      IF ( CHI1 .LT. (2.*CHI) ) GOTO 10
      CALL DIBUJA(SWCONV,ENERGY,NUMP)
C
      I = 0
20    CFRAC2 = CFRAC2 * 1.01
      I = I + 1
      IF(I .GT. 100) THEN
       DELCFRAC = 1.
       RETURN
      END IF
       CALL CONVOLVE(ENERGY,DELZ,CFRAC2,SWCONV)
       CALL PUTBACKG(ENERGY,SWEXP,SWCONV,NUMP)
       CALL GETCHI(SWCONV,SWEXP,CHI2,NUMP)
      WRITE(INFO,25) I,CFRAC,CFRAC2
25    FORMAT( 'I,CFRAC,CFRAC2 ',I4,2(G12.6),'        ' )
      CALL LETRERO(INFO,8)
      WRITE(INFO,26) CHI,CHI2
26    FORMAT( 'CHI,CHI2 ',2(G12.6),'        ' )
      CALL LETRERO(INFO,9)
      IF ( CHI2 .LT. (2.*CHI) ) GOTO 20
C
      DELCFRAC = AMAX1(CFRAC-CFRAC1, CFRAC2-CFRAC)
    WRITE(INFO,*) 'CFRAC1, CFRAC, CFRAC2 ',CFRAC1, CFRAC, CFRAC
      CALL LETRERO(INFO,10)
    WRITE(INFO,*) 'DEL1,DEL2,DELCFRAC ',CFRAC-CFRAC1,
  &          CFRAC2-CFRAC,DELCFRAC
      CALL LETRERO(INFO,11)
C
      RETURN
      END
C-----------------------------------------------------------------------
    SUBROUTINE GETPARAM(PARAMFILE,DELZ,CFRAC,
  &                 OSCKILL,BKCORRECT,DCTY,FCTY)
```

```
      IMPLICIT NONE
      REAL DELZ,CFRAC
      CHARACTER*255 PARAMFILE
      CHARACTER OSCKILL
      CHARACTER BKCORRECT
      REAL DCTY,FCTY
C
      REAL ENERO,EXTRA
      REAL GAMMA,A,PLANE,DEPTH,COSRATIO
      COMPLEX FH,FMINH,FO
      COMPLEX FGA(2049)
      INTEGER*4 NUMP,ITER
      LOGICAL SYMMETRIC
      COMMON ENERO,EXTRA
      COMMON GAMMA,A,PLANE,DEPTH,COSRATIO
      COMMON FH,FMINH,FO
      COMMON FGA(2049)
      COMMON NUMP,ITER
      COMMON SYMMETRIC
C
      REAL  REFOIN,IMFOIN,REFHIN,IMFHIN
      REAL  REFOP,IMFOP,REFHP,IMFHP
      CHARACTER*8  REFLE
C
      REAL IMAX
      CHARACTER*255 INFO
      COMPLEX FACTOR1, FACTOR2
      REAL RITER
      REAL COSTETA,DISTANCE
      CHARACTER CHARSYMM
C
       WRITE(INFO,*) 'NOW GETTING THE PARAMETERS          '
       CALL LETRERO(INFO,0)
C
      OPEN (UNIT=1,STATUS='OLD',FILE=TRIM(PARAMFILE))
C
```

```
      READ (1,10) REFOIN,IMFOIN,REFHIN,IMFHIN
      READ (1,10) REFOP,IMFOP,REFHP,IMFHP
      READ (1,20) REFLE
      READ (1,10) A
      READ (1,10) CFRAC,DELZ       !INITIAL VALUE
      READ (1,10) RITER
      READ (1,20) OSCKILL
      READ (1,10) DEPTH
      READ (1,20) CHARSYMM
      READ (1,10) COSRATIO              !COSGAMA TO COSTETA RATIO
      READ (1,20) BKCORRECT
      READ (1,10) DCTY,FCTY       !TOTAL YIELD
10    FORMAT (F12.0)
20    FORMAT (A)
C  CALCULATE THE PARAMETERS
      ITER = INT(RITER+.1)
C
     IF( (CHARSYMM .EQ. 'Y') .OR. (CHARSYMM .EQ. 'y') ) THEN
       SYMMETRIC = .TRUE.
     ELSE IF( (CHARSYMM .EQ. 'N') .OR. (CHARSYMM .EQ. 'n') ) THEN
       SYMMETRIC = .FALSE.
      ELSE
       WRITE(9,*) 'SYMMETRIC OR NOT? PLEASE ABORT '
       PAUSE 'SYMMETRIC OR NOT? PLEASE ABORT '
      END IF
C
      IF(REFLE .EQ. '[200]') THEN
        FACTOR1 = -1.
        FACTOR2 = -1.
        PLANE = 2.
        WRITE(9,*) 'REFLECTION ',REFLE
      ELSE IF(REFLE .EQ. '[111]') THEN
        FACTOR1 = -CMPLX(0.,1.)
        FACTOR2 = CMPLX(0.,1.)
        PLANE = SQRT(3.)
      ELSE IF(REFLE .EQ. '[-1-1-1]') THEN
```

```
          FACTOR1 = CMPLX(0.,1.)
          FACTOR2 = -CMPLX(0.,1.)
          PLANE = SQRT(3.)
          WRITE(9,*) 'REFLECTION ',REFLE
        ELSE IF(REFLE .EQ. '[220]' .OR. REFLE .EQ. '[400]') THEN
          FACTOR1 = 1.
          FACTOR2 = 1.
          PLANE = SQRT(8.)
          IF (REFLE .EQ. '[400]') PLANE = 4.
        ELSE
          WRITE(9,*) 'ERROR IN READING REFLECTION '
          WRITE(9,*) 'ERROR IN READING REFLECTION '
          PAUSE 'PLEASE ABORT '
        END IF
        FH = CMPLX(REFHIN,IMFHIN) + FACTOR1*CMPLX(REFHP,IMFHP)
        FMINH = CMPLX(REFHIN,IMFHIN) + FACTOR2*CMPLX(REFHP,IMFHP)
        FO = CMPLX(REFOIN,IMFOIN) + CMPLX(REFOP,IMFOP)
        GAMMA = 5512.97/(A*A*A*ENERO*ENERO)
C  CORRECTION FOR ENERO
      ENERO = ENERO - GAMMA*FO*A*A*ENERO**3/(2.*(6201.5*PLANE)**2)
C
      COSTETA = 6201.5*PLANE/A/ENERO
        DISTANCE = REAL(FO) * GAMMA*ENERO/COSTETA**2/2.
      EXTRA = 2.*DISTANCE
C
        CLOSE(1)
        RETURN
        END
C---------------------------------------------------------------------------
       SUBROUTINE GETCFRAC(DELZ,CFRAC,ENERGY,SWEXP,CHI,SWCAL,
     & DATA,OSCKILL)
        IMPLICIT NONE
        REAL DELZ,CFRAC
        REAL ENERGY(260), SWEXP(260),SWCAL(260)
        REAL CHI
        CHARACTER*255 DATA
```

```
      CHARACTER OSCKILL
C
      REAL ENERO,EXTRA
      REAL GAMMA,A,PLANE,DEPTH,COSRATIO
      COMPLEX FH,FMINH,FO
      COMPLEX FGA(2049)
      INTEGER*4 NUMP,ITER
      LOGICAL SYMMETRIC
      COMMON ENERO,EXTRA
      COMMON GAMMA,A,PLANE,DEPTH,COSRATIO
      COMMON FH,FMINH,FO
      COMMON FGA(2049)
      COMMON NUMP,ITER
      COMMON SYMMETRIC
C
    REAL SWCAL1(260), SWCAL2(260)
      REAL FACTOR
      REAL CFRAC1, CFRAC2, CHI1, CHI2
      REAL DELZ1, DELZ2
      INTEGER*4 I
      CHARACTER*255 INFO
      CHARACTER CHAR
C
      FACTOR = 1.1                   !INITIAL VALUE
      DELZ1 = DELZ
      DELZ2 = DELZ
CX      CALL CONVOLVE(ENERGY,DELZ,CFRAC,SWCAL)
CX      CALL PUTBACKG(ENERGY,SWEXP,SWCAL,NUMP)
CX      CALL DIBUJA(SWCAL,ENERGY,NUMP)
C
     IF( (OSCKILL .EQ. 'Y') .OR. (OSCKILL .EQ. 'y') )
  &  CALL KILLOSCIL(ENERGY,DELZ,CFRAC)           ! CHANGES FGA
C
      CALL AXESFOR(SWEXP,ENERGY,NUMP)
      CALL DIBUJA(SWEXP,ENERGY,NUMP)
        CALL CONVOLVE(ENERGY,DELZ,CFRAC,SWCAL)
```

```
          CALL PUTBACKG(ENERGY,SWEXP,SWCAL,NUMP)
          CALL DIBUJA(SWCAL,ENERGY,NUMP)
C
        CALL GETDELZ(DELZ,CFRAC,ENERGY,SWEXP,SWCAL,CHI)
C
10      CFRAC1 = CFRAC * FACTOR
     CALL GETDELZ(DELZ1,CFRAC1,ENERGY,SWEXP,SWCAL1,CHI1)
C
C
         WRITE(INFO,140) FACTOR,DATA
140      FORMAT('GETCFRAC1    FACTOR ',G12.5,'   FILENAME ',A20)
         CALL LETRERO(INFO,5)
        WRITE(INFO,44) CHI,CHI1
144     FORMAT('CHI,CHI1= ',2(G12.5),'           ')
      CALL LETRERO(INFO,6)
       WRITE(INFO,47) CFRAC,CFRAC1
147       FORMAT('CFRAC,CFRAC1 ',2(G12.5),'           ')
         CALL LETRERO(INFO,7)
       WRITE(INFO,*) 'DELZ,DELZ1 ',DELZ,DELZ1
         CALL LETRERO(INFO,8)
C
C
        IF (CHI1 .LT. CHI) THEN
          CHI = CHI1
          CFRAC = CFRAC1
          DELZ = DELZ1
          DO 200, I = 1, NUMP
200        SWCAL(I) = SWCAL1(I)
          CALL DIBUJA(SWCAL,ENERGY,NUMP)
          GOTO 10
        END IF
C
C
20      CFRAC2 = CFRAC / FACTOR
     CALL GETDELZ(DELZ2,CFRAC2,ENERGY,SWEXP,SWCAL2,CHI2)
C
```

```
C
      WRITE(INFO,40) FACTOR,DATA
40    FORMAT('GETCFRAC2   FACTOR ',G12.5,'   FILENAME ',A20)
      CALL LETRERO(INFO,5)
     WRITE(INFO,44) CHI,CHI1,CHI2
44   FORMAT('CHI,CHI1,CHI2= ',3(G12.5),'    ')
   CALL LETRERO(INFO,6)
    WRITE(INFO,47) CFRAC,CFRAC1,CFRAC2
47    FORMAT('CFRAC,CFRAC1,CFRAC2 ',3(G12.5),'    ')
      CALL LETRERO(INFO,7)
    WRITE(INFO,*) 'DELZ,DELZ1,DELZ2 ',DELZ,DELZ1,DELZ2
      CALL LETRERO(INFO,8)
C
     IF (CHI2 .LT. CHI) THEN
       CHI = CHI2
       CFRAC = CFRAC2
       DELZ = DELZ2
       DO 300, I = 1, NUMP
300     SWCAL(I) = SWCAL2(I)
       CALL DIBUJA(SWCAL,ENERGY,NUMP)
       GOTO 20
     END IF
C
     IF (FACTOR > 1.001) THEN
      FACTOR = SQRT(FACTOR)
       CALL DIBUJA(SWCAL,ENERGY,NUMP)
      GOTO 10
     END IF
C
     INFO = 'END OF GETCFRAC, RETURN TO CONTINUE '
     CALL LETRERO(INFO,20)
     CALL AXESFOR(SWEXP,ENERGY,NUMP)
     CALL DIBUJA(SWEXP,ENERGY,NUMP)
     CALL DIBUJA(SWCAL,ENERGY,NUMP)
C
     RETURN
```

```
      END
C--------------------------------------------------------------------------
      SUBROUTINE KILLOSCIL(ENERGY,DELZ,CFRAC)
      IMPLICIT NONE
      REAL ENERGY(260)
      REAL DELZ,CFRAC
C
      REAL ENERO,EXTRA
      REAL GAMMA,A,PLANE,DEPTH,COSRATIO
      COMPLEX FH,FMINH,FO
      COMPLEX FGA(2049)
      INTEGER*4 NUMP,ITER
      LOGICAL SYMMETRIC
      COMMON ENERO,EXTRA
      COMMON GAMMA,A,PLANE,DEPTH,COSRATIO
      COMMON FH,FMINH,FO
      COMMON FGA(2049)
      COMMON NUMP,ITER
      COMMON SYMMETRIC
C
      COMPLEX FSW(1025)
      COMPLEX FT2(1025)
      REAL EINTERP(1025)
C
      INTEGER*4 I
      REAL Y(1025)
      REAL X(1025)
      CHARACTER*255 INFO
      INTEGER*4 INIT, FINAL
      REAL ENER,STEP
      REAL SWFUNCTION
C
    STEP = (ENERGY(NUMP)-ENERGY(1)+2.*EXTRA)/(ITER-1.)
C
      ENER = ENERGY(1) - EXTRA
       DO 6, I=1,ITER
```

```
         FSW(I) = CMPLX(SWFUNCTION(DELZ,CFRAC,ENER),0.)
          EINTERP(I) = ENER
          ENER = ENER + STEP
6        CONTINUE
C
        CALL FOUR1(FSW,ITER,1)
C
200     CONTINUE
C
        DO 50, I=1,30
         X(I) = I - 30.
         X(I+30) = I
         Y(I) = REAL( FGA(ITER - 30 + I) )
         Y(I+30) = REAL( FGA(I) )
50      CONTINUE
        CALL AXESFOR(Y,X,60)
        CALL DIBUJA(Y,X,60)
        PAUSE
C
        WRITE(9,*) 'WHICH ONES? INIT, FINAL (X ESCALE  -30 30) '
        READ(9,*) INIT, FINAL
        IF(INIT .LT. 0) THEN
         INIT = ITER + INIT
         FINAL = ITER + FINAL
        END IF
C
        DO 60, I=INIT, FINAL
      FGA(I) = FGA(INIT) + (FGA(FINAL)-FGA(INIT))/(FINAL - INIT)*
     &  (I - INIT)
60      CONTINUE
C
        DO 222, I=1,ITER
         FT2(I) = FGA(I) * FSW(I)
222     CONTINUE
C
        CALL FOUR1(FT2,ITER,-1)
```

```
      DO 231, I=1, ITER
       Y(I) = REAL(FT2(I))
231   CONTINUE
C
      CALL AXESFOR(Y,EINTERP,ITER)
      CALL DIBUJA(Y,EINTERP,ITER)
C
C
      WRITE(9,*) 'AGAIN? (1 FOR YES) '
      WRITE(9,*) 'AGAIN? (1 FOR YES) '
      READ(9,*) I
      IF (I .EQ. 1) GOTO 200
C
      RETURN
      END
C-----------------------------------------------------------------------------
     SUBROUTINE GETDELZ(DELZ,CFRAC,ENERGY,SWEXP,SWCONV,CHI)
      IMPLICIT NONE
      REAL DELZ,CFRAC,CHI
      REAL ENERGY(260), SWEXP(260), SWCONV(260)
C
      REAL ENERO,EXTRA
      REAL GAMMA,A,PLANE,DEPTH,COSRATIO
      COMPLEX FH,FMINH,FO
      COMPLEX FGA(2049)
      INTEGER*4 NUMP,ITER
      LOGICAL SYMMETRIC
      COMMON ENERO,EXTRA
      COMMON GAMMA,A,PLANE,DEPTH,COSRATIO
      COMMON FH,FMINH,FO
      COMMON FGA(2049)
      COMMON NUMP,ITER
      COMMON SYMMETRIC
C
      REAL FACTOR
      REAL DELZ1, DELZ2, CHI1, CHI2
```

```
      INTEGER*4 I
      CHARACTER*255 INFO
C
      FACTOR = 1.1                    !INITIAL VALUE
       CALL CONVOLVE(ENERGY,DELZ,CFRAC,SWCONV)
       CALL PUTBACKG(ENERGY,SWEXP,SWCONV,NUMP)
       CALL GETCHI(SWCONV,SWEXP,CHI,NUMP)
C
10    DELZ1 = DELZ * FACTOR
       CALL CONVOLVE(ENERGY,DELZ1,CFRAC,SWCONV)
       CALL PUTBACKG(ENERGY,SWEXP,SWCONV,NUMP)
       CALL GETCHI(SWCONV,SWEXP,CHI1,NUMP)
C
      IF (CHI1 < CHI) THEN
         CHI = CHI1
        DELZ = DELZ1
        GOTO 10
      END IF
C
20    DELZ2 = DELZ / FACTOR
       CALL CONVOLVE(ENERGY,DELZ2,CFRAC,SWCONV)
       CALL PUTBACKG(ENERGY,SWEXP,SWCONV,NUMP)
       CALL GETCHI(SWCONV,SWEXP,CHI2,NUMP)
C
      IF (CHI2 < CHI) THEN
         CHI = CHI2
        DELZ = DELZ2
        GOTO 20
      END IF
C
      IF (FACTOR > 1.001) THEN
       FACTOR = SQRT(FACTOR)
C
          WRITE(INFO,40)
40        FORMAT('SUBROUTINE GETDELZ')
          CALL LETRERO(INFO,0)
```

```
          WRITE(INFO,44) CHI,CHI1,CHI2
44          FORMAT('CHI,CHI1,CHI2= ',3(G12.5),'   ')
      CALL LETRERO(INFO,1)
        WRITE(INFO,47) DELZ,DELZ1,DELZ2
47          FORMAT('DELZ,DELZ1,DELZ2 ',3(G12.5),'   ')
            CALL LETRERO(INFO,2)
          WRITE(INFO,49) ENERO,FACTOR
49          FORMAT('ENERO,FACTOR ',3(G12.5),'   ')
          CALL LETRERO(INFO,3)
C
        GOTO 10
      END IF
C
      RETURN
      END
C------------------------------------------------------------------------
      SUBROUTINE CONVOLVE(ENERGY,DELZ,CFRAC,SWCONV)
      IMPLICIT NONE
      REAL ENERGY(260), SWCONV(260)
      REAL DELZ,CFRAC
C
      REAL ENERO,EXTRA
      REAL GAMMA,A,PLANE,DEPTH,COSRATIO
      COMPLEX FH,FMINH,FO
      COMPLEX FGA(2049)
      INTEGER*4 NUMP,ITER
      LOGICAL SYMMETRIC
      COMMON ENERO,EXTRA
      COMMON GAMMA,A,PLANE,DEPTH,COSRATIO
      COMMON FH,FMINH,FO
      COMMON FGA(2049)
      COMMON NUMP,ITER
      COMMON SYMMETRIC
C
      INTEGER*4 I,J
      REAL SWOFFNORMAL
```

```
      REAL SWFUNCTION
      CHARACTER OFFNOR
      REAL STEP
C
      COMPLEX FSWCAL(2049), FT(2049)
      REAL ENER
      REAL DELTA
C
    STEP = (ENERGY(NUMP)-ENERGY(1)+2.*EXTRA)/(ITER-1.)
C
      ENER = ENERGY(1) - EXTRA
       DO 6, I=1,ITER
        FSWCAL(I) = CMPLX(SWFUNCTION(DELZ,CFRAC,ENER),0.)
        ENER = ENER + STEP
6      CONTINUE
C
      CALL FOUR1(FSWCAL,ITER,1)
      DO 20, I=1,ITER
       FT(I) = FSWCAL(I) * FGA(I) / ITER
20    CONTINUE
      CALL FOUR1(FT,ITER,-1)
C
      DO 30, I=1, NUMP
       J = INT( (ENERGY(I)-ENERGY(1) + EXTRA)/STEP )
       DELTA = (ENERGY(I)-ENERGY(1) + EXTRA)/STEP - J
     SWCONV(I) = (1.-DELTA)*REAL(FT(J+1)) + DELTA*REAL(FT(J+2))
30    CONTINUE
C
      RETURN
      END
C-----------------------------------------------------------------------
    FUNCTION REFLFUNCTION(ENER)
    IMPLICIT NONE
     REAL ENER
     REAL REFLFUNCTION
C
```

```
      REAL ENERO,EXTRA
      REAL GAMMA,A,PLANE,DEPTH,COSRATIO
      COMPLEX FH,FMINH,FO
      COMPLEX FGA(2049)
      INTEGER*4 NUMP,ITER
      LOGICAL SYMMETRIC
      COMMON ENERO,EXTRA
      COMMON GAMMA,A,PLANE,DEPTH,COSRATIO
      COMMON FH,FMINH,FO
      COMMON FGA(2049)
      COMMON NUMP,ITER
      COMMON SYMMETRIC
C
      COMPLEX  ETA
      COMPLEX AIOO1,AIOO2
      REAL AIO1,AIO2
      REAL REFLNONSYMM
C
      REAL COSTETA
C
      IF(.NOT. SYMMETRIC) THEN
       REFLFUNCTION = REFLNONSYMM(ENER)
       RETURN
      END IF
C
      COSTETA = 6201.5 * PLANE / A / ENERO
       GAMMA = 5512.97/(A*A*A*ENER*ENER)
     ETA = (-2.*(ENER-ENERO)/ENER*COSTETA**2+GAMMA*FO)
    &        /GAMMA/CSQRT(FH*FMINH)
C
      AIOO1 = - CSQRT(FH/FMINH) * ( ETA - CSQRT( ETA*ETA - 1. ) )
      AIO1 =  CABS( AIOO1 ) **2
C
      AIOO2 = - CSQRT(FH/FMINH) * ( ETA + CSQRT( ETA*ETA - 1. ) )
      AIO2 =  CABS( AIOO2 ) * CABS( AIOO2 )
C
```

```
      IF (AIO2 .LE. 1.) THEN
        REFLFUNCTION = AIO2
       ELSE
        REFLFUNCTION = AIO1
      END IF
C
      RETURN
      END
C-----------------------------------------------------------------------
    FUNCTION REFLNONSYMM(ENER)
    IMPLICIT NONE
     REAL ENER
     REAL REFLNONSYMM
C
      REAL ENERO,EXTRA
      REAL GAMMA,A,PLANE,DEPTH,COSRATIO
      COMPLEX FH,FMINH,FO
      COMPLEX FGA(2049)
      INTEGER*4 NUMP,ITER
      LOGICAL SYMMETRIC
      COMMON ENERO,EXTRA
      COMMON GAMMA,A,PLANE,DEPTH,COSRATIO
      COMMON FH,FMINH,FO
      COMMON FGA(2049)
      COMMON NUMP,ITER
      COMMON SYMMETRIC
C
      COMPLEX  ETA, AIOO
      COMPLEX AIOO1,AIOO2
      REAL AIO1,AIO2
      INTEGER*4 I
C
      REAL ANGLE
      REAL AGEO,COSTETA
C
     ANGLE = - ACOS(6201.5 * SQRT(3.) / A / ENERO ) +
```

```
    &              ACOS(SQRT(2./3.))
         AGEO = 0.33333   +   SQRT(8.)/3. * TAN(ANGLE)
      COSTETA = SQRT(2./3.) * COS(ANGLE) + 1./SQRT(3.) * SIN(ANGLE)
         GAMMA = 5512.97/(A*A*A*ENER*ENER)
      ETA = ( -2.*(ENER-ENERO)/ENER*(COSTETA)**2  +
    &      GAMMA*FO*(0.66666 + SQRT(2.)/3. * TAN(ANGLE) ) )
    &      / ( GAMMA*CSQRT(FH*FMINH)*SQRT(AGEO) )
C
     AIOO1 = - CSQRT(FH/FMINH) / SQRT(AGEO) *
    &         ( ETA - CSQRT( ETA*ETA - 1. ) )
        AIO1 =  CABS( AIOO1 ) **2
C
     AIOO2 = - CSQRT(FH/FMINH) / SQRT(AGEO) *
    &         ( ETA + CSQRT( ETA*ETA - 1. ) )
        AIO2 =  CABS( AIOO2 ) * CABS( AIOO2 )
C
        IF (AIO2 .LE. AIO1) THEN
          REFLNONSYMM = AIO2
        ELSE
          REFLNONSYMM = AIO1
        END IF
C
        RETURN
        END
C---------------------------------------------------------------------------
      FUNCTION SWFUNCTION(DELZ,CFRAC,ENER)
      IMPLICIT NONE
      REAL DELZ,CFRAC
      REAL ENER, SWFUNCTION
C
        REAL ENERO,EXTRA
        REAL GAMMA,A,PLANE,DEPTH,COSRATIO
        COMPLEX FH,FMINH,FO
        COMPLEX FGA(2049)
        INTEGER*4 NUMP,ITER
        LOGICAL SYMMETRIC
```

```
      COMMON ENERO,EXTRA
      COMMON GAMMA,A,PLANE,DEPTH,COSRATIO
      COMMON FH,FMINH,FO
      COMMON FGA(2049)
      COMMON NUMP,ITER
      COMMON SYMMETRIC
C
      COMPLEX  ETA, AIOO
      COMPLEX AIOO1,AIOO2
      REAL AIO1,AIO2
      REAL SWO1, SWO2
      INTEGER*4 I
      REAL COSTETA,ALFA1,ALFA2
      REAL COSGAMA
      REAL SWNONSYMM
C
      IF(.NOT. SYMMETRIC) THEN
       SWFUNCTION = SWNONSYMM(DELZ,CFRAC,ENER)
       RETURN
      END IF
C
       COSTETA = 6201.5 * PLANE / A / ENERO
CX     COSGAMA = COSTETA / SQRT(3.)              ! FOR THE 111 REFLECTION WITH
100 WAFERS
CX     COSGAMA = COSTETA                   ! FOR THE 400 REFLECTION
CX     COSGAMA = COSTETA/SQRT(2.)                ! FOR THE 220 REFLECTION
CX     COSGAMA = COSTETA                   ! FOR BACK REFLECTION
       COSGAMA = COSTETA/COSRATIO
       GAMMA = 5512.97/(A*A*A*ENER*ENER)
    ETA = (-2.*(ENER-ENERO)/ENER*COSTETA**2+GAMMA*FO)
  &       /GAMMA/CSQRT(FH*FMINH)
C
      AIOO1 = - CSQRT(FH/FMINH) * ( ETA - CSQRT( ETA*ETA - 1. ) )
      AIO1 =  CABS( AIOO1 ) **2
   SWO1 = 2. * CFRAC * REAL( AIOO1*
  &      CMPLX( COS(6.2832*DELZ),- SIN(6.2832*DELZ) ) )
```

```
    &     + 1. + AIO1
      ALFA1 = ENER*GAMMA/COSGAMA/197.32 * AIMAG( FMINH*AIOO1+FO )
C  hc = 197.32 eV nm.  nm BECAUSE THE PROFILE DEPTH IS IN nm
C
          AIOO2 = - CSQRT(FH/FMINH) * ( ETA + CSQRT( ETA*ETA - 1. ) )
          AIO2 =  CABS( AIOO2 ) * CABS( AIOO2 )
      SWO2 = 2. * CFRAC * REAL( AIOO2*
    &       CMPLX( COS(6.2832*DELZ),- SIN(6.2832*DELZ) ) )
    &     + 1. + AIO2
      ALFA2 = ENER*GAMMA/COSGAMA/197.32 * AIMAG( FMINH*AIOO2+FO )
C
          IF (AIO2 .LE. 1.) THEN
            SWFUNCTION = SWO2 / ALFA2 * (1. - EXP(-DEPTH*ALFA2))
           ELSE
         SWFUNCTION = SWO1 / ALFA1 * (1. - EXP(-DEPTH*ALFA1))
          END IF
C
          RETURN
          END
C-----------------------------------------------------------------------------
     FUNCTION SWNONSYMM(DELZ,CFRAC,ENER)
     IMPLICIT NONE
     REAL DELZ,CFRAC
     REAL ENER, SWNONSYMM
C
          REAL ENERO,EXTRA
          REAL GAMMA,A,PLANE,DEPTH,COSRATIO
          COMPLEX FH,FMINH,FO
          COMPLEX FGA(2049)
          INTEGER*4 NUMP,ITER
          LOGICAL SYMMETRIC
          COMMON ENERO,EXTRA
          COMMON GAMMA,A,PLANE,DEPTH,COSRATIO
          COMMON FH,FMINH,FO
          COMMON FGA(2049)
          COMMON NUMP,ITER
```

```
      COMMON SYMMETRIC
C
      COMPLEX  ETA, AIOO
      COMPLEX AIOO1,AIOO2
      REAL AIO1,AIO2
      REAL SWO1, SWO2
      INTEGER*4 I
C
      REAL ANGLE
      REAL AGEO,COSTETA
C
     ANGLE = - ACOS(6201.5 * SQRT(3.) / A / ENERO ) +
   &              ACOS(SQRT(2./3.))
       AGEO = 0.33333  +  SQRT(8.)/3. * TAN(ANGLE)
     COSTETA = SQRT(2./3.) * COS(ANGLE) + 1./SQRT(3.) * SIN(ANGLE)
C
       GAMMA = 5512.97/(A*A*A*ENER*ENER)
     ETA = ( -2.*(ENER-ENERO)/ENER*(COSTETA)**2  +
   &      GAMMA*FO*(0.66666 + SQRT(2.)/3. * TAN(ANGLE) ) )
   &      / ( GAMMA*CSQRT(FH*FMINH)*SQRT(AGEO) )
C
     AIOO1 = - CSQRT(FH/FMINH) / SQRT(AGEO) *
   &          ( ETA - CSQRT( ETA*ETA - 1. ) )
       AIO1 =  CABS( AIOO1 ) **2
     SWO1 = 2. * CFRAC * REAL( AIOO1*
   &      CMPLX( COS(6.2832*DELZ),- SIN(6.2832*DELZ) ) )
   &     +  1. + AIO1
C
     AIOO2 = - CSQRT(FH/FMINH) / SQRT(AGEO) *
   &          ( ETA + CSQRT( ETA*ETA - 1. ) )
       AIO2 =  CABS( AIOO2 ) * CABS( AIOO2 )
     SWO2 = 2. * CFRAC * REAL( AIOO2*
   &      CMPLX( COS(6.2832*DELZ),- SIN(6.2832*DELZ) ) )
   &     +  1. + AIO2
C
       IF (AIO2 .LE. AIO1) THEN
```

```
           SWNONSYMM = SWO2
          ELSE
           SWNONSYMM = SWO1
         END IF
C
         RETURN
         END
C----------------------------------------------------------------------------
         SUBROUTINE PUTBACKG(ENERGY,EXPDAT,CALDAT,NUMP)
C  MINIMIZES  SUM [ ( ALFA+BETA(E-E(0)) )*CAL - EXP ]**2
C  THE ARGUMENT IS THAT I=I(0)+ALFA(E-E(0))
         IMPLICIT NONE
         REAL ENERGY(260), EXPDAT(260), CALDAT(260)
         REAL AN(2), B(2), C(2)
         REAL ALFA,BETA
         INTEGER*4 I
C
         DO 5, I=1,2
         AN(I) = 0.
         B(I) = 0.
5        C(I) = 0.
C
         DO 10, I=1, NUMP
          AN(1) = AN(1) + CALDAT(I)**2
          AN(2) = AN(2) + ( ENERGY(I) - ENERGY(1) ) * CALDAT(I)**2
          B(1) = B(1) + ( ENERGY(I) - ENERGY(1) ) * CALDAT(I)**2
          B(2) = B(2) + ( ENERGY(I) - ENERGY(1) )**2 * CALDAT(I)**2
          C(1) = C(1) + EXPDAT(I)*CALDAT(I)
       C(2) = C(2) + EXPDAT(I)*CALDAT(I)*(ENERGY(I) - ENERGY(1))
10       CONTINUE
C
         ALFA = ( C(1)*B(2) - C(2)*B(1) ) / ( AN(1)*B(2) - AN(2)*B(1) )
         BETA = ( AN(1)*C(2) - AN(2)*C(1) ) / ( AN(1)*B(2) - AN(2)*B(1) )
C
         DO 20, I = 1, NUMP
20      CALDAT(I)=( ALFA+BETA*(ENERGY(I) - ENERGY(1)) ) * CALDAT(I)
```

```
C
      RETURN
      END
C-----------------------------------------------------------------------
      SUBROUTINE PUTINFILE(SWCAL,ENERGY,OUTFILE,POINTS)
      IMPLICIT NONE
      REAL SWCAL(1025), ENERGY(1025)
      CHARACTER*255 OUTFILE
      INTEGER*4 POINTS
C
      INTEGER*4 I
C
      CLOSE(4)
      OPEN ( UNIT=4,STATUS='NEW',FILE=TRIM(OUTFILE) )
C
      DO 20, I=1, POINTS
       WRITE(4,10) ENERGY(I),CHAR(9),SWCAL(I)
20    CONTINUE
10    FORMAT( 4(G13.7,A) )
C
      CLOSE(4)
      RETURN
      END
C-----------------------------------------------------------------------
      SUBROUTINE DIBUJA(IO,ENERGY,POINTS)
      IMPLICIT NONE
      REAL IO(1025), ENERGY(1025)
      INTEGER*4 POINTS
C
      INTEGER*4 I
C
      CALL MOVEA (ENERGY(1),IO(1))
      DO 10, I=1, POINTS
     CALL DRAWA (ENERGY(I),IO(I))
10    CONTINUE
C
```

```
        RETURN
        END
C-------------------------------------------------------------------------
        SUBROUTINE AXESFOR(Y,ENERGY,POINTS)
        IMPLICIT NONE
        REAL Y(1025), ENERGY(1025)
        INTEGER*4 POINTS
C
        REAL MINY,MAXY
        REAL XMIN,XMAX,YMIN,YMAX
C
    XMIN = ENERGY(1)
    XMAX = ENERGY(POINTS)
    CALL MINMAX(Y,MINY,MAXY,POINTS)
        YMIN = MINY
        YMAX = MAXY
C Draw the axes
     CALL GRAPH(XMIN, XMAX, YMIN, YMAX)
C
        RETURN
        END
C-------------------------------------------------------------------------
        SUBROUTINE MINMAX(Y,MINY,MAXY,POINTS)
        IMPLICIT NONE
        REAL MINY,MAXY
        REAL Y(1025)
        INTEGER*4 I
C
        INTEGER*4 POINTS
C
        MINY = Y(1)
        MAXY = Y(1)
        DO 10, I=1,POINTS
         IF (MINY > Y(I) ) MINY = Y(I)
         IF (MAXY < Y(I) ) MAXY = Y(I)
10      CONTINUE
```

```
C
        RETURN
        END
C-----------------------------------------------------------------------
        SUBROUTINE LETRERO(INFO,NUM)
        IMPLICIT NONE
        CHARACTER*255 INFO
        INTEGER*4 NUM
C
        INTEGER*4 H, V
        INTEGER*2 PENLOC(2)
        INTEGER GETPEN, MOVETO
      parameter (GETPEN=Z'89A30000',MOVETO=Z'89309000')
C
C
C  AND TO WRITE OUT THE INFO
        CALL TOOLBX(GETPEN, PENLOC)
        CALL TOOLBX (MOVETO, 10, 30+NUM*10)
C
         WRITE(9,44) INFO
44       FORMAT(A)
C
C  AND PUT THE PEN BACK WHERE IT WAS
        H = PENLOC(2)
        V = PENLOC(1)
        CALL TOOLBX (MOVETO, H, V)
C
        RETURN
        END
C-----------------------------------------------------------------------
        SUBROUTINE RCHAR(CHAR,NUM)
        IMPLICIT NONE
        CHARACTER CHAR
        INTEGER*4 NUM
C
        INTEGER*4 H, V
```

```
      INTEGER*2 PENLOC(2)
      INTEGER GETPEN, MOVETO
     parameter (GETPEN=Z'89A30000',MOVETO=Z'89309000')
C
C
C AND TO WRITE OUT THE INFO
      CALL TOOLBX(GETPEN, PENLOC)
      CALL TOOLBX (MOVETO, 10, 30+NUM*10)
C
       READ(9,*) CHAR
C
C AND PUT THE PEN BACK WHERE IT WAS
      H = PENLOC(2)
      V = PENLOC(1)
      CALL TOOLBX (MOVETO, H, V)
C
      RETURN
      END
C-----------------------------------------------------------------------
      SUBROUTINE RINT(INUM,NUM)
      IMPLICIT NONE
      INTEGER*4 INUM
      INTEGER*4 NUM
C
      INTEGER*4 H, V
      INTEGER*2 PENLOC(2)
      INTEGER GETPEN, MOVETO
     parameter (GETPEN=Z'89A30000',MOVETO=Z'89309000')
C
C
C AND TO WRITE OUT THE INFO
      CALL TOOLBX(GETPEN, PENLOC)
      CALL TOOLBX (MOVETO, 10, 30+NUM*10)
C
       READ(9,*) INUM
C
```

```
C  AND PUT THE PEN BACK WHERE IT WAS
         H = PENLOC(2)
         V = PENLOC(1)
         CALL TOOLBX (MOVETO, H, V)
C
         RETURN
         END
C-----------------------------------------------------------------------
         SUBROUTINE RREAL(RNUM,NUM)
         IMPLICIT NONE
         REAL RNUM
         INTEGER*4 NUM
C
         INTEGER*4 H, V
         INTEGER*2 PENLOC(2)
         INTEGER GETPEN, MOVETO
      parameter (GETPEN=Z'89A30000',MOVETO=Z'89309000')
C
C
C  AND TO WRITE OUT THE INFO
         CALL TOOLBX(GETPEN, PENLOC)
         CALL TOOLBX (MOVETO, 10, 30+NUM*10)
C
          READ(9,*) RNUM
C
C  AND PUT THE PEN BACK WHERE IT WAS
         H = PENLOC(2)
         V = PENLOC(1)
         CALL TOOLBX (MOVETO, H, V)
C
         RETURN
         END
C-----------------------------------------------------------------------
         SUBROUTINE GETCHI(CAL,EXPE,CHI,POINTS)
         IMPLICIT NONE
         REAL CAL(260), EXPE(260)
```

```
      REAL CHI
      INTEGER*4 POINTS
C
      INTEGER*4 I
C
      CHI = 0.
      DO 90, I=1,POINTS
       CHI = CHI + ( EXPE(I) - CAL(I) ) **2
90    CONTINUE
C
      RETURN
      END
C-----------------------------------------------------------------------
      SUBROUTINE DUM
      COMMON /K/ ARY(8000)
      RETURN
      END
C
      INCLUDE GRAPH.INC
```

Appendix 4 Program "AVERAGE"

This program was used to average the experimental data (see Section 6.3). The criteria to obtain the apropiate shift and interpolation is by maximizing the correlation of the reflectivity or of the total yield.

```
C
      PROGRAM AVERAGE
      IMPLICIT NONE
      REAL ENERGY(260)
      REAL IO(260),SW(260),TY(260)
      REAL IOTOT(260),SWTOT(260),TYTOT(260)
      REAL IOS(260),SWS(260),TYS(260)
      REAL IOB(260), SWB(260)
      CHARACTER*64 INFO
      CHARACTER CH
      INTEGER*4 I
      CHARACTER*255 OUTFILE, DATA, REPSTR
      REAL FRACTION
      INTEGER*4 SHIFT
      REAL MULBKG
      INTEGER*4 NUMFILES
      INTEGER*4 JOFMAX, JOFMAXTOT, MAXSHIFT
      REAL STEP, E1
      CHARACTER AORS
      CHARACTER AUGERBKG
      REAL ENERGY1,ENERGY2,BKG1,BKG2,BKG2REAL
C
    INTEGER*4
ENERCHANNEL,REFCHANNEL,SWCHANNEL,TYCHANNEL,NORMCHANNEL
    INTEGER*4 SKIPLINES
      CHARACTER NORMALIZE
C
      INTEGER*4 NUMP
      COMMON NUMP
```

```
C
      OPEN(5, FILE='AVERFILES', STATUS='OLD')
      READ(5,*) ENERCHANNEL
      READ(5,*) REFCHANNEL
      READ(5,*) SWCHANNEL
      READ(5,*) TYCHANNEL
      READ(5,*) NORMCHANNEL
      READ(5,*) NORMALIZE
      READ(5,*) SKIPLINES
      READ(5,*) AUGERBKG
      READ(5,*) ENERGY1, ENERGY2
      READ(5,*) BKG1, BKG2
      READ(5,*) BKG2REAL
      READ(5,*) MULBKG
C
      WRITE(9,*) ' repeated string? '
      READ(5,*) REPSTR
      WRITE(9,*) ' MAIN FILE? (I PUT ',TRIM(REPSTR)
      READ(5,*) DATA
      DATA = TRIM(DATA)
      DATA = TRIM(TRIM(DATA)//TRIM(REPSTR))
      WRITE(9,*) DATA
C
      CALL GETENERGY(DATA,ENERGY,ENERCHANNEL,SKIPLINES)
C
    CALL
GETEXPDATA(DATA,IOTOT,SWTOT,TYTOT,REFCHANNEL,SWCHANNEL,
   &        TYCHANNEL,NORMCHANNEL,SKIPLINES,NORMALIZE)
      NUMFILES = 1
    CALL GETJOFMAX(IOTOT,JOFMAXTOT)
      MAXSHIFT = 0
C
20    CONTINUE
      WRITE(9,*) ' NEXT FILE? (I PUT ',TRIM(REPSTR)
      WRITE(9,*) ' NEXT FILE? (I PUT ',TRIM(REPSTR)
      READ(5,*,ERR=850,END=850) DATA,AORS
```

```
        DATA = TRIM(DATA)
        DATA = TRIM(TRIM(DATA)//TRIM(REPSTR))
      CALL GETEXPDATA(DATA,IO,SW,TY,REFCHANNEL,SWCHANNEL,
     &          TYCHANNEL,NORMCHANNEL,SKIPLINES,NORMALIZE)
C
        CALL AXESFOR(IOTOT,ENERGY)
        CALL DIBUJA(IOTOT,ENERGY)
        CALL PUTBACKG(ENERGY,IOTOT,IO,IOB)
        CALL DIBUJA(IOB,ENERGY)
        WRITE(INFO,*) ' LIKE IT? (Y/N) '
C
        CALL LETRERO(INFO,19)
        CALL RECHAR(CH,20)
        IF(CH .EQ. 'N') GOTO 800
C
        CALL AXESFOR(SW,ENERGY)
        CALL DIBUJA(SW,ENERGY)
        WRITE(INFO,*) ' STILL LIKE IT? (Y/N) '
        CALL LETRERO(INFO,19)
        CALL RECHAR(CH,20)
        IF(CH .EQ. 'N') GOTO 800
C
      CALL GETJOFMAX(IO,JOFMAX)
      SHIFT = - JOFMAX + JOFMAXTOT
        CALL MAKESHIFT(SHIFT,IO,IOS)
        CALL MAKESHIFT(SHIFT,SW,SWS)
        CALL MAKESHIFT(SHIFT,TY,TYS)
        IF( ABS(SHIFT) .GT. ABS(MAXSHIFT) ) MAXSHIFT = SHIFT
C
        CALL GETSHIFT(ENERGY,IOTOT,IOS,SHIFT,FRACTION)
        CALL MAKESHIFT(SHIFT,IOS,IO)
        CALL MAKESHIFT(SHIFT,SWS,SW)
        CALL MAKESHIFT(SHIFT,TYS,TY)
        CALL INTERPOLATE(FRACTION,IO,IOS)
        CALL INTERPOLATE(FRACTION,SW,SWS)
        CALL INTERPOLATE(FRACTION,TY,TYS)
```

```
C
      WRITE(INFO,*) TRIM(DATA)
      CALL LETRERO(INFO,18)
C
    CALL GETTOTAL(MULBKG,IOS,SWS,TYS,IOTOT,SWTOT,TYTOT,
  &
NUMFILES,AORS,AUGERBKG,ENERGY1,ENERGY2,BKG1,BKG2,BKG2REAL)
800   CONTINUE
      WRITE(INFO,*) 'ANOTHER FILE? (Y/N) '
      CALL LETRERO(INFO,21)
      CALL RECHAR(CH,22)
      IF(CH .NE. 'N') GOTO 20
C
850   CONTINUE
      WRITE(9,*) 'CORRECT ENERGY SCALE? '
      WRITE(9,*) 'CORRECT ENERGY SCALE? '
      READ(9,*) CH
      IF(CH .EQ. 'Y') THEN
       WRITE(9,*) 'ENERGY SCALE CORRECTED '
C IF THE PEAK COMES EARLIER, WE HAVE TO EXPAND THE SCALE
       STEP = STEP * (1. + MAXSHIFT/NUMFILES/NUMP)
C
       ENERGY(1) = E1
       DO 6, I=2,NUMP
     ENERGY(I) = ENERGY(I-1) + STEP
6      CONTINUE
C
       CALL GETENERGY(DATA,ENERGY,STEP,E1)
      ELSE
       WRITE(9,*) 'ENERGY SCALE NOT NOT NOT CORRECTED '
      END IF
C
      CALL LESSSMALLER(IOTOT)
C
      OUTFILE = 'SUM.TXT'
      CALL PUTINFILE(OUTFILE,ENERGY,IOTOT,SWTOT,TYTOT)
```

```
900     CONTINUE
        PAUSE 'DONE'
        STOP
        END
C-----------------------------------------------------------------------
        SUBROUTINE GETJOFMAX(IO,JOFMAX)
        IMPLICIT NONE
        REAL IO(260)
        INTEGER*4 JOFMAX
C
        INTEGER*4 NUMP
        COMMON NUMP
C
        REAL IMAX
        INTEGER*4 I
C
        IMAX = IO(1)
        JOFMAX = 1
        DO 810, I=1, NUMP
         IF(IO(I) .GT. IMAX) THEN
          IMAX = IO(I)
          JOFMAX = I
         END IF
810     CONTINUE
C
        RETURN
        END
C-----------------------------------------------------------------------
        SUBROUTINE LESSSMALLER(IO)
        IMPLICIT NONE
        REAL IO(260)
C
        INTEGER*4 NUMP
        COMMON NUMP
C
        REAL IMIN
```

```
      INTEGER*4 I
C
      IMIN = IO(1)
      DO 810, I=1, NUMP
       IF(IO(I) .LT. IMIN) IMIN = IO(I)
810   CONTINUE
C
      DO 820, I=1, NUMP
       IO(I) = IO(I) - IMIN
820   CONTINUE
C
      RETURN
      END
C-----------------------------------------------------------------------
      SUBROUTINE
GETEXPDATA(DATA,IO,SW,TY,REFCHANNEL,SWCHANNEL,
   &        TYCHANNEL,NORMCHANNEL,SKIPLINES,NORMALIZE)
      IMPLICIT NONE
      CHARACTER*255 DATA
      REAL IO(260), SW(260), TY(260)
    INTEGER*4 REFCHANNEL,SWCHANNEL,TYCHANNEL,NORMCHANNEL
    INTEGER*4 SKIPLINES
      CHARACTER NORMALIZE
C
      INTEGER*4 I, J, K
      REAL GAR(10)
      CHARACTER CH
C
      INTEGER*4 NUMP
      COMMON NUMP
C
       WRITE(9,*) 'NOW GETTING THE DATA          '
      OPEN (UNIT=10,STATUS='OLD',FILE=TRIM(DATA) )
C
      DO 34, I=1,SKIPLINES
       READ(10,35) CH
```

```
34      CONTINUE
35       FORMAT(A)
C
        K = MAX0(REFCHANNEL,SWCHANNEL,TYCHANNEL,NORMCHANNEL)
        DO 6, I=1,NUMP
       READ(10,*,END=10,ERR=10) ( GAR(J), J=1, K )
       IF( NORMALIZE .EQ. 'Y' ) THEN
          IO(I) = GAR(REFCHANNEL)/GAR(NORMCHANNEL)
          SW(I) = GAR(SWCHANNEL)/GAR(NORMCHANNEL)
          TY(I) = GAR(TYCHANNEL)/GAR(NORMCHANNEL)
         ELSE
          IO(I) = GAR(REFCHANNEL)
          SW(I) = GAR(SWCHANNEL)
          TY(I) = GAR(TYCHANNEL)
         END IF
6       CONTINUE
C
        CLOSE(10)
        RETURN
10      WRITE(9,*) 'ERROR READING THIS FILE '
        PAUSE 'ERROR READING THIS FILE '
        PAUSE ' PLEASE ABORT '
        RETURN
        END
C-------------------------------------------------------------------------
        SUBROUTINE
GETENERGY(DATA,ENERGY,ENERCHANNEL,SKIPLINES)
        IMPLICIT NONE
        CHARACTER*255 DATA
        REAL ENERGY(260)
        INTEGER*4 ENERCHANNEL, SKIPLINES
C
        REAL STEP,E1
C
        INTEGER*4 I, J
        CHARACTER CH
```

```
        REAL GAR
        REAL ENER
C
        INTEGER*4 NUMP
        COMMON NUMP
C
         WRITE(9,*) 'NOW GETTING THE ENERGY          '
        OPEN (UNIT=10,STATUS='OLD',FILE=TRIM(DATA) )
C
        DO 34, I=1,SKIPLINES
         READ(10,35) CH
34      CONTINUE
35       FORMAT(A)
C
        ENER = E1
        DO 6, I=1,260
       READ(10,*,END = 10, ERR=10) ( ENERGY(I), J=1,ENERCHANNEL )
6       CONTINUE
C
10      CONTINUE
        NUMP = I - 1
C
        CLOSE(10)
        RETURN
        END
C---------------------------------------------------------------------------
      SUBROUTINE GETSHIFT(ENERGY,IOTOT,IO,SHIFT,FRACTION)
        IMPLICIT NONE
        REAL ENERGY(260),IOTOT(260),IO(260)
        INTEGER*4 SHIFT
        REAL FRACTION
C
        INTEGER*4 NUMP
        COMMON NUMP
C
        REAL IOB(260),IOS(260),IOF(260)
```

```
      REAL CHI,CHI1
      INTEGER*4 I
      CHARACTER*64 INFO
C
      CALL AXESFOR(IOTOT,ENERGY)
      CALL DIBUJA(IOTOT,ENERGY)
      CALL PUTBACKG(ENERGY,IOTOT,IO,IOB)
      CALL GETCHI(IOTOT,IOB,CHI)
      SHIFT = 1
      CALL MAKESHIFT(SHIFT,IO,IOS)
      CALL PUTBACKG(ENERGY,IOTOT,IOS,IOB)
      CALL GETCHI(IOTOT,IOB,CHI1)
      IF(CHI1 .LT. CHI) THEN
       CALL DIBUJA(IOB,ENERGY)
15     CONTINUE
       CHI = CHI1
       CALL MAKESHIFT(SHIFT+1,IO,IOS)
       CALL PUTBACKG(ENERGY,IOTOT,IOS,IOB)
       CALL GETCHI(IOTOT,IOB,CHI1)
       IF(CHI1 .LT. CHI) THEN
        SHIFT = SHIFT + 1
        CALL DIBUJA(IOB,ENERGY)
        GOTO 15
       END IF
      ELSE
       SHIFT = 0
16     CONTINUE
       CALL MAKESHIFT(SHIFT-1,IO,IOS)
       CALL PUTBACKG(ENERGY,IOTOT,IOS,IOB)
       CALL GETCHI(IOTOT,IOB,CHI1)
       IF(CHI1 .LT. CHI) THEN
        SHIFT = SHIFT - 1
        CHI = CHI1
        CALL DIBUJA(IOB,ENERGY)
        GOTO 16
       END IF
```

```
      END IF
C
      CALL MAKESHIFT(SHIFT,IO,IOS)
      FRACTION = 0.1
      CALL INTERPOLATE(FRACTION,IOS,IOF)
      CALL PUTBACKG(ENERGY,IOTOT,IOF,IOB)
      CALL GETCHI(IOTOT,IOB,CHI1)
      IF(CHI1 .LT. CHI) THEN
       CALL DIBUJA(IOB,ENERGY)
17     CONTINUE
       CHI = CHI1
       CALL INTERPOLATE(FRACTION+0.1,IOS,IOF)
       CALL PUTBACKG(ENERGY,IOTOT,IOF,IOB)
       CALL GETCHI(IOTOT,IOB,CHI1)
       IF(CHI1 .LT. CHI) THEN
        FRACTION = FRACTION + 0.1
        CALL DIBUJA(IOB,ENERGY)
        GOTO 17
       END IF
      ELSE
       FRACTION = 0
18     CONTINUE
       CALL INTERPOLATE(FRACTION - 0.1,IOS,IOF)
       CALL PUTBACKG(ENERGY,IOTOT,IOF,IOB)
       CALL GETCHI(IOTOT,IOB,CHI1)
       IF(CHI1 .LT. CHI) THEN
        FRACTION = FRACTION - 0.1
        CHI = CHI1
        CALL DIBUJA(IOB,ENERGY)
        GOTO 18
       END IF
      END IF
C
      RETURN
      END
C-----------------------------------------------------------------------
```

```
      SUBROUTINE MAKESHIFT(SHIFT,IO,IOS)
      IMPLICIT NONE
      INTEGER*4 SHIFT
      REAL IO(260), IOS(260)
C
      INTEGER*4 NUMP
      COMMON NUMP
C
      INTEGER*4 SHIFT2
      INTEGER*4 I
C
      IF(SHIFT .EQ. 0) THEN
       DO 10, I=1, NUMP
10      IOS(I) = IO(I)
      ELSE IF(SHIFT .GT. 0) THEN
       DO 20, I=1,SHIFT
20      IOS(I) = IO(1)
       DO 30, I=SHIFT+1,NUMP
30      IOS(I) = IO(I-SHIFT)
      ELSE
       SHIFT2 = - SHIFT
       DO 40, I=1, NUMP-SHIFT2
40      IOS(I) = IO(I+SHIFT2)
       DO 50, I=NUMP-SHIFT2+1, NUMP
50      IOS(I) = IO(NUMP)
      END IF
C
      RETURN
      END
C-----------------------------------------------------------------------
      SUBROUTINE INTERPOLATE(FRACTION,IOS,IOF)
      IMPLICIT NONE
      REAL FRACTION
      REAL IOS(260), IOF(260)
C
      INTEGER*4 NUMP
```

```
      COMMON NUMP
C
      REAL FRACTION2
      INTEGER*4 I
C
      IF(FRACTION .GE. 0.0) THEN
       DO 10, I=1,NUMP-1
10        IOF(I) = (1.-FRACTION)*IOS(I) + FRACTION*IOS(I+1)
     IOF(NUMP) = IOS(NUMP)
    ELSE
     FRACTION2 = 1 + FRACTION
     DO 20, I=2, NUMP
20        IOF(I) = (1.-FRACTION2)*IOS(I-1) + FRACTION2*IOS(I)
       IOF(1) = IOS(1)
      END IF
C
      RETURN
      END
C----------------------------------------------------------------------------
    SUBROUTINE GETTOTAL(MULBKG,IO,SW,TY,IOTOT,SWTOT,TYTOT,
  &
NUMFILES,AORS,AUGERBKG,ENERGY1,ENERGY2,BKG1,BKG2,BKG2REAL)
      IMPLICIT NONE
      REAL MULBKG
      REAL IO(260),SW(260),TY(260)
      REAL IOTOT(260),SWTOT(260),TYTOT(260)
      INTEGER*4 NUMFILES
      CHARACTER AORS
      CHARACTER AUGERBKG
      REAL ENERGY1,ENERGY2,BKG1,BKG2,BKG2REAL
C
      CHARACTER*64 INFO
      REAL CONST1
      REAL DELTA, CONST2
      INTEGER*4 I
C
```

```
      INTEGER*4 NUMP
      COMMON NUMP
C
      IF(AORS .EQ. 'A') THEN
        CONST1 =  1.
        CONST2 = 0.
      ELSE IF(AORS .EQ. 'S') THEN
        IF( AUGERBKG .EQ. 'Y' .OR. AUGERBKG .EQ. 'y' ) THEN
       DELTA = ( BKG2 * ENERGY1 - BKG1 * ENERGY2 ) /
   &           (ENERGY2 - ENERGY1 ) * BKG2REAL / BKG2
       CONST1 = - ENERGY1/ENERGY2
       CONST2 =  - ( ENERGY1/ENERGY2 - 1. ) * DELTA
        ELSE
         CONST1 =  - MULBKG
         CONST2 = 0.
        END IF
      ELSE
        WRITE(9,*) ' ADD OR SUBSTRACT? '
        PAUSE ' ADD OR SUBSTRACT? '
      END IF
C
      WRITE(INFO,5) CONST1, CONST2, DELTA
5    FORMAT( 'CONST1 ', G12.5, '  CONST2 ', G12.5, '  DELTA ',G12.5)
      CALL LETRERO(INFO,5)
C
      DO 10, I=1,NUMP
       IOTOT(I) = IOTOT(I) + IO(I)
       SWTOT(I) = SWTOT(I) + ( CONST1 * SW(I) + CONST2 )
       TYTOT(I) = TYTOT(I) + TY(I)
10    CONTINUE
      NUMFILES = NUMFILES + 1
C
      RETURN
      END
C-----------------------------------------------------------------------
      SUBROUTINE GETCHI(CAL,EXPE,CHI)
```

```
      IMPLICIT NONE
      REAL CAL(260), EXPE(260)
      REAL CHI
      INTEGER*4 I
C
      INTEGER*4 NUMP
      COMMON NUMP
C
      CHI = 0.
      DO 90, I=1,NUMP
       CHI = CHI + ( EXPE(I) - CAL(I) ) **2
90    CONTINUE
C
      RETURN
      END
C-----------------------------------------------------------------------
      SUBROUTINE DIBUJA(IO,ENERGY)
      IMPLICIT NONE
      REAL IO(260), ENERGY(260)
      INTEGER*4 I
C
      INTEGER*4 NUMP
      COMMON NUMP
C
      CALL MOVEA (ENERGY(1),IO(1))
      DO 10, I = 1, NUMP
     CALL DRAWA (ENERGY(I),IO(I))
10    CONTINUE
C
      RETURN
      END
C-----------------------------------------------------------------------
      SUBROUTINE PUTBACKG(ENERGY,IOTOT,IO,IOB)
C MINIMIZES SUM[ ( ALFA+BETA(E-E(0)) )*CAL(I) + DELTA  - EXP(I) ]**2
C  THE ARGUMENT IS THAT I=I(0)+ALFA(E-E(0))
      IMPLICIT NONE
```

```
      REAL ENERGY(260), IOTOT(260), IO(260), IOB(260)
      REAL AN(3), B(3), C(3), D(3)
      REAL ALFA,BETA,DELTA
      REAL DETER
      INTEGER*4 I
C
      INTEGER*4 NUMP
      COMMON NUMP
C
      DO 3, I=1,NUMP
       IO(I) = IO(I) + 1.
3     CONTINUE
C
      DO 5, I=1,3
      AN(I) = 0.
      B(I) = 0.
      C(I) = 0.
5     D(I) = 0.
C
      DO 10, I=1, NUMP
       AN(1) = AN(1) + IO(I)**2
       AN(2) = AN(2) + ( ENERGY(I) - ENERGY(1) ) * IO(I)**2
       AN(3) = AN(3) + IO(I)
       B(1) = B(1) + ( ENERGY(I) - ENERGY(1) ) * IO(I)**2
       B(2) = B(2) + ( ENERGY(I) - ENERGY(1) )**2 * IO(I)**2
       B(3) = B(3) + ( ENERGY(I) - ENERGY(1) ) * IO(I)
       C(1) = C(1) + IO(I)
       C(2) = C(2) + IO(I) * ( ENERGY(I) - ENERGY(1) )
       C(3) = C(3) + 1.
       D(1) = D(1) + IOTOT(I)*IO(I)
     D(2) = D(2) + IOTOT(I)*IO(I)*(ENERGY(I) - ENERGY(1))
       D(3) = D(3) + IOTOT(I)
10    CONTINUE
C
      ALFA = DETER(D,B,C) / DETER(AN,B,C)
      BETA = DETER(AN,D,C) / DETER(AN,B,C)
```

```
      DELTA = DETER(AN,B,D) / DETER(AN,B,C)
C
      DO 20, I = 1, NUMP
    IOB(I)=( ALFA+BETA*(ENERGY(I) - ENERGY(1)) ) *
  &                IO(I) + DELTA
20    CONTINUE
C
C
      RETURN
      END
C-----------------------------------------------------------------------
      FUNCTION DETER(A2,B,C)
      IMPLICIT NONE
      REAL A2(3), B(3), C(3)
      REAL DETER
C
      DETER = A2(1) * ( B(2)*C(3) - B(3)*C(2) )
  &        - A2(2) * ( B(1)*C(3) - B(3)*C(1) )
  &          + A2(3) * ( B(1)*C(2) - B(2)*C(1) )
C
      RETURN
      END
C-----------------------------------------------------------------------
      SUBROUTINE AXESFOR(Y,ENERGY)
      IMPLICIT NONE
      REAL Y(260), ENERGY(260)
      REAL MINY,MAXY
      REAL XMIN,XMAX,YMIN,YMAX
C
      INTEGER*4 NUMP
      COMMON NUMP
C
   XMIN = ENERGY(1)
   XMAX = ENERGY(NUMP)
   CALL MINMAX(Y,MINY,MAXY)
      YMIN = MINY
```

```
C       YMIN = AMIN1(MINY,0.)
        YMAX = MAXY
C Draw the axes
     CALL GRAPH(XMIN, XMAX, YMIN, YMAX)
C
        RETURN
        END
C------------------------------------------------------------------------
        SUBROUTINE MINMAX(Y,MINY,MAXY)
        IMPLICIT NONE
        REAL MINY,MAXY
        REAL Y(260)
        INTEGER*4 I
C
        INTEGER*4 NUMP
        COMMON NUMP
C
        MINY = Y(1)
        MAXY = Y(1)
        DO 10, I=1,NUMP
         IF (MINY > Y(I) ) MINY = Y(I)
         IF (MAXY < Y(I) ) MAXY = Y(I)
10      CONTINUE
C
        RETURN
        END
C------------------------------------------------------------------------
        SUBROUTINE PUTINFILE(OUTFILE,ENERGY,IOTOT,SWTOT,TYTOT)
        IMPLICIT NONE
        REAL SWTOT(260), TYTOT(260), ENERGY(260), IOTOT(260)
        CHARACTER*255 OUTFILE
C
        INTEGER*4 I
C
        INTEGER*4 NUMP
        COMMON NUMP
```

```
C
      CLOSE(4)
      OPEN ( UNIT=4,STATUS='NEW',FILE=TRIM(OUTFILE) )
C
      DO 20, I=1,NUMP
       WRITE(4,10) ENERGY(I),CHAR(9),IOTOT(I),CHAR(9),
     &      SWTOT(I),CHAR(9),TYTOT(I)
20    CONTINUE
10    FORMAT( F10.3,A,4(G12.5,A) )
C
      CLOSE(4)
      RETURN
      END
C-------------------------------------------------------------------------
      SUBROUTINE LETRERO(INFO,NUM)
      IMPLICIT NONE
      CHARACTER*64 INFO
      INTEGER*4 NUM
C
      INCLUDE QUICKDRAW.INC
      INTEGER*4 H, V
      INTEGER*2 PENLOC(2)
C
C AND TO WRITE OUT THE INFO
      CALL TOOLBX(GETPEN, PENLOC)
CX    CALL TOOLBX (MOVETO, 10, 30)
      CALL TOOLBX (MOVETO, 10, 30+NUM*10)
C
       WRITE(9,44) INFO
44     FORMAT(A)
C
C AND PUT THE PEN BACK WHERE IT WAS
      H = PENLOC(2)
      V = PENLOC(1)
      CALL TOOLBX (MOVETO, H, V)
C
```

```
      RETURN
      END
C------------------------------------------------------------------------
      SUBROUTINE PAULETRERO(INFO,NUM)
      IMPLICIT NONE
      CHARACTER*64 INFO
      INTEGER*4 NUM
C
      INCLUDE QUICKDRAW.INC
      INTEGER*4 H, V
      INTEGER*2 PENLOC(2)
C
C  AND TO WRITE OUT THE INFO
      CALL TOOLBX(GETPEN, PENLOC)
      CALL TOOLBX (MOVETO, 10, 30+NUM*10)
C
       WRITE(9,44) INFO
44     FORMAT(A)
       PAUSE 'RETURN TO CONTINUE   '
C
C  AND PUT THE PEN BACK WHERE IT WAS
      H = PENLOC(2)
      V = PENLOC(1)
      CALL TOOLBX (MOVETO, H, V)
C
      RETURN
      END
C------------------------------------------------------------------------
      SUBROUTINE RECHAR(CH,NUM)
      IMPLICIT NONE
      INTEGER*4 NUM
      CHARACTER CH
C
      INCLUDE QUICKDRAW.INC
      INTEGER*4 H, V
      INTEGER*2 PENLOC(2)
```

```
C
C  AND TO WRITE OUT THE INFO
        CALL TOOLBX(GETPEN, PENLOC)
        CALL TOOLBX (MOVETO, 10, 30+NUM*10)
C
         READ(9,*) CH
C
C  AND PUT THE PEN BACK WHERE IT WAS
        H = PENLOC(2)
        V = PENLOC(1)
        CALL TOOLBX (MOVETO, H, V)
C
        RETURN
        END
C-----------------------------------------------------------------------------
        SUBROUTINE DUM
        COMMON /K/ ARY(8000)
        RETURN
        END
C
        INCLUDE GRAPH.INC
```